UNIVERSITÄT PADERBORN
Die Universität der Informationsgesellschaft

FAKULTÄT FÜR
ELEKTROTECHNIK,
INFORMATIK UND
MATHEMATIK

Title

Design and Performance Analysis of Improper Gaussian Signaling Schemes for Interference-limited Systems

Der Fakultät für Elektrotechnik, Informatik und Mathematik
der Universität Paderborn

zur Erlangung des akademischen Grades

Doktor der Ingenieurwissenschaften (Dr.-Ing.)

vorgelegte Dissertation

von

M. Sc. Mohammad Soleymani
geboren am 30.07.1989 in Arak, Iran

Erster Gutachter: Prof. Dr. Peter J. Schreier
Zweiter Gutachter: Prof. Dr. Ignacio Santamaria

Tag der mündlichen Prüfung: 15.12.2020

Paderborn 2020

EIM-E/357

UNIVERSITÄT PADERBORN
Die Universität der Informationsgesellschaft

FAKULTÄT FÜR
ELEKTROTECHNIK,
INFORMATIK UND
MATHEMATIK

Abstract for the dissertation:

Design and Performance Analysis of Improper Gaussian Signaling Schemes for Interference-limited Systems

by **Mohammad Soleymani**

In this thesis, we design various improper Gaussian signaling (IGS) schemes to improve the performance of different interference-limited systems and analyze the performance of IGS as an interference-management technique. In an improper signal, the real and imaginary parts of the signal are correlated and/or have unequal powers. The performance of modern wireless communication systems is mainly restricted by interference from other users, which implies the importance of interference-management techniques. We propose some IGS schemes to improve spectral and energy efficiency of different single-antenna and multiple-antenna interference-limited systems with realistic assumptions regarding hardware and channel knowledge.

We first consider the K-user multiple-input, multiple-output (MIMO) interference channel (IC) with imperfect hardware. To fully characterize the performance of IGS, we consider various optimization problems such as the rate region, sum-rate maximization, energy-efficiency (EE) region and global EE maximization problems. To solve these non-convex problems, we first formulate a general optimization problem that encompasses all performance metrics under study and then, employ a majorization-minimization framework to obtain solutions for each problem. This optimization framework converges to a stationary point of every optimization problem in MIMO interference-limited systems with treating interference as noise (TIN) in which either the objective function and/or constraints are linear functions of rates. Our numerical results show that IGS can outperform the K-user MIMO IC with hardware impairment, where its benefits increase with K and the imbalance level and decrease with the number of antennas. We also consider the K-user single-input, single-output (SISO) IC with imperfect devices and derive the corresponding achievable rate region by proposing two iterative algorithms with different computational complexity.

We also investigate the robustness of IGS against imperfect channel state information (CSI) on the transmitter side in a 2-user and Z SISO IC. Following a worst-case robustness approach, we study the rate-region boundary of the ICs for the worst channels and show the superiority of IGS. Additionally, we study the performance of IGS over a 2-user Rayleigh SISO IC. We assume that the receivers have perfect CSI, while the transmitters have access to only statistical CSI. We derive the ergodic rate region for the 2-user fading IC and show that, in the moderate and strong interference regimes, IGS outperforms the proper Gaussian signaling scheme.

In addition to the rate analysis, we consider EE of IGS and propose energy-efficient IGS designs for the K-user SISO IC and underlay cognitive radio (UCR). We show that IGS can be beneficial from EE point of view. In UCR, we derive closed-form necessary and sufficient conditions for the optimality of IGS.

To summarize, we propose some spectral or energy efficient IGS schemes and show that IGS can improve the spectral and EE of different interference-limited systems with realistic assumptions regarding channel knowledge and hardware. Moreover, we show that the benefits of IGS increases with the number of users and decreases with the number of (either spatial or frequency) resources. We also show that the EE benefits of IGS are less than its rate benefits.

UNIVERSITÄT PADERBORN
Die Universität der Informationsgesellschaft

FAKULTÄT FÜR
ELEKTROTECHNIK,
INFORMATIK UND
MATHEMATIK

Zusammenfassung der Dissertation

Design und Leistungsanalyse von Improper Gaussian Signaling-Schemata für Systeme mit begrenzter Interferenz

des **Herrn Mohammad Soleymani**

In dieser Arbeit wurde verschiedene Improper Gaussian Signaling (IGS)-Schemata entworfen, um die Leistung verschiedener störungsbegrenzter Systeme zu verbessern, und die Leistung von IGS als Interferenzmanagementtechnik wird untersucht. Als improper bezeichnet man komplexwertige Signale deren Real- und Imaginärteil korreliert sind und/oder unterschiedliche Leistung haben. Ziel dieser Dissertation war es, die Spektral- und Energieeffizienzsteigerungen durch verschiedene IGS Schemata. Diese reichen von unterschiedlichen interferenzbegrenzten Einzelantennen- bis Mehrantennensysteme unter Berücksichtigung realer Annahmen bezüglich Hardware- und Kanalkenntnisse.

Zunächst wurde der K-Nutzer Mehrantenneninterferenzkanal (multiple input, multiple-output (MIMO) interference channel (IC)) mit imperfekter Hardware betrachtet. Zur Charakterisierung der Performanz des IGS werden verschiedene Optimierungen betrachtet, wie z.B. die Datenratenregion, Summen-Raten Maximierung, Energieeffizienz (EE-)Region und globale EE-Max-imierung. Um diese nicht-konvexen Probleme zu lösen, wird zunächst ein allgemeines Optimierungsproblem formuliert, das alle Metriken umfasst um anschließend das Majorisierungs-/Minimierungsverfahren anzuwenden, wodurch Lösungen für jedes der Einzelprobleme gefunden werden kann. Numerische Auswertungen haben gezeigt, dass IGS die Performanz des K-Nutzer-MIMO-IC unter Berücksichtigung von Hardwareeinfluss verbessern kann. Dabei hat sich herausgestellt, dass der Nutzen mit K und dem Ungleichgewicht zwischen Stärke des Real- und Imaginärteils zunimmt, aber mit der Anzahl der Antennen sinkt. Weiterhin wurde auch der K-Nutzer Single-Input, Single-Output (SISO) IC mit imperfekter Hardware betrachtet. Indem zwei iterative Algorithmen unterschiedlicher Rechenkomplexität entwickelt wurden, konnten die entsprechenden Ratenregionen hergeleitet werden.

Darüber hinaus wurde in dieser Arbeit die Robustheit von IGS gegenüber imperfekten Kanalzustandsinformationen (channel state information (CSI)) auf Seiten des Empfängers in einem 2-Nutzer- und Z SISO-IC untersucht. Basierend auf einem Worst-Case-Robustheit Ansatz haben wir die Überlegenheit des IGS, durch Untersuchung der Grenze der Ratenregion des IC für den schlechtesten Kanal, gezeigt. Zusätzlich wurde die Performanz von IGS gegenüber einem 2-Nutzer Rayleigh SISO IC untersucht. Dafür wurde angenommen, dass die Empfänger perfekte CSI haben, während die Sender nur Zugang zu statistischen CSI haben. Die ergodische Ratenregion für die 2-Nutzer Fading IC wurde hergeleitet und es konnte gezeigt werden, dass im moderat bis starken Interferenzbereich, IGS dem Proper-Gaussian-Signaling-Schema überlegen ist.

Zusätzlich zur Analyse der Datenrate, wurde die EE von IGS betrachtet und es konnte ein energieeffizientes IGS Design für K-Nutzer-SISO-IC und Underlay Cognitive Radio (UCR) bestimmt werden. Dabei hat sich herausgestellt, dass IGS aus EE Sicht vorteilhaft ist. Für UCR wurden außerdem notwendige und hinreichende Bedingungen für die Optimalität von IGS hergeleitet.

Zusammenfassend wurden in dieser Arbeit verschiedene spektrale oder energieeffiziente IGS-Schemata vorgeschlagen. Es wurde gezeigt, dass IGS beide Aspekte verschiedener interferenzbegrenzter Systeme mit realistischen Annahmen bezüglich Kanalwissen und Hardware, verbessert. Außerdem wurde demonstriert, dass die Vorteile von IGS mit der Anzahl der Nutzer steigt, aber mit der Anzahl der (räumlichen oder Frequenz-) Ressourcen sinkt. Darüber hinaus wurde gezeigt, dass die EE-Vorteile des IGS geringer sind als seine Ratenvorteile.

Declaration

I hereby declare that I have completed the work on this PhD dissertation with my own efforts and no part of this work or documentation has been copied from any other source. It is also assured that this work is not submitted to any other institution for award of any degree or certificate.

Paderborn, August 14, 2020

Mohammad Soleymani

Dedication

To my parents, my wife, and my sister

Acknowledgements

First and foremost, I would like to express my highest gratitude to my supervisor, Prof. Dr. Peter J. Schreier, for his continuous support, his friendliness, patience, motivation, and effort during my PhD studies. I appreciate the opportunity that I had, under his supervision, to pursue my research directions, which has made my PhD study a joyful and unforgettable journey. I am also deeply grateful to Prof. Dr. Ignacio Santamaria for being a great collaborator in the last three years. It could not be possible to accomplish my PhD study without their priceless advice and their effort, which substantially helped me to grow as a research scientist. I also appreciate the time and effort of my other collaborators, Dr. Christian Lameiro and Dr. Behrouz Maham, which improved the quality of our works. Furthermore, I sincerely thank my colleagues at the Signal and System Theory (SST) group for the fruitful discussion and the friendly and inspiring atmosphere, which created an ideal research environment.

Last but not the least, I am very thankful to my parents, my wife, and my sister for their unconditional love and believing in me. Their love and support gave me the power to follow my dreams.

Contents

List of Figures

List of Abbreviations

AF	Amplify and Forward
BC	Broadcast Channel
CR	Cognitive Radio
CSI	Channel State Information
CSIR	Channel State Information at Receiver
CSIT	Channel State Information at Transmitter
DCP	Difference of Convex Programming
DF	Decode and Forward
DoF	Degree of Freedom
EE	Energy Efficiency
FP	Fractional Programming
GDA	Generalized Dinkelbach Algorithm
GDoF	Generalized Degree of Freedom
HWI	Hardware Impairment
IA	Interference Alignment
IC	Interference Channel
ICR	Interweave Cognitive Radio
IGS	Improper Gaussian Signaling
i.i.d	Independent and Identically Distributed
MIMO	Multiple Input Multiple Output
MISO	Multiple Input Single Output
MM	Majorization Minimization
mmW	Millimeter Wave
NOMA	Non-orthogonal Multiple Access
OCR	Overlay Cognitive Radio
OFDM	Orthogonal Frequency Division Multiplexing
PGS	Proper Gaussian Signaling
PSINR	Pseudo Signal to Interference plus Noise Ratio
PU	Primary User
QoS	Quality of Service
RSI	Residual Self Interference
SCP	Sequential Convex Programming
SDP	Semidefinite Programming
SI	Self Interference
SIC	Successive Interference Cancellation
SIMO	Single Input Multiple Output

SISO	Single Input Single Output
SINR	Signal to Interference plus Noise Ratio
SNR	Signal to Noise Ratio
SU	Secondary User
TIN	Treating Interference as Noise
TS	Time Sharing
UCR	Underlay Cognitive Radio
WMEE	Weighted Minimum Energy Efficiency

List of Notations

x	Scalar
$\mathbf{x}$	Vector
$\mathbf{X}$	Matrix
$\Re\{x\}$	Real part of x
$\Im\{x\}$	Imaginary part of x
$\underline{x}$	Real decomposition of x
$\det(\mathbf{X})$	Determinant of $\mathbf{X}$
$\text{Tr}(\mathbf{X})$	Trace of $\mathbf{X}$
$\text{diag}(\mathbf{X})$	Diagonal of $\mathbf{X}$
$\mathbb{E}\{x\}$	Mathematical expectation of x
$\mathbf{x}^T/\mathbf{X}^T$	Transpose of vector $\mathbf{x}$/matrix $\mathbf{X}$
$\mathbf{x}^H/\mathbf{X}^H$	Transpose and complex conjugate (Hermitian) of vector $\mathbf{x}$/matrix $\mathbf{X}$
$\mathbf{I}_N$	$N \times N$ identity matrix

1 Motivation, Background, and Contributions

1.1 Motivation

The increasing number of devices with wireless connectivity, on the one hand, and the limited availability of radio resources, on the other hand, motivate the design of techniques to exploit the spectrum more efficiently. Additionally, energy expenses and global warming make energy-efficient techniques more and more important in modern wireless communication systems. Hence, it is expected that energy-efficient and spectral-efficient designs, which are the main concern of this thesis, will continue to play essential roles in wireless communication systems [15].

One of the main targets for 5G is to reach a data rate more than 1000 times of the data rate of current cellular systems [5]. Reaching the goal is not possible without increasing the spectral efficiency and overcoming many challenges such as interference, hardware non-idealities, implementation costs and so on. A consequence of increasing the spectral efficiency is to tolerate more interference from other users as modern wireless communications systems are mostly *interference-limited*. Handling interference is always among the primary issues in modern wireless communication systems, and interference management techniques play a key role in the current and next generations of wireless communications [5].

Global warming has been among the urgent environmental issues in the last decades. It is estimated that information and communication technology systems are responsible for 5% of the global CO_2 emission, and it is predicted that this percentage will increase [15, 33, 128]. Maximizing energy efficiency (EE) is also beneficial from economical point of view. Energy is usually very expensive, and in order to make the implementation costs affordable, we should use energy resources as efficient as possible. Thus, energy-efficient designs are essential for upcoming wireless communication systems.

In order to quantify the EE, a metric has to be defined. In general, the more data transmitted by a scheme per energy unit, the more energy efficient the scheme is. Following this concept, the EE of a user is defined as the ratio of its achievable rate to its total power consumption [15, 126]. There are different approach to extend this metric to determine the EE of a system, consisting of several users. An approach can be, for instance, to consider the global EE for a system, which is defined as the ratio of the achievable rate of the system to the total power consumption of the system [126]. Note that such metrics is not the only way to propose energy-aware schemes. It is also possible to design energy-aware schemes by minimizing the power consumption for a fixed performance level. This performance metric can be, in general, the achievable rate, outage probability and/or system throughput [15]. By this approach, the minimum required performance level for a system is firstly determined. Then, the parameters are set in such a way that the power to meet this requirement is minimized. These two main approaches for proposing energy-aware schemes might seem similar, but they lead to different

resource allocations. Obviously, to account for EE metrics in the system design can result in more energy-efficient schemes [15].

To improve the spectral and/or energy efficiency entails many challenge. One of the main challenges in spectral and energy efficiency is hardware non-idealities. Devices are never completely ideal in practice, which can significantly degrade the system performance especially when the hardware non-idealities are not considered in the system design. The impact of hardware imperfections has become even more vital in modern wireless communication systems. In particular, in millimeter wave (mmW) and wideband communications, which are the main trends for 5G and beyond, the communication systems may severely suffer from hardware imperfections [45]. Additionally, in modern wireless communications, we sometimes have to employ low-cost devices in order to make the implementation expenses affordable. Obviously, low-cost devices can be imperfect. In general, hardware impairment (HWI) may happen due to imperfections in hardwares such as quantization noise, phase noise, amplifier nonlinearities, and I/Q imbalance [8–11, 22, 34, 59, 64, 83, 93, 111, 112, 120, 123, 131–135].

Another critical challenge in the design of wireless communication systems is to acquire perfect channel state information (CSI), which may require lots of signaling overhead depending on the scenario. In practical scenarios, the CSI is always imperfect, and the system performance would be highly affected if this imperfectness is not considered in the design. In general, it can be reasonable to assume that a receiver knows the CSI perfectly since acquiring CSI at the receiver side is relatively easy with training sequences or applying blind/semi-blind estimation methods [89, 97, 115]. The channel information is typically quantized and then sent to the transmitters through a noisy feedback link, which results in noisy CSI at transmitter side (CSIT). Even this noisy CSIT can be useful and improve the system performance. However, neglecting these CSI imperfections in the system design can result in a huge performance degradation, which motivates us to study robust designs against imperfect CSI. A way to propose robust designs is to follow the concept of the worst-case robustness in which we consider the worst-case channels and derive the parameters such that the worst-case performance is improved. In other words, we design the system for the worst-case scenario and ensure that the performance cannot be worse than it.

In addition to robust design, it is also common to consider only the statistics of the CSI at the transmitter side and design the system based on the probability distribution of the channel [3,4,36,37]. In this case, a goal can be to maximize the long-term achievable rate, which is also called the ergodic rate and is defined as the mathematical expectation of the instantaneous rate. Another possible performance metric for this case can be the outage probability for a given target rate. In general, by this approach, the need for instantaneous CSIT is relaxed, which reduces signaling overheads. For instance, if the channels vary fast, the available CSIT might be outdated, and the signaling overhead for the CSI has to be increased in order to send the latest update of the channels. It might not be possible to allocate lots of signaling overhead for CSI in every implementations, which can enforce us to consider only statistical CSI in the system design.

In this thesis, we propose some spectral and energy-efficient schemes with practical assumptions regarding hardware and channel knowledge. We focus on interference-limited systems and try to manage interference by improper Gaussian signaling, which is briefly described in Section 1.2. To this end, we need some optimization tools such as convex optimization, majorization minimization, fractional programming and so on. Thus, in this work, we first provide the basic analytical tools and then, propose our schemes for different scenarios.

1.2 Role of improper signaling in communications

A zero-mean complex Gaussian signal is called improper if its real and imaginary parts are correlated and/or have unequal powers [2, 94]. In a zero-mean proper Gaussian signals, the real and imaginary parts are independent and identically distributed (iid). The concept of proper and improper signals can be extended to non-Gaussian and/or discrete signals. We will describe improper signals with more details in Chapter 2.

Improper signals and improper signaling have existed so long in communication systems. For instance, some of discrete constellations are improper such as binary phase shift keying (BPSK), pulse amplitude modulation (PAM) and 8-quadratic amplitude modulation (QAM). These discrete constellations actually fall into improper signaling. Additionally, in some scenarios, the signal and/or the noise might be improper signals. For example, when there exists an imbalance between the in-phase and quadrature (I/Q) signal paths, the signal becomes improper. I/Q imbalance yields to capacity loss, which degrades the system performance, and has to be compensated either at the transmitter and/or receiver. Indeed, when the noise is proper at the receiver side of a point-to-point communication, improper signal is rather undesired than being useful. However, when signal at the receiver side is proper, making the noise improper can improve the system performance. It has been an inspiration to employ improper signaling to improve the performance of interference-limited systems. The main idea of this application is that if we make the signal of a user improper, it has less undesired interference effects on other users with the cost of losing some capacity for the user. Improper signaling can be beneficial only if the former pays off, and the gain we can get by reducing the undesired interference effects becomes more than the capacity we lose by making the signals improper. In the last decade, this idea has been applied to different scenarios, and it has been shown that improper Gaussian signaling (IGS) can improve the performance of various interference-limited systems [4, 17, 36, 54, 59, 67–71, 86, 121, 129]. We will discuss this application with more details in the next subsection.

1.2.1 IGS as an interference-management technique

It is known that proper Gaussian signaling (PGS) achieves the capacity of traditional wireless communication channels such as point-to-point communications [24]. However, it is very complicated to find the capacity achieving signaling for every interference-limited systems. An important example of interference-limited systems is the interference channel (IC), which is a fundamental communication scenario where multiple users share the same frequency and time resources for the transmission of the desired messages. Interference channels have been vastly studied over the last decades [32, 38, 42, 84], but their capacity is still unknown in the general case [32, 42, 84]. In some particular cases such as the very strong and very weak interference regimes, the capacity-achieving schemes are known [42]. For example, in the very strong interference regime, the capacity of the 2-user IC is achieved by successive interference cancellation (SIC), in which the interfering signals are firstly decoded and then canceled from the received signal [42]. In other words, in the strong interference regime, the interference has to be decoded in order to achieve capacity. Obviously, SIC is not a linear operation and has a high computational cost, specially in a multiuser setting. On the other hand, when the interference level is very low, which is also referred to as the very weak interference regime, treating interference as noise (TIN) is the capacity achieving strategy [42, 84]. TIN is a simple and practical decoding

strategy, which turns out to be optimal from generalized degree of freedom (GDoF) point of view in low interference regimes [38].

In summary and at a coarse level, if the interference is strong, the optimal interference management approach is to decode it along with the desired signal, whereas if the interference is weak, then the interference management approach is to treat interference as noise. If the strength of the interference is comparable to the strength of the desired signal, the degrees-of-freedom (DoF) optimal interference management approach is to apply interference alignment (IA) [16, 57, 79]. IA designs transmit precoders that reduce the dimension of the interference subspace, in such a way that the interference can be zero-forced at each receiver thus getting an interference-free subspace for the transmission of the desired signals. IA techniques actually optimize DoF, which operates in the asymptotic regime, i.e., when the signal-to-noise ratio (SNR) is very high. Furthermore, the feasibility of IA for channels with constant coefficients depends on the number of antennas and hence packing the interference into a low-dimensional subspace is not always possible. Hence, in some practical scenarios, we have to tolerate and manage interference to improve the system performance. As a result, in modern wireless communication systems non-orthogonal multiple access (NOMA) schemes play an essential role [28, 29].

Another approach to handle interference is to employ IGS. The main idea of employing IGS is to manage interference by making the interference improper, but there is actually a trade off in the employment of improper signals. On the one hand, the ability to reject interference increases if the interference has more structure. On the other hand, we lose some achievable rates since the entropy of a signal decreases when the signal is structured. Hence, we should design parameters such that, in the end, the overall performance is improved. An example of this idea can be found in [70], where the authors considered an underlay cognitive radio (UCR) system. They maximized the rate of the secondary user (SU) by employing IGS while satisfying the rate requirement of the primary user (PU). In the paper, it was shown that the rate of the SU decreases with the degree of impropriety; however, the SU can transmit with more power without violating the rate requirement of the PU. They showed that the power increment can compensate the rate loss and derived a necessary and sufficient condition on the ratio between the gain of the interference and direct channel coefficients for IGS to outperform PGS.

Employing IGS has also another advantage, which is to provide more optimization parameters. In a zero-mean proper Gaussian signal, the real and imaginary parts are i.i.d. However, in improper Gaussian signals, this constraint is relaxed, and the real and imaginary parts can be correlated and/or have unequal powers. In other words, the powers of the real and imaginary parts can be considered as two different optimization variables. This feature has been used for the first time in [17], where the authors showed that by considering different powers for real and imaginary parts, we can increase the DoF of the 3-user single-input single-output (SISO) IC. Later, this idea has been employed in other scenarios when interference is treated as noise. For instance in [130], the authors first derived the achievable rate by PGS for the K-user multiple-input, single-output (MISO) IC and then optimize over complementary variances to improve over the PGS rate. By this approach, it is ensured that the proposed IGS scheme does not perform worse than the existing PGS scheme. Note that PGS schemes can never outperform the optimal IGS scheme since IGS includes PGS as a special case.

IGS has been applied to many interference-limited systems, and it is shown that IGS can improve the performance of different interference-limited systems from two main performance metrics. First, IGS with interference alignment can increase the DoF of different ICs [17, 73, 99, 121]. Second, IGS can provide some gain from achievable rate and/or power/energy-efficiency

perspectives when interference is treated as noise [4, 36, 54, 67–71, 85, 86, 113, 129]. In the following, we describe these benefits with more details.

The paper in [17] showed that IGS can increase the DoF of the 3-user SISO IC with constant channel coefficients. In [73], this result was extended to the 4-user SISO IC and, in [121], the authors showed that IGS can also increase the DoF of the 2-user multiple-input, multiple-output (MIMO) X interference channel[1]. The paper in [99] proposed an IA strategy with IGS for 3-cell SISO interference broadcast channels and showed the benefits of employing IGS as an IA technique. In these papers, it is shown that IGS with IA can improve the DoF of different interference-limited systems. However, as indicated, IGS can also be beneficial from rate and/or power/energy-efficiency point of view when interference is treated as noise as described below.

The benefits of IGS with TIN was considered in different interference-limited systems such as different ICs, relay channels and broadcast channels. For instance, the paper in [54] showed that IGS can improve the performance of the SISO 2-user interference channel, while in [129] IGS was used to optimize the rate of the K-user MIMO interference channel. Moreover, the authors in [129] derived the rate region of the 2-user SISO IC with TIN by solving a semidefinite programming (SDP) problem, showing that IGS can enlarge the rate region and improve the performance of the system. The paper in [86] showed that IGS can reduce the symbol error rate of the K-user IC. The superiority of IGS over PGS schemes for the Z-IC[2] was also established in several works [67, 69, 71]. Additionally, the authors in [36] showed that IGS can improve the performance of full-duplex relaying systems with fading channels. Similarly, the authors in [4] considered an overlay CR system, in which the SU can employ IGS, and showed the rate benefits by IGS for the SU. They showed that the outage probability of the SU for a fixed achievable rate decreases by employing IGS. In [85], the authors showed that IGS can increase the minimum achievable rate of the users in the MIMO broadcast channel. The paper [113] investigated the performance improvements by IGS in non-orthogonal multiple access systems.

To summarize, IGS may improve the system performance in interference-limited systems and/or in the presence of improper noise, and PGS is definitely optimal in interference-free systems with proper noise. Up to now, it has been shown that IGS can improve the performance of several interference-limited systems, such as IC [17, 54, 67, 69, 71, 73, 86, 121, 129], underlay and overlay cognitive radio (CR) systems [3, 4, 70], relay channels [37, 53, 59], and broadcast channels (BC) with (widely) linear transceivers [46, 48], to mention a few.

1.3 Related Work

In this section, we provide a brief review on the related works in the literature, which consider more realistic assumptions regarding hardware and channel knowledge. We focus more on the papers related to IGS since it is the main concern of this thesis. We first present some papers on hardware imperfections and then, consider some related works with realistic channel assumptions. Finally, we present a brief review on EE.

[1] The 2-user X-IC is a generalization of the 2-user IC where there is an independent message from each transmitter to each receiver [55].

[2] Z-IC is a special case of the 2-user IC, in which only one of the users interferes with the other user.

1.3.1 Hardware imperfections

Hardware imperfections are among the main issues in modern wireless communications. Depending on the application, we sometimes have to employ low-cost devices/antennas to make the implementation expenses affordable [8, 135]. Hence, we have to tolerate some hardware imperfections in practice and deal with these imperfections in the design level. The impact of hardware imperfections has been studied in various scenarios in [8–11, 22, 34, 59, 64, 83, 111, 112, 120, 123, 131–135]. For instance, [9, 59, 64, 111] considered different interference-limited scenarios with single-antenna transceivers subject to additive hardware distortions (AHWD). When there is AHWD, the distortion power is a linear function of the signal power at the corresponding antenna [9, 59, 64, 111]. In [9], the authors investigated the effect of AHWD on the performance of a dual-hop relay with both amplify-and-forward and decode-and-forward protocols and derived closed-form expressions for outage probabilities, as well as an upper bound for the ergodic capacity. The outage probability for a device-to-device mmW communication system with complex proper AHWD was derived in [111]. However, AHWD may be, in general, improper due to I/Q imbalance [12, 59–64]. The authors in [59] considered a relay channel with improper AHWD and maximized the achievable rate of the system by optimizing over complementary variances. In [64], the authors considered a full-duplex multihop relay channel with improper AHWD.

Hardware imperfections are even more critical in multiple antenna systems especially in massive MIMO communications. Due to a huge number of antennas in massive MIMO systems, employing low-complexity devices has received lots of attentions in order to keep the implementation costs affordable [8, 135]. Obviously, low-complexity devices may generate significant HWI, which makes HWI-aware schemes important in upcoming multiple antenna systems.

The performance of various multiple antenna systems with hardware nonidealities has been investigated in many papers (see, e.g., [8, 10, 11, 22, 34, 120, 123, 131–135]). For instance, the papers in [11, 134, 135] studied secure communications for massive MIMO systems with AHWD in different scenarios. The paper in [8] investigated the impact of AHWD on the performance of a cellular communication in which the base station employs a massive number of antennas. The papers in [120, 131, 133] studied the performance of massive MIMO systems with AHWD in fading channels in different scenarios. In [34], the authors investigated the system performance of a two-way massive MIMO relay channel with AHWD. In [22], the authors considered beamforming designs for a dual-hop MIMO amplify-and-forward relay channel in the presence of AHWD and analyzed the outage probabilities for the system. In [10], the authors studied the capacity limit and multiplexing gain of MIMO point-to-point systems with AHWD at both transmitter and receiver sides.

In addition to AHWD, there might be other sources of hardware imperfections and impairments like I/Q imbalance[3]. When I/Q imbalance occurs, the received signal can be modeled through a widely linear transformation of the transmitted signal and the aggregated noise. A widely linear transformation is a linear combination of the signal and its conjugate. Hence, the received signal can be improper even if the transmitted signal and aggregated noise are proper [63]. It has been shown that IGS can improve the system performance in the presence of improper additive noise [12, 59–64, 101]. For example, it is shown in [60] that IGS is the optimal

[3] In this dissertation, AHWD noise refers to the model in [8–11, 101, 120, 131, 135] in which the power of the AHWD noise is a linear function of the power of the received signal. On the other hand, I/Q imbalance refers to the model in [12, 63], where the received signal is a function of the widely linear transform of the transmitted signal and noise, and the variance of the noise is fixed and independent of signal powers.

signaling for a point-to-point single-input, multiple-output (SIMO) system with asymmetric or improper AHWD.

1.3.2 Channel state information

Acquiring perfect and instantaneous CSI at both receiver and transmitter sides is very challenging in practice. It becomes even more complicate to acquire global and perfect CSI at every transmitter in multiuser systems, where assuming global and perfect CSI at every transmitter is very restrictive. Therefore, a great deal of work has aimed at relaxing this assumption and exploiting either imperfect or statistical CSIT. For instance, the paper in [3] considers an UCR network in which the SU has only statistical CSIT and optimizes its transmit power and degree of impropriety to maintain a given PU outage probability. A more challenging UCR scenario where the PU is assumed to work using full-duplex mode is considered in [36] for Rayleigh fading channels. In [4], the authors considered both global CSI and partial CSI scenarios in an overlay CR system. Specifically, with partial CSIT the primary user has access only to the average CSI. In this setting, the authors showed that IGS reduces the outage probability of the PU link. Nevertheless, references [3,4,36] only consider block fading models and the probability of outage as the figure of merit to optimize. In [37], the authors studied a full-duplex relay system over Nakagami-m fading channels. They derived the outage probability for a given target rate as well as the ergodic rate of the system and showed the benefits of IGS.

In these papers, it was assumed that the existing CSI, either instantaneous or statistical, is perfect. However, in practical scenarios, the CSI is always imperfect. Furthermore, acquiring the CSI at the transmitter side is more difficult than at the receiver side. Thus, it is critical to investigate whether IGS is still beneficial when the available CSI is imperfect. To design the PGS scheme, only the channel gains are required. However, IGS typically requires the phases of the channels in addition to the gains in order to design the optimal complementary variances. Since IGS needs more detailed CSI than PGS, it might be reasonable to expect that IGS is more affected by imperfect CSI and its benefit will decrease when the CSI quality decreases as well.

On the other hand, the use of IGS in combination with IA obtains DoF improvements in certain scenarios such as 3-user IC [17] or 2-user MIMO X-IC [121]. In other scenarios, such as the 2-user IC with partial or full transmitter cooperation, the use of IGS does not offer DoF advantages, although IA still offers improvements in terms of generalized degrees of freedom (GDoFs), which are a refinement of the DoF metric. However, these asymptotic (in the high SNR regime) DoF or GDoF benefits are typically lost under finite precision CSIT, a phenomenon known as DoF collapse. For instance, under limited CSIT, the DoF collapse for the 2-user MISO BC even when perfect channel knowledge for one user is available [26, 110]. It is also shown in [27] that, under finite precision CSIT, the sum GDoF of the 2-user X channel and 2-user BC collapse and hence, the benefits of IA are entirely lost under finite precision CSIT.

In this work, we do not study possible DoF or GDoF benefits of IGS, but rather the advantages that IGS can provide in terms of rate and/or EE with TIN. The optimal IGS parameters typically depend on the gains and phases of the channels, so the following question arises: *Is IGS still beneficial in the presence of imperfect CSI?* We will address this question for the 2-user SISO IC and Z-IC in this work.

1.3.3 Energy efficiency

Energy is very precious from both economical and environmental perspectives and has to be employed very efficiently. As indicated, the EE of a user is defined as the ratio of its achievable rate to its total power consumption [15, 126]. For a system, there can be different utility functions for the EE metric [15]. For instance, an extension of the definition of EE to include a system is the global EE, which is defined as the ratio of the total achievable rate (sum rates of the users) to the total power consumption of the system (the summation of the total power consumption of each user). This metric is the system-wide EE measure and does not consider the EE of each individual user [15]. There is also another approach to measure the EE for a system by considering the EE of each individual users. In general, we can propose more fair schemes if we consider the individual EE of each user in the objective and/or constraint functions. According to [15], the three most frequently used objective functions for EE in the literature are: weighted sum EE, weighted product, and weighted minimum EE. Throughout this dissertation, we mostly consider the EE region, which can be obtained by solving the weighted minimum EE [126]. The reason is that EE region shows all possible operational points for specific channels. Additionally, we can enhance the fairness EE by maximizing the minimum EE of a system. It is often that the EE problems are solved by considering a constraint on the quality of service (QoS) for users to ensure meeting the minimum requirements of the system [15, 126]. This QoS constraint can be on, for example, minimum achievable rate [127], maximum tolerable delay [96], interference temperature [116, 117] and so on.

There are many works that study the energy-efficiency of PGS in various networks (please refer to [15, 126] and the references therein), but the question of how these results translate to the IGS schemes remains unanswered. In this dissertation, we provide an answer and show that IGS can be beneficial in different interference-limited systems in terms of EE.

1.4 Contribution

In this work, we study the performance of IGS as an interference-management technique in various single-antenna and multiple-antenna interference-limited systems with realistic assumptions. We first present some HWI models such as I/Q imbalance and AHWD for SISO and MIMO systems. We then consider some interference-limited systems with TIN. Throughout this work, we consider two main performance metrics: achievable rate and EE. Note that achievable rate is a metric for spectral efficiency. We show that IGS can outperform PGS from both achievable rate and energy-efficiency perspectives in various interference-limited systems such as the K-user SISO and MIMO ICs, 2-user SISO IC, SISO Z-IC, and underlay cognitive radio under realistic assumptions regarding CSIT and hardwares. In the following, we present our main contributions for multiple-antenna and single-antenna systems in separate subsections.

1.4.1 Multiple-antenna systems

The performance of IGS in the 2-user and/or K-user SISO ICs has been vastly studied, e.g., in [17, 54, 86, 129]. However, it still requires further investigations how IGS performs in the K-user MIMO IC. In SISO systems, it is shown that the benefits of IGS become negligible when the number of resources, e.g., time or frequency channel uses, increases. For instance, in [52], the authors proved that PGS is optimal in the 2-user IC if coded time-sharing is allowed

in which the average power consumption is constrained instead of the *instantaneous power*. Hence, it seems that increasing the number of temporal or frequency dimensions provides a more flexible power allocation for PGS, which might lead to minor improvements by IGS. In MIMO systems, the number of resources increases by allowing more antennas at transceivers. Thus, the following questions arise: *how does IGS perform in the K-user MIMO ICs? Is IGS still beneficial when the number of spatial dimensions (antennas) increases?* In this thesis, we answer these questions and analyze the performance of IGS by considering different rate and energy-efficiency metrics and solving various optimization problems.

We consider two main performance metrics: the achievable rate and the EE. We show that IGS can be beneficial in MIMO systems in terms of achievable rate and EE. Interestingly, IGS provides more relative gain in terms of achievable rate than in terms of energy efficiency. Moreover, although there are some benefits for IGS in terms of global EE for the K-user MIMO IC, as we will show, these benefits may not be significant. In other words, our numerical results suggest that IGS does not provide a significant gain in terms of global EE for the K-user MIMO IC.

In order to analyze the performance of IGS, we consider different optimization problems such as achievable rate region, maximum sum-rate, energy efficiency region and global energy efficiency. To solve these non-convex problems, we first formulate a general optimization problem that encompasses all performance metrics under study and then, employ a majorization-minimization framework to obtain solutions for each problem. The main idea of this framework is based on the structure of the achievable rate or energy-efficiency functions in interference-limited systems when interference is treated as noise. Specifically, the achievable rate with TIN is a difference of two concave/convex functions. We exploit this feature and employ a majorization-minimization (MM) approach to derive a stationary point[4] of every optimization problem in interference-limited systems with TIN in which the objective function and/or the constraints are linear functions of the rates. Note that MM is an iterative algorithm and consists of two steps in every iteration: i) majorization, and ii) minimization [108]. In the majorization step, the objective function is approximated by a surrogate function. Then, the approximated problem is solved in the minimization step. In other words, MM solves a non-convex optimization problem by solving a sequence of surrogate optimization problems, which can be solved easier than the original problem [108].

We provide some numerical examples for the framework in the K-user MIMO IC with HWI including I/Q imbalance and with AHWD. In the presence of HWI, the received signal is a function of the widely linear transform of the transmitted signal and the aggregated noise. Note that the widely linear transform of a signal is the linear combination of the signal and its conjugate. Thus, the aggregated noise can be improper, which motivates us to consider IGS. We also investigate the performance of IGS as an interference-management technique in the K-user MIMO IC with HWI. We observe that the benefits of IGS decreases with the number of antennas either at the transmitter or receiver sides for a fixed number of users. This is due to the fact that interference can be managed easier by PGS when there are more resources, and consequently, IGS provides less gain as an interference-management technique. We also observe that, for a fixed number of antennas, the benefits of IGS is increasing in K. The reason is that the interference level increases with K, and the more interference, the better performance for IGS. Additionally, our results show that the benefits of IGS increases with the HWI level. The more improper, the

[4] In a constrained optimization problem, a stationary point of satisfies the corresponding Karush-Kuhn-Tucker (KKT) conditions [75].

noise is, the more benefits can be achieved by IGS.

We also consider the achievable rate region of a K-user MIMO IC with AHWD at the transmitters and provide some numerical solutions for this scenario. We assume that the transmitters are imperfect and produce AHWD with Gaussian distribution [8–11, 120, 131, 135]. Our proposed scheme outperforms the scheme, which disregards AHWD. Moreover, the benefits of employing our scheme increase with K and the level of AHWD. Our results show that AHWD may significantly degrade the performance of the K-user MIMO IC, especially at high SNR regimes.

The main contributions of this work for MIMO interference-limited systems can be summarized as follows:

- We propose HWI-aware IGS schemes for the K-user MIMO IC. We study two general performance metrics, i.e., the achievable rate and EE and solve four different optimization problems. We derive a stationary point of the rate region, sum-rate maximization, EE region and global EE maximization problems.

- To solve these optimization problems, we cast them as a typical optimization problem in which the objective function and/or the constraints are linear functions of the achievable rates. We then apply a unified framework to obtain a stationary point of these optimization problems by majorization-minimization algorithms.

- Our results show that IGS can improve the performance of the K-user MIMO IC with HWI in terms of achievable rate and EE. We show that IGS provides more benefits in terms of achievable rate than in terms of energy efficiency.

- Our numerical simulations suggest that the benefit of IGS schemes increases with K and with the level of impairment for a fixed number of antennas. However, IGS provides minor gains with respect to PGS when the number of antennas grows for a fixed number of users.

1.4.2 Single-antenna systems

In addition to MIMO systems, we study the performance of IGS in various single-antenna systems. The number of optimization parameters is less in single-antenna systems than in multiple-antenna systems, which can allow us to propose simplified algorithms for SISO systems. In this work, we consider different SISO systems from both achievable rate and EE perspectives with realistic assumptions. As indicated, the EE of IGS schemes has not been well studied in different scenarios, and this question has to be answered: *How energy-efficient can IGS schemes be?* We provide an answer by proposing energy-efficient IGS schemes for the UCR and K-user IC.

It is also critical to investigate the performance of IGS with realistic assumptions regarding CSIT and devices. In some scenarios, transmitters have access only to statistical CSIT. Moreover, when it is possible to provide instantaneous CSIT, the instantaneous CSIT can be imperfect, which might affect the performance of IGS more than PGS. The reason is that, to design the PGS scheme, only the channel gains are required. However, IGS typically requires the phases of the channels in addition to the gains in order to design the optimal complementary variances. Hence, the following question arises: *Does IGS outperform PGS in the presence of imperfect and/or statistical CSIT?* We will also address this question in this work. As indicated,

devices are not always perfect in practice, and we have to consider such imperfections in the design. Thus, we also propose AHWD-aware IGS schemes for the K-user IC.

We, moreover, study an orthogonal frequency division multiplexing (OFDM) UCR system in this thesis. IGS outperforms PGS in many scenarios in single-carrier interference-limited systems. It can be interesting to investigate whether a similar behavior happens when we increase the number of frequency resources by employing OFDM. As we will show, the benefits of IGS disappears when the number of subbands grows. In the following, we will describe our main contributions with more details.

OFDM underlay cognitive radio

In Chapter 5, we consider an OFDM UCR system with improper signaling. Because improper signaling has been so successful at increasing the achievable rates in many interference-limited scenarios, one might expect the same in an OFDM UCR system. However, the parallel channels in OFDM allow the SU to allocate its power more flexibly compared to the single carrier case. Moreover, in relatively low load traffic, when the constraint is on the total rate of the PU, the PU can neglect some subcarriers without violating the rate constraint. This allows the SU to transmit proper signals with maximum power on those subbands. This is why our results show that the benefit of improper signaling is fairly small and decreases further with increasing number of subbands. Our study therefore reveals that the use of improper signaling in interference channels needs to be justified for each individual case.

K-user SISO IC with asymmetric AHWD

In Chapter 6, we consider the K-user SISO IC with asymmetric AHWD and derive the achievable rate region of the system. We assume that the transceivers of both users produce asymmetric AHWD noise, and model the hardware distortion as an additive improper Gaussian noise, similar to [59–61, 64]. We devise two iterative algorithms to derive suboptimal solutions for the achievable rate region. To this end, we rewrite the rate region as a pseudo-signal-to-interference-plus-noise-ratio (PSINR) region and employ sequential optimization approaches to solve the resulting problems.

In our first proposed algorithm, we employ MM as well as fractional programming (FP) and the well-known generalized Dinkelbach algorithm (GDA). In our algorithm, to solve each surrogate problem, we apply the GDA, which is a powerful tool to solve multiple ratio maximin problems [25, 126]. In Dinkelbach-based algorithms, an iterative optimization is performed, in which the fractional functions are replaced by surrogate functions at each iteration. The GDA permits solving fractional programming efficiently and results in the global optimal solution of the original optimization problem if the optimization problem at each iteration is perfectly solved, i.e., its global optimum is obtained [25, 30, 98, 126].

In our second proposed algorithm, we employ a separate optimization of powers and complementary variances. We first optimize the powers transmitted by the users by employing the well-known bisection method, which transforms the original problem into a sequence of feasibility problems, and derive a closed-form solution for the feasibility problem in the 2-user IC. In order to obtain the complementary variances, we employ difference of convex programming (DCP), which is a special case of sequential convex programming (SCP) and falls into MM [75, 108]. In DCP, the objective function and/or constraints are difference of two con-

vex/concave functions. DCP solves a non-convex problem by solving a sequence of convex optimization problems and converges to a stationary point.

The main contributions of this work for the K-user SISO IC with asymmetric AHWD are as in the following:

- We first propose an iterative algorithm based on a sequential optimization method, in which we solve a sequence of fractional optimization problems [6, 108]. We derive the global optimal solution of each surrogate problem by FP and the generalized Dinkelbach algorithm. Our first proposed algorithm obtains a stationary point of the PSINR region.

- We also propose a simplified algorithm that is computationally less expensive than our proposed algorithm with FP. This simplified algorithm is based on a separate optimization of powers and complementary variances of users. We employ a bisection method to obtain the powers and derive a closed-form solution for powers in each iteration. Then, we employ DCP to find the complementary variances.

- Our results show that IGS improves the achievable rate of the K-user IC in the presence of asymmetric AHWD, and that there is a significant performance improvement by IGS for highly asymmetric AHWD noise. Moreover, both of our proposed algorithms outperform existing PGS and other existing IGS algorithms.

Energy-efficient IGS schemes

IGS is usually claimed to be energy-efficient either by showing that it increases the achievable rates for given transmit power or by showing that it reduces the transmit power to achieve target data rates. However, there is a trade-off between data rate and transmit power in IGS schemes, which cannot be fully characterized when one of them is kept fixed. In order to shed light onto this trade-off, we consider the EE metric and propose energy-efficient IGS schemes for the K-user SISO IC and UCR in Chapter 7.

For the K-user SISO IC, we derive the EE region of IGS by casting the corresponding optimization problem as maximizing the weighted minimum EE (WMEE) [126]. To solve this optimization problem, we employ a sequential optimization method, in which we first maximize the WMEE over the powers considering PGS, i.e., when the complementary variances are zero. We then maximize the WMEE over the complementary variances for the given powers. This suboptimal approach guarantees that the proposed IGS scheme is not worse than the PGS scheme. Our results show that IGS can substantially enlarge the EE region of the K-user IC.

In the UCR, we derive a necessary and sufficient condition in closed form for IGS to be more energy efficient than PGS. We leverage this result to numerically obtain the optimal transmission parameters by the well-known bisection method. Our results show that IGS can improve the EE of the SU in UCR when interference is treated as noise.

Robust IGS for 2-user IC and Z-IC

In this work, we also investigate the robustness of IGS against imperfect CSIT in the 2-user IC and Z-IC. To this end, we employ a *worst-case* robustness approach to derive optimal robust IGS designs [7, 82, 88, 95, 114, 116]. Thereby, we assume that the true channels are within a known bounded region around the available CSI estimate with a certain probability, which we

call the uncertainty region. Robustness is then achieved by performing an optimization for the worst-case channels within the uncertainty region.

We consider a scenario in which the transmitters have access to a noisy estimate of the channel coefficients, and we propose closed-form robust designs of the transmission parameters that achieve the robust rate region of the 2-user IC and Z-IC with TIN. To this end, we first extend the results in [70] to derive a worst-case robust design for the 2-user IC. In [70], an UCR scenario was considered, in which the PU, unaware of the SU, employs PGS and transmits with maximum power. In UCR, there are two types of users, PUs and SUs. PUs are licensed users and have priorities to use the resources; on the other hand, SUs can transmit only if they do not disturb the communications of the PUs. However, in the 2-user IC, a higher degree of cooperation between users may be allowed to achieve a better performance. Thus, we derive the Pareto-optimal boundary of the robust rate region for the 2-user IC when at most one user employs IGS, which makes the scheme robust against imperfect CSI and represents a generalization of the scenario studied in [70]. We then extend the design in [71] to a robust design for the Z-IC. The main challenge of the robust design for the Z-IC is to consider the phase uncertainty, which makes the optimization problems more difficult than in the setting of [71].

The main contributions of this work for the robust design in the 2-user SISO IC and Z-IC are the following:

- We first consider a 2-user IC scenario and derive a robust scheme in closed-form by allowing only one of the users to employ IGS. An important advantage of this suboptimal scheme is that it is independent of the channel phase information at the transmitters. We derive a sufficient and necessary condition for the proposed IGS scheme to outperform PGS in this scenario.

- Although the results for the 2-user IC can be applied to the Z-IC, we propose another robust design for the Z-IC that allows both users to employ IGS simultaneously. We also derive closed-form conditions for this IGS scheme to outperform PGS. These conditions, which depend on the accuracy of the CSI at the transmitter side, provide a robust version of the design in [71].

- Our results show that even in the presence of imperfect CSI, robust IGS can substantially outperform robust PGS designs. This is in contrast to non-robust IGS designs, which may be strongly affected by uncertain CSI. Our results show that improper signaling is even more robust to imperfect CSI than its proper counterpart when the transmission parameters are optimized in a robust way.

Ergodic rate analysis for 2-user IC

We also study the achievable ergodic rates of IGS schemes over the 2-user fading IC when interference is treated as noise. For the case where at most one user employs IGS (denoted as PGS/IGS scheme), we derive closed-form expressions for the ergodic rates for both users. These rates can be attained using fixed-rate codebooks and no optimization is involved. For the more general IGS/IGS scheme where both users can employ improper signaling no closed-form expressions for the rates exist and hence we compute numerically the optimal transmission parameters and the boundary of the rate region. In our model, the users have perfect and instantaneous CSI at the receiver side (CSIR) but they only have access to statistical CSIT. In other

words, the transmitters know the parameters defining the Rayleigh fading distributions of the direct and interfering links. Note that the perfect instantaneous CSIR can be achieved using, for example, training sequences. Under these assumptions, we derive the achievable ergodic rates when the users transmit proper and improper Gaussian codewords.

The main contributions of this paper for the ergodic rates of IGS schemes over the 2-user fading IC are as follows:

- We derive closed-form expressions for the achievable ergodic rate of the PGS and IGS users. We also characterize the achievable ergodic rate region of the mixed PGS/IGS scheme by allowing power control.
- Our proposed scheme incurs no additional overhead at the transmitter side when both users transmit at maximum power. Moreover, in order to operate at a specific Pareto-optimal point, the transmitters (or a central entity implementing the power control module) should be informed about the average gain of the direct and interference links, which are scalar values and can be easily sent to the transmitters. Hence, the PGS/IGS scheme is simple to implement in practice.
- Through numerical examples, we show that our proposed PGS/IGS scheme substantially outperforms the PGS scheme in moderate and strong interference regimes. Moreover, we analyze the maximum sum-rate point for the symmetric 2-user IC when both users transmit at maximum power. Under this condition, the sum-rate point is attained either with PGS or with PGS/MIGS (maximally IGS); that is, one user transmits proper signals while the other user employs maximally improper signaling. Then, the maximum sum-rate point does not require any optimization and/or power control.
- We also compare our results with the more general scheme where both users can employ IGS and their transmission parameters are numerically optimized. Our numerical results show that the union of the PGS and PGS/MIGS schemes with time sharing attains almost the whole Pareto-optimal points in the rate region and little is gained by allowing both users to employ IGS.

Summary of contributions for SISO systems

We consider various SISO interference-limited systems with realistic assumptions regarding the CSIT and hardware non-ideality and show superiority of IGS in different scenarios as described. Our main findings about for single antenna systems can be summarized as:

- The benefits of IGS increases with the number of users in the K-user SISO IC, similar to the K-user MIMO IC. This is due to the fact that the more users, the more interference, and consequently the more benefits by IGS as an interference-management technique.
- We show that IGS can outperform PGS from both achievable rate and EE perspectives, while the rate benefits of IGS are higher than its EE benefits. This is also in line with our findings in MIMO systems.
- IGS is not beneficial in OFDM UCR systems. Indeed, the IGS benefits may vanish by increasing the number of resources since we can have a more flexible power allocation when more resources are available. We also observe a similar behavior in MIMO systems, where the benefits of IGS decreases with the number of antennas.

- IGS can outperform PGS in the 2-user SISO IC with imperfect CSIT or with statistical CSIT. Hence, IGS can be beneficial with realistic CSIT assumptions even though it requires more detailed CSIT than PGS.

1.4.3 Outline

This thesis is organized as follows. Chapter 2 provides some preliminaries on improper signaling. Chapter 3 describes some multiple-antenna interference-limited systems and states the corresponding achievable rates when interference is treated as noise. In this chapter, we show that the rates with TIN can be written as a difference of two concave/convex functions. In Chapter 4, we present an optimization framework for MIMO interference-limited systems with TIN and imperfect hardware. In Chapters 5-8, we consider SISO interference-limited systems since it allows us to propose computationally less expensive designs. In Chapter 5, investigates the performance of IGS in OFDM UCR. In Chapter 6, we derive the rate region of the K-user SISO IC with asymmetric AHWD. We propose energy-efficient IGS schemes in Chapter 7 for the K-user SISO IC and UCR. Finally, Chapter 8 studies the performance of IGS in the 2-user IC and Z-IC with realistic assumptions regarding CSIT.

2 Preliminaries on Improper Signaling

Throughout this work, we deal with complex-valued signals and try to optimize the achievable rate and/or energy-efficiency functions, which are real-valued, continuous and differentiable. We apply improper signaling to improve the performance of various interference-limited systems. In this chapter, we present the concept of impropriety and discuss the analytical tools for modeling improper signals. We consider complex-valued variables and show how to write the expressions in real-valued domain, which might simplify analysis in some scenarios. Moreover, we present the complex-valued analysis for modeling improper signals. Finally, we briefly discuss the applications of improper signaling in communications.

2.1 Concept of impropriety

In this subsection, we discuss the main concept of propriety and impropriety of a signal. To this end, we first consider scalar complex Gaussian random variables and then, extend the definitions of impropriety to a vector form as well as non-Gaussian signals.

2.1.1 Scalar Gaussian random variables

Consider a scalar zero-mean complex Gaussian random variable x. The random variable x can be uniquely specified by its variance, $p_x = \mathbb{E}\{|x|^2\}$, and complementary variance, $q_x = \mathbb{E}\{x^2\}$ [2, 94]. In the following definitions, we describe the main features of x, which are used throughout this thesis.

Definition 2.1 ([2, 94]) *The circularity coefficient of x is defined as the ratio of the absolute value of the complementary variance of x to its power, i.e., $\kappa = \frac{|q|}{p}$, which takes values between 0 and 1.*

Definition 2.2 ([2,94]) *The complex Gaussian random variable x is called proper if $\kappa_x = 0$, or equivalently $q_x = 0$; otherwise, x is called improper. Moreover, x is called maximally improper if $\kappa_x = 1$.*

Remark 2.1 *The complementary variance of x can be written as $q_x = p_x \kappa_x e^{j\phi_x}$, where ϕ_x is the phase of $q_x = \mathbb{E}\{x^2\}$.*

Remark 2.2 *The absolute value of the complementary variance is less than or equal to the power, i.e., $|q_x| \leq p_x$.*

The concept of improper signaling can be understood easier by considering the real and imaginary parts of a signal. When the random variable x is improper, its real and imaginary parts are not independent and identically distributed (i.i.d). In other words, in a zero-mean improper signal, the real and imaginary parts of the signal do not have the same statistics, and/or they are correlated. It is in contrast with proper signals in which the real and imaginary parts are i.i.d. In Fig. 2.1, we show the probability-density contours of a complex Gaussian random

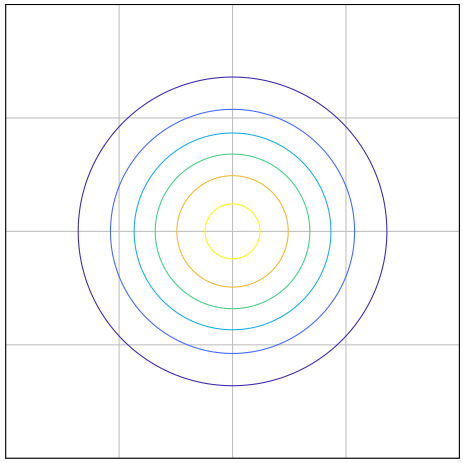

(a) $q_x = 0$ (proper).

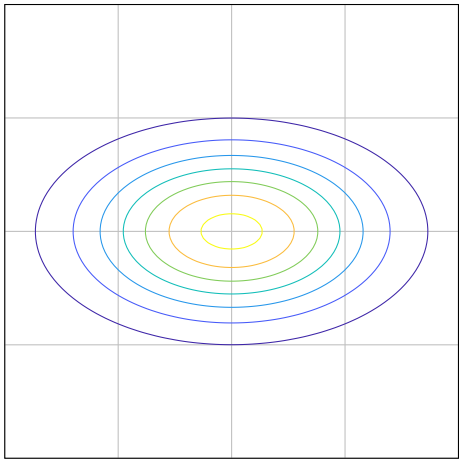

(b) $q_x/p_x = 0.5$ (improper).

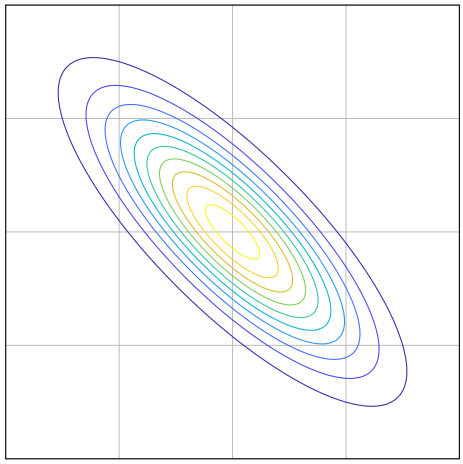

(c) $q_x/p_x = 0.8e^{j3\pi/2}$ (improper).

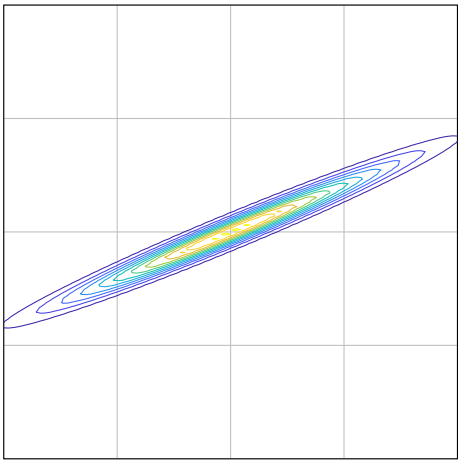

(d) $q_x/p_x = 0.99e^{j\pi/4}$ (near to maximally improper).

Figure 2.1: Probability-density contours of complex Gaussian random variable x with different complementary variance q_x.

variable with different complementary variance q_x. As can be observed, the probability-density contours are circular for a proper Gaussian random variable. That is why, proper Gaussian random variables are also called *circular* or *circularly symmetric*. The concept of circularly symmetric is provided in the following definition.

Definition 2.3 ([2]) *A complex random variable is called circularly symmetric if its probability distribution is rotationally invariant. In other words, if x and $\hat{x} = xe^{j\phi}$ have the same probability distribution for any arbitrary real value ϕ, the random variable x is circularly symmetric.*

We also observe that the probability-density contours are ellipses for an improper Gaussian random variable and become lines for the maximally improper case. This is the reason that improper Gaussian signals are also called *noncircular* or *circularly asymmetric*. It should be emphasized that, in general, there is a difference between the concept of "propriety/impropriety" (which is a second-order concept) and "circular/noncircular" (which is defined in terms of probability distribution). These terms are the same only for Gaussian signals, and these cannot be generalized to non-Gaussian proper/improper signals.

2.1.2 Vector Gaussian random variables

The definition of improper scalar variables can be easily extended to vectors. A zero-mean complex Gaussian random vector $\mathbf{x} \in \mathbb{C}^{N\times 1}$ with covariance matrix $\mathbf{P} = \mathbb{E}\{\mathbf{x}\mathbf{x}^H\}$ is called proper if $\mathbf{Q} = \mathbb{E}\{\mathbf{x}\mathbf{x}^T\} = \mathbf{0}$; otherwise, it is improper [2, 94]. As indicated before, a Gaussian random variable can be uniquely specified by its first (mean) and second order (covariance and complementary covariance matrices) statistics. In other words, we only need the covariance and complementary covariance matrices of a zero-mean complex Gaussian signal to fully define it.

There are two main approaches to model improper signals: augmented covariance matrix and real-decomposition method. In the following, we provide the definition of these approaches. Note that we consider vector variables in these definitions; however, they also include scalar variables as a special case.

Definition 2.4 ([2,94]) *The augmented covariance matrix of a random vector* $\mathbf{x}$ *is defined as*

$$\mathbf{C} = \mathbb{E}\left\{ \begin{bmatrix} \mathbf{x} \\ \mathbf{x}^* \end{bmatrix} \begin{bmatrix} \mathbf{x} \\ \mathbf{x}^* \end{bmatrix}^H \right\} = \begin{bmatrix} \mathbf{P} & \mathbf{Q} \\ \mathbf{Q}^* & \mathbf{P}^* \end{bmatrix}. \tag{2.1}$$

Lemma 2.1 $\mathbf{P}$ *and* $\mathbf{Q}$ *are a valid covariance and complementary covariance pair if and only if* $\mathbf{C} = \begin{bmatrix} \mathbf{P} & \mathbf{Q} \\ \mathbf{Q}^* & \mathbf{P}^* \end{bmatrix}$ *is Hermitian positive semidefinite.*

Remark 2.3 *The augmented covariance matrix cannot be any arbitrary Hermitian positive semidefinite matrix and has to fulfill the structure in* (2.1)*.*

Remark 2.4 *The augmented covariance matrix of scalar variable* x *is*

$$\mathbf{C} = \mathbb{E}\left\{ \begin{bmatrix} x \\ x^* \end{bmatrix} \begin{bmatrix} x \\ x^* \end{bmatrix}^H \right\} = \begin{bmatrix} p & \kappa p e^{j\phi} \\ \kappa p e^{-j\phi} & p \end{bmatrix}, \tag{2.2}$$

where p*,* κ*, and* ϕ *are, respectively, the power, circularity coefficient, and the phase of the complementary variance of* x*.*

We can also employ the real-decomposition method to represent the covariance matrix of improper and improper random vectors. By the real-decomposition method, the real-domain covariance matrix of $\mathbf{x}$ is define as $\underline{\mathbf{P}} = \mathbb{E}\{\underline{\mathbf{x}}\,\underline{\mathbf{x}}^T\}$, where the notation $\underline{\mathbf{x}} = [\ \Re\{\mathbf{x}\}^T \quad \Im\{\mathbf{x}\}^T\ ]^T$ refers to the real-decomposition of vector $\mathbf{x}$. Throughout this dissertation, we represent the real-decomposition of a typical vector $\mathbf{t}$ by $\underline{\mathbf{t}}$.

Lemma 2.2 *In the real-decomposition model, an improper random vector can have any arbitrary symmetric and positive semi-definite covariance matrix. However, a proper Gaussian signal has a covariance matrix with the specific structure [94]*

$$\underline{\mathbf{P}} = \mathbb{E}\left\{ \begin{bmatrix} \Re\{\mathbf{x}\} \\ \Im\{\mathbf{x}\} \end{bmatrix} \begin{bmatrix} \Re\{\mathbf{x}\} \\ \Im\{\mathbf{x}\} \end{bmatrix}^T \right\} = \begin{bmatrix} \mathbf{A} & \mathbf{B} \\ \mathbf{B} & \mathbf{A} \end{bmatrix}, \tag{2.3}$$

where $\mathbf{A} \in \mathbb{R}^{N\times N}$ *is symmetric and positive semi-definite, and* $\mathbf{B} \in \mathbb{R}^{N\times N}$ *is skew-symmetric.*

Definition 2.5 *Matrix* $\mathbf{B}$ *is skew-symmetric if and only if* $\mathbf{B} = -\mathbf{B}^T$*. It implies that diagonal elements of* $\mathbf{B}$ *are zero.*

In the next section, we state the rate expressions by each analytical approach and discuss their

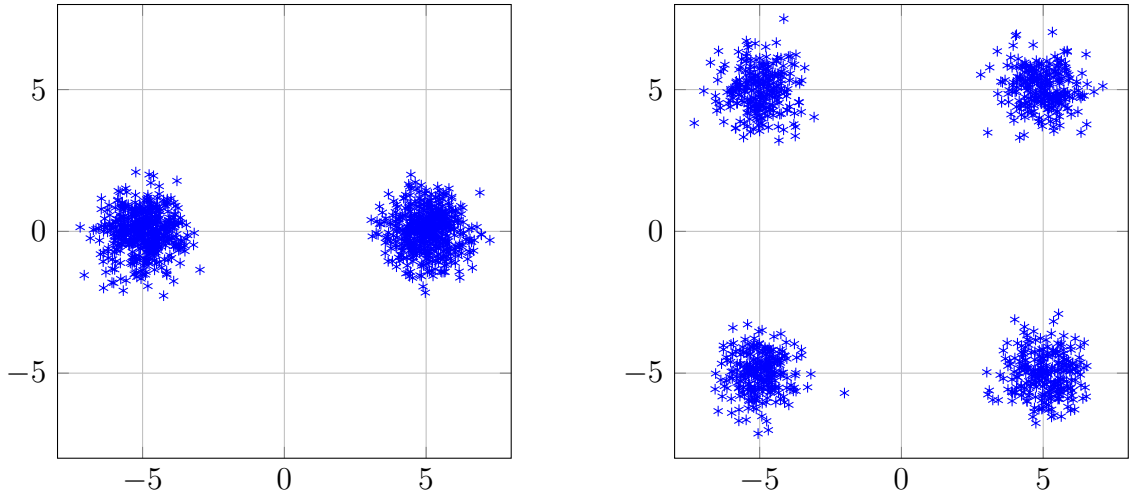

(a) BPSK (maximally improper constellation). **(b)** 4-QAM (proper constellation).

Figure 2.2: Constellation of a maximally improper and proper discrete signaling contaminated by a proper complex Gaussian additive noise.

advantages and drawbacks.

2.1.3 Discrete constellations

The concept of propriety/impropriety can be employed in discrete constellation as well [1, 2, 94]. For instance, in Fig. 2.2, we depict two proper and maximally improper constellations, which are contaminated by a proper complex Gaussian additive noise. The binary phase shift keying (BPSK) signaling is a maximally improper discrete signaling (Fig. 2.2a). Moreover, 4-quadrature amplitude modulation (QAM) with equal transmission probability of each symbol is a proper signaling (Fig. 2.2b) [1, 2]. For more details and discussions on improper discrete signals, please refer to [65].

2.2 Analytical tools for improper signaling

In this subsection, we discuss the common analytical tools for modeling improper signaling. In general, to deal with improper signals, there are two approaches: augmented covariance matrix [2] and real-decomposition method [49]. In the augmented-covariance-matrix approach, complex-domain signals are considered, and the optimized variables are covariance and complementary covariance matrices. However, in the real-decomposition method, every variable is written in the real domain, and the optimization variable is the covariance matrix of the real decomposition of the signals. The main differences of these two approaches are in the structure of the optimization variables as well as corresponding optimization problems. That is, a complementary covariance matrix has to follow a specific structure for improper signals, while the real covariance matrices are required to be only positive semi-definite. Each approach has some advantages and drawbacks. We should be careful about choosing the right analytical tool for our problem. In general, the augmented-covariance-matrix approach can provide insights into the behavior of the signals. However, depending on the scenario, the optimization over the real

domain might be simpler. In this section, we discuss the analytical approaches in details.

2.2.1 Real-decomposition method

There are powerful analytical tools for analyzing complex-valued signals. However, in some cases, it might be easier to rewrite everything in real-valued domain and deal with only real-valued signals. By real-decomposition method, we are able to convert a complex-domain problem to a real-domain one. That is, we consider the real and imaginary parts of signals separately as independent real values, which leads to a doubling of the dimension. For example, consider the following complex-valued equation

$$\begin{aligned} y = hx + n &= (\Re\{h\} + j\Im\{h\})\,(\Re\{x\} + j\Im\{x\}) + \Re\{n\} + j\Im\{n\} \\ &= (\Re\{h\}\Re\{x\} - \Im\{h\}\Im\{x\} + \Re\{n\}) + j\,(\Im\{h\}\Re\{x\} + \Re\{h\}\Im\{x\} + \Im\{n\}) \\ &= \Re\{y\} + j\Im\{y\}, \end{aligned} \tag{2.4}$$

where y, x, h, and n are arbitrary complex-value scalar. Additionally, $\Re\{x\}$ and $\Im\{x\}$ take the real and imaginary parts of x, respectively. The expression in (2.4) can be written in a vector/matrix form as

$$\begin{bmatrix} \Re\{y\} \\ \Im\{y\} \end{bmatrix} = \begin{bmatrix} \Re\{h\} & -\Im\{h\} \\ \Im\{h\} & \Re\{h\} \end{bmatrix} \begin{bmatrix} \Re\{x\} \\ \Im\{x\} \end{bmatrix} + \begin{bmatrix} \Re\{n\} \\ \Im\{n\} \end{bmatrix}. \tag{2.5}$$

As can be observed, the dimension of the signals is increased by a factor of 2, and each variable is written in a real-valued domain.

The real-decomposition method can be simply applied to vector cases as well. For instance, consider the following equation describing a point-to-point communication system

$$\mathbf{y} = \mathbf{H}\mathbf{x} + \mathbf{n}, \tag{2.6}$$

where $\mathbf{y} \in \mathbb{C}^{N_R \times 1}$, $\mathbf{x} \in \mathbb{C}^{N_T \times 1}$, $\mathbf{n} \in \mathbb{C}^{N_R \times 1}$, and $\mathbf{H} \in \mathbb{C}^{N_R \times N_T}$ are, respectively, the received signal, transmitted signal, noise vector, and the channel matrix. The real-decomposition model for the link is

$$\underline{\mathbf{y}} = \begin{bmatrix} \Re\{\mathbf{H}\} & -\Im\{\mathbf{H}\} \\ \Im\{\mathbf{H}\} & \Re\{\mathbf{H}\} \end{bmatrix} \underline{\mathbf{x}} + \underline{\mathbf{n}}, \tag{2.7}$$

where the notation $\underline{\mathbf{y}}$, $\underline{\mathbf{x}}$, and $\underline{\mathbf{n}}$ are, respectively, the real-decomposition of vectors $\mathbf{y}$, $\mathbf{x}$, and $\mathbf{n}$. We can also easily derive the achievable rate of this link for Gaussian additive noise by the real-decomposition method. Assume $\mathbf{n}$ is a random vector with Gaussian distribution as $\mathbf{n} \sim \mathcal{CN}(\mathbf{0}, \mathbf{P}_n)$. The achievable rate of the system is [24]

$$R = \frac{1}{2}\log_2 \det\left(\underline{\mathbf{P}}_n + \underline{\mathbf{H}}\,\underline{\mathbf{P}}\,\underline{\mathbf{H}}^T\right) - \frac{1}{2}\log_2 \det\left(\underline{\mathbf{P}}_n\right), \tag{2.8}$$

where $\underline{\mathbf{P}}_n$ is the covariance matrix of $\underline{\mathbf{n}}$, $\underline{\mathbf{P}}$ is the covariance matrix of $\underline{\mathbf{x}}$, and $\underline{\mathbf{H}}$ is

$$\underline{\mathbf{H}} = \begin{bmatrix} \Re\{\mathbf{H}\} & -\Im\{\mathbf{H}\} \\ \Im\{\mathbf{H}\} & \Re\{\mathbf{H}\} \end{bmatrix}. \tag{2.9}$$

Remark 2.5 ([24]) *The achievable rate of a link is defined as the difference between the entropy*

of the received signal and the entropy of the noise at the receiver.

The real-decomposition method may simplify complex-domain optimization problems especially when the real and imaginary parts of the optimization variables do not *necessarily* have the same statistics, which is referred to as improper signaling [2, 94]. As can be observed through (2.8), the rate is a concave function in $\underline{\mathbf{P}}$ and a difference of two concave functions in $\underline{\mathbf{P}}_n$.

To sum up, by the real-decomposition method, the dimension of the signals is doubled, which can increase the computational expenses especially when the analysis in the complex domain are not complicated. However, in some cases, the analysis might be intractable if we employ complex-domain representations. We will elaborate more on how the real-decomposition method can simplify optimization of improper signaling in the next subsection.

2.2.2 Augmented-covariance-matrix analysis

In this subsection, we provide simple examples to state the rate expressions by the augmented-covariance-matrix approach. To this end, we consider a point-to-point communication with possibly improper Gaussian noise and signal, similar to the model in Section 2.2.1, as

$$\mathbf{y} = \mathbf{H}\mathbf{x} + \mathbf{n}, \tag{2.10}$$

where the parameters are define as in (2.6). In this case, the achievable rate by the augmented-covariance-matrix method is [2, 129]

$$R = \frac{1}{2}\log_2 \frac{\left|\mathbf{C}_n + \mathbf{H}\mathbf{C}\mathbf{H}^H\right|}{|\mathbf{C}_n|} \tag{2.11}$$

where $\mathbf{C}$, $\mathbf{C}_n$, and $\mathbf{H}$ are, respectively, the covariance of transmitted signal, covariance of noise, and the channel matrix. The rate can be simplified as [2, 129]

$$\begin{aligned} R_{\text{IGS}} = & \underbrace{\log_2 \frac{\left|\mathbf{P}_n + \mathbf{H}\mathbf{P}\mathbf{H}^H\right|}{|\mathbf{P}_n|}}_{R_{\text{PGS}}} \\ & + \underbrace{\frac{1}{2}\log_2 \frac{\left|\mathbf{I} - \left(\mathbf{P}_n + \mathbf{H}\mathbf{P}\mathbf{H}^H\right)^{-1}\left(\mathbf{Q}_n + \mathbf{H}\mathbf{Q}\mathbf{H}^T\right)\left(\mathbf{P}_n + \mathbf{H}\mathbf{P}\mathbf{H}^H\right)^{-T}\left(\mathbf{Q}_n + \mathbf{H}\mathbf{Q}\mathbf{H}^T\right)^H\right|}{|\mathbf{I} - \mathbf{P}_n^{-1}\mathbf{Q}_n\mathbf{P}_n^{-T}\mathbf{Q}_n^H|}}_{\tilde{R}}, \end{aligned} \tag{2.12}$$

where $\mathbf{P}$, $\mathbf{P}_n$, $\mathbf{Q}$, and $\mathbf{Q}_n$ are, respectively, the covariance of transmitted signal, covariance of noise, complementary covariance of transmitted signal and complementary covariance of noise. As can be observed through (2.12), the rate of IGS can be written as the rate of PGS, R_{PGS}, plus an additional term $\tilde{R}$. When the noise is proper ($\mathbf{Q}_n = \mathbf{0}$), the additional term is always non-positive ($\tilde{R} \leq 0$), and is maximized at $\mathbf{Q} = \mathbf{0}$. In other words, when the noise is proper, the signal has to be proper to maximize the achievable rate. This representation allows us to interpret easier the behavior of improper signals. However, the optimization over the parameters is very complicated in this case. The reason is that, the rate function in (2.12) has a very com-

plicated form and is neither jointly convex nor jointly concave in $\mathbf{P}$ and $\mathbf{Q}$, which makes the optimization of the rate sophisticated. This is in contrast with the real-decomposition method, where the rate is concave in $\underline{\mathbf{P}}$ and a difference of two concave functions in $\underline{\mathbf{P}}_n$ (please see (2.8)). This feature of the real-decomposition method enables us to apply the well-know optimization methods such as majorization minimization to obtain numerical solutions for various problems in multiple-antenna systems. Hence, the real-decomposition method suits more for optimizations in multiple-antenna systems.

In single-antenna systems, we deal with scalars, and the representation of the rate expression is simplified. Let us consider a simple example of a point-to-point single-antenna system. In this case, the achievable rate in (2.12) can be simplified as [71]

$$R = \frac{1}{2}\log_2\left(\frac{(p+p_n)^2 - |q+q_n|^2}{p_n^2 - |q_n|^2}\right), \tag{2.13}$$

where p, p_n, q, and q_n are, respectively, the power of signal, power of noise, complementary variance of signal and complementary variance of noise. To make it more illustrative, we simplify the scenario and assume that the desired signal is proper, i.e., $q = 0$. In this case, considering $|q_n| = p_n\kappa_n$, we simplify the rate as

$$R = \frac{1}{2}\log_2\left(\frac{(p_s+p_n)^2 - (p_n\kappa_n)^2}{p_n^2(1-\kappa_n^2)}\right), \tag{2.14}$$

where κ_n is the circularity coefficient of the noise. Now it is easy to verify that R is monotonically increasing in κ_n. In other words, by this method, we could simply show that the rate can be increased by making the noise improper for a fixed noise power. However, it might not be completely straightforward to prove this statement by the real-decomposition method. The reason is that, the real-decomposition method convert the SISO system with complex variables to a 2×2 MIMO system with real variables and optimize over 2 by 2 covariance matrices, as indicated in Section 2.2.1 and Equation (2.8). Note that we consider a very simple scenario here, and it would be even much more complicated to derive necessary and/or sufficient conditions for optimality of improper/proper signaling by the real-decomposition method in more realistic scenarios.

In the following, we provide a simple example to describe the main idea of employing the augmented-covariance-matrix method for deriving conditions on the optimality of IGS. Assume that we want to optimize a performance metric over a scalar optimization variable, which can be improper. A sufficient condition for optimality of IGS can be derived by taking a derivative of the desired performance metric with respect to the circularity coefficient, κ, of the optimization variable. Then, we derive conditions such that the performance metric is increasing in κ around $\kappa = 0$ or equivalently, the derivative is positive at $\kappa = 0$. These conditions imply that there exists at least a κ, which improves the system performance over PGS. In other words, under these conditions, IGS definitely outperforms PGS, which provides a sufficient condition for the optimality of IGS. Moreover, if we are able to show that the system performance is always monotone in κ, these conditions would be the necessary condition as well. A practical example of this approach is provided in Section 7.2. Unfortunately, these analysis are not straightforward for multiple-antenna systems as discussed before.

2.2.3 Discussions on the analysis tool

There are two main approaches to analyze improper signals, and each analytical tool has its own advantages and drawbacks. We should choose the most adequate formulation for the problems based on our goal and the format of the problem. In this thesis, we employ both the augmented-covariance-matrix and the real-decomposition methods depending on the considered scenario. In single-antenna systems, we mostly consider the augmented-covariance-matrix method since it allows us to discuss on the optimality of improper/proper signaling in some specific scenarios. As an example, in Section 7.2, we derive the necessary and sufficient conditions for the optimality of IGS from an EE point of view in UCR by this approach. However, we employ the real-decomposition method in multiple-antenna systems in Chapter 4. The reason is that, we are able to simplify the considered optimization problems by this method and derive numerical solutions for the studied problems in the multiple-antenna systems.

2.3 Widely linear transformation

The widely linear transformation of complex-domain vector $\mathbf{x}$ is defined as a linear combination of $\mathbf{x}$ and its conjugate, $\mathbf{x}^*$, as

$$\mathbf{y} = \mathbf{A}_1\mathbf{x} + \mathbf{A}_2\mathbf{x}^*, \tag{2.15}$$

where $\mathbf{A}_1$ and $\mathbf{A}_2$ are coefficients, and $\mathbf{y}$ is the widely linear transformation of $\mathbf{x}$. We can express the widely linear transformation in a real domain as

$$\underline{\mathbf{y}} = \begin{bmatrix} \Re\{\mathbf{A}_1 + \mathbf{A}_2\} & -\Im\{\mathbf{A}_1 - \mathbf{A}_2\} \\ \Im\{\mathbf{A_1} + \mathbf{A_2}\} & \Re\{\mathbf{A_1} - \mathbf{A_2}\} \end{bmatrix} \underline{\mathbf{x}}. \tag{2.16}$$

Assume $\mathbb{E}\{\mathbf{x}\mathbf{x}^H\} = \mathbf{P}$ and $\mathbb{E}\{\mathbf{x}\mathbf{x}^T\} = \mathbf{0}$. Then, we have

$$\mathbb{E}\{\mathbf{y}\mathbf{y}^T\} = \mathbf{A}_1\mathbf{P}\mathbf{A}_2^T + \mathbf{A}_2\mathbf{P}^*\mathbf{A}_1^T. \tag{2.17}$$

In other words, the complementary covariance of $\mathbf{y}$ is in general non-zero. This is an important feature of the widely linear transformation, which makes the output signal improper even if the input signal is proper.

One of the applications of the widely linear transformation in wireless communications is to model I/Q imbalance at transceivers [63]. I/Q imbalance happens due to imperfections at devices. Another application of this transformation is to optimize the parameters of improper signals [46, 68, 69]. It might also simplify the implementation of improper signaling since we can apply this transformation to the existing proper signaling schemes and convert them to improper signaling.

2.4 Wirtinger calculus

In wireless communications, we usually optimize a real-valued utility/cost function over complex-valued optimization parameters. Hence, we have to be able to take the derivative of real-valued functions with respect to the complex-domain parameters. Unfortunately, real-valued functions are not analytic as will be discussed. A general framework for differentiating non-analytical

functions is Wirtinger calculus [1]. In this section, we provide some basic definitions for derivative of complex-valued functions with complex domain and state the Wirtinger calculus.

Consider a complex-valued function $f(z) = u(z) + jv(z)$ with complex domain $\mathbb{A}$, where $u(z), v(z) \in \mathbb{R}$, and $z = x + jy \in \mathbb{A}$ with $x, y \in \mathbb{R}$. In the following, we provide the definition of complex differentiability for the typical function f as well as the definition of complex analytical functions.

Definition 2.6 ([1, 2]) *The function f is complex differentiable at $z_0 \in \mathbb{A}$ if the limit*

$$\lim_{z \to z_0} \frac{f(z) - f(z_0)}{z - z_0} \tag{2.18}$$

uniquely exists and is independent of how z approaches to z_0.

Definition 2.7 ([1, 2]) *The function f is called analytical or holomorphic if f is complex differentiable on its entire domain.*

Not that there is a difference between the definition of real analytic and complex analytic functions. A necessary condition for f to be complex analytic is that the Cauchy-Reimann equations have to be satisfied on the entire domain $\mathbb{A}$, where the Cauchy-Reimann equations are [1, 2]

$$\frac{\partial u(x,y)}{\partial x} = \frac{\partial v(x,y)}{\partial y} \qquad \text{and} \qquad \frac{\partial u(x,y)}{\partial y} = -\frac{\partial v(x,y)}{\partial x}. \tag{2.19}$$

When f is a real-valued function, $v(x, y) = 0$. It implies that the Cauchy-Reimann equations cannot be satisfied on the entire domain $\mathbb{A}$, and consequently, f cannot be complex analytic and complex differentiable even if f is analytic in x or y. A way to take the differential $\mathrm{d}f$ of a non-analytical complex-valued function f is to employ the Wirtinger calculus, which is defined as

$$\mathrm{d}f = \frac{\partial f(z)}{\partial z}\mathrm{d}z + \frac{\partial f(z)}{\partial z^*}\mathrm{d}z^*. \tag{2.20}$$

In the Wirtinger calculus, z and z^* are treated as two independent variables as

$$\frac{\partial z^*}{\partial z} = \frac{\partial z}{\partial z^*} = 0. \tag{2.21}$$

Additionally, the partial-derivative operators $\frac{\partial}{\partial z}$ and $\frac{\partial}{\partial z}$, which are referred to as the Wirtinger derivatives [119], are defined as

$$\frac{\partial}{\partial z} = \frac{1}{2}\left(\frac{\partial}{\partial x} - j\frac{\partial}{\partial y}\right) \qquad \text{and} \qquad \frac{\partial}{\partial z^*} = \frac{1}{2}\left(\frac{\partial}{\partial x} + j\frac{\partial}{\partial y}\right). \tag{2.22}$$

When f is a real-domain function, the differential $\mathrm{d}f$ in (2.20) is simplified to [14]

$$\mathrm{d}f = 2\Re\left\{\frac{\partial f(z)}{\partial z}\mathrm{d}z\right\} = 2\Re\left\{\frac{\partial f(z)}{\partial z^*}\mathrm{d}z^*\right\}. \tag{2.23}$$

To illustrate the concept of complex analytic and the Wirtinger calculus, we provide two simple examples. Consider $f(z) = z^2$. Then $f(z)$ is complex analytical and $\frac{\partial f(z)}{\partial z} = 2z$. Now consider $f(z) = |z|^2$. In this case, although $f(z)$ is analytic in either z or z^*, $f(z)$ is not complex

analytic. The differential $\mathrm{d}f$ is

$$\mathrm{d}f = z^*\mathrm{d}z + z\mathrm{d}z^* = 2\Re\left\{z^*\mathrm{d}z\right\} = 2\Re\left\{z\mathrm{d}z^*\right\}. \tag{2.24}$$

In this section, we consider only scalar variables; however, the concept of the Wirtinger calculus can be easily extended to the vector and matrix forms. There are many applications for the Wirtinger calculus in wireless communications specially when we want to optimize a performance metric over complex-domain parameters. An example of applying the Wirtinger calculus can be found in Section 6.6, where we find suitable surrogate functions when we optimize over complementary variances.

2.5 Applications of improper signaling in communications

In this section, we discuss some applications of improper signaling in communication with more emphasis on its wireless communications applications. As indicated in Section 2.1, the concept of improper signaling can be applied to discrete constellations. For instance, 8-QAM, pulse-amplitude modulation (PAM) and BPSK are among discrete improper signaling. Thus, improper signals have been used vastly in communications. Furthermore, there might be improper noise or distortions in many practical scenarios in communication systems. For example, the transceivers might suffer from I/Q imbalance, which leads to improper noise as well as improper signal [63]. In the presence of I/Q imbalance, the improper signal at the receiver side is undesired and has to compensated since it leads to rate loss. This impropriety can be compensated by employing improper signaling.

In addition to aforementioned applications, improper signaling has received lots of attentions as an interference-management technique in the last decade. It has been shown that the performance of different interference-limited systems is enhanced by transmitting improper signals [4, 17, 36, 54, 59, 67–71, 86, 121, 129]. In other words, by intentionally making the signals improper, we are able to reduce the harmful effects of interference on non-intended receivers. Throughout this work, we focus on this application of improper signaling in wireless communications. In the following, we briefly explain the main idea of employing IGS as an interference-management technique.

Proper signaling is the optimal signaling in the presence of proper noise for a point-to-point link [24]. However, the system performance can be improved by improper signaling in the presence of interference. To understand the basic idea of employing IGS as an interference-management technique, we provide two illustrative examples of a single-antenna point-to-point communication. We first consider a proper signal with an improper noise. The achievable rate of this system is given by (2.14), which is rewritten here as

$$R = \frac{1}{2}\log_2\left(\frac{(p+p_n)^2 - (p_n\kappa_n)^2}{p_n^2(1-\kappa_n^2)}\right), \tag{2.25}$$

where the parameters are defined as in (2.14). As discussed, the rate is increasing in κ_n (see

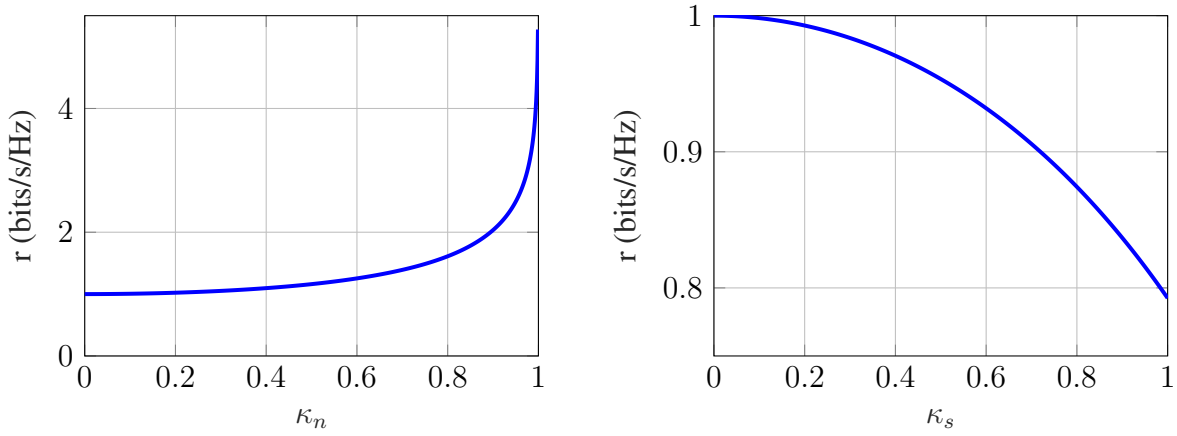

(a) Proper signal with improper noise.

(b) Improper signal with proper noise.

Figure 2.3: Achievable rate versus the circularity coefficient for $p_s = p_n = 1$.

Fig. 2.3a). To elaborate more on the behavior in Fig. 2.3a, we rewrite the rate as

$$R = \frac{1}{2}\log_2\left(1 + \frac{p}{p_n(1-\kappa_n)}\right) + \frac{1}{2}\log_2\left(1 + \frac{p}{p_n(1+\kappa_n)}\right). \tag{2.26}$$

When the noise is maximally improper, i.e., $\kappa_n = 1$, there is a noise-free dimension on which infinite date can be transmitted. Of course, maximally improper noise is never practical, but this example shows the main trend of making the noise (or generally interference plus noise) improper.

Now we consider an improper signal with proper noise. In this case, the achievable rate is

$$R = \frac{1}{2}\log_2\left(\frac{(p+p_n)^2 - (p\kappa)^2}{p_n^2}\right), \tag{2.27}$$

where κ is the circularity coefficient of the signal. It is easy to verify that the rate is decreasing in κ as depicted in Fig. 2.3b. This behavior can be explained as follows. Let rewrite the rate in (2.27) as

$$R = \frac{1}{2}\log_2\left(1 + \frac{p(1+\kappa)}{p_n}\right) + \frac{1}{2}\log_2\left(1 + \frac{p(1-\kappa)}{p_n}\right). \tag{2.28}$$

As can be observed, the rate consist of two parts. The reason is that the real and imaginary parts of improper signals can be correlated. The circularity coefficient κ, somehow, measures the correlation between the real and imaginary parts of a signal. When $\kappa = 0$, there is no correlation between the real and imaginary parts, and they are i.i.d. In this case, the rate is actually

$$R = \frac{1}{2}\log_2\left(1 + \frac{p}{p_n}\right) + \frac{1}{2}\log_2\left(1 + \frac{p}{p_n}\right). \tag{2.29}$$

It means that the transmission power is equally divided in both dimensions. When $\kappa = 1$, the

full transmission power is allocated to only one dimension as

$$R = \frac{1}{2}\log_2\left(1 + \frac{2p}{p_n}\right). \tag{2.30}$$

Indeed, we loss one dimension when we employ maximally improper signaling, which results in reducing the the achievable data rate and diversity. Hence, improper Gaussian signals have less differential entropy than proper ones. This feature can typically be exploited to make interference less harmful to non-intended receivers with the cost of losing some data rates.

These two examples are inspiring for the applications of IGS as an interference-management technique. In some practical scenarios, interference from other users is treated as noise. As shown in Fig. 2.3, the more improper the noise is, the better rate performance can be achieved. This motivates us to employ IGS to reduce the undesired consequences of interference on other users. It is clear that the undesired consequences of interference can be reduced when the interference has spatial or statistical structure that can be optimized for the benefit of the whole network. However, the rate of a user is decreasing in its degree of impropriety. Hence, transmitting IGS signals always involves a trade-off: it reduces its own rate (because the differential entropy of a Gaussian random variable decreases when its circularity coefficient increases), but it allows to increase the rate of other users. When properly optimized, the reduction in rate can sometimes be compensated by an increase in transmitted power (which in turn increases the transmitted rate) with an overall benefit for the system.

In summary, IGS gives us an extra degree of freedom to optimize the systems performance, which enables us to handle interference with more flexibility. The real and imaginary parts of a proper Gaussian signal are i.i.d random variables. However, this constraint is relaxed when improper Gaussian signals are transmitted since the real and imaginary parts of IGS can have unequal power and/or be correlated. Thus, we can consider for instance the power allocated to the real and imaginary parts as two different optimization parameters (subject to a total power constraint). This basic idea has been exploited in [17] for the first time to increase the DoF of the 3-user SISO IC. Later, this idea was applied to different interference-limited wireless communication scenarios in which the interference was treated as noise to improve the achievable rate and/or power/energy performances. For instance, the authors in [129] derived the achievable rate of IGS for the K-user MIMO IC with TIN. In [129, eq (10)], it is shown that the achievable rate of IGS can be written as the summation of the rate of PGS and an additional term, which is a function of the complementary variances. This equation shows that we may be able to increase the rate by optimizing over the complementary variances. A suboptimal way to propose IGS schemes is that we can first optimize over powers (or covariance matrices) of users, which results in a proper design. Then we can optimize over complementary variances (or complementary covariance matrices) to improve the system performance. We employ this technique to propose suboptimal algorithms for single-antenna systems in Section 6.3 and Section 7.1.

Throughout this thesis, we do not consider any possible DoF improvement by IGS and focus on the rate and/or energy efficiency improvements of IGS. DoF considerations are always asymptotic and hence not always of practical relevance. Note that IGS includes PGS as a special case and thus, PGS can never outperform the optimal IGS scheme.

2.6 Summary

In this chapter, we provided some preliminaries on improper signals as well as improper signaling. We stated the most common analytical tools to model improper signals and discussed about their advantages and drawbacks. Moreover, we briefly described the main applications of improper signaling in wireless communications and shortly explained the main idea of employing IGS as an interference-management technique.

3 Interference-limited systems

In this chapter, we present some well-known interference-limited systems. The performance of interference-limited systems is mainly restricted by the interference from other users. There are many different types of interference-limited systems such as various interference channels, relay channels, cognitive radio systems, multiple access channels, broadcast channels, etc. In this work, we focus on different interference channels and underlay cognitive radio systems. We consider treating interference as noise (TIN) as decoding strategy and state the achievable rates in different interference-limited systems. As will be observed in this chapter, the achievable rate in interference-limited systems with TIN is a difference of two concave/convex functions when the real-decomposition method is employed. This feature of the rate can be exploited for solving some rate-dependent optimization problems as will be discussed in Chapter 4.

3.1 Hardware imperfection models

In this section, we present the most common hardware imperfection models in the literature. We first discuss the I/Q imbalance model in Section 3.1.1. Then, we describe the AHWD model in Section 3.1.2.

3.1.1 I/Q imbalance

In this section, we present hardware impairment model for a point-to-point multiple antenna system with N_T transmitter antennas and N_R receiver antennas (see Fig. 3.1). To this end, we employ the hardware imperfection model in [63]. The I/Q imbalance at the transmitter side is modeled as a widely linear transform of the transmit signal $\mathbf{x} \in \mathbb{C}^{N_T \times 1}$ as

$$\tilde{\mathbf{x}} = \mathbf{V}_1 \mathbf{x} + \mathbf{V}_2 \mathbf{x}^*, \tag{3.1}$$

where the matrices $\mathbf{V}_1 \in \mathbb{C}^{N_T \times N_T}$ and $\mathbf{V}_2 \in \mathbb{C}^{N_T \times N_T}$ capture the amplitude and rotational errors and can be derived as [63]

$$\mathbf{V}_1 = \frac{\mathbf{I}_{N_T} + \mathbf{A}_T e^{j\boldsymbol{\theta}_T}}{2}, \tag{3.2}$$

$$\mathbf{V}_2 = \mathbf{I}_{N_T} - \mathbf{V}_1^* = \frac{\mathbf{I}_{N_T} - \mathbf{A}_T e^{-j\boldsymbol{\theta}_T}}{2}. \tag{3.3}$$

Moreover, the matrices $\mathbf{A}_T$ and $\boldsymbol{\theta}_T$ are diagonal and, respectively, reflect the amplitude and phase errors of each branch at the transmitter side [63]. There are different methods to estimate the parameters of I/Q imbalance [18, 23, 39, 109]. It is worth mentioning that there is no I/Q imbalance if $\mathbf{A}_T = \mathbf{I}$ and $\boldsymbol{\theta}_T = \mathbf{0}$ or equivalently, $\mathbf{V}_1 = \mathbf{I}$ and $\mathbf{V}_2 = \mathbf{0}$.

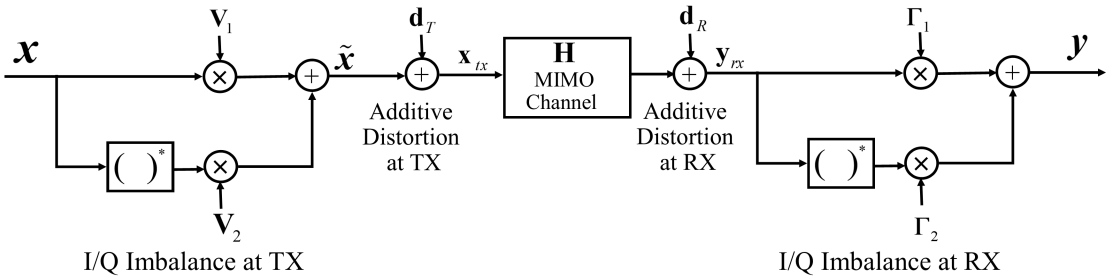

Figure 3.1: The transceiver model of a point-to-point communications link with HWI.

We also assume that the transmitter is not perfect and may generate an additive proper Gaussian noise in addition to the I/Q imbalance with probability distribution $\mathbf{d}_T \in \mathbb{C}^{N_T \times 1} \sim \mathcal{CN}(\mathbf{0}, \mathbf{C}_T)$ [63]. Hence, the transmitted signal is

$$\mathbf{x}_{tx} = \tilde{\mathbf{x}} + \mathbf{d}_T. \tag{3.4}$$

The transmitted signal is delivered to the receiver over a MIMO channel with additive white Gaussian noise. Thus, the received signal over a multipath channel is

$$\mathbf{y}_{rx} = \mathbf{H}\mathbf{x}_{tx} + \mathbf{d}_R, \tag{3.5}$$

where $\mathbf{H} \in \mathbb{C}^{N_R \times N_T}$ is the matrix of the channel coefficients. Moreover, the matrix $\mathbf{d}_R \in \mathbb{C}^{N_R \times 1}$ is the aggregate effect of the additive white Gaussian noise of the channel and the additive distortion of the received devices. The receiver can cause an I/Q imbalance similar to the transmitter. Thus, the received signal after I/Q imbalance is

$$\mathbf{y} = \mathbf{\Gamma}_1 \mathbf{y}_{rx} + \mathbf{\Gamma}_2 \mathbf{y}_{rx}^*, \tag{3.6}$$

where the matrices $\mathbf{\Gamma}_1 \in \mathbb{C}^{N_R \times N_R}$ and $\mathbf{\Gamma}_2 \in \mathbb{C}^{N_R \times N_R}$ are, respectively, given by

$$\mathbf{\Gamma}_1 = \frac{\mathbf{I}_{N_R} + \mathbf{A}_R e^{j\boldsymbol{\theta}_R}}{2} \tag{3.7}$$

$$\mathbf{\Gamma}_2 = \mathbf{I}_{N_R} - \mathbf{\Gamma}_1^* = \frac{\mathbf{I}_{N_R} - \mathbf{A}_R e^{-j\boldsymbol{\theta}_R}}{2}. \tag{3.8}$$

Similar to $\mathbf{A}_T$ and $\boldsymbol{\theta}_T$, the matrices $\mathbf{A}_R$ and $\boldsymbol{\theta}_R$ are diagonal and, respectively, reflect the amplitude and phase errors of each branch at the receiver side [63]. In following lemmas, we present the aggregate effect of the impairments at the transmitter and receiver sides.

Lemma 3.1 *The transceiver of MIMO system with HWI can be modeled as*

$$\mathbf{y} = \bar{\mathbf{H}}_1 \mathbf{x} + \bar{\mathbf{H}}_2 \mathbf{x}^* + \mathbf{z}, \tag{3.9}$$

where

$$\bar{\mathbf{H}}_1 = \mathbf{\Gamma}_1 \mathbf{H} \mathbf{V}_1 + \mathbf{\Gamma}_2 \mathbf{H}^* \mathbf{V}_2^* \in \mathbb{C}^{N_R \times N_T}, \tag{3.10}$$

$$\bar{\mathbf{H}}_2 = \mathbf{\Gamma}_1 \mathbf{H} \mathbf{V}_1 + \mathbf{\Gamma}_2 \mathbf{H}^* \mathbf{V}_2^* \in \mathbb{C}^{N_R \times N_T}, \tag{3.11}$$

$$\mathbf{z} = \mathbf{\Gamma}_1 (\mathbf{H}\mathbf{d}_T + \mathbf{d}_R) + \mathbf{\Gamma}_2 (\mathbf{H}\mathbf{d}_T + \mathbf{d}_R)^* \in \mathbb{C}^{N_R \times 1}. \tag{3.12}$$

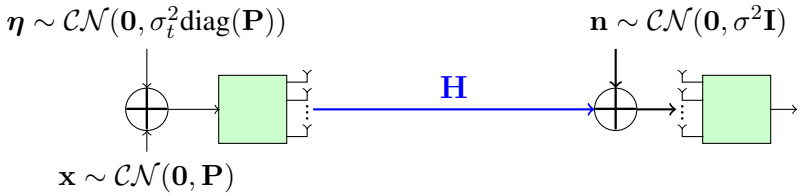

Figure 3.2: Point-to-point MIMO system with AHWD at transmitters.

Proof. Please refer to [63, Lemma 1]. □

Lemma 3.2 *The real decomposition of the HWI model in Lemma* 3.1 *is*

$$\underline{\mathbf{y}} = \tilde{\mathbf{H}}\underline{\mathbf{x}} + \underline{\mathbf{z}}, \tag{3.13}$$

where $\underline{\mathbf{y}} = \begin{bmatrix} \Re\{\mathbf{y}\}^T & \Im\{\mathbf{y}\}^T \end{bmatrix}^T$, $\underline{\mathbf{x}} = \begin{bmatrix} \Re\{\mathbf{x}\}^T & \Im\{\mathbf{x}\}^T \end{bmatrix}^T$, *and* $\underline{\mathbf{z}} = \begin{bmatrix} \Re\{\mathbf{z}\}^T & \Im\{\mathbf{z}\}^T \end{bmatrix}^T$ *are, respectively, the real decomposition of* $\mathbf{y}$, $\mathbf{x}$, *and* $\mathbf{z}$ *in* (3.9). *Moreover,* $\tilde{\mathbf{H}}$ *is*

$$\tilde{\mathbf{H}} = \begin{bmatrix} \Re\{\bar{\mathbf{H}}_1 + \bar{\mathbf{H}}_2\} & -\Im\{\bar{\mathbf{H}}_1 - \bar{\mathbf{H}}_2\} \\ \Im\{\bar{\mathbf{H}}_1 + \bar{\mathbf{H}}_2\} & \Re\{\bar{\mathbf{H}}_1 - \bar{\mathbf{H}}_2\} \end{bmatrix}. \tag{3.14}$$

The statics of the vector $\underline{\mathbf{z}} \in \mathbb{R}^{2N_R \times 1}$ *is* $\mathbb{E}\{\underline{\mathbf{z}}\} = \mathbf{0}$, *and*

$$\mathbb{E}\{\underline{\mathbf{z}}\,\underline{\mathbf{z}}^T\} = \underline{\mathbf{C}}_z = \underline{\mathbf{\Gamma}}\mathbf{C}_d\underline{\mathbf{\Gamma}}^T, \tag{3.15}$$

where $\underline{\mathbf{H}}\,\underline{\mathbf{C}}_T\underline{\mathbf{H}}^T + \underline{\mathbf{C}}_R$, *and*

$$\underline{\mathbf{\Gamma}} \triangleq \begin{bmatrix} \Re\{\mathbf{\Gamma}_1 + \mathbf{\Gamma}_2\} & -\Im\{\mathbf{\Gamma}_1 - \mathbf{\Gamma}_2\} \\ \Im\{\mathbf{\Gamma}_1 + \mathbf{\Gamma}_2\} & \Re\{\mathbf{\Gamma}_1 + \mathbf{\Gamma}_2\} \end{bmatrix}. \tag{3.16}$$

Additionally, $\underline{\mathbf{H}}$, $\underline{\mathbf{C}}_T$, *and* $\underline{\mathbf{C}}_R$ *are, respectively, the real decomposition of* $\mathbf{H}$, $\mathbf{C}_T$, *and* $\mathbf{C}_R$. *For example, if* $\mathbf{C}_T = \sigma^2\mathbf{I}_{N_T}$, *then* $\underline{\mathbf{C}}_T = \frac{1}{2}\sigma^2\mathbf{I}_{2N_T}$.

Proof. We can easily construct the real decomposition model in (3.13) from the complex model in (3.9). Now we want to derive the statistics of $\underline{\mathbf{z}}$ in (3.13). To this end, we first write the real decomposition of $\mathbf{z}$ in (3.12) as

$$\begin{bmatrix} \Re\{\mathbf{z}\} \\ \Im\{\mathbf{z}\} \end{bmatrix} = \begin{bmatrix} \Re\{\mathbf{\Gamma}_1 + \mathbf{\Gamma}_2\} & -\Im\{\mathbf{\Gamma}_1 - \mathbf{\Gamma}_2\} \\ \Im\{\mathbf{\Gamma}_1 + \mathbf{\Gamma}_2\} & \Re\{\mathbf{\Gamma}_1 + \mathbf{\Gamma}_2\} \end{bmatrix} \begin{bmatrix} \Re\{\mathbf{H}\mathbf{d_T} + \mathbf{d_R}\} \\ \Im\{\mathbf{H}\mathbf{d}_T + \mathbf{d}_R\} \end{bmatrix}, \tag{3.17}$$

which can be represented as $\underline{\mathbf{z}} = \underline{\mathbf{\Gamma}}\,(\underline{\mathbf{H}}\,\underline{\mathbf{d}}_T + \underline{\mathbf{d}}_R)$, where $\underline{\mathbf{d}}_T$ and $\underline{\mathbf{d}}_R$ are, respectively, the real decomposition of $\mathbf{d}_T$ and $\mathbf{d}_R$. The average of $\underline{\mathbf{z}}$ is simply $\mathbf{0}$ since $\mathbf{d}_R$ and $\mathbf{d}_T$ are a zero-mean random vectors. Furthermore, the covariance matrix of $\underline{\mathbf{z}}$ can be derived as (3.15). □

3.1.2 Additive hardware distortion

In this subsection, we present a model for AHWD noise based on the model in papers [8–10, 101, 111, 120, 131, 135] for a point-to-point communication system (see Fig. 3.2). That is, we

assume that the received signal is

$$\mathbf{y} = \mathbf{H}(\mathbf{x} + \boldsymbol{\eta}) + \mathbf{n}, \tag{3.18}$$

where $\mathbf{x} \in \mathbb{C}^{N_t \times 1}$, $\boldsymbol{\eta} \in \mathbb{C}^{N_t \times 1}$, $\mathbf{H} \in \mathbb{C}^{N_t \times N_r}$, and $\mathbf{n} \in \mathbb{C}^{N_r \times 1}$ are, respectively, the transmit symbol, the additive hardware distortion noise, the channel matrix between, and the additive noise at receiver k. We represent the covariance matrix of the transmitted signal by $\mathbf{P} = \mathbb{E}\{\mathbf{x}\mathbf{x}^H\}$. We consider $\mathbb{E}\{\mathbf{n}\mathbf{n}^H\} = \sigma^2 \mathbf{I}_{N_r}$, where σ^2 is the variance of each noise component. We employ the proposed framework in [8,10,120,131,135] to model the AHWD. Thus, the probability distribution of $\boldsymbol{\eta}$ is $\mathcal{CN}(\mathbf{0}, \sigma_t^2 \text{diag}(\mathbf{P}))$, where σ_t^2 is the proportionality coefficient [8]. It is worth emphasizing that the covariance matrix of the AHWD noise is diagonal, which means that there is no correlation between noise components. Moreover, the variance of each noise component is a linear function of the signal transmission power at the corresponding antenna. Thus, the higher transmission power at an antenna, the higher AHWD at the corresponding antenna.

Note that the aggregated noise in the presence of proper AHWD is proper. It is in contrast with I/Q imbalance, which makes a proper noise improper noise as indicated in Section 3.1.1. Since the noise is proper, we consider proper signals as well. However, it can be easily extended to improper signals by considering the real-decomposition method in Section 2.2.1.

Asymmetric additive hardware distortion for SISO systems

In this part, we present a hardware imperfection model for single antenna systems. We employ the distortion model in [59–61, 64] and model the aggregated effect of hardware distortion on the transceiver of a communication link with an improper Gaussian additive noise as

$$y = \sqrt{P} h(x + \eta) + n, \tag{3.19}$$

where y, x, P, h, η, and n are the received signal, transmitted symbol, transmission power, channel coefficient, aggregated hardware distortion noise and additive complex proper Gaussian noise, respectively. The aggregated hardware distortion noise is modeled as an improper complex Gaussian random variable with probability distribution $\eta \sim \mathcal{CN}(0, \sigma_\eta^2, \tilde{\sigma}_\eta^2)$, where $\sigma_\eta^2 = \sigma_{\eta_{\text{TX}}}^2 + \sigma_{\eta_{\text{RX}}}^2$ and $\tilde{\sigma}_\eta^2 = \tilde{\sigma}_{\eta_{\text{TX}}}^2 + \tilde{\sigma}_{\eta_{\text{RX}}}^2$ are the variance and complementary variance of η, respectively, both of which are composed of contributions at the transmitter side (denoted TX) and the receiver side (denoted RX). Note that we are able to simplify the system and consider the aggregated noise since the noises are scalar. This is in contrast with MIMO systems in which the noises at transmitters and receivers are vectors with different lengths. Please refer to [64, Lemma 1] for more details about this model.

Note that this model is an extension of the AHWD model, where the hardware distortion is modeled as additive proper Gaussian noise. However, as indicated in Section 3.1.1, the aggregated hardware distortion is, in general, improper due to I/Q imbalance. Note that the variances and complementary variances of AHWD noise are not only a function of device parameters, but also a linear function of the transmission power and channel gain, meaning that higher transmission power results in higher AHWD noise [60, 64]. Moreover, even if the channel noise is proper, the aggregated distortion is improper due to the asymmetric AHWD.

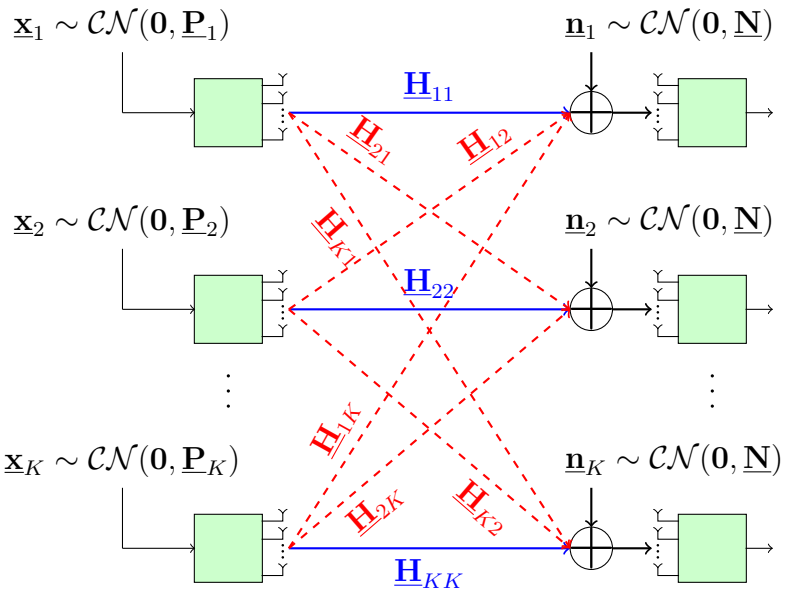

Figure 3.3: The real-decomposition channel model for the K-user MIMO IC with perfect devices.

3.2 MIMO interference-limited systems

In this section, we consider some well-known interference-limited MIMO systems and state the corresponding achievable rates when interference is treated as noise. To this end, we employ the real-decomposition method, which simplifies the representation of the rate expressions. We first consider the K-user IC with different hardware imperfection models. Then, we state the rates for underlay cognitive radio and relay channels, which can be seen as special cases of the K-user IC. As will be shown, the rates of MIMO interference-limited systems can be written as a difference of two concave functions in the covariance matrices of users when treating interference as noise. We exploit this feature to propose different IGS schemes for MIMO interference-limited systems in Chapter 4. Throughout this section, we assume that, without loss of generality, the transceivers have the same number of antennas and generate noise with the same statistics to simplify the representation of equations. Obviously, it is straightforward to extend the model to the most general case with asymmetric devices.

3.2.1 K-user interference channel

In this subsection, we consider the K-user MIMO IC with ideal and non-ideal devices. In the K-user IC, there are K transceivers in which transmitter k transmits its message to receiver k. All transceivers in the K-user IC employ the same resources, which results in interference at receiver sides as depicted in Fig. 3.3. In the following, we present the signal model for the K-user MIMO IC and state the achievable rates with different hardware assumptions. We first consider ideal devices and then study different sources of hardware imperfections.

Ideal devices

We consider a K-user MIMO IC with ideal transceivers, as shown in Fig. 3.3. In order to model impropriety, we employ the real-decomposition method in Section 2.2.1. Note it is straightfor-

ward and very similar to write the equations in a complex domain. The real decomposition of the received signal at the receiver of user k is

$$\underline{\mathbf{y}}_k = \sum_{i=1}^{K} \underline{\mathbf{H}}_{ki}\underline{\mathbf{x}}_i + \underline{\mathbf{n}}_k = \underbrace{\underline{\mathbf{H}}_{kk}\underline{\mathbf{x}}_k}_{\text{desired signal}} + \underbrace{\sum_{i=1,i\neq k}^{K} \underline{\mathbf{H}}_{ki}\underline{\mathbf{x}}_i}_{\text{interference}} + \underbrace{\underline{\mathbf{n}}_k}_{\text{noise}}, \tag{3.20}$$

where $\underline{\mathbf{x}}_i$, $\underline{\mathbf{n}}_k$, and $\underline{\mathbf{H}}_{ki}$ are, respectively, the real decompositions of the transmitted signal of user i, the noise at receiver k, and the channel matrix for the link between transmitter i and receiver k, $\mathbf{H}_{ki}$. Please refer to Section 2.2.1 for more details.

When interference is treated as noise, the rate of user $k \in \{1, 2, ..., K\}$ can be derived by [24, 94]

$$R_k = \underbrace{\frac{1}{2}\log_2 \det\left(\underline{\mathbf{N}} + \sum_{i=1}^{K} \underline{\mathbf{H}}_{ki}\,\underline{\mathbf{P}}_i\,\underline{\mathbf{H}}_{ki}^T\right)}_{\triangleq r_{k,1}} - \underbrace{\frac{1}{2}\log_2 \det\left(\underline{\mathbf{N}} + \sum_{i=1,i\neq k}^{K} \underline{\mathbf{H}}_{ki}\,\underline{\mathbf{P}}_i\,\underline{\mathbf{H}}_{ki}^T\right)}_{\triangleq r_{k,2}}, \tag{3.21}$$

where $\mathbf{P}_i$ is the covariance matrix of user i, using the real-decomposition method. Furthermore, $\underline{\mathbf{N}}$ is the covariance matrix of $\underline{\mathbf{n}}_k$ for all k. As can be observed through (4.36), the rate of a typical user k is a difference of two concave functions, i.e., $R_k = r_{k,1} - r_{k,2}$, where $r_{k,1}$ and $r_{k,2}$ are concave.

Devices with HWI and I/Q imbalance

Now, we consider a K-user MIMO IC with HWI including I/Q imbalance at transceivers, as shown in Fig. 3.4. In the presence of I/Q imbalance, the effective noise can be improper even if the noise is proper. Since the signals can be improper due to I/Q imbalance, we employ the real-decomposition method, which simplifies the analysis. To this end, we employ the HWI model in Lemma 3.2. Thus, the real decomposition of the received signal at the receiver of user k is

$$\underline{\mathbf{y}}_k = \sum_{i=1}^{K} \tilde{\mathbf{H}}_{ki}\underline{\mathbf{x}}_i + \underline{\mathbf{z}}_k = \underbrace{\tilde{\mathbf{H}}_{kk}\underline{\mathbf{x}}_k}_{\text{desired signal}} + \underbrace{\sum_{i=1,i\neq k}^{K} \tilde{\mathbf{H}}_{ki}\underline{\mathbf{x}}_i}_{\text{interference}} + \underbrace{\underline{\mathbf{z}}_k}_{\text{noise}}, \tag{3.22}$$

where $\underline{\mathbf{x}}_i$ is the real decomposition of the transmitted signal of user i, and

$$\tilde{\mathbf{H}}_{ki} = \begin{bmatrix} \Re\{\bar{\mathbf{H}}_{1,ki} + \bar{\mathbf{H}}_{2,ki}\} & -\Im\{\bar{\mathbf{H}}_{1,ki} - \bar{\mathbf{H}}_{2,ki}\} \\ \Im\{\bar{\mathbf{H}}_{1,ki} + \bar{\mathbf{H}}_{2,ki}\} & \Re\{\bar{\mathbf{H}}_{1,ki} - \bar{\mathbf{H}}_{2,ki}\} \end{bmatrix}, \tag{3.23}$$

where $\bar{\mathbf{H}}_{1,ki}$ and $\bar{\mathbf{H}}_{2,ki}$ can be derived, respectively, by replacing $\mathbf{H}$ with $\mathbf{H}_{ki}$ in (3.10) and (3.11). Note that $\mathbf{H}_{ki}$ is the channel matrix for the link between transmitter i and receiver k. Moreover, $\underline{\mathbf{z}}_k$ is the real decomposition of the noise vector $\mathbf{z}_k$, which is given by

$$\mathbf{z}_k = \mathbf{\Gamma}_1(\sum_{i=1}^{K} \mathbf{H}_{ki}\mathbf{d}_{T,i} + \mathbf{d}_{R,k}) + \mathbf{\Gamma}_2(\sum_{i=1}^{K} \mathbf{H}_{ki}\mathbf{d}_{T,i} + \mathbf{d}_{R,k})^*. \tag{3.24}$$

According to Lemma 3.2, the covariance matrix of $\underline{\mathbf{z}}_k$ is

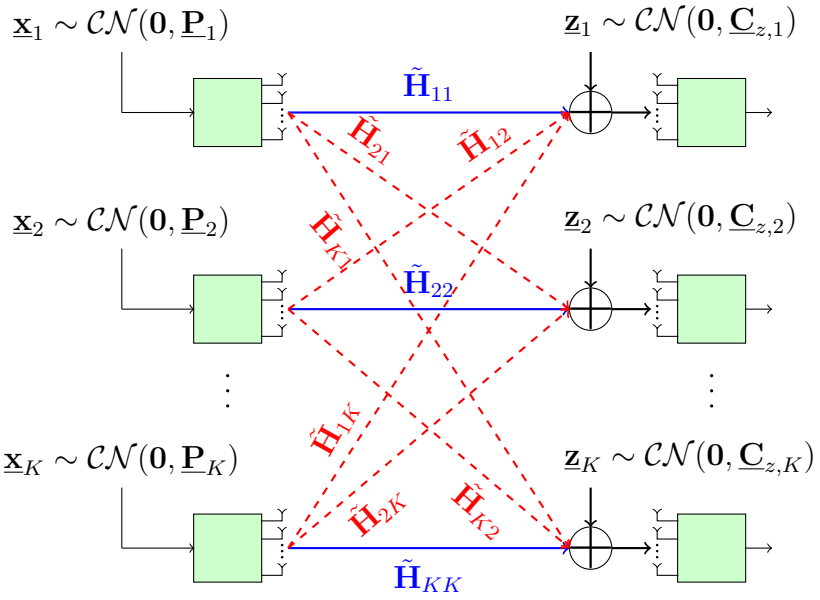

Figure 3.4: The real-decomposition channel model for the K-user MIMO IC.

$$\underline{\mathbf{C}}_{z,k} = \underline{\mathbf{\Gamma}} \left(\sum_{i=1}^{K} \underline{\mathbf{H}}_{ki} \underline{\mathbf{C}}_T \underline{\mathbf{H}}_{ki}^T + \underline{\mathbf{C}}_R \right) \underline{\mathbf{\Gamma}}^T, \tag{3.25}$$

where $\underline{\mathbf{H}}_{ki}$ is the real decomposition of $\mathbf{H}_{ki}$, and $\underline{\mathbf{\Gamma}}$ is given by (3.16). The rate of user $k \in \{1, 2, ..., K\}$ with TIN is [24, 94]

$$R_k = \underbrace{\frac{1}{2} \log_2 \det \left(\underline{\mathbf{C}}_{z,k} + \sum_{i=1}^{K} \tilde{\mathbf{H}}_{ki} \underline{\mathbf{P}}_i \tilde{\mathbf{H}}_{ki}^T \right)}_{\triangleq r_{k,1}} - \underbrace{\frac{1}{2} \log_2 \det \left(\underline{\mathbf{C}}_{z,k} + \sum_{i=1, i \neq k}^{K} \tilde{\mathbf{H}}_{ki} \underline{\mathbf{P}}_i \tilde{\mathbf{H}}_{ki}^T \right)}_{\triangleq r_{k,2}}. \tag{3.26}$$

Similar to the case with perfect devices, the rate of a typical user k is a difference of two concave functions, i.e., $R_k = r_{k,1} - r_{k,2}$, where $r_{k,1}$ and $r_{k,2}$ are concave.

Devices with AHWD

Now, we consider a K-user MIMO IC with AHWD shown in Fig. 3.5. To model the AHWD, we employ the model in Section 3.1.2. Similar to Section 3.1.2, it is not necessary to employ the real-decomposition method since the noise is proper. However, in order to model IGS, we employ the real-decomposition method. The received signal of user k is

$$\underline{\mathbf{y}}_k = \sum_{i=1}^{K} \underline{\mathbf{H}}_{ki} (\underline{\mathbf{x}}_i + \underline{\boldsymbol{\eta}}_i) + \underline{\mathbf{n}}_k = \underbrace{\underline{\mathbf{H}}_{kk} \underline{\mathbf{x}}_k}_{\text{desired signal}} + \underbrace{\sum_{i=1, i \neq k}^{K} \underline{\mathbf{H}}_{ki} \underline{\mathbf{x}}_i}_{\text{interference}} + \underbrace{\sum_{i=1}^{K} \underline{\mathbf{H}}_{ki} \underline{\boldsymbol{\eta}}_i + \underline{\mathbf{n}}_k}_{\text{aggregated noise}}, \tag{3.27}$$

where $\underline{\mathbf{x}}_i \in \mathbb{R}^{2N_T \times 1}$, $\underline{\boldsymbol{\eta}}_i \in \mathbb{R}^{2N_T \times 1}$, $\underline{\mathbf{H}}_{ki} \in \mathbb{R}^{2N_T \times 2N_R}$, and $\underline{\mathbf{n}}_k \in \mathbb{R}^{2N_R \times 1}$ are, respectively, the real decomposition of the transmit symbol of user i, the additive hardware distortion noise, the channel matrix between transmitter i and receiver k, and the additive noise at receiver k.

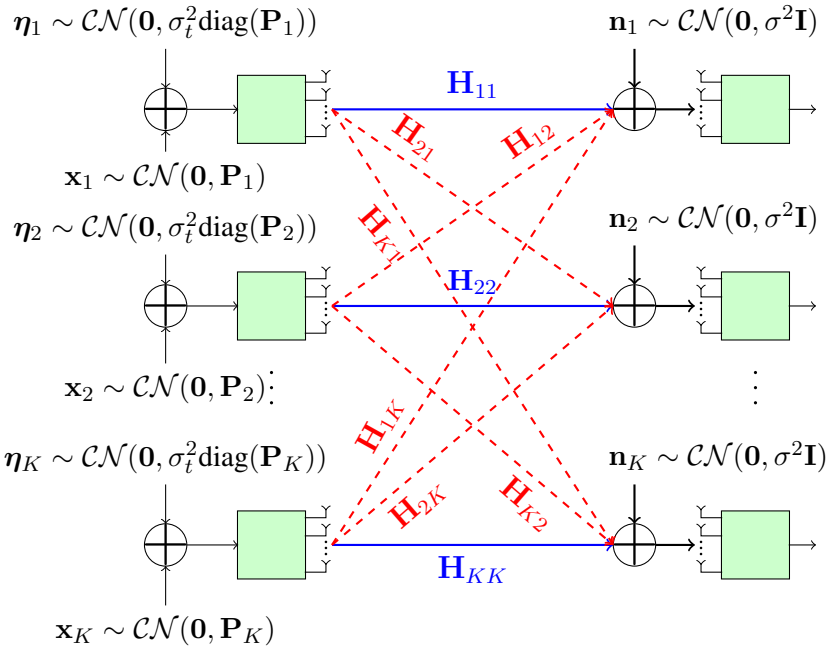

Figure 3.5: Channel model for the SISO K-user IC with ideal devices.

When interference is treated as noise, the achievable rate of user k is [24, 94]

$$R_k = \underbrace{\frac{1}{2}\log_2 \det\left(\underline{\boldsymbol{\Phi}}_{k,1}\left(\{\underline{\mathbf{P}}_i\}_{i=1}^K\right)\right)}_{\triangleq r_{k,1}} - \underbrace{\frac{1}{2}\log_2 \det\left(\underline{\boldsymbol{\Phi}}_{k,2}\left(\{\underline{\mathbf{P}}_i\}_{i=1}^K\right)\right)}_{\triangleq r_{k,2}}, \tag{3.28}$$

where

$$\underline{\boldsymbol{\Phi}}_{k,1}\left(\{\underline{\mathbf{P}}_i\}_{i=1}^K\right) = \sum_{i=1}^K \underline{\mathbf{H}}_{ki}\underline{\mathbf{P}}_i\underline{\mathbf{H}}_{ki}^T + \frac{1}{2}\sigma_t^2\sum_{i=1}^K \underline{\mathbf{H}}_{ki}\text{diag}(\underline{\mathbf{P}}_i)\underline{\mathbf{H}}_{ki}^T + \frac{1}{2}\sigma^2\mathbf{I}_{N_r}, \tag{3.29}$$

$$\underline{\boldsymbol{\Phi}}_{k,2}\left(\{\underline{\mathbf{P}}_i\}_{i=1}^K\right) = \underline{\boldsymbol{\Phi}}_{k,1}\left(\{\underline{\mathbf{P}}_i\}_{i=1}^K\right) - \underline{\mathbf{H}}_{kk}\underline{\mathbf{P}}_k\underline{\mathbf{H}}_{kk}^T. \tag{3.30}$$

Note that the rate of typical user k is a difference of two concave functions in $\{\underline{\mathbf{P}}_i\}_{i=1}^K$, i.e., $r_{k,1}$ and $r_{k,2}$ are concave in $\{\underline{\mathbf{P}}_i\}_{i=1}^K$.

For the sake of completeness, we also write the rate in complex domain signals when PGS is employed. That is,

$$R_k = \underbrace{\log_2 \det\left(\boldsymbol{\Phi}_{k,1}\left(\{\mathbf{P}_i\}_{i=1}^K\right)\right)}_{\triangleq r_{k,1}} - \underbrace{\log_2 \det\left(\boldsymbol{\Phi}_{k,2}\left(\{\mathbf{P}_i\}_{i=1}^K\right)\right)}_{\triangleq r_{k,2}}, \tag{3.31}$$

where

$$\boldsymbol{\Phi}_{k,1}\left(\{\mathbf{P}_i\}_{i=1}^K\right) = \sum_{i=1}^K \mathbf{H}_{ki}\mathbf{P}_i\mathbf{H}_{ki}^H + \sigma_t^2\sum_{i=1}^K \mathbf{H}_{ki}\text{diag}(\mathbf{P}_i)\mathbf{H}_{ki}^H + \sigma^2\mathbf{I}_{N_R}, \tag{3.32}$$

$$\boldsymbol{\Phi}_{k,2}\left(\{\mathbf{P}_i\}_{i=1}^K\right) = \boldsymbol{\Phi}_{k,1}\left(\{\mathbf{P}_i\}_{i=1}^K\right) - \mathbf{H}_{kk}\mathbf{P}_k\mathbf{H}_{kk}^H, \tag{3.33}$$

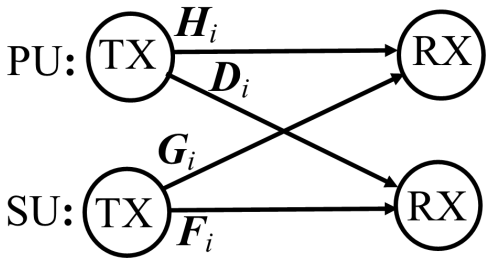

Figure 3.6: The channel model for the UCR system in subband i

where $\mathbf{P}_i$ is the complex-domain covariance matrix of user i. Note that if the users employ PGS, (3.28) would be simplified to (3.31).

3.2.2 Cognitive radio

Employing cognitive radio (CR) systems is a way to improve spectral efficiency [40,44]. In CR systems, there are two types of users, primary users (PUs) and secondary users (SUs). PUs are the licensed users, and SUs can transmit only if they do not disturb the PUs' communications. There are three types of CR systems: interweave, underlay and overlay. In interweave CR (ICR), the SUs can transmit only if the PUs do not employ the resources. In other words, the SU should listen to channel and detect the signal of the PUs. Hence, ICR is interference free. In underlay and overlay CR, which are interference limited, the SU can simultaneously transmit with PUs, but the SU should meet a quality of service (QoS) constraint for the PUs. Precisely, the rate of the PU has to be greater than a given threshold. The main difference of the underlay and overlay CR systems is in the cooperation between the SU and the PU. In underlay CR (UCR) systems, the PU is unaware of the SU. However, in overlay CR (OCR), the SU allocates parts of its transmission power to transmit the PU signals.

CR systems can be considered as a special case of the 2-user (or generally K-user) IC, and the rate expressions are very similar. On contrary, the main difference is in the priority of the users and the considered objective functions. For instance, in the K-user IC, we may want to maximize the minimum rate of users or the sum rate of the system while there is no difference between the users, and all users have the same priority. However, as indicated, the PU has a higher priority in CR, and we want to optimize a performance metric for the SU while a QoS metric for the PU is met. Another difference between the K-user IC and UCR is that the secondary system in UCR can be completely independent of the primary communication as long as the QoS constraint for the PUs is met. For instance, the secondary communication can be a multiple-access channel or a device-to-device communication, while the primary communication is a point-to-point system.

Similar to the K-user IC, there might be different CR systems such as single-antenna or multiple-antenna systems. In this subsection, we provide a simple example of an UCR system, in which both the primary and secondary systems are point-to-point-communication links as shown in Fig. 3.6. We assume that the PU and SU employ OFDM with N subbands. We further assume that the PU and SU employ N_T transmit and N_R receive antennas. We represent the transmit covariance of the PU at the ith subband with $\underline{\mathbf{P}}_{\text{PU},i}$ and the transmit covariance of the SU at the ith subband with $\underline{\mathbf{P}}_{\text{SU},i}$. The achievable rates of the PU and SU in subband i with

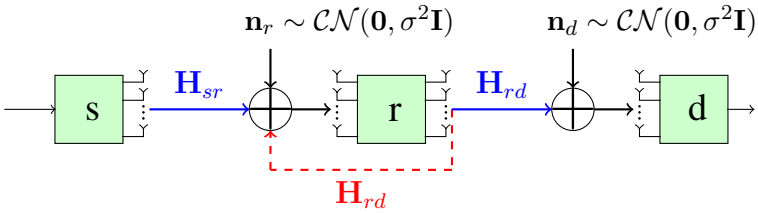

Figure 3.7: Single-hop MIMO relay channel with full-duplex relay node.

TIN are

$$R_{p,i} = \underbrace{\frac{1}{2}\log_2\left|\frac{1}{2}\sigma^2\mathbf{I} + \underline{\mathbf{H}}_i\underline{\mathbf{P}}_{\text{PU},i}\underline{\mathbf{H}}_i^T + \underline{\mathbf{G}}_i\underline{\mathbf{P}}_{\text{SU},i}\underline{\mathbf{G}}_i^T\right|}_{\triangleq r_{p,1}} - \underbrace{\frac{1}{2}\log_2\left|\frac{1}{2}\sigma^2\mathbf{I} + \underline{\mathbf{G}}_i\underline{\mathbf{P}}_{\text{SU},i}\underline{\mathbf{G}}_i^T\right|}_{\triangleq r_{p,2}},$$
$$R_{s,i} = \underbrace{\frac{1}{2}\log_2\left|\frac{1}{2}\sigma^2\mathbf{I} + \underline{\mathbf{F}}_i\underline{\mathbf{P}}_{\text{SU},i}\underline{\mathbf{F}}_i^H + \underline{\mathbf{D}}_i\underline{\mathbf{P}}_{\text{PU},i}\underline{\mathbf{D}}_i^T\right|}_{\triangleq r_{s,1}} - \underbrace{\frac{1}{2}\log_2\left|\frac{1}{2}\sigma^2\mathbf{I} + \underline{\mathbf{D}}_i\underline{\mathbf{P}}_{\text{PU},i}\underline{\mathbf{D}}_i^T\right|}_{\triangleq r_{s,2}}, \quad (3.34)$$

respectively, where σ^2, $\underline{\mathbf{H}}_i$, $\underline{\mathbf{G}}_i$, $\underline{\mathbf{F}}_i$, and $\underline{\mathbf{D}}_i$ are the variance of the additive noise, and the real decomposition of the PU-PU, SU-PU, SU-SU and PU-SU channels, respectively (see Fig. 3.6). The total achievable rate of the OFDM systems is the summation of the rates of the subbands, i.e., $R_p = \sum_{i=1}^{N} R_{p,i}$ and $R_s = \sum_{i=1}^{N} R_{s,i}$. As can be observed, the rate of the PU is a difference of two concave/convex functions is $\underline{\mathbf{P}}_{\text{SU},i}$. Furthermore, the rate of the SU is a concave function in $\underline{\mathbf{P}}_{\text{SU},i}$ when the devices are ideal. Indeed, the rate of the direct link is concave in the corresponding covariance matrix when the devices are ideal, and the rate of the interference link can be written as a difference of two concave/convex functions in the covariance matrix of the interfering users. Note that the rates in (3.34) are written base on the real-domain analysis; however, it is straightforward to apply the complex-decomposition method to derive the rates.

3.2.3 Relay channels

In a relay channel, there is no direct link between the source and destination (or the direct link is very weak), and the transmit signal of the source has to be relayed to the destination (see Fig. 3.7). Similar to CR, the relay channels can be considered as a special case of the K-user IC. The relay can be either single-hop or multi-hop. There are two main types of relay channels, amplify-and-forward (AF) relays and decode-and-forward (DF) relays. In AF relays, the relay node amplifies the received signal, which means that it amplifies both the received signal and the noise component. In DF relays, the relay node firstly decodes the signal and then, transmits the decode signal. In this section, we provide a simple example of a single-hop one-way DF relay with a full-duplex-relay node as depicted in Fig. 3.7.

Full-duplex nodes can simultaneously transmit and receive at the same channel. One of the main challenges of employing full-duplex nodes is self interference (SI), which is very complicated to be completely canceled. The received signal of the relay node in the presence of residual SI (RSI) is

$$\underline{\mathbf{y}}_r = \underbrace{\underline{\mathbf{H}}_{sr}\underline{\mathbf{x}}_s}_{\text{desired signal}} + \underbrace{\underline{\mathbf{H}}_{rr}\underline{\mathbf{x}}_r}_{\text{RSI}} + \underbrace{\underline{\mathbf{n}}_r}_{\text{noise}}, \quad (3.35)$$

where $\underline{\mathbf{x}}_s$, $\underline{\mathbf{x}}_r$, $\underline{\mathbf{n}}_r$, $\underline{\mathbf{H}}_{sr}$, and $\underline{\mathbf{H}}_{rr}$ are, respectively, the real representation of the transmit signal of the source node, the transmit signal of the relay node, the noise at the receiver of the relay node, the source-relay, and rely-relay channels. Additional, the received signal at the destination is

$$\underline{\mathbf{y}}_d = \underbrace{\underline{\mathbf{H}}_{rd}\underline{\mathbf{x}}_r}_{\text{desired signal}} + \underbrace{\underline{\mathbf{n}}_d}_{\text{noise}}, \tag{3.36}$$

where $\underline{\mathbf{n}}_d$, and $\underline{\mathbf{H}}_{rd}$ are, respectively, the real representation of the noise at the destination and the relay-destination channel.

Treating RSI as noise, we can state the achievable rate of source-relay and relay-destination links as

$$\begin{aligned} R_{sr} &= \underbrace{\frac{1}{2}\log_2\left|\frac{1}{2}\sigma^2\mathbf{I} + \underline{\mathbf{H}}_{sr}\underline{\mathbf{P}}_s\underline{\mathbf{H}}_{sr}^H + \underline{\mathbf{H}}_{rr}\underline{\mathbf{P}}_r\underline{\mathbf{H}}_{rr}^H\right|}_{\triangleq r_{sr,1}} - \underbrace{\frac{1}{2}\log_2\left|\frac{1}{2}\sigma^2\mathbf{I} + \underline{\mathbf{H}}_{rr}\underline{\mathbf{P}}_r\underline{\mathbf{H}}_{rr}^H\right|}_{\triangleq r_{sr,2}}, \\ R_{rd} &= \frac{1}{2}\log_2\left|\frac{1}{2}\sigma^2\mathbf{I} + \underline{\mathbf{H}}_{rd}\underline{\mathbf{P}}_r\underline{\mathbf{H}}_{rd}^H\right| - \frac{1}{2}\log_2\left|\frac{1}{2}\sigma^2\mathbf{I}\right|, \end{aligned} \tag{3.37}$$

respectively, where σ^2, $\underline{\mathbf{P}}_s$, and $\underline{\mathbf{P}}_r$ are, respectively, the variance of the additive noise, the covariance matrices of the transmitted signal of the source and relay nodes. As can be obeserved, the rate of the source-relay link can be written as a difference of two concave functions in $\underline{\mathbf{P}}_r$. The total rate of this relay channel is $R = \min\{R_{sr}, R_{rd}\}$.

3.3 SISO interference-limited systems

In this section, we consider single-antenna interference-limited systems. Although the achievable rate of the K-user SISO IC can be also derive with the real-decomposition method in Section 3.2, we employ a complex representation for the K-user SISO IC because it can allow us to derive computationally less expensive algorithms. Since there are less optimization parameters in SISO systems, we might be able to derive closed-form solutions for different optimization problems. The complex-domain representations help us to simplify the equations for SISO systems and get some interpretations about the performance of IGS schemes. In the following, we state the rates for the K-user SISO IC, and Z-IC.

3.3.1 K-user SISO interference channel

In this subsection, we consider the K-user SISO IC with ideal and non-ideal devices. We state the achievable rates by employing complex representations of the signals. We represent the power and complementary variance of user k by p_k and q_k, respectively. We define the feasible set of the design parameters as

$$\Omega = \{p_k, q_k \colon 0 \leq p_k \leq P_k, |q_k| \leq p_k, k = 1, 2, \cdots, K\}, \tag{3.38}$$

where P_k is the power budget of user k. Since q_k is the complementary variance of user k, its absolute value has to be not greater than the transmission power of user k, i.e., $|q_k| \leq p_k$ as indicated in Remark 2.2.

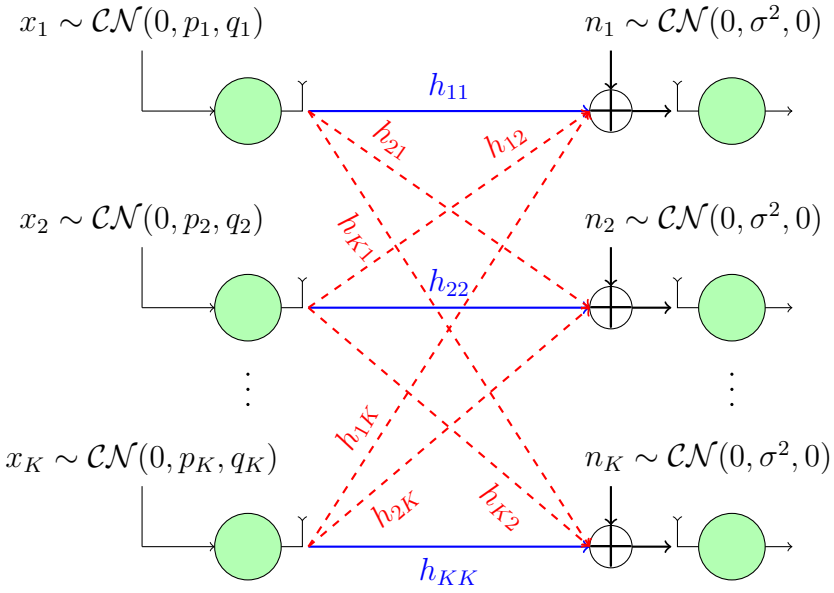

Figure 3.8: Channel model for the K-user SISO IC with ideal devices.

Ideal devices

Here, we assume that the devices are ideal. Hence, the received signal of user k is

$$y_k = \sum_{i=1}^{K} h_{ki}x_i + n_k = \underbrace{h_{kk}x_k}_{\text{desired signal}} + \underbrace{\sum_{i=1, i\neq k}^{K} h_{ki}x_i}_{\text{interference}} + \underbrace{n_k}_{\text{noise}}, \tag{3.39}$$

where x_i, h_{ki}, and n_k for $i \in \{1, \cdots, K\}$ are the transmit signal of user i, channel coefficient of the link between transmitter i and receiver k, and independent zero-mean proper complex Gaussian noise with variance σ^2, respectively.

We assume that each user is allowed to employ IGS. Thus, the achievable rate of user k is [129]

$$R_k = \frac{1}{2}\log_2\left(\frac{\left(\sigma^2 + \sum_{i=1}^{K} p_i|h_{ki}|^2\right)^2 - \left|\sum_{i=1}^{K} q_i h_{ki}^2\right|^2}{\left(\sigma^2 + \sum_{i=1, i\neq k}^{K} |h_{ki}|^2 p_i\right)^2 - \left|\sum_{i=1, i\neq k}^{K} q_i h_{ki}^2\right|^2}\right), \tag{3.40}$$

where p_i, and q_i are, respectively, the transmission power, and complementary variance of the transmitted signal of user i. We can represent the rate of user k in vector form as

$$R_k(\mathbf{p}, \mathbf{q}) = \frac{1}{2}\log_2\left(\frac{(\sigma^2 + \mathbf{a}_k^T\mathbf{p})^2 - |\mathbf{f}_k^H\mathbf{q}|^2}{(\sigma^2 + \mathbf{b}_k^T\mathbf{p})^2 - |\mathbf{g}_k^H\mathbf{q}|^2}\right), \tag{3.41}$$

where

$$\mathbf{a}_k = \begin{bmatrix} |h_{k1}|^2 & |h_{k1}|^2 & \cdots & |h_{kK}|^2 \end{bmatrix}^T, \quad \mathbf{b}_k = \mathbf{a}_k - \begin{bmatrix} 0 & 0 & \cdots & |h_{kk}|^2 & \cdots & 0 \end{bmatrix}^T, \tag{3.42}$$

$$\mathbf{f}_k = \begin{bmatrix} h_{k1}^2 & h_{k2}^2 & \cdots & h_{kK}^2 \end{bmatrix}^H, \quad \mathbf{g}_k = \mathbf{f}_k - \begin{bmatrix} 0 & 0 & \cdots & h_{kk}^2 & \cdots & 0 \end{bmatrix}^H, \tag{3.43}$$

$$\mathbf{q} = \begin{bmatrix} q_1 & q_2 & \cdots & q_K \end{bmatrix}^H, \quad \mathbf{p} = \begin{bmatrix} p_1 & p_2 & \cdots & p_K \end{bmatrix}^T. \tag{3.44}$$

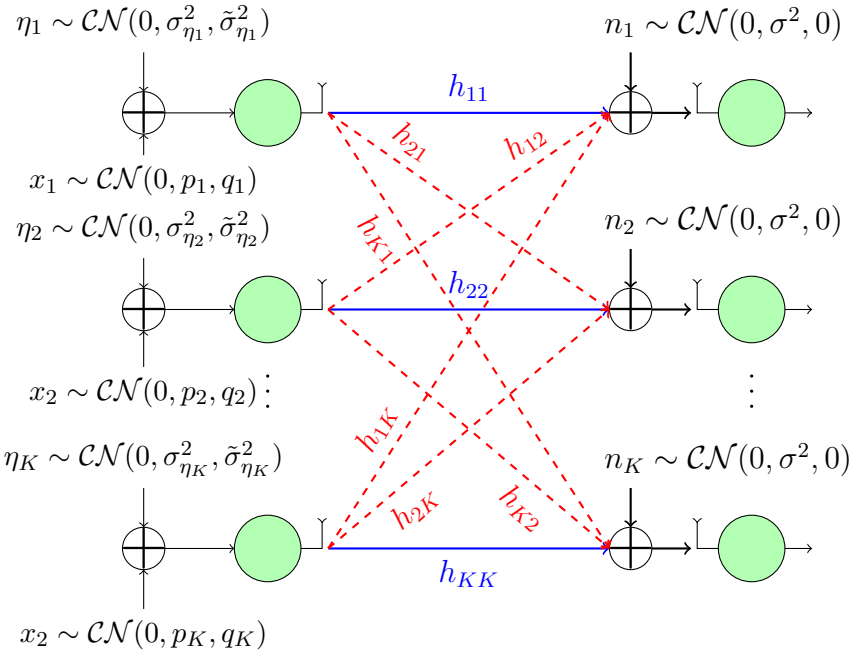

Figure 3.9: Equivalent channel model for the SISO K-user IC with AHWD.

Devices with asymmetric AHWD

Now, we consider a SISO K-user IC with asymmetric AHWD at the transceivers of users. The received signals at receiver k is

$$y_k = \sum_{i}^{K} \sqrt{p_i} h_{ki}(x_i + \eta_{ki}) + n_k = \underbrace{\sqrt{p_k} h_{kk} x_k}_{\text{desired signal}} + \underbrace{\sum_{i=1, i\neq k}^{K} \sqrt{p_i} h_i x_i}_{\text{interference}} + \underbrace{\sum_{i}^{K} \sqrt{p_i} h_{ki} \eta_i + n_k}_{\text{aggregated noise}}, \quad (3.45)$$

respectively, where x_k, h_{ki}, n_k, and η_i for $k, i \in \{1, 2, \cdots, K\}$ are the transmit signal of user k, channel between transmitter i and receiver k, independent zero-mean proper complex Gaussian noise with variance σ^2, and the aggregated hardware distortion noise of the link between transmitter i and receiver k, respectively.

Since the transmitted signals x_k for $k \in \{1, 2, \cdots, K\}$ are improper complex Gaussian, the achievable rate of user k is [59, 71, 129]

$$R_k = \frac{1}{2} \log_2 \left(\frac{\left(\sigma^2 + \sum_{i=1}^{K} p_i |h_{ki}|^2 (1 + \sigma^2_{\eta_i})\right)^2 - \left|\sum_{i=1}^{K} (q_i + p_i \tilde{\sigma}^2_{\eta_i}) h^2_{ki}\right|^2}{\left(\sigma^2 + \sum_{i=1}^{K} p_i |h_{ki}|^2 (1 + \sigma^2_{\eta_i}) - p_k |h_{kk}|^2\right)^2 - \left|\sum_{i=1}^{K} (q_i + p_i \tilde{\sigma}^2_{\eta_i}) h^2_{ki} - q_k h^2_{kk}\right|^2} \right), \quad (3.46)$$

where p_k, q_k, $\sigma^2_{\eta_i}$, and $\tilde{\sigma}^2_{\eta_i}$ for $k, i \in \{1, 2, \cdots, K\}$ are, respectively, the transmission power of user k, the complementary variance of the transmitted signal of user k, the aggregated variance and the complementary variance of the AHWD noise for user i. The rate of user k can be written using vector notation as

$$R_k = \frac{1}{2} \log_2 \left(\frac{(\sigma^2 + \mathbf{a}_k^T \mathbf{p})^2 - |\mathbf{f}_k^H \mathbf{q} + \tilde{\mathbf{f}}_k^H \mathbf{p}|^2}{(\sigma^2 + \mathbf{b}_k^T \mathbf{p})^2 - |\mathbf{g}_k^H \mathbf{q} + \tilde{\mathbf{f}}_k^H \mathbf{p}|^2} \right), \quad (3.47)$$

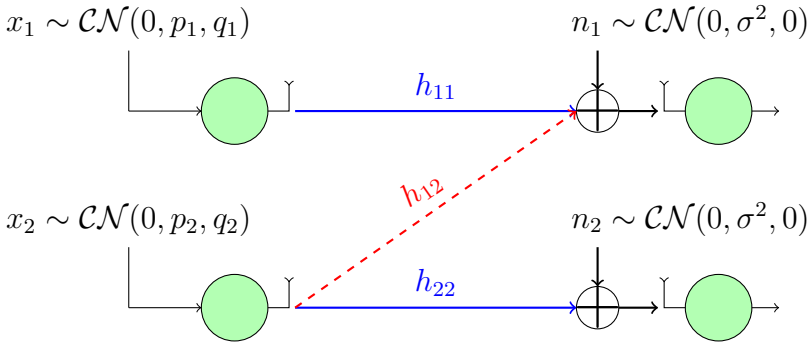

Figure 3.10: Channel model for the SISO K-user IC with ideal devices.

where $\mathbf{f}_k$, $\mathbf{g}_k$, $\mathbf{p}$, and $\mathbf{q}$ are defined in (3.43) and (3.44), and $\mathbf{a}_k$, $\mathbf{b}_k$, and $\tilde{\mathbf{f}}_k$ are given by

$$\mathbf{a}_k = \left[\begin{array}{cccc} |h_{1k}|^2(1+\sigma_{\eta_1}^2) & |h_{2k}|^2(1+\sigma_{\eta_2}^2) & \cdots & |h_{Kk}|^2(1+\sigma_{\eta_K}^2) \end{array} \right]^T, \tag{3.48}$$

$$\mathbf{b}_k = \mathbf{a}_k - \left[\begin{array}{ccccccc} 0 & 0 & \cdots & |h_{kk}|^2 & \cdots & 0 \end{array} \right]^T, \quad \tilde{\mathbf{f}}_k = \left[\begin{array}{cccc} h_{1k}^2\tilde{\sigma}_{\eta_1}^2 & h_{2k}^2\tilde{\sigma}_{\eta_2}^2 & \cdots & h_{Kk}^2\tilde{\sigma}_{\eta_K}^2 \end{array} \right]^H. \tag{3.49}$$

3.3.2 Z interference channels

Z interference channel (Z-IC) is a special case of the 2-user IC in which only one user interferes with the other user as depicted in Fig. 3.10. Assuming ideal deices, the rates of users are

$$R_1 = \frac{1}{2}\log_2\left(\frac{(\sigma^2 + |h_{11}|^2p_1 + |h_{12}|^2p_2)^2 - |h_{11}^2q_1 + h_{12}^2q_2|^2}{(\sigma^2 + |h_{12}|^2p_2)^2 - |h_{12}^2q_2|^2}\right), \tag{3.50}$$

$$R_2 = \frac{1}{2}\log_2\left(\frac{(\sigma^2 + |h_{22}|^2p_2)^2 - |h_{22}^2q_2|^2}{\sigma^4}\right), \tag{3.51}$$

where the parameters are defined as in (3.40). As can be observed, the rate expressions in the Z-IC are less complicated than those for the K-user IC, which allows us to derive simplified algorithms for the Z-IC, as will be shown in Section 8.1.4.

3.4 Summary

In this chapter, we presented some interference-limited systems with different hardware assumptions. We stated the achievable rates of the users with TIN. As indicated, the rates have a specific structures. Precisely, each rate is either a concave function (for direct links with ideal channels) or can be written as a difference of two concave/convex functions (for interference links and/or for direct links with AHWD). This feature actually comes from the definition of the capacity of a channel, which is the difference of the entropy of the received signal and the received noise [24]. The capacity achieving signaling of a point-to-point link with additive Gaussian noise is Gaussian. Moreover, the entropy of Gaussian signals involves logarithmic functions, which are concave. Hence, the achievable rate of PGS and/or IGS scheme with TIN can be written as a difference of two concave/convex functions. This feature can be exploited in optimizing different system parameters as will be discussed in the next chapter.

4 Optimization framework for MIMO interference-limited systems with TIN

In this chapter, we evaluate the performance of IGS in the K-user MIMO IC with imperfect devices by considering various utility functions. To this end, we solve different optimization problems such as the achievable rate region, sum-rate maximization, EE region and global EE maximization. In order to solve these non-convex problems, we employ an optimization framework based on majorization minimization, which can be applied to any interference-limited multiple-antenna systems with TIN. This optimization framework is an iterative suboptimal algorithm, which obtains a stationary point of every optimization problem in which the objective and/or the constraint functions are linear functions of the achievable rates. We first state the preliminaries on optimizations in Section 4.1. We then present the optimization framework in Section 4.2 and apply this framework to the aforementioned optimization problems in Section 4.3. We finally presents some numerical results in Section 4.8. Our numerical results show that IGS can be beneficial from both spectral and energy efficiency points of view in the K-user MIMO IC with imperfect devices. The results and the optimization framework, which is presented in this chapter, have been published in [106, 107].

4.1 Preliminaries on optimization algorithms

In this section, we provide some preliminaries on optimization algorithms. We first introduce convex optimization problems. We then consider non-convex optimization problems and provide some well-known optimization techniques to derive numerical solutions for some non-convex optimization problems with continuous and differentiable objective and constrain functions.

4.1.1 Convex optimization problems

Consider the following optimization problem

$$\min_{\{\mathbf{P}_k\}_{k=1}^K \in \mathcal{P}} \quad f_0\left(\{\mathbf{P}_k\}_{k=1}^K\right) \tag{4.1a}$$

$$\text{s.t.} \quad f_i\left(\{\mathbf{P}_k\}_{k=1}^K\right) \leq 0, \qquad i = 1, 2, ..., I, \tag{4.1b}$$

$$g_j\left(\{\mathbf{P}_k\}_{k=1}^K\right) = 0, \qquad j = 1, 2, ..., J, \tag{4.1c}$$

where $\{\mathbf{P}_k\}_{k=1}^K$ and $\mathcal{P}$ are, respectively, the optimization variables and the feasibility set of the variables, which is a convex set. If $f_0(\cdot)$ and $f_i(\cdot)$ for $i = 1, 2, ..., I$ are convex, and $g_j(\cdot)$ for

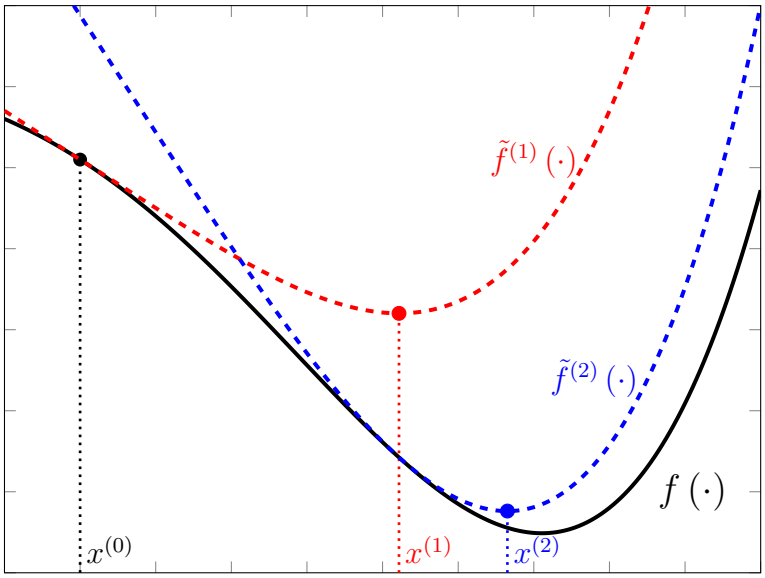

Figure 4.1: Majorization-minimization method.

$j = 1, 2, ..., J$ are affine, the optimization problem (4.1) is known as convex and can be solved in polynomial time [13]. There are powerful numerical tools to solve convex optimization problems. Among them is CVX, which is a tool box in MATLAB [41]. Throughout this thesis, we employ CVX in order to numerically solve convex optimization problems.

4.1.2 Majorization minimization

Unfortunately, most of optimization problems from practical scenarios are non-convex. In this subsection, we consider non-convex optimization problems and present an iterative approach to solve such problems numerically. In general, there is no optimization tool to derive the global optimal solution of every non-convex optimization problems in polynomial time. However, there are some powerful tools to obtain suboptimal solutions for such problems. Among them is majorization minimization[1] (MM), which includes many iterative optimization techniques such as expectation maximization (EM), sequential convex programming (SCP) and difference of convex programming (DCP) [108].

The main concept of MM is depicted in Fig. 4.1. The MM algorithm starts with a feasible arbitrary initial point, e.g., x_0 in Fig. 4.1, and consists of two steps at each iteration: majorization and minimization. In the majorization step, the algorithm majorize the non-convex optimization objective (and/or constraints) function $f(\cdot)$ by a suitable surrogate function $\tilde{f}^{(l)}(\cdot)$ in the lth iteration. In other words, the function $f(\cdot)$ is approximated (majorized) by the upper-bound function $\tilde{f}^{(l)}(\cdot)$. Then, the corresponding surrogate problem is solved in the minimization step, which gives the new point $x^{(l)}$. This procedure continues till a convergence metric is met. In the following, we describe the MM algorithm mathematically.

[1] It is also called minorization maximization for maximization problems [43].

Consider the optimization problem

$$\min_{\{\mathbf{P}_k\}_{k=1}^K \in \mathcal{P}} \quad f_0\left(\{\mathbf{P}_k\}_{k=1}^K\right) \tag{4.2a}$$

$$\text{s.t.} \quad f_i\left(\{\mathbf{P}_k\}_{k=1}^K\right) \leq 0, \qquad i = 1, 2, ..., I. \tag{4.2b}$$

If $f_0(\cdot)$ and $f_i(\cdot)$ for $i = 1, 2, ..., I$ are neither convex nor pseudo-convex, it is not straightforward to derive the global optimal solution of (4.2) in polynomial time [6,13,108,122]. However, we can obtain a suboptimal solution for (4.2) by MM. In the following lemma, we present convergence conditions of iterative algorithms such as MM.

Lemma 4.1 ([6]) *Let us define $\tilde{f}_i^{(l)}(\cdot)$ for $l \in \mathbb{N}$ as surrogate functions of $f_i(\cdot)$ for $i = 0, 1, 2, ..., I$ such that the following conditions are fulfilled:*

- $\tilde{f}_i^{(l-1)}\left(\{\mathbf{P}_k^{(l-1)}\}_{k=1}^K\right) = f_i\left(\{\mathbf{P}_k^{(l-1)}\}_{k=1}^K\right)$ *for* $i = 0, 1, 2, \cdots, I$.
- $\frac{\partial \tilde{f}_i^{(l)}\left(\{\mathbf{P}_k^{(l-1)}\}_{k=1}^K\right)}{\partial \mathbf{P}_k} = \frac{\partial f_i\left(\{\mathbf{P}_k^{(l-1)}\}_{k=1}^K\right)}{\partial \mathbf{P}_k}$ *for* $i = 0, 1, 2, \cdots, I$ *and* $k = 1, 2, \cdots, K$.
- $\tilde{f}_i^{(l)}(\cdot) \geq f_i(\cdot)$ *for* $i = 0, 1, 2, \cdots, I$ *for all feasible* $\{\mathbf{P}_k\}_{k=1}^K$,

where $\{\mathbf{P}_k^{(l-1)}\}_{k=1}^K$ is the initial point at the lth iteration of the MM algorithm, which is obtained by solving

$$\max_{\{\mathbf{P}_k\}_{k=1}^K \in \mathcal{P}} \quad \tilde{f}_0^{(l-1)}\left(\{\mathbf{P}_k\}_{k=1}^K\right) \qquad \text{s.t.} \quad \tilde{f}_i^{(l-1)}\left(\{\mathbf{P}_k\}_{k=1}^K\right) \geq 0, \quad i = 1, 2, ..., I. \tag{4.3}$$

Then, the sequence of $\{\mathbf{P}_k^{(l)}\}_{k=1}^K$ converges to a stationary point of (4.2).

Remark 4.1 *The surrogate optimization problem* (4.3) *is not necessarily convex; however, we can obtain the global optimal solution of* (4.3) *much easier than* (4.2).

Remark 4.2 *The MM algorithm depends on the initial point since this algorithm generally converges to a stationary point of the original problem.*

The challenging part in MM algorithms is to find suitable surrogate functions, which depends on the structure of the objective and constraint functions. In general, there are different approaches to obtain a surrogate function (see, e.g., [108]), and the main difference of MM algorithms is in the approach for finding the corresponding surrogate functions. Throughout this thesis, we mainly optimize the achievable rate and/or energy-efficiency of users. Hence, we focus only on MM algorithms, which might be required for such optimizations.

The rate functions are continuous and differentiable in the powers/covariance matrices of users. Depending on the considered scenario, a rate function can be concave, convex or a difference of two concave/convex functions in the powers/covariance matrices of users, as will be discussed in Chapter 3. Thus, we are able to derive suitable surrogate functions for achievable rates by the concave-convex (and/or convex-concave) procedure (CCP). The idea of CCP comes from Fig. 4.2. Suppose that we have a convex function f_{cvx}, an affine function f_{aff}, and a concave function f_{ccv}, which have the same value and the same derivative at point $x^{(\star)}$. Then for all feasible x, the following inequality holds

$$f_{\text{ccv}}(x) \leq f_{\text{aff}}(x) \leq f_{\text{cvx}}(x). \tag{4.4}$$

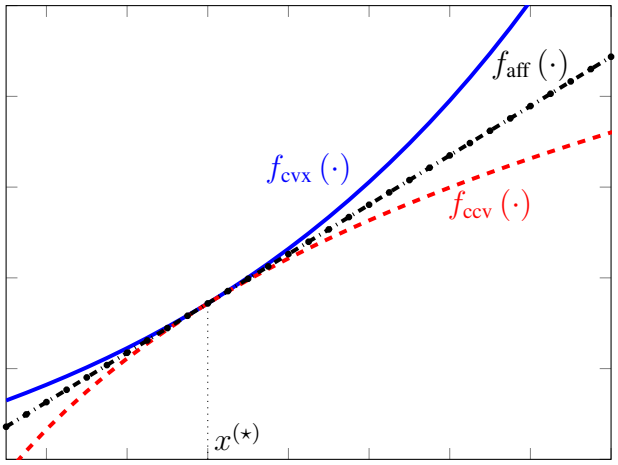

Figure 4.2: Majorization-minimization method.

It means that we can derive an upper (lower) bound for a concave (convex) function by approximating it with an affine (linear) function. A way to approximate a function by a linear function is to employ the first-order Taylor expansion, which is the main idea for the CCP as presented in the following lemma.

Lemma 4.2 (Concave-convex procedure [75]) *An upper (lower) bound for a concave (convex) function $g(\cdot)$ can be derived by*

$$g\left(\{\mathbf{P}_k\}_{k=1}^K\right) \leq g\left(\{\mathbf{P}_k^{(\star)}\}_{k=1}^K\right) + \sum_{k=1}^K \left(\frac{\partial g\left(\{\mathbf{P}_k^{(\star)}\}_{k=1}^K\right)}{\partial \mathbf{P}_k}\right)^H \left(\mathbf{P}_k - \mathbf{P}_k^{(\star)}\right), \tag{4.5}$$

where $\{\mathbf{P}_k\}_{k=1}^K$ are the variables and $\{\mathbf{P}_k^{(\star)}\}_{k=1}^K$ is an arbitrary feasible point.

In this thesis, we mostly employ SCP and DCP among all MM algorithms. In SCP, the surrogate functions are chosen such that the surrogate optimization problem is convex. In other words, SCP obtains a stationary point of a non-convex optimization problem by solving a sequence of convex problems. A special case of SCP is DCP in which the objective and/or constraints are a difference of two convex/concave functions. In this case, we can apply CCP to approximate the concave parts of functions by affine functions, which makes the surrogate optimization problem convex. Examples of DCP and SCP are provided in Chapters 4, 6, 7, 5, where we applied these techniques to different practical scenarios in IGS. For more details about CCP, the readers can refer to [75].

4.1.3 Semi-definite relaxation (SDR) for quadratic optimization problems

In this subsection, we consider non-convex quadratic optimization problems and present a suboptimal approach to derive numerical solutions for such problems. Let us consider the following

non-convex complex-domain optimization problem

$$\min_{\mathbf{x}} \quad \mathbf{x}^H \mathbf{A}_0 \mathbf{x} \tag{4.6a}$$

$$\text{s.t.} \quad \mathbf{x}^H \mathbf{A}_i \mathbf{x} \trianglerighteq_i b_i, \qquad i = 1, 2, ..., I, \tag{4.6b}$$

where $\mathbf{x}$ is the optimization vector, $\mathbf{A}_i$ and b_i for $i = 0, 1, \cdots, I$ are constant and given. Additionally, $\trianglerighteq$ is chosen to simplify the notations and can be either "$\leq$", "$=$", or "$\geq$". The optimization problem (4.6) is in general non-convex due to the constraints with "$\geq$". A way to derive a suboptimal solution for (4.6) is to employ semi-definite programming (SDP) and semi-definite relaxation (SDR), which follows a simple idea as describe in the following.

Consider the quadratic term $\mathbf{x}^H \mathbf{A} \mathbf{x}$, which is scalar. We can simply verify that

$$\mathbf{x}^H \mathbf{A} \mathbf{x} = \text{Tr}\left(\mathbf{x}^H \mathbf{A} \mathbf{x}\right) = \text{Tr}\left(\mathbf{A} \mathbf{x} \mathbf{x}^H\right). \tag{4.7}$$

Let us define $\mathbf{X} = \mathbf{x}\mathbf{x}^H$, which is a rank-one Hermitian matrix. Now we rewrite (4.6) as

$$\min_{\mathbf{X}} \quad \text{Tr}\left(\mathbf{A}_0 \mathbf{X}\right) \tag{4.8a}$$

$$\text{s.t.} \quad \text{Tr}\left(\mathbf{A}_0 \mathbf{X}\right) \trianglerighteq_i b_i, \qquad i = 1, 2, ..., I, \tag{4.8b}$$

$$\mathbf{X} \succcurlyeq 0, \qquad \text{rank}(\mathbf{X}) = 1. \tag{4.8c}$$

The optimization problem (4.8), which is equivalent to (4.6), is still non-convex and difficult to solve. The main idea of SDR is to relax the rank-one constraint and solve the following linear optimization problem

$$\min_{\mathbf{X}} \quad \text{Tr}\left(\mathbf{A}_0 \mathbf{X}\right) \tag{4.9a}$$

$$\text{s.t.} \quad \text{Tr}\left(\mathbf{A}_0 \mathbf{X}\right) \trianglerighteq_i b_i, \qquad i = 1, 2, ..., I, \tag{4.9b}$$

$$\mathbf{X} \succcurlyeq 0. \tag{4.9c}$$

The optimization problem (4.9) is convex, and its global optimal solution $\mathbf{X}^{(\star)}$ can be easily obtained. If $\mathbf{X}^{(\star)}$ is rank one, it is also the global optimal solution of (4.6). Otherwise, it is not a valid solution for (4.6). Unfortunately, it is not ensured that $\mathbf{X}^{(\star)}$ is rank one for every quadratic optimization problem, which means that the solution of (4.9) cannot be taken for (4.6). However, we may be able to use $\mathbf{X}^{(\star)}$ to generate a good suboptimal solution for (4.6). There are few approaches to obtain solutions for (4.6) from $\mathbf{X}^{(\star)}$. Among them is Gaussian randomization [78]. That is, we generate many random vectors $\mathbf{x}$ from a zero-mean proper complex Gaussian distribution with covariance matrix $\mathbf{X}^{(\star)}$ and choose the best solution, $\mathbf{x}^{(\star)}$, among them.

The optimization problem in (4.6) is a homogeneous quadratic problem. SDR can be also applied to inhomogeneous quadratic problems such as

$$\min_{\mathbf{x}} \quad \mathbf{x}^H \mathbf{A}_0 \mathbf{x} + 2\mathfrak{R}\left\{\mathbf{b}_0^H \mathbf{x}\right\} \tag{4.10a}$$

$$\text{s.t.} \quad \mathbf{x}^H \mathbf{A}_i \mathbf{x} + 2\mathfrak{R}\left\{\mathbf{b}_i^H \mathbf{x}\right\} \trianglerighteq_i c_i, \qquad i = 1, 2, ..., I, \tag{4.10b}$$

where $\mathbf{A}_i \mathbf{x}$, $\mathbf{b}_i$, and c_i for $i = 1, 2, ..., I$ are given and constant. In order to apply SDR to (4.10),

we introduce a new scalar real-valued variable t and rewrite (4.10) as

$$\min_{\mathbf{x},t} \quad \left[\begin{array}{cc} \mathbf{x}^H & t \end{array}\right] \left[\begin{array}{cc} \mathbf{A}_0 & \mathbf{b}_0 \\ \mathbf{b}_0^H & 0 \end{array}\right] \left[\begin{array}{c} \mathbf{x} \\ t \end{array}\right] \tag{4.11a}$$

$$\text{s.t.} \quad \left[\begin{array}{cc} \mathbf{x}^H & t \end{array}\right] \left[\begin{array}{cc} \mathbf{A}_i & \mathbf{b}_i \\ \mathbf{b}_i^H & 0 \end{array}\right] \left[\begin{array}{c} \mathbf{x} \\ t \end{array}\right] \trianglerighteq_i c_i, \qquad i = 1, 2, ..., I, \tag{4.11b}$$

$$t^2 = 1. \tag{4.11c}$$

Now we define new parameters $\mathbf{x}' = \left[\begin{array}{cc} \mathbf{x}^H & t \end{array}\right]^H$ and

$$\mathbf{A}_i' = \left[\begin{array}{cc} \mathbf{A}_i & \mathbf{b}_i \\ \mathbf{b}_i^H & 0 \end{array}\right], \tag{4.12}$$

for $i = 0, 1, 2, ..., I$. Substituting these parameters in (4.11), we have

$$\min_{\mathbf{x}} \quad \mathbf{x'}^H \mathbf{A}_0' \mathbf{x}' \tag{4.13a}$$

$$\text{s.t.} \quad \mathbf{x'}^H \mathbf{A}_i' \mathbf{x}' \trianglerighteq_i b_i, \qquad i = 1, 2, ..., I, \tag{4.13b}$$

which is similar to (4.6) and thus, can be solved similarly.

Comparison to MM

Note that SDR is in general a suboptimal algorithm similar to MM-based algorithms. If we compare these algorithms, we can say that MM-based algorithms are generally more powerful since they can be applied to a wide-range of optimization problem. Moreover, MM algorithms converge to a stationary point of the problem; however, SDR algorithms do not fulfill any optimality constraint due to the Gaussian randomization. In [78], it is suggested that in some applications, we can use MM-based algorithms and SDR algorithms as a complementary of each other rather than competitors. That is, MM algorithms depend on an initial point, which can be obtained by SDR algorithms. The readers are referred to [78] for more details and applications of SDR in signal processing.

4.1.4 Dinkelbach-based algorithms for fractional problems

In this section, we consider fractional-programming (FP) and present a powerful solver for fractional optimization problems. An example of fractional functions in wireless communications is an energy-efficiency (EE) function, which is defined as the ratio of the achievable rate to the total power consumption as will be discussed with more details in Section 4.5, Section 4.6, Chapter 6, and Chapter 7. Fractional optimization problems can be divided into two main categories: single-ratio optimizations and max-min optimizations. In single-ratio FP, a single fractional function is optimized over a compact set. However, in max-min FP, the minimum of multiple fractional functions is maximized, which is more challenging. Note that the optimization parameters can be scalars, vectors and even matrices in this subsection.

Single-ratio fractional programming

Consider the following optimization problem

$$\max_{\mathbf{x}\in\mathcal{X}} \ \frac{u(\mathbf{x})}{v(\mathbf{x})}, \tag{4.14}$$

where $\mathbf{x}$ is the optimization variable, and $\mathcal{X}$ is the feasiblity set, which is a compact set. The optimization problem (4.14) is called single-ratio fractional programming. We assume $u(\mathbf{x}) \geq 0$ and $v(\mathbf{x}) > 0$ are continuous real-valued functions, which is the case in the considered optimization problems in this thesis. A way to solve (4.14) is to employ Dinkelbach algorithm, which falls into parametric algorithms [25, 30, 126]. Parametric algorithms are iterative, similar to MM algorithms, and we solve an optimization problem by solving a sequence of surrogate problems, which can be solved easier than the original problem [58, 126]. However, surrogate functions for parametric algorithms are generally chosen in a different way comparing to MM algorithms.

Dinkelbach's algorithm is a powerful tool that can achieve the global optimal solution of (4.14). This algorithm was originally proposed for the case that $u(\mathbf{x})$ is concave, and $v(\mathbf{x})$ is convex. However, the algorithm can still converge to the optimal solution of (4.14) even if $u(\mathbf{x})$ and $-v(\mathbf{x})$ are not concave as will be discussed in the following. The Dinkelbach algorithm is an iterative algorithm, which employs the following function in each iteration

$$V(\mu) = \max_{\mathbf{x}\in\mathcal{X}} \ u(\mathbf{x}) - \mu v(\mathbf{x}), \tag{4.15}$$

This function satisfies the conditions presented in the following lemma, which are essential for the convergence of the Dinkelbach algorithm.

Lemma 4.3 ([30, 58, 126]) *Consider the fractional function $\frac{u(\mathbf{x})}{v(\mathbf{x})}$, where $u(\mathbf{x})$ and $v(\mathbf{x})$ are continuous in $\mathbf{x}$, $v(\mathbf{x})$ is strictly positive in $\mathbf{x}$, and $\mathbf{x}$ is a vector with dimension n that belongs to a compact set $\mathcal{X}$. Let us define*

$$V(\mu) = \max_{\mathbf{x}\in\mathcal{X}} \ u(\mathbf{x}) - \mu v(\mathbf{x}), \tag{4.16}$$

$$\mu^{(\star)} = \max_{\mathbf{x}} \ \frac{u(\mathbf{x})}{v(\mathbf{x})}, \tag{4.17}$$

where $V(\mu)$, $\mu^{(\star)}$, and μ are real and scalar, and have the following properties.

1. *$V(\mu)$ is continuous and strictly decreasing in μ.*
2. *The optimization problems* (4.26) *and* (4.27) *always have optimal solutions.*
3. *$\mu^{(\star)}$ is finite and $V(\mu^{(\star)}) = 0$.*
4. *$V(\mu)$ has a unique root, and $V(\mu) = 0$ implies $\mu = \mu^{(\star)}$.*

The Dinkelbach algorithm employs the results in Lemma 4.3 to obtain the global optimal solution of (4.14). According to Lemma 4.3, there is a connection between $V(\mu)$ and the optimization problem in (4.14). Particularly, $V(\mu)$ is strictly decreasing in μ and has a unique root

$\mu^{(\star)}$, which is the global optimal solution of (4.14), i.e., $\mu^{(\star)} = \frac{u(\mathbf{x}^{(\star)})}{v(\mathbf{x}^{(\star)})}$, where $\mathbf{x}^{(\star)}$ is

$$\mathbf{x}^{(\star)} = \arg \max_{\mathbf{x}\in\mathcal{X}} \frac{u(\mathbf{x})}{v(\mathbf{x})}. \tag{4.18}$$

Dinkelbach proposed an algorithm in [30] to obtain the unique root of $V(\mu)$. Note that there might be other algorithms such as the bisection method to derive the unique root of $V(\mu)$, and the Dinkelbach algorithm is not the only way to obtain $\mu^{(\star)}$.

The Dinkelbach algorithm is an iterative algorithm, which employs the surrogate function $V(\mu)$ in (4.14) and tries to find its unique root $\mu^{(\star)}$. The algorithm starts with an initial point, e.g., $\mu^{(0)} = \frac{u(\mathbf{x}^{(0)})}{v(\mathbf{x}^{(0)})}$, where $\mathbf{x}^{(0)}$ is an arbitrary feasible point. Then the algorithm updates μ to obtain $\mu^{(\star)}$. Since $V(\mu)$ is continuous and strictly decreasing in μ, μ is chosen monotonically increasing at each iteration ($\mu^{(l)} > \mu^{(l-1)}$) until $V(\mu)$ approaches 0. At the lth iteration, $\mu^{(l)}$ is

$$\mu^{(l)} = \frac{u(\mathbf{x}^{(l)})}{v(\mathbf{x}^{(l)})} > 0, \tag{4.19}$$

where $\mathbf{x}^{(l)}$ is

$$\mathbf{x}^{(l)} = \arg \max_{\mathbf{x}} \left(u(\mathbf{x}) - \mu^{(l-1)} v(\mathbf{x}) \right). \tag{4.20}$$

The Dinkelbach algorithm updates $\mu^{(l)}$ and $\mathbf{x}^{(l)}$ based on (4.19) and (4.20), respectively, until a convergence metric is met, e.g., $V(\mu^{(l)}) < \varepsilon$, where $\varepsilon > 0$. We summarize the Dinkelbach algorithm in the following lemma.

Lemma 4.4 *Consider the following fractional optimization problem*

$$\max_{\{\mathbf{x}\}\in\mathcal{X}} \frac{v(\mathbf{x})}{u(\mathbf{x})}, \tag{4.21}$$

where $\mathcal{X}$ is a compact set. The global optimal solution of (4.21) *can be derived, iteratively, by the Dinkelbach algorithm, i.e., by solving*

$$\max_{\{\mathbf{x}\}\in\mathcal{X}} v(\mathbf{x}) - \mu^{(l)} u(\mathbf{x}), \tag{4.22}$$

where $\mu^{(l)}$ is constant and given by

$$\mu^{(l)} = \frac{v\left(\mathbf{x}^{(l)}\right)}{u\left(\mathbf{x}^{(l)}\right)}, \tag{4.23}$$

where $\mathbf{x}^{(l)}$ is the solution of (4.22) *at the $(l-1)$th iteration. Note that the Dinkelbach algorithm converges to the global optimal solution of* (4.14) *with a super-linear rate.*

Proof. Please refer to [25, 101, 126]. □

Remark 4.3 *The Dinkelbach algorithm converges to the global optimal solution of* (4.14) *only if the global optimal solution of* (4.22) *is obtained.*

According to Remark 4.3, the optimization problem (4.22) should be perfectly solved in order to ensure the convergence of the algorithm to the global optimal solution. When $v(\mathbf{x})$ and $-u(\mathbf{x})$ are concave for $v \geq 0$ and $u > 0$, the optimization problem (4.22) is convex, and its global optimal solution can be achieved easily. When (4.22) is non-convex, it might be challenging to obtain its global optimal solution as discussed in Section 4.1. However, it is still possible to apply the Dinkelbach algorithm to such problems, and only the optimization part might be challenging.

Remark 4.4 *The Dinkelbach algorithm still converges even if the global optimal solution of* (4.22) *is not attained. However, it is not ensured that the algorithm converges to the global optimal solution. Indeed, the Dinkelbach algorithm converges to a suboptimal solution if a suboptimal solution of* (4.22) *is obtained.*

We can still apply Dinkelbach algorithm to obtain suboptimal solutions for the cases that (4.22) is non-convex and very difficult to be perfectly solved, as indicated in Remark 4.4. That is, we can combine the Dinkelbach algorithm with MM algorithms. In such case, we first apply the MM algorithm to $\frac{v}{u}$ to obtain a suitable surrogate function $\frac{\tilde{v}}{\tilde{u}}$, which can be easily solved by the Dinkelbach algorithm. An example of this approach is provided in Section 4.6, where we maximize the global EE of the K-user MIMO IC, which is a non-concave single-ratio fractional function.

Max-min fractional programming

Consider the following fractional optimization problem

$$\max_{\{\mathbf{x}\}\in\mathcal{X}} \quad \min_{1\leq k\leq K} \left\{ \frac{v_k(\mathbf{x})}{u_k(\mathbf{x})} \right\}, \tag{4.24}$$

where $\mathcal{X}$ is a compact set. It is called max-min FP or multiple-ratio FP. A way to solve (4.24) is to extend the Dinkelbach algorithm, which is called the generalized Dinkelbach algorithm (GDA). The GDA is a modified version of the Dinkelbach algorithm to solve maximin multiple-ratio problems [25]. Similar to the Dinkelbach algorithm, the GDA is an iterative approach in which the fractional functions are approximated by surrogate functions at each iteration. The only difference between the Dinkelbach algorithm and the GDA is that the GDA employs the following surrogate function

$$V(\mu) = \max_{\mathbf{x}} \ \min_{k} \left(u_k(\mathbf{x}) - \mu v_k(\mathbf{x}) \right), \tag{4.25}$$

which is also similar to (4.14) and follows the same properties as discussed in the following lemma.

Lemma 4.5 ([25, 126]) *Consider the fractional functions* $\frac{u_k(\mathbf{x})}{v_k(\mathbf{x})}$*, where* $u_k(\mathbf{x})$ *and* $v_k(\mathbf{x})$ *are continuous in* $\mathbf{x}$*,* $v_k(\mathbf{x})$ *is strictly positive in* $\mathbf{x}$*, and* $\mathbf{x}$ *is a vector with dimension* n *that belongs to a compact set* $\mathcal{X}$*. Let us define*

$$V(\mu) = \max_{\mathbf{x}} \ \min_{k} \left(u_k(\mathbf{x}) - \mu v_k(\mathbf{x}) \right), \tag{4.26}$$

$$\mu^{(\star)} = \max_{\mathbf{x}} \ \min_{k} \left(\frac{u_k(\mathbf{x})}{v_k(\mathbf{x})} \right), \tag{4.27}$$

where $V(\mu)$, $\mu^{(\star)}$, and μ are real and scalar, and have the following properties.

1. *$V(\mu)$ is continuous and strictly decreasing in μ.*
2. *The optimization problems* (4.26) *and* (4.27) *always have optimal solutions.*
3. *$\mu^{(\star)}$ is finite and $V(\mu^{(\star)}) = 0$.*
4. *$V(\mu)$ has a unique root, and $V(\mu) = 0$ implies $\mu = \mu^{(\star)}$.*

The GDA follows the same concept and approach as the Dinkelbach algorithm and converges to the global optimal solution of (4.24) if the optimization problem in (4.25) is perfectly solved, similar to the Dinkelbach algorithm. It is worth noting that the GDA converges linearly to the optimal solution [25], but the Dinkelbach algorithm converges super linearly to the optimal solution [126]. Since the GDA performs very similar to the Dinkelbach algorithm, we present only a summary of the GDA in the following lemma and refer the readers to the Dinkelbach for more details and discussions.

Lemma 4.6 *Consider the following fractional optimization problem*

$$\max_{\{\mathbf{x}\}\in\mathcal{X}} \quad \min_{1\leq k\leq K} \left\{ \frac{v_k(\mathbf{x})}{u_k(\mathbf{x})} \right\}, \tag{4.28}$$

where $\mathcal{X}$ is a compact set. The global optimal solution of (4.28) *can be derived, iteratively, by the GDA, i.e., by solving*

$$\max_{t,\{\mathbf{x}\}\in\mathcal{X}} \quad t \tag{4.29a}$$

$$\text{s.t.} \qquad v(\mathbf{x}) - \mu^{(l)} u(\mathbf{x}) \geq t, k = 1, 2, ..., K, \tag{4.29b}$$

where $\mu^{(l)}$ is constant and given by

$$\mu^{(l)} = \min_{1\leq k\leq K} \left\{ \frac{v\left(\mathbf{x}^{(l)}\right)}{u\left(\mathbf{x}^{(l)}\right)} \right\}, \tag{4.30}$$

where $\mathbf{x}^{(l)}$ is the solution of (4.29) *at the $(l-1)$th iteration.*

Proof. Please refer to [25, 101, 126]. □

The discussions about the Dinkelbach algorithm can be extended to the GDA. For instance, in order to apply the GDA, it is not required that $u_k(\mathbf{x})$ and $v_k(\mathbf{x})$ fulfill any other condition (except those in the lemma), which makes this algorithm a powerful tool to solve different types of fractional problems. If $u_k(\mathbf{x})$ and $v_k(\mathbf{x})$ are concave and convex functions, respectively, the optimization problem at each iteration is convex and can easily be solved. However, in the general case, it might be difficult to efficiently solve the optimization problem at each iteration. Furthermore, the GDA can be combine with MM algorithms to obtain suboptimal solutions as mentioned in the previous subsection. We will discuss this approach and apply it to solve non-convex optimization problems in Section 4.5, Chapter 6, and Chapter 7 for different network scenarios as well as different objective functions.

4.2 Optimization framework for MIMO systems

In this section, we present a framework based on MM to solve different optimization problems in which either the objective function and/or constraints are linear functions of the rates. In this approach, we employ the real-decomposition method because, by this method, the rates can be written as a difference of two concave functions, which enables us to employ MM and solve the corresponding optimization problem iteratively. The proposed framework can be applied to both IGS and PGS schemes. Since we employ the real-decomposition method, the only difference of IGS and PGS schemes is the feasibility set of the covariance matrices. As indicated in Lemma 2.2, an improper Gaussian random variable can have an arbitrary symmetric and positive semi-definite covariance matrix. Thus, the feasibility set of the covariance matrices of users $\{\underline{\mathbf{P}}_k\}_{k=1}^K$ for IGS is

$$\mathcal{P}_{\text{IGS}} = \left\{ \{\underline{\mathbf{P}}_k\}_{k=1}^K : \text{Tr}(\underline{\mathbf{P}}_k) \leq P_k,\ \underline{\mathbf{P}}_k \succcurlyeq \mathbf{0}, k = 1, 2, \cdots, K \right\}, \tag{4.31}$$

where P_k is the power budget of user K. It is in contrast to a proper Gaussian signal, which has a covariance matrix with the specific structure in Lemma 2.2. In this case, the feasibility set is

$$\mathcal{P}_{\text{PGS}} = \left\{ \{\underline{\mathbf{P}}_k\}_{k=1}^K : \text{Tr}(\underline{\mathbf{P}}_k) \leq P_k,\ \underline{\mathbf{P}}_k = \underline{\mathbf{P}}_{x_k},\ \underline{\mathbf{P}}_k \succcurlyeq \mathbf{0},\ k = 1, 2, \cdots, K \right\}, \tag{4.32}$$

where $\underline{\mathbf{P}}_{x_k}$ has the structure in (2.3). In order to include both IGS and PGS schemes in the derivations to follow, we denote the feasibility set of the covariance matrices as $\mathcal{P}$ hereafter.

We can apply this framework to different sources of hardware imperfections such as I/Q imbalance and/or AHWD. As shown in Section 3.2.1, the rate of user k with theses imperfections can be written as a difference of two concave function as

$$R_k = r_{k,1}\left(\{\underline{\mathbf{P}}_i\}_{i=1}^K\right) - r_{k,2}\left(\{\underline{\mathbf{P}}_i\}_{i=1}^K\right). \tag{4.33}$$

This allows us to apply CCP to obtain a suitable surrogate function. That is, we approximate the convex part of the rate expressions, $-r_{k,2}$, as a linear function by the first-order Taylor expansion. By MM and CCP, we are able to obtain a stationary point of different optimization problems in which either the objective or constraint functions are linear functions of the rates of the users. In the following lemmas, we present the surrogate functions for the rates.

Lemma 4.7 ([106]) *Using CCP, we can obtain an affine upper bound for* $\log\det(\mathbf{Q})$ *as*

$$\log\det(\mathbf{Q}) \leq \log\det\left(\mathbf{Q}^{(l)}\right) + \text{Trace}((\mathbf{Q}^{(l)})^{-1}(\mathbf{Q} - \mathbf{Q}^{(l)})), \tag{4.34}$$

where $\mathbf{Q}^{(l)}$ *is any feasible fixed point.*

Proof. A concave function can be majorized by an affine function if these two functions have the same value and the same derivative in a point [108]. The logarithmic function is concave. Furthermore, the left-hand and the right-hand sides of (4.34) hold these condition at $\mathbf{Q} = \mathbf{Q}^{(l)}$. Thus, the upper-bound in (4.34) holds for all feasible $\mathbf{Q}$. Note that the derivative of $\log\det(\mathbf{Q})$ with respect to $\mathbf{Q}$ is $\mathbf{Q}^{-1}$. □

Lemma 4.8 *A concave approximation of the rates in* (4.33) *can be obtained by CCP as*

$$R_k \geq \tilde{R}_k^{(l)} = r_{k,1} - r_{k,2}\left(\{\underline{\mathbf{P}}_i^{(l)}\}_{i=1}^K\right) - \text{Tr}\left(\sum_{i=1}^K \frac{\partial r_{k,2}\left(\{\underline{\mathbf{P}}_i^{(l)}\}_{i=1}^K\right)^T}{\partial \underline{\mathbf{P}}_i}(\underline{\mathbf{P}}_i - \underline{\mathbf{P}}_i^{(l)})\right) \tag{4.35}$$

where $r_{k,1}$ and $r_{k,2}$ are, respectively, the concave and convex parts of R_k in (3.26)*. Moreover, $\frac{\partial r_{k,2}\left(\{\underline{\mathbf{P}}_i^{(l)}\}_{i=1}^K\right)}{\partial \underline{\mathbf{P}}_i}$ is the derivative of $r_{k,2}$ with respect to $\underline{\mathbf{P}}_i$ at the previous iteration. Note that $r_{k,2}\left(\{\underline{\mathbf{P}}_i^{(l)}\}_{i=1}^K\right)$ is constant and is given by $r_{k,2}$ at the previous step. Additionally, R_k and $\tilde{R}_k^{(l)}$ fulfill the conditions in Lemma* 4.1.

Remark 4.5 *This optimization framework can be applied to both real-domain and complex-domain problems. Note that if we want to model IGS (or generally* improper signals*), we should employ the real-decomposition method to be able to use this optimization framework. However, if we deal with only proper signals, we can use complex representations, which is much easier than the real representation for proper signals. Note that we should use Hermitian in* (4.35) *instead of transpose when we employ complex-domain signals.*

In the following lemmas, we state the derivative of $r_{k,2}\left(\{\underline{\mathbf{P}}_i\}_{i=1}^K\right)$ with respect to $\underline{\mathbf{P}}_i$ with different hardware nonideality assumptions. We first state the derivative of $r_{k,2}$ for the HWI model including I/Q imbalance, presented in Section 3.2.1, in which the rate expression is stated in (3.26). For the ease of readers, we restate the rate as

$$R_k = \underbrace{\frac{1}{2}\log_2\det\left(\underline{\mathbf{C}}_{z,k} + \sum_{i=1}^{K}\tilde{\mathbf{H}}_{ki}\underline{\mathbf{P}}_i\tilde{\mathbf{H}}_{ki}^T\right)}_{\triangleq r_{k,1}} - \underbrace{\frac{1}{2}\log_2\det\left(\underline{\mathbf{C}}_{z,k} + \sum_{i=1,i\neq k}^{K}\tilde{\mathbf{H}}_{ki}\underline{\mathbf{P}}_i\tilde{\mathbf{H}}_{ki}^T\right)}_{\triangleq r_{k,2}}. \quad (4.36)$$

Lemma 4.9 *Let us consider the HWI model including I/Q imbalance in Section* 3.2.1*. The derivative of $r_{k,2}(\cdot)$ in* (4.36) *with respect to $\underline{\mathbf{P}}_i$ for $i \neq k$ is*

$$\frac{\partial r_{k,2}\left(\{\underline{\mathbf{P}}_i^{(l)}\}_{i=1,i\neq k}^K\right)}{\partial \underline{\mathbf{P}}_i} = \frac{1}{2\ln 2}\tilde{\mathbf{H}}_{ki}^T\left(\underline{\mathbf{C}}_{z,k} + \sum_{i=1,i\neq k}^{K}\tilde{\mathbf{H}}_{ki}\underline{\mathbf{P}}_i^{(l)}\tilde{\mathbf{H}}_{ki}^T\right)^{-1}\tilde{\mathbf{H}}_{ki}, \quad (4.37)$$

where $\tilde{\mathbf{H}}_{ki}^T$ and $\underline{\mathbf{C}}_{z,k}$ are, respectively, defined in (3.23) *and* (3.25)*. Moreover, $\underline{\mathbf{P}}_i$ is the covariance matrix of user i, using the real-decomposition method. Note that $r_{k,2}(\cdot)$ in* (3.26) *is independent of $\underline{\mathbf{P}}_k$, and consequently, $\frac{\partial r_{k,2}\left(\{\underline{\mathbf{P}}_i^{(l)}\}_{i=1,i\neq k}^K\right)}{\partial \underline{\mathbf{P}}_k} = \mathbf{0}$.*

Now we consider consider the AHWD model in Section 3.2.1 in which the rate of user k is stated in (3.28). For simplifying the reading, we restate (3.28) as

$$R_k = \underbrace{\frac{1}{2}\log_2\det\left(\underline{\boldsymbol{\Phi}}_{k,1}\left(\{\underline{\mathbf{P}}_i\}_{i=1}^K\right)\right)}_{\triangleq r_{k,1}} - \underbrace{\frac{1}{2}\log_2\det\left(\underline{\boldsymbol{\Phi}}_{k,2}\left(\{\underline{\mathbf{P}}_i\}_{i=1}^K\right)\right)}_{\triangleq r_{k,2}}. \quad (4.38)$$

The derivative of $r_{k,2}(\cdot)$ with respect to $\underline{\mathbf{P}}_i$ for this model is presented in the following lemma.

Lemma 4.10 *Let us consider the AHWD model in Section* 3.2.1*. The derivative of $r_{k,2}(\cdot)$ in* (3.28) *with respect to $\underline{\mathbf{P}}_i$ is*

$$\frac{\partial r_{k,2}(\cdot)}{\partial \underline{\mathbf{P}}_i} = \begin{cases} \frac{\sigma_t^2}{2\ln 2}\mathrm{diag}\left(\underline{\mathbf{H}}_{kk}^T\underline{\boldsymbol{\Phi}}_{k,2}^{-1}\left(\{\underline{\mathbf{P}}_i\}_{i=1}^K\right)\underline{\mathbf{H}}_{kk}\right) & \text{for} \quad i=k, \\ \frac{\sigma_t^2}{2\ln 2}\mathrm{diag}\left(\underline{\mathbf{H}}_{ki}^T\underline{\boldsymbol{\Phi}}_{k,2}^{-1}\left(\{\underline{\mathbf{P}}_i\}_{i=1}^K\right)\underline{\mathbf{H}}_{ki}\right) + \frac{1}{2\ln 2}\underline{\mathbf{H}}_{ki}^T\underline{\boldsymbol{\Phi}}_{k,2}^{-1}\left(\{\underline{\mathbf{P}}_i\}_{i=1}^K\right)\underline{\mathbf{H}}_{ki} & \text{for} \quad i\neq k. \end{cases} \quad (4.39)$$

where $\underline{\boldsymbol{\Phi}}_{k,2}\left(\{\underline{\mathbf{P}}_i\}_{i=1}^K\right)$ *is defined in* (3.30).

4.3 Achievable rate region

The achievable rate region is defined as the set of all rates that can be achieved by feasible covariance matrices of the users as

$$\mathcal{R} = \bigcup_{\{\mathbf{P}_k\}_{k=1}^K \in \mathcal{P}} (R_1, R_2, \cdots, R_K). \tag{4.40}$$

In order to derive the achievable rate region, we can employ the following definition of the Pareto boundary for the achievable rate region.

Definition 4.1 ([66]) *The rate vector* $(r_1, r_2, \cdots, r_K)$ *is called Pareto-optimal if the rate vector* $(r'_1, r'_2, \cdots, r'_K)$ *with* $(r'_1, r'_2, \cdots, r'_K) \geq (r_1, r_2, \cdots, r_K)$ *and* $(r'_1, r'_2, \cdots, r'_K) \neq (r_1, r_2, \cdots, r_K)$ *is not achievable, where the the inequality is taken component-wise.*

There are different approaches to derive the achievable rate region. A way to derive the achievable rate region is the rate-profile technique, which yields [129]

$$\max_{R, \{\underline{\mathbf{P}}_k\}_{k=1}^K \in \mathcal{P}} \quad R \qquad \text{s.t.} \quad R_k \geq \alpha_k R, \qquad k = 1, 2, \cdots, K, \tag{4.41}$$

where $\alpha_k \geq 0$ for $k = 1, 2, \cdots, K$ are given constants, and $\sum_{k=1}^K \alpha_k = 1$. The boundary of the achievable rate region can be derived by solving (4.41) for different values of α_ks. The optimization problem (4.41) is not convex; however, we can derive its stationary point by the framework proposed in Section 4.2. That is, we solve (4.41) iteratively, and in each iteration, we employ the surrogate function in Lemma 4.8 for the rates. Since the corresponding surrogate optimization problem is convex, we can efficiently derive the global optimal solution of each surrogate optimization problem and consequently, obtain a stationary point of (4.41).

Remark 4.6 *The concept of the achievable rate region can be applied to different interference-limited systems such as various interference channels and relay channels.*

4.4 Maximizing weighted sum-rate

The weighted-sum-rate maximization of a MIMO interference-limited system with K users can be written as

$$\max_{\{\underline{\mathbf{P}}_k\}_{k=1}^K \in \mathcal{P}} \quad \sum_{k=1}^K \alpha_k R_k \tag{4.42a}$$

$$\text{s.t.} \quad R_k \geq R_{\text{th},k}, \qquad k = 1, 2, ..., K, \tag{4.42b}$$

where (4.42b) is the quality of service (QoS) constraint, and $R_{\text{th},k}$ is a given threshold for the rate of user k. Moreover, $\{\alpha_k \geq 0\}_{k=1}^K$ are the corresponding weights for the rates. Note that $R_{\text{th},k}$s have to be set in a way that (4.42) is feasible. Similar to (4.41), we can solve (4.42) by the framework in Section 4.2 and obtain its stationary point. Note that each surrogate optimization problem is convex, which can be solved efficiently.

4.5 Energy-efficiency region

In this section, we consider the EE region for a MIMO interference-limited system with K users. The EE of user k is defined as the ratio of its achievable rate to its total power consumption [126]

$$E_k = \frac{R_k}{\eta_k \text{Tr}(\underline{\mathbf{P}}_k) + P_{c,k}}, \qquad \text{(bits/Joule)} \tag{4.43}$$

where η_k^{-1}, and $P_{c,k}$ are, respectively, the power transmission efficiency of user k, and the constant power consumption of the kth transceiver. The EE function is a linear function of the rates, which allows us to apply the framework in Section 4.2 to optimize the EE. Note that the EE function has a fractional structure, which makes its optimization more difficult than the rate analysis, as will be discussed in the following.

The EE region of a MIMO interference-limited system with K users can be derived by solving [126]

$$\max_{E,\{\underline{\mathbf{P}}_k\}_{k=1}^K \in \mathcal{P}} \quad E \tag{4.44a}$$

$$\text{s.t.} \quad E_k = \frac{R_k}{\eta_k \text{Tr}(\underline{\mathbf{P}}_k) + P_{c,k}} \geq \alpha_k E, \qquad k = 1, 2, \cdots, K, \tag{4.44b}$$

$$R_k \geq R_{\text{th},k}, \qquad k = 1, 2, ..., K, \tag{4.44c}$$

where $\alpha_k \geq 0$ for $k = 1, 2, \cdots, K$ and $\sum_{k=1}^K \alpha_k = 1$. Moreover, the constraint (4.44c) is the QoS constraint, similar to (4.42b), and $R_{\text{th},k}$ has to be chosen in a way that the feasibility set of parameters is not empty. Similar to (4.41), the boundary of the EE region can be derived by solving (4.44) for all possible α_ks. Since E_k is a linear function of R_k, we can apply the framework in Section 4.2 to derive a stationary point of (4.44). The surrogate optimization problem at the lth iteration is

$$\max_{E,\{\underline{\mathbf{P}}_k\}_{k=1}^K \in \mathcal{P}} \quad E \tag{4.45a}$$

$$\text{s.t.} \quad \tilde{E}_k^{(l)} = \frac{\tilde{R}_k^{(l)}}{\eta_k \text{Tr}(\underline{\mathbf{P}}_k) + P_{c,k}} \geq \alpha_k E, \qquad k = 1, 2, \cdots, K, \tag{4.45b}$$

$$\tilde{R}_k^{(l)} \geq R_{\text{th},k}, \qquad k = 1, 2, ..., K, \tag{4.45c}$$

where $\tilde{R}_k^{(l)}$ is given by (4.35). Note that we can rewrite (4.45) as a maximin fractional optimization problem by removing E as

$$\max_{\{\underline{\mathbf{P}}_k\}_{k=1}^K \in \mathcal{P}} \quad \min_{1 \leq k \leq K} \left\{ \frac{\tilde{E}_k^{(l)}}{\alpha_k} \right\} \quad \text{s.t.} \quad \tilde{R}_k^{(l)} \geq R_{\text{th},k}, \quad k = 1, 2, ..., K. \tag{4.46}$$

The optimization problem (4.45) (or equivalently (4.46)) is not convex; however, its global optimal solution can be derived by employing the GDA, which is given in Section 4.1.4.

Applying the GDA in Lemma 4.6 to (4.45), we have

$$\max_{E,\{\underline{\mathbf{P}}_k\}_{k=1}^K \in \mathcal{P}} \quad E \tag{4.47a}$$

$$\text{s.t.} \quad \tilde{R}_k^{(l)} - \mu^{(m)} \left(\eta_k \text{Tr}(\underline{\mathbf{P}}_k) + P_{c,k}\right) \geq \alpha_k E, \qquad k = 1, 2, \cdots, K, \tag{4.47b}$$

$$\tilde{R}_k^{(l)} \geq R_{\text{th},k}, \qquad k = 1, 2, ..., K, \tag{4.47c}$$

where

$$\mu^{(m)} = \min_{1 \leq k \leq K} \left\{ \frac{E_k \left(\{\underline{\mathbf{P}}_i^{(l,m-1)}\}_{i=1}^K \right)}{\alpha_k} \right\}, \tag{4.48}$$

where $\{\underline{\mathbf{P}}_i^{(l,m-1)}\}_{i=1}^K$ is the solution of (4.47) at the $(m-1)$th iteration. Note that the GDA converges to the global optimal solution of (4.45) linearly, and the whole algorithm converges to a stationary point of (4.44).

4.6 Global energy-efficiency

The global energy-efficiency (GEE) of a system with K users is defined as the ratio of its total achievable rate to its total power consumption as [126]

$$G = \frac{\sum_{k=1}^K R_k}{\sum_{k=1}^K \left(\eta_k \text{Tr}(\underline{\mathbf{P}}_k) + P_{c,k}\right)}. \tag{4.49}$$

Hence, the GEE maximization problem is [126]

$$\max_{\{\mathbf{P}_k\}_{k=1}^K \in \mathcal{P}} \quad G = \frac{\sum_{k=1}^K R_k}{\sum_{k=1}^K \left(\eta_k \text{Tr}(\underline{\mathbf{P}}_k) + P_{c,k}\right)} \tag{4.50a}$$

$$\text{s.t.} \quad R_k \geq R_{\text{th},k}, \qquad k = 1, 2, ..., K, \tag{4.50b}$$

where (4.50b) is the QoS constraint similar to (4.44c) and (4.42b). Since the GEE is a linear function of the rates, we can apply the framework in Section 4.2 to obtain a stationary point of (4.50). Thus, the surrogate optimization problem at the lth iteration is

$$\max_{\{\mathbf{P}_k\}_{k=1}^K \in \mathcal{P}} \quad \tilde{G} = \frac{\sum_{k=1}^K \tilde{R}_k}{\sum_{k=1}^K \left(\eta_k \text{Tr}(\underline{\mathbf{P}}_k) + P_{c,k}\right)} \qquad \text{s.t.} \quad \tilde{R}_k \geq R_{\text{th},k}, \quad k = 1, 2, ..., K, \tag{4.51}$$

Similar to (4.45), the optimization problem is not convex; however, its global optimal solution can be derived by the Dinkelbach algorithm. That is, we obtain $\underline{\mathbf{P}}_i^{(l,m)}$ by solving

$$\max_{\{\underline{\mathbf{P}}_k\}_{k=1}^K \in \mathcal{P}} \quad \sum_{k=1}^K \tilde{R}_k - \mu^{(m)} \sum_{k=1}^K \left(\eta_k \text{Tr}(\underline{\mathbf{P}}_k) + P_{c,k}\right) \tag{4.52a}$$

$$\text{s.t.} \quad \tilde{R}_k \geq R_{\text{th},k}, \qquad k = 1, 2, ..., K, \tag{4.52b}$$

where $\mu^{(m)} = \tilde{G}\left(\{\underline{\mathbf{P}}_i^{(l,m-1)}\}_{i=1}^K\right)$, in which $\{\underline{\mathbf{P}}_i^{(l,m-1)}\}_{i=1}^K$ is the solution of (4.52) at the $(m-1)$th iteration. The global optimal solution of (4.51) can be achieved by iteratively solving (4.52) and updating $\mu^{(m)}$ until a convergence metric is met. Moreover, as indicated, the whole algorithm converges to a stationary point of (4.50).

4.7 Rate maximization of the secondary user in UCR

The optimization framework in Section 4.2 can be also applied other MIMO interference-limited systems with TIN. In this section, we present a simple example of a MIMO OFDM UCR with ideal devices, which is described in Section 3.2.2. Here, we assume that the SU may employ IGS while the PU, which is unaware of the SU, transmits with a fixed transmission strategy $\{\underline{\mathbf{P}}_{\text{PU},i}\}_{i=1}^N$. Our goal is to find a transmission strategy, $\{\underline{\mathbf{P}}_{\text{SU},i}\}_{i=1}^N$, for the SU that maximizes its rate, R_s, under the constraint that the rate of the PU, R_p, is ensured to be above a threshold, $\overline{R}$. It is assumed that the transmission power of the PU is given, and the power budget of the SU is $P_{\text{SU,max}}$. The optimization problem can be formulated as

$$\max_{\{\underline{\mathbf{P}}_{\text{SU},i}\}_{i=1}^N \in \mathcal{P}_{\text{SU}}} \quad R_s = \sum_{i=1}^N R_{s,i} \qquad \text{s.t.} \qquad R_p = \sum_{i=1}^N R_{p,i} \geqslant \overline{R}, \tag{4.53}$$

where $R_{p,i}$ and $R_{s,i}$ are given by (3.34). Additionally, $\underline{\mathbf{P}}_{\text{SU},i}$ is the feasibility set of the covariance matrices for the SU, which is given by

$$\mathcal{P}_{\text{SU}} = \left\{\underline{\mathbf{P}}_{\text{SU},i} : \sum_{i=1}^N \text{Tr}(\underline{\mathbf{P}}_{\text{SU},i}) \leqslant P_{\text{SU,max}}, \underline{\mathbf{P}}_{\text{SU},i} \succeq \mathbf{0}, i = 1, 2, ..., N\right\}. \tag{4.54}$$

The optimization problem in (4.53) is not convex since the rate of the PU is a convex function of $\{\underline{\mathbf{P}}_{\text{SU},i}\}_{i=1}^N$ rather than concave. However, we can derive its stationary point by the framework in Section 4.2. That is, we approximate the rate of the PU by the lower bound given in Lemma 4.8 and solve (4.53) iteratively. Note that we can apply the framework in Section 4.2 to other optimization problems in UCR systems such as energy-efficiency maximization.

4.8 Numerical examples for the K-user MIMO IC with HWI at transceivers

In this section, we provide some numerical examples for the K-user MIMO IC with HWI at transceivers based on the HWI model in Section 3.1.1. We employ Monte Carlo simulations and average the results over 100 channel realizations. In each channel realization, the elements of the channels are taken from a zero-mean complex proper Gaussian distribution with unit variance, i.e., $\mathcal{CN}(0,1)$. For all simulation, the maximum number of the iterations of the MM algorithm is 40. We also consider $\mathbf{C}_T = \sigma_T^2\mathbf{I}_{N_T}$ and $\mathbf{C}_R = \sigma_R^2\mathbf{I}_{N_R}$ [63], or equivalently $\underline{\mathbf{C}}_T = \frac{1}{2}\sigma_T^2\mathbf{I}_{2N_T}$ and $\underline{\mathbf{C}}_R = \frac{1}{2}\sigma_R^2\mathbf{I}_{2N_R}$. In all simulations, we assume $\sigma_T^2 = 0.2$ and $\sigma_R^2 = 1$. We assume that the I/Q imbalance by each antenna is symmetric. In other words, the matrices $\mathbf{A}_T = a_T\mathbf{I}_{N_T}$, $\boldsymbol{\theta}_T = \phi_T\mathbf{I}_{N_T}$, $\mathbf{A}_R = a_R\mathbf{I}_{N_R}$, and $\boldsymbol{\theta}_R = \phi_R\mathbf{I}_{N_R}$ are scaled identity matrices. We consider $\phi_T = \phi_R = 5$ degrees in all simulations. We also define the signal-to-noise ratio (SNR) as the ratio of the power budget to σ^2, i.e., SNR$= \frac{P}{\sigma^2}$.

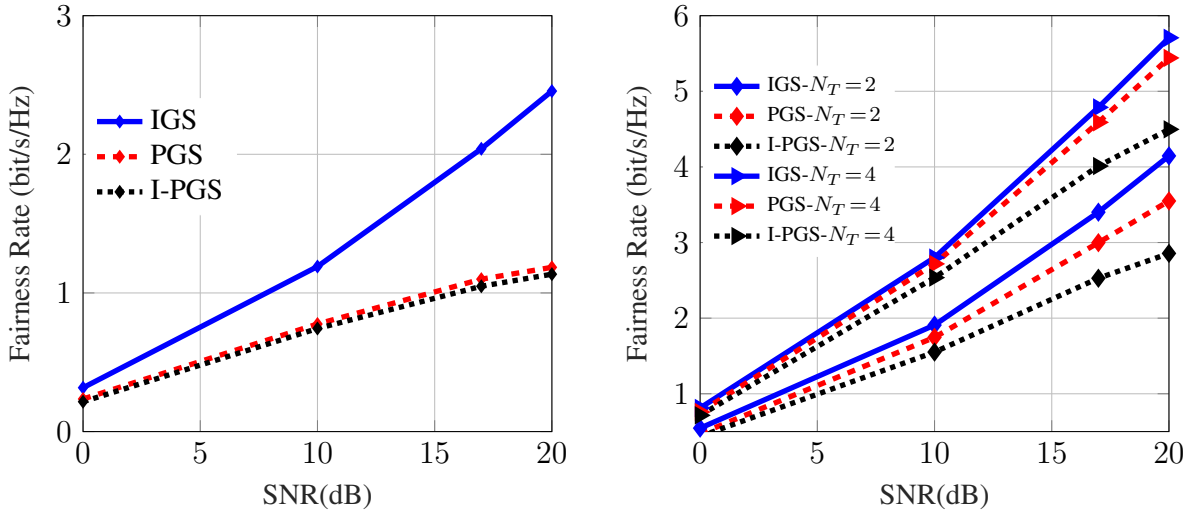

(a) SISO. **(b)** MISO.

Figure 4.3: Fairness rate versus SNR for SISO and MISO.

We compare our proposed algorithms for PGS and IGS schemes with the PGS algorithm for ideal devices. The considered schemes in this section are as follows:

- **IGS**: The proposed IGS scheme.
- **PGS**: The proposed PGS scheme.
- **I-PGS**: The PGS scheme for K-user IC without considering the I/Q imbalance in the design.

Note that MM algorithms depend on the initial point. In PGS and I-PGS algorithms, we start with a uniform power allocation $\mathbf{P}_k = \frac{P}{2N_T}\mathbf{I}_{2N_T}$ for $k = 1, \cdots, K$ in optimization problems (4.41) and (4.42) and $\mathbf{P}_k = \frac{0.3P}{2N_T}\mathbf{I}_{2N_T}$ for $k = 1, \cdots, K$ in optimization problems (4.44) and (4.50). However, the IGS algorithm takes the solution of the PGS algorithm as an initial point.

4.8.1 Achievable rate region

In this subsection, we consider a specific point of the rate region, which maximizes the minimum rate of users. The minimum rate of the K-user MIMO IC is maximized for $\alpha_k = \frac{1}{K}$. This point is also referred as the maximin fairness point. Hereafter, we call the minimum rate as the fairness rate. We show the fairness rate of the 2-user SISO and MISO IC for $a_T = 0.6$ and different number of antennas at the transmitter side in Fig. 4.3. As can be observed, there is a huge performance improvement by IGS in the 2-user SISO IC, especially at high SNR. However, the benefits of employing IGS become negligible by increasing the number of antennas. This is due to the fact that, by increasing the number of resources for a fixed number of users, the interference can be easier managed, and hence, IGS as an interference-management tool does not provide significant gain. This is in line with the results in [103], in which it was shown that IGS cannot provide considerable benefits in OFDM UCR systems due to existence of parallel channels. Moreover, in [52], it was shown that the benefits of IGS disappears with time sharing

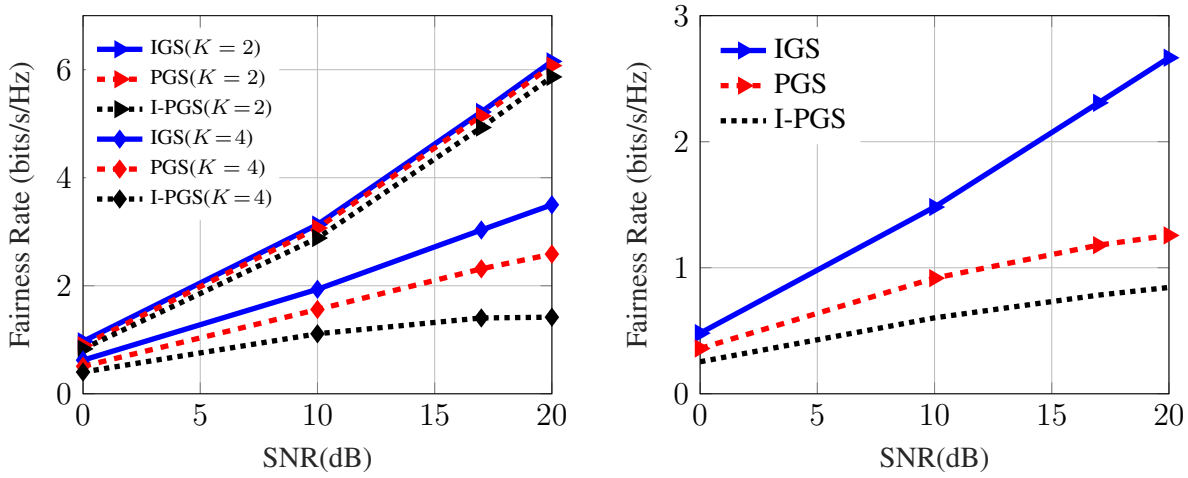

(a) $K = 2$ and $K = 4$. **(b)** $K = 6$.

Figure 4.4: Fairness rate versus SNR for 2×2 MIMO.

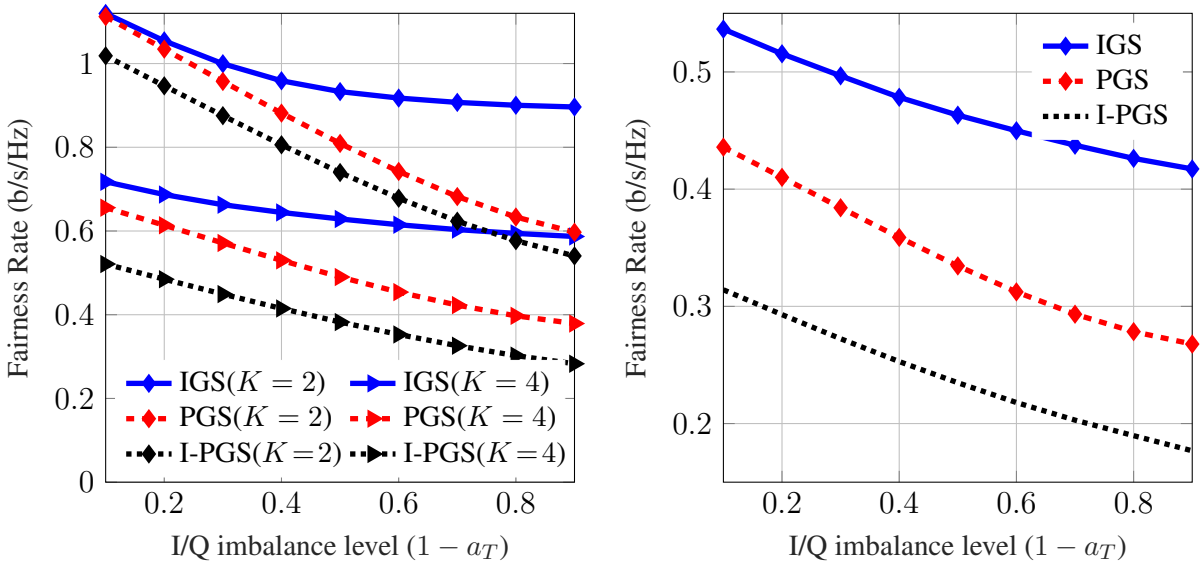

(a) $K = 2$ and $K = 4$. **(b)** $K = 6$.

Figure 4.5: Fairness rate versus the I/Q imbalance level for 2×2 MIMO.

when the average power consumption is constrained, instead of the *instantaneous power*, which allows a more flexible power allocation. To sum up, the benefits of IGS decrease or even vanish by increasing the number of resources either by increasing the number of antennas or number of time slots, by time sharing, and/or the number of parallel channels by OFDM. It is worth mentioning that, even with high number of antennas, IGS and PGS, which are aware of the HWI, outperform PGS, which is designed for ideal devices.

In Fig. 4.4, we consider the effect of the power budget on the fairness rate of the K-user 2×2 MIMO IC for $a_T = 0.6$. As can be observed, there are minor benefit for IGS when $K = 2$. However, by increasing the number of users, the performance improvement of IGS increases. The reason is that, by increasing the number of users, the interference level increases, which results in more performance improvements by IGS as an interference-management technique.

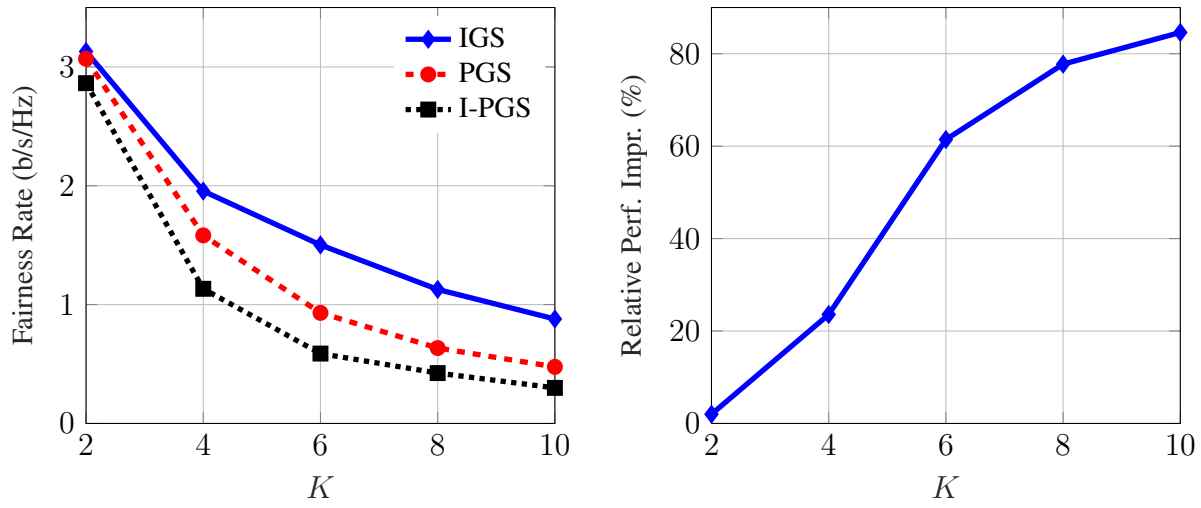

(a) Achievable rate **(b)** Relative improvement of IGS over PGS

Figure 4.6: Fairness rate versus the number of users for 2×2 MIMO.

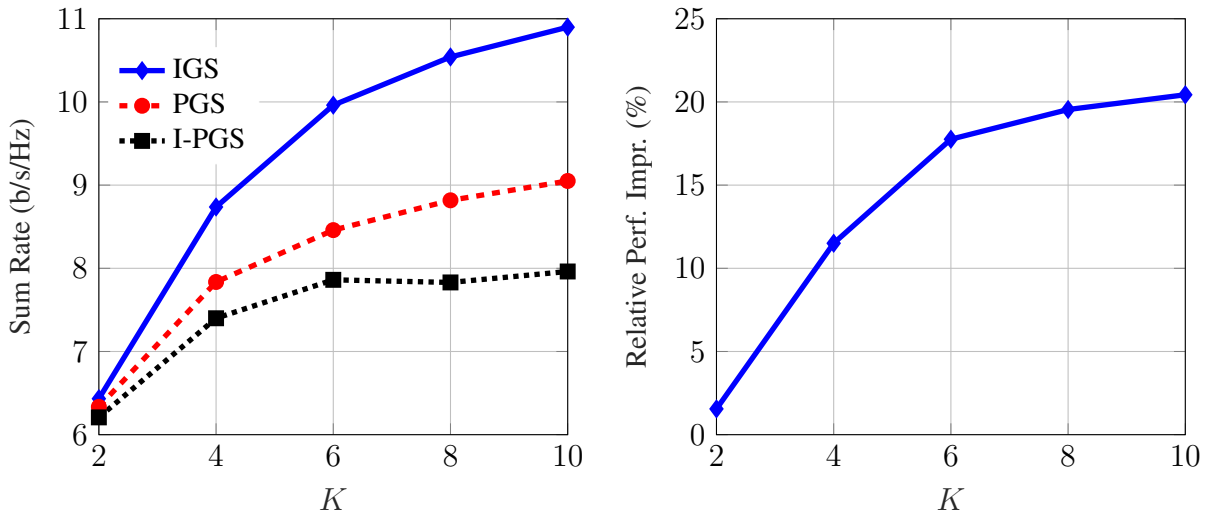

(a) Achievable sum-rate **(b)** Relative improvement of IGS over PGS

Figure 4.7: Achievable sum-rate and relative performance of IGS versus the number of users for 2×2 MIMO.

Moreover, IGS performs much better in high SNR for $K = 6$, similar to the SISO 2-user IC as depicted in Fig. 4.3a.

Figure 4.5 shows the fairness rate versus the level of the I/Q imbalance, i.e., $1 - a_T$ for SNR$=$ 10dB and $N_T = N_R = 2$. Note that $a_T = 1$ means that there is no I/Q imbalance. As can be observed, the IGS design is less affected by the HWI level for different K. In $K = 2$, the IGS and PGS schemes perform very similarly in low HWI level. However, the performance of the PGS scheme drastically decreases with the HWI level, while the fairness rate of the IGS scheme decreases slightly. In $K = 4$ and $K = 6$, the same behavior is observed, but the relative performance of the IGS scheme over the PGS scheme is increasing in K. Moreover, for a given K, the benefits of IGS is increasing in the level of the I/Q imbalance, as expected.

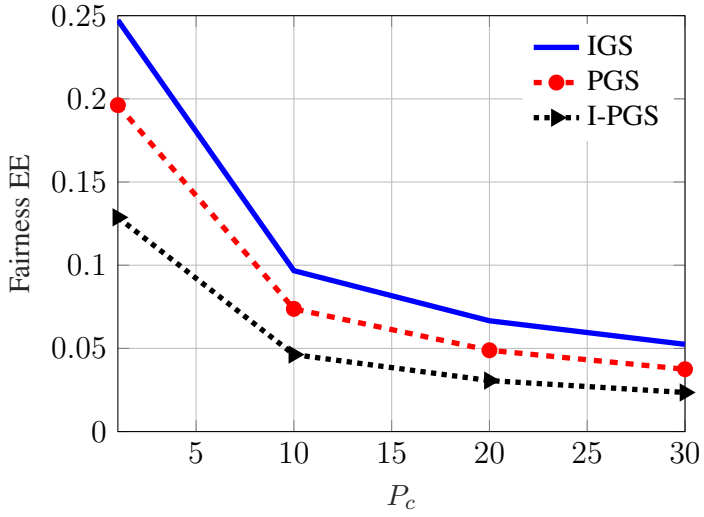

Figure 4.8: Fairness EE of the 6-user 2×2 MIMO IC versus P_c.

Figure 4.6 considers the effect of the number of users on the fairness rate as well as the performance of IGS. As can be observed, the fairness rates are related to K^{-1}. Additionally, the relative performance improvement by IGS is increasing in K, where there is more than 80% improvements over PGS for $K = 10$. The reason is that, the more users yields the more interference, which results in more improvements by IGS as indicated before.

4.8.2 Achievable sum-rate

In Fig. 4.7, we show the effect of the number of users on the achievable sum-rate of the K-user 2×2 MIMO IC. In this figure, we set the threshold in (4.42) to $R_{\text{th},k} = 0$. We can observe that the sum-rate and also the relative performance of IGS over PGS are increasing in K. Since we maximize the sum-rate without considering a QoS constraint, the rate of some users with weak direct link might be even 0, which causes less interference. As a result, the relative performance improvement of IGS is less than the improvements for the fairness rate in Fig. 4.6.

4.8.3 Energy efficiency region

In this subsection, we consider the EE region in (4.44). In general, IGS provides less EE benefits than rate benefits. For example, in [104], it was shown that there are more constraints for optimality of IGS in an UCR system from EE point of view than from the achievable rate perspective. In other words, it might happen that IGS provides more rate benefits for the secondary user; however, PGS is the energy-efficient optimal scheme for the SU.

In Fig. 4.8, we show the symmetric or fairness EE of the 6-user 2×2 MIMO IC versus P_c for $a_T = 0.6$. As can be observed, the fairness EE decreases with P_c. Moreover, our proposed IGS scheme outperforms the PGS scheme as well as I-PGS. Figure 4.9 shows the relative performance improvement by our IGS scheme with respect to the PGS and I-PGS schemes for the results in Fig. 4.8. As can be observed in these figures, the fairness EE decreases with P_c; however, the benefits of employing IGS is increasing in P_c. The reason is that when P_c is very large, the EE region optimization problem is simplified to the achievable rate region problem,

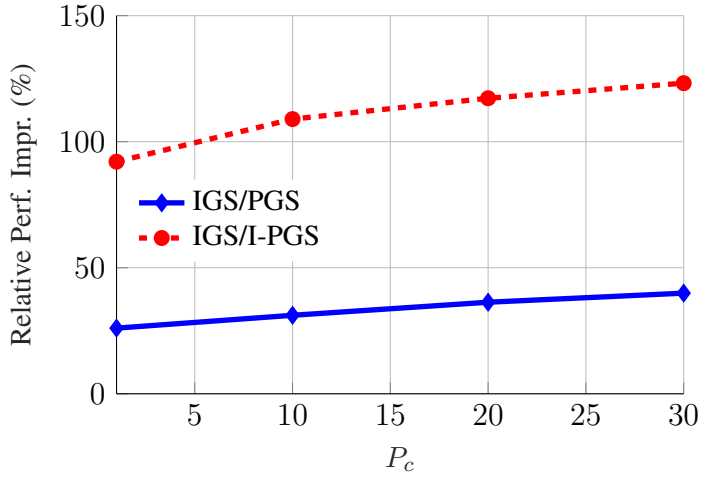

Figure 4.9: Relative performance of IGS with respect to PGS and I-PGS versus P_c for the 6-user 2×2 MIMO IC.

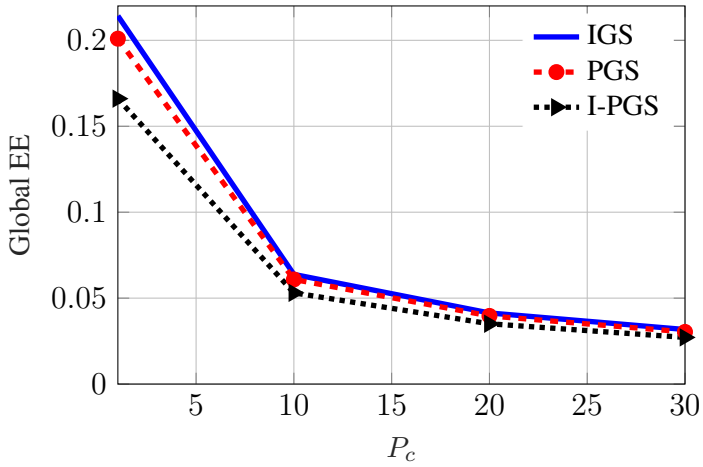

Figure 4.10: Global EE of the 6-user 2×2 MIMO IC versus P_c.

and as indicated, IGS can provide more gain in achievable rate optimizations.

4.8.4 Global Energy efficiency

Figure 4.10 shows the global EE of the 6-user 2×2 MIMO IC versus P_c for $a_T = 0.6$. In this figure, we consider $R_{\text{th},k} = 0$ in (4.50). As can be observed, IGS provides minor benefits for the global EE. Since the QoS constraint is not considered, it might happen that some users do not transmit, which causes less interference. Moreover, the lower interference level, the less need for interference-management techniques. Thus, we can expect that the benefits of employing IGS become less in global EE with respect to EE.

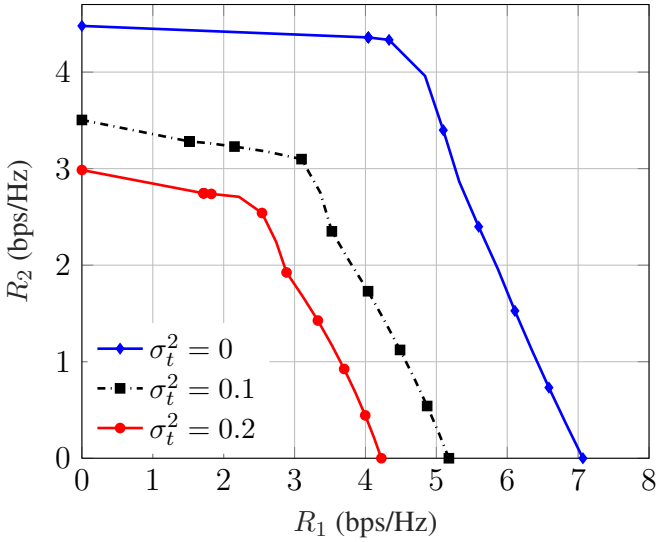

Figure 4.11: The achievable rate region of the 2-user IC 2×2 MIMO with SNR$= 10$ dB and different σ_t^2.

4.9 Numerical examples for the K-user MIMO IC with AHWD at transmitters

In this section, we provide some numerical results for the achievable rate region of the K-user MIMO IC with AHWD at transmitters. As observed in Section 4.8, the benefits of employing IGS decrease with the number of antennas at transceivers. Hence, in this section, we do not consider IGS. Here, we assume $\sigma^2 = 1$ and equal power budget for all users, i.e., $P_1 = P_2 = \cdots = P_K = P$. We define the SNR as SNR$= \frac{P}{\sigma^2}$. The maximum number of iterations of the DCP algorithm is 30.

There are generally two types of performance metrics for rate-region analysis in the literature [102]. One is to consider a specific channel realization and derive the whole rate region for the given channel realization, which is presented in Section 4.9.1. In such figures, we can observe the whole possible operational points for a specific channel realization. Even though these figures vary for different channel realizations, they show us the main trends for the considered system performance. To cope with this dependency on channel realizations, there is also another type of performance evaluation, which employs Monte Carlo simulations for a specific point of the rate region. In this approach, the results are averaged over a large number of channel realizations for the specific point of the region as described in Section 4.9.2.

4.9.1 Rate region

In this subsection, we depict the achievable rate region for a typical channel realization. As indicated, we have to consider a channel realization in order to depict the whole rate region. To this end, we choose a random channel realization. In Fig. 4.11, we show the achievable rate region for a 2-user 2×2 MIMO IC with SNR$= 10$ dB, $\sigma_t^2 = 0, 0.1, 0.2$ and the following

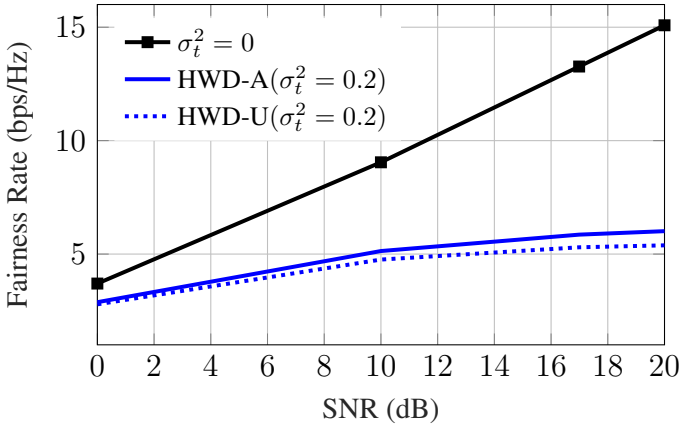

(a) $\sigma_t^2 = 0, 0.2$.

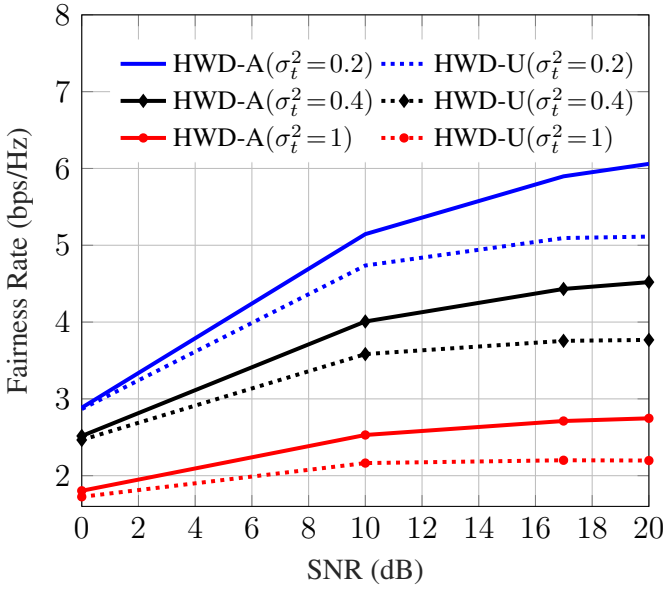

(b) $\sigma_t^2 = 0.2, 0.4, 1$.

Figure 4.12: The average fairness rate versus SNR for the 2-user 4×4 MIMO IC with different σ_t^2.

channel realization

$$\mathbf{H}_{11} = \begin{bmatrix} -0.0582 - 1.0619i & 0.6289 + 0.4246i \\ -0.6971 - 0.4074i & -1.4091 - 0.5512i \end{bmatrix},$$
$$\mathbf{H}_{12} = \begin{bmatrix} 0.0168 + 0.1373i & 0.5545 + 0.3165i \\ 0.6714 + 0.4017i & 0.6933 + 0.3237i \end{bmatrix},$$
$$\mathbf{H}_{21} = \begin{bmatrix} 0.4203 + 0.7962i & 1.1189 - 0.6048i \\ -0.7680 + 0.1541i & -1.3321 - 0.0836i \end{bmatrix},$$
$$\mathbf{H}_{22} = \begin{bmatrix} 0.5857 + 0.2984i & 0.5236 - 1.1194i \\ -0.1130 + 0.3857i & -0.1024 - 0.0475i \end{bmatrix}.$$

As can be observed, the achievable rate region significantly shrinks when the AHWD level σ_t^2 increases. Note that we just choose a typical channel to show the impact of the AHWD level on

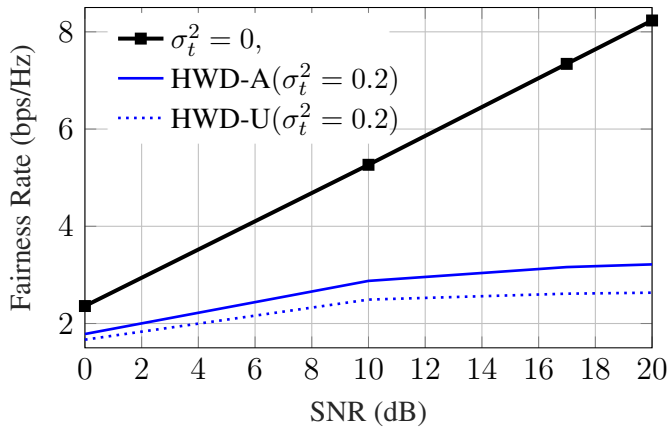

Figure 4.13: The average fairness rate versus SNR for the 3-user 3×3 MIMO IC with different σ_t^2.

the rate region. Obviously, the rate region highly depends on the considered channel realization; however, a similar behavior will be observed in other channel realizations.

4.9.2 Fairness (symmetric) rate

The results in this subsection have been obtained by averaging 100 independent channel realizations. Every element of each channel matrix is drawn from a complex zero-mean Gaussian distribution with unit variance. We consider the fairness rate, which is obtained for $\alpha_k = \frac{1}{K}$ for $k = 1, \cdots, K$. In this case, each user receives the same achievable rate, and we indeed maximize the minimum achievable rate of the system. That is why this point of the rate region is referred to as the "fairness point". We compare our proposed HWD-aware algorithm (labeled "HWD-A") with the scheme that does not consider AHWD (labeled "HWD-U").

In Fig. 4.12, we show the effect of σ_t^2 on the average achievable fairness rate of the 2-user 4×4 MIMO IC. In order to make the figure clearer, plots (a) and (b) use a different scale for different values of σ_t^2, and we consider only the 2-user MIMO IC. We consider the 3-user IC with a different number of antennas later in Fig. 4.13. As can be observed in Fig. 4.12, the achievable fairness rate drastically decreases when the devices are not ideal especially at high SNR, where the average fairness rate by our scheme is 15.08 bps/Hz for ideal devices and 6 bps/Hz for $\sigma_t^2 = 0.2$ in this example, which means more than 70 % performance loss by AHWD. The reason is that the AHWD level increases with the transmission power, which causes a severe performance degradation in high SNR.

Figure 4.13 shows the average fairness rate of the 3-user 3×3 MIMO IC with $\sigma_t^2 = 0, 0.2$. As can be observed, the average fairness rate significantly decreases with AHWD similar to the 2-user 4×4 MIMO IC, shown in Fig. 4.12a. Additionally, our AHWD-aware scheme provides more benefits in the 3-user IC. In other words, we observe that when the number of users or antennas increase, to account for AHWD is more important.

In Fig. 4.14, we depict the relative performance improvement by our scheme for the 2-user and 3-user 3×3 MIMO ICs with different σ_t^2. In this figure, both the 2-user and 3-user ICs employ the same number of antennas. As can be observed, the benefits of our scheme increase with power budget and σ_t^2. The reason is that the AHWD at each antenna is a linear function of the transmission power at the corresponding antenna. Thus, AHWD level increases with the transmission power, and the higher AHWD is, the higher performance improvement is achieved

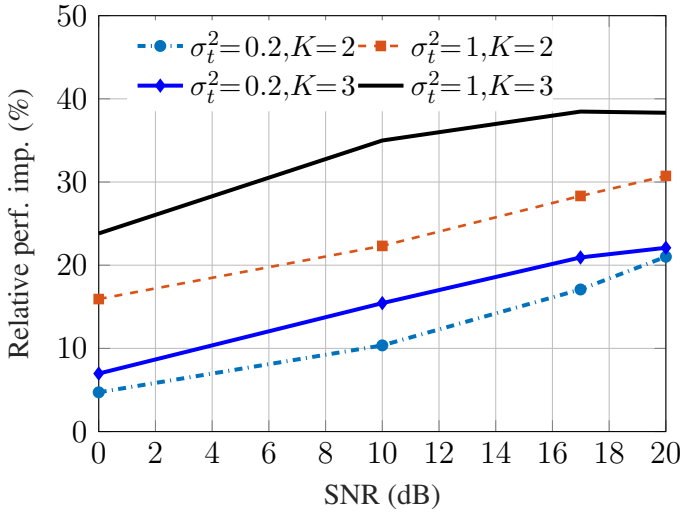

Figure 4.14: The relative performance improvement of our algorithm versus SNR for the 2-user and 3-user 3×3 MIMO ICs with different σ_t^2 with respect to the scheme "HWD-U".

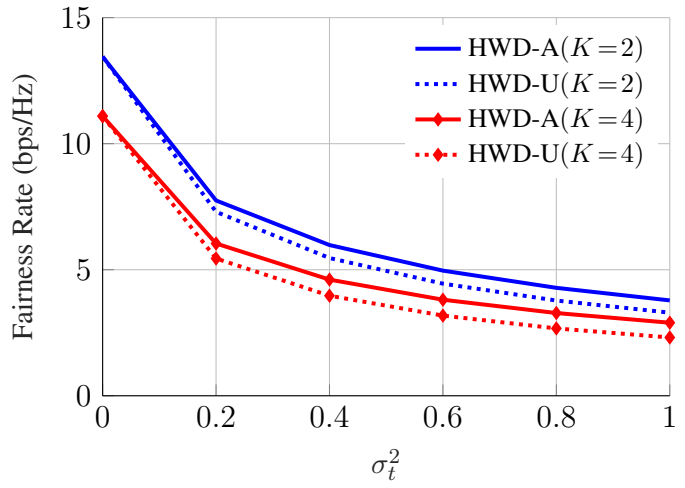

Figure 4.15: The average fairness rate versus σ_t^2 for the 2-user and 3-user 6×6 MIMO IC with SNR$=$ 10 dB.

by our scheme. Furthermore, as indicated in Fig. 4.13, when K increases it is more important to account for AHWD. This is due to the fact that when there are more transmitters with a similar AHWD, the receiver experiences more AHWD.

In Fig. 4.15, we show the impact of the AHWD level on the average fairness rate of the 2-user and 3-user 6×6 MIMO ICs with SNR$=$ 10 dB. As can be observed, AHWD can significantly degrade the system performance. Moreover, we observe again that considering AHWD in design is more important when the number of users increases.

In Fig. 4.16, we show the effect of K on the average fairness rate of the K-user 3×5 MIMO IC with $\sigma_t^2 = 0.5$, and SNR$=$ 0 dB. As can be observed, the fairness rate is decreasing in K. However, the benefits of our AHWD-aware scheme increase with K, which shows the importance of our scheme in practical scenarios. As indicated, the AHWD at each receiver increases with K for a fixed $\sigma_t^2 > 0$. Hence, our AHWD-aware scheme can provide more benefits when K grows due to the increase in AHWD level.

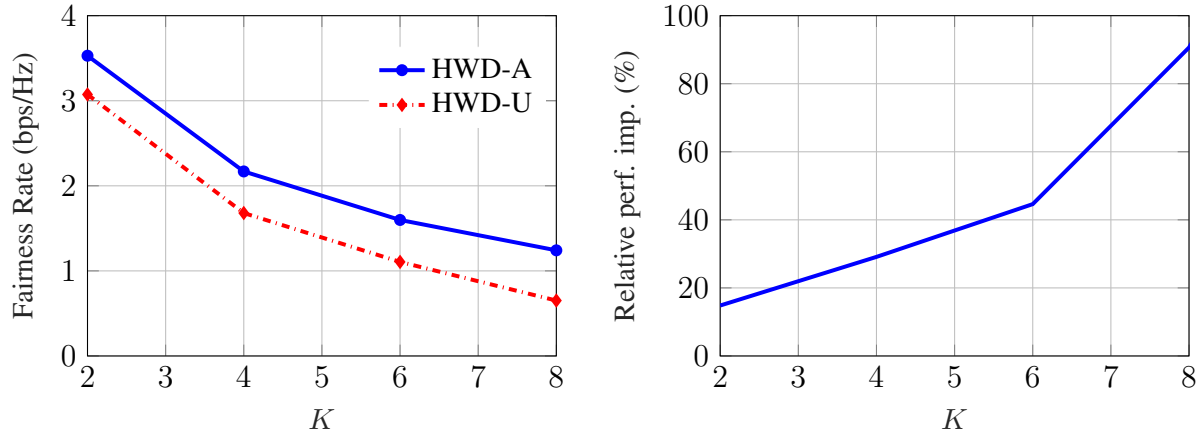

(a) Symmetric rate.

(b) Relative performance improvement.

Figure 4.16: The average fairness rate and relative performance of our proposed scheme versus K for the K-user 5×3 MIMO IC with $\sigma_t^2 = 0.5$, and SNR$= 0$ dB.

4.10 Summary

In this chapter, we presented a suboptimal algorithm for multiple-antenna interference-limited systems with TIN. The optimization framework obtains a stationary point of any optimization problem in which either the objective function or constraints are linear functions of achievable rates. This framework can be applied to different sources of non-idealities at devices such as I/Q imbalance and/or AHWD. In the presence of I/Q imbalance, the received signal is a function of the widely linear transform of the transmitted signal and the aggregated noise, which implies that the effective noise can be improper at the receiver side. We considered achievable rate region, weighted-sum-rate maximization, energy-efficiency region and global energy-efficiency maximization problems as well as the rate maximization of the SU in a MIMO OFDM UCR as some examples of the optimization problems, which can be solved by the optimization framework.

In the numerical sections, we first considered a K-user MIMO IC with HWI including I/Q imbalance. Our numerical results showed that the benefits of IGS as an interference-management technique increase with the number of users and decrease with the number of antennas. This is due to the fact that the higher interference level results in the more need for interference management and consequently, the more improvements by IGS. We also observed that the benefit of employing IGS increases with imbalance level. Additionally, we observed that IGS provides more benefits from achievable rate point of view than from EE perspective.

In this chapter, we also provided some numerical examples for the K-user MIMO IC with AHWD at transmitters. In the numerical results, we observed that the performance of the system is highly affected by AHWD at transmitters. Our proposed AHWD-aware scheme outperforms the scheme that does not consider non-idealities at transmitters. Furthermore, the benefit of employing our AHWD-aware scheme increases with the number of users.

5 Improper Signaling for SISO OFDM Underlay Cognitive Radio Systems

In this chapter, we investigate the performance of improper signaling in a SISO OFDM UCR system. To this end, we consider two different QoS constraints for the PU. Because improper signaling has been so successful at increasing the achievable rates in many interference-limited scenarios, one might expect the same in a UCR OFDM system. However, the parallel channels in OFDM allow the SU to allocate its power more flexibly compared to the single carrier case. For example, in relatively low load traffic, the PU can neglect some subcarriers without violating the rate constraint. This allows the SU to transmit proper signals with maximum power on those subbands. This is why our results show that the benefit of improper signaling is fairly small and decreases further with increasing number of subbands. Our study therefore reveals that the use of improper signaling in interference channels needs to be justified for each individual case. Note that the algorithm in Section 4.7 can be also applied to single-antenna systems. However, in this chapter, we employ the augmented covariance matrices to elaborate more on the behavior of improper signaling. This study is presented in [103].

5.1 System Model

In this chapter, we consider a UCR system, in which both primary and secondary users employ OFDM with N subbands. In order to model improper signals, we employ complex representations and consider the augmented covariance matrix of the signals throughout this chapter. We assume that the PU transmits proper Gaussian signals, while the SU is allowed to employ IGS. Thus, according to Remark 2.4, the augmented covariance matrices of the signal transmitted by the PU and SU in subband i are $\mathbf{C}_{\text{PU},i} = p_{\text{PU},i}\mathbf{I}$ and

$$\mathbf{C}_{\text{SU},i} = \begin{bmatrix} p_{\text{SU},i} & \kappa_i p_{\text{SU},i} e^{-j\phi_i} \\ \kappa_i p_{\text{SU},i} e^{j\phi_i} & p_{\text{SU},i} \end{bmatrix}, \tag{5.1}$$

respectively, where $p_{\text{PU},i}$, $p_{\text{SU},i}$, κ_i, and ϕ_i denote the transmission power of the PU, transmission power of the SU, circularity coefficient of the SU, and the phase of the complementary variance of the SU in subband i, respectively. Hence, the rates of the PU and SU in subband i are [129]

$$\begin{aligned} R_{p,i} &= \frac{1}{2}\log_2 |\mathbf{I} + (\sigma^2\mathbf{I} + \mathbf{G}_i\mathbf{C}_{\text{SU},i}\mathbf{G}_i^H)^{-1}\mathbf{H}_i\mathbf{C}_{\text{PU},i}\mathbf{H}_i^H|, \\ R_{s,i} &= \frac{1}{2}\log_2 |\mathbf{I} + (\sigma^2\mathbf{I} + \mathbf{D}_i\mathbf{C}_{\text{PU},i}\mathbf{D}_i^H)^{-1}\mathbf{F}_i\mathbf{C}_{\text{SU},i}\mathbf{F}_i^H|, \end{aligned} \tag{5.2}$$

respectively, where σ^2, $\mathbf{H}_i$, $\mathbf{G}_i$, $\mathbf{F}_i$, and $\mathbf{D}_i$ are the variance of the additive noise, PU-PU, SU-PU, SU-SU and PU-SU channels, respectively. In Fig. 5.1, we show the channel coefficients of

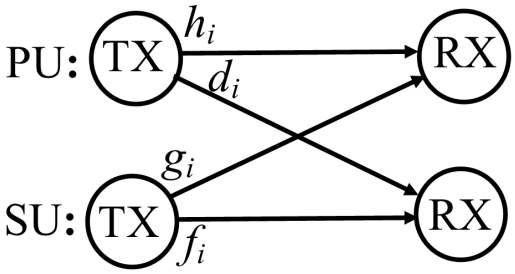

Figure 5.1: The channel model for the UCR system in subband i

the UCR system for subband i. Note that the channel matrices are diagonal and can be written as a product of the channel coefficient and the identity matrix (e.g., $\mathbf{H}_i = h_i\mathbf{I}$). Moreover, since only the SU transmits improper signals, the rate is independent of $\phi_i =$. Thus, we choose $\phi_i = 0$ without loss of generality.

5.2 Problem Statement

In this chapter, we aim at finding a transmission strategy, $\{\mathbf{C}_{\text{SU},i}\}_{i=1}^{N}$, for the SU that maximizes its rate, R_s, under the constraint that the rate of the PU, R_p, is ensured to be above a threshold, $\overline{R}$. We assume that the transmission power of the PU is given, and the power budget of the SU is $P_{\text{SU,max}}$. The optimization problem can be formulated as

$$\max_{\{\mathbf{C}_{\text{SU},i}\}_{i=1}^{N}} \quad R_s = \sum_{i=1}^{N} R_{s,i} \tag{5.3a}$$

$$\text{s.t.} \quad \sum_{i=1}^{N} R_{p,i} \geqslant \overline{R}, \tag{5.3b}$$

$$\sum_{i=1}^{N} \text{Tr}(\mathbf{C}_{\text{SU},i}) \leqslant 2P_{\text{SU,max}}, \tag{5.3c}$$

$$\mathbf{C}_{\text{SU},i} \succeq \mathbf{0}, \qquad \text{for} \quad i = 1, 2, ..., N, \tag{5.3d}$$

$$[\mathbf{C}_{\text{SU},i}]_{11} = [\mathbf{C}_{\text{SU},i}]_{22}, \quad \text{for} \quad i = 1, 2, ..., N, \tag{5.3e}$$

where $[\mathbf{C}_{\text{SU},i}]_{kk}$ is the kth element in the kth row of $\mathbf{C}_{\text{SU},i}$. We consider two different scenarios, in which the rate constraints are different. In the first scenario, the total rate is greater than a threshold, and thus, (5.3b) is equivalent to $\sum_{i=1}^{N} R_{p,i} \geqslant \overline{R}$. In the second, the rate in each subband is greater than a threshold, and thus, (5.3b) is replaced by the N constraints $R_{p,i} \geqslant \overline{R}_i$, for $i = 1, 2, ..., N$.

5.3 Proposed Transmission Strategies

In this section, we solve the optimization problem in (5.3), which is not convex since the rate of the PU is a convex function of $\{\mathbf{C}_{\text{SU},i}\}_{i=1}^{N}$ rather than concave. We first consider the constraint on the total rate in Section 5.3.1, and then in Section 5.3.2, we solve (5.3) when there is a constraint on the rate of each subband, which is a more restricted assumption.

5.3.1 Constraint on the total rate

In this subsection, we solve (5.3) when there is a constraint on the total rate. To this end, we employ sequential convex programming (SCP), which falls into MM [108]. In this approach, the optimization problem is approximated by a convex optimization problem, and solved iteratively. At each iteration, the non-concave constraint is approximated by a concave function. It is known that this approach converges to to a stationary point of (5.3) [81, 108]. Note that the initial point should be in the feasible set of the original problem. Since the channel and PU's power matrices are scaled identity matrices, we will show that (5.3e) is automatically satisfied in each iteration if the initial point satisfies (5.3e). Thus, we can safely drop (5.3e) and consider only (5.3a)-(5.3d) in each iteration.

In order to solve (5.3), at each iteration we approximate the rate of the PU by an affine function, which is the closest concave function. We employ the first-order term in the Taylor series expansion of the rate of the PU with respect to $\mathbf{C}_{\text{SU},i}$ at point $\mathbf{C}_{\text{SU},i}^{(l-1)}$, which is given by the previous iteration. That is

$$R_{p,i}(\mathbf{C}_{\text{SU},i}) \simeq R_{p,i}(\mathbf{C}_{\text{SU},i}^{(l-1)}) + \text{Tr}\left[\nabla_{\mathbf{C}_{\text{SU},i}} R_{p,i}(\mathbf{C}_{\text{SU},i}^{(l-1)}) \left(\mathbf{C}_{\text{SU},i} - \mathbf{C}_{\text{SU},i}^{(l-1)}\right)\right], \tag{5.4}$$

where $\nabla_{\mathbf{C}_{\text{SU},i}} R_{p,i}(\mathbf{C}_{\text{SU},i}^{(l-1)})$ is the derivative of the PU rate with respect to $\mathbf{C}_{\text{SU},i}$, which is

$$\begin{aligned}\nabla_{\mathbf{C}_{\text{SU},i}} R_{p,i} = &-\mathbf{G}_i^H(\sigma^2\mathbf{I} + \mathbf{G}_i\mathbf{C}_{\text{SU},i}\mathbf{G}_i^H)^{-1}\mathbf{H}_i\mathbf{C}_{\text{PU},i}\mathbf{H}_i^H \\ &\times \left(\mathbf{I} + (\sigma^2\mathbf{I} + \mathbf{G}_i\mathbf{C}_{\text{SU},i}\mathbf{G}_i^H)^{-1}\mathbf{H}_i\mathbf{C}_{\text{PU},i}\mathbf{H}_i^H\right)^{-1}(\sigma^2\mathbf{I} + \mathbf{G}_i\mathbf{C}_{\text{SU},i}\mathbf{G}_i^H)^{-1}\mathbf{G}_i. \end{aligned}\tag{5.5}$$

By this approximation, the optimization problem at each iteration turns into:

$$\max_{\{\mathbf{C}_{\text{SU},i}\}_{i=1}^N} \quad R_s = \sum_{i=1}^N R_{s,i} \qquad \text{s.t.} \quad \sum_{i=1}^N \text{Tr}\left(\mathbf{A}_i^{(l-1)}\mathbf{C}_{\text{SU},i}\right) \leqslant B^{(l-1)}, \tag{5.6a}$$

$$\sum_{i=1}^N \text{Tr}(\mathbf{C}_{\text{SU},i}) \leqslant 2P_{\text{SU,max}}, \tag{5.6b}$$

$$\mathbf{C}_{\text{SU},i} \succeq 0, \quad \text{for} \quad i = 1, 2, ..., N. \tag{5.6c}$$

In (5.6), the coefficients $\mathbf{A}_i^{(l-1)}$ and $B^{(l-1)}$ can be obtained as

$$\mathbf{A}_i^{(l-1)} = -\nabla_{\mathbf{C}_{\text{SU},i}} R_{p,i}(\mathbf{C}_{\text{SU},i}^{(l-1)}), \tag{5.7a}$$

$$B^{(l-1)} = \sum_{i=1}^N R_{p,i}(\mathbf{C}_{\text{SU},i}^{(l-1)}) - \overline{R} - \sum_{i=1}^N \text{Tr}\left(\nabla_{\mathbf{C}_{\text{SU},i}} R_{p,i}(\mathbf{C}_{\text{SU},i}^{(l-1)})\mathbf{C}_{\text{SU},i}^{(l-1)}\right). \tag{5.7b}$$

The solution of (5.6) can be derived by using the dual function and KKT approach. The Lagrangian for the optimization problem (5.6) can be written as

$$\begin{aligned}\mathcal{L}(\{\mathbf{U}_i\}_{i=1}^N, \lambda, \mu) = \mu(\sum_{i=1}^N \text{Tr}(\mathbf{C}_{\text{SU},i}) - 2Q_{\max}) - \sum_{i=1}^N \frac{1}{2}\log_2|\mathbf{I} + (\sigma^2\mathbf{I} + \mathbf{D}_i\mathbf{C}_{\text{PU},i}\mathbf{D}_i^H)^{-1}\mathbf{F}_i\mathbf{C}_{\text{SU},i}\mathbf{F}_i^H| \\ - \sum_{i=1}^N \text{Tr}(\mathbf{U}_i\mathbf{C}_{\text{SU},i}) + \lambda(\sum_{i=1}^N \text{Tr}(\mathbf{A}_i^{(l-1)}\mathbf{C}_{\text{SU},i}) - B^{(l-1)}),\end{aligned}\tag{5.8}$$

Algorithm I Proposed solution for constraint on the total rate
Initialize $\mathbf{C}_{\text{SU},i}^{(0)}$ in the feasible set of the problem (5.3) Compute $\mathbf{A}_i^{(0)}$ and $B^{(0)}$ using (5.7) Set $l = 1$
While $\|\|\mathbf{C}_{\text{SU},i}^{(l)} - \mathbf{C}_{\text{SU},i}^{(l-1)}\|\|_2 \geq \varepsilon$ for at least one subband **do** $\mathbf{C}_{\text{SU},i}^{(l)} = \left[(\lambda \mathbf{A}_i^{(l-1)} + \mu \mathbf{I})^{-1} - \frac{\sigma^2 + \|d_i\|^2 p_i}{\|f_i\|^2}\mathbf{I}\right]^+$ where $\text{Tr}(\mathbf{A}_i^{(l-1)}\mathbf{C}_{\text{SU},i}) = B^{(l-1)}$ and $\sum_{i=1}^{N} \text{Tr}(\mathbf{C}_{\text{SU},i}) = 2P_{\text{SU,max}}$ Update $\mathbf{A}_i^{(l)}$ and $B^{(l)}$ using (5.7) Set $l = l + 1$ **End (While)**

where λ, μ, and $\{\mathbf{U}_i\}_{i=1}^N$ are the Lagrangian multipliers of the constraints (5.6b), (5.6c), and (5.6d), respectively [13]. Equating the derivative of the Lagrangian to zero we obtain

$$\frac{\partial \mathcal{L}}{\partial \mathbf{C}_{\text{SU},i}} = \mathbf{0} \Rightarrow -\mathbf{F}_i^H \left[\mathbf{I} + (\sigma^2 \mathbf{I} + \mathbf{D}_i \mathbf{C}_{\text{PU},i} \mathbf{D}_i^H)^{-1} \mathbf{F}_i \mathbf{C}_{\text{SU},i} \mathbf{F}_i^H\right]^{-1} \mathbf{F}_i (\sigma^2 \mathbf{I} + \mathbf{D}_i \mathbf{C}_{\text{PU},i} \mathbf{D}_i^H)^{-1} - \mathbf{U}_i + \lambda \mathbf{A}_i^{l-1} + \mu \mathbf{I} = \mathbf{0}. \quad (5.9)$$

Since the coefficient matrices are scaled identity matrices, we can simplify (5.9) as

$$-\frac{\|f_i\|^2}{\sigma^2 + \|d_i\|^2 p_i}\left[\mathbf{I} + \frac{\|f_i\|^2}{\sigma^2 + \|d_i\|^2 p_i}\mathbf{C}_{\text{SU},i}\right]^{-1} - \mathbf{U}_i + \lambda \mathbf{A}_i^{(l-1)} + \mu \mathbf{I} = \mathbf{0}. \quad (5.10)$$

Note that if a constraint is not active, its corresponding Lagrangian multiplier is zero. Thus, if the solution of (5.10), $\mathbf{C}_{\text{SU},i}$, is positive semidefinite for $\mathbf{U}_i = \mathbf{0}$, (5.6d) is not active, and consequently, its corresponding Lagrangian multiplier, $\mathbf{U}_i$, is zero. Otherwise, $\mathbf{U}_i$ should be determine in a way that the eigenvalues of $\mathbf{C}_{\text{SU},i}$ are non-negative. The eigenvectors of $\mathbf{C}_{\text{SU},i}$ affect only constraint (5.6b), which implies that the eigenvectors of $\mathbf{C}_{\text{SU},i}$ are equal to the eigenvectors of $\mathbf{A}_i^{(l-1)}$ (see [72, Lemma 2]). Hence, the optimal solution can be obtained by solving (5.10) for $\mathbf{U}_i = \mathbf{0}$ and replacing the negative eigenvalues of $\mathbf{C}_{\text{SU},i}$, if there are any, by zero. Finally, the closed-form solution for $\mathbf{C}_{\text{SU},i}$ is

$$\mathbf{C}_{\text{SU},i} = \left[(\lambda \mathbf{A}_i^{(l-1)} + \mu \mathbf{I})^{-1} - \frac{\sigma^2 + \|d_i\|^2 p_{\text{PU},i}}{\|f_i\|^2}\mathbf{I}\right]^+, \quad (5.11)$$

where $\mathbf{Q} = [\mathbf{X}]^+$ denotes an operator that replaces negative eigenvalues of $\mathbf{X}$ with zeros. The Lagrangian multipliers μ and λ can be derived by solving $\sum_{i=1}^{N} \text{Tr}(\mathbf{C}_{\text{SU},i}) = 2P_{\text{SU,max}}$ and $\sum_{i=1}^{N} \text{Tr}\left(\mathbf{A}_i^{(l-1)}\mathbf{C}_{\text{SU},i}\right) = B^{(l-1)}$. Through (5.11), it can be easily observed that $\mathbf{C}_{\text{SU},i}$ follows the feasibility structure (5.3e) if $\mathbf{A}_i^{(l-1)}$, and consequently the initial point, satisfies (5.3e). This solution is iterated until convergence. We summarize the solution in Algorithm I.

When the power constraint is the only active constraint, the optimal solution is PGS, which can be obtained by the well-known water-filling approach. Thus, IGS may be beneficial only if the rate constraint is active. This is due to the fact that the rate of the SU is a decreasing function of the circularity coefficients; hence, a proper signal maximizes the rate when there is only a

power budget constraint. However, when the transmitted power is restricted by interference, the allowed transmission power can be increased by using improper signaling, which may result in a higher achievable rate [70]. But even in this case, the optimal solution may still turn out to be proper, depending on the channel coefficients.

5.3.2 Constraint on the rate of each subband

We now solve problem (5.3) assuming a constraint on the rate of the PU in each subband. We employ the analytical results in [70] to implement an algorithm for this optimization problem. In [70], a similar optimization problem for a single-carrier scenario is considered. Here, we extend the results to the OFDM scenario. In this subsection, in order to simplify the notations, we represent the power of the SU by q_i, i.e., $p_{\text{SU},i} = q_i$.

Lemma 5.1 *The signal transmitted on subband i is improper if and only if the following two conditions are met:*

1. *The corresponding channel coefficients satisfy $\frac{|g_i|^2(\sigma^2+p_{PU,i}|d_i|^2)}{|f_i|^2\sigma^2} > 1 - \frac{p_{PU,i}|h_i|^2}{\sigma^2(2^{2\overline{R}_i}-1)}$.*

2. *The power allocated to subband i is greater than a given threshold $q_{i,0}^{thr}$, which we derive further below.*

Proof. According to Theorem 1 in [70], improper signaling in subband i is only beneficial if $\frac{|g_i|^2(\sigma^2+p_{\text{PU},i}|d_i|^2)}{|f_i|^2\sigma^2}$ is greater than a threshold that does not depend on the channel coefficients. When improper signaling is rate-maximizing on a subband, this is due to the fact the maximum allowed power on that subband can be increased by using improper signaling. If the power allocated to this subband is greater than a threshold, which depends on the channel coefficients, the optimal transmission is improper. According to [70][Eq. (11)], the maximum allowed power $q_i^{\max}$ is a function of the circularity coefficient, hence we can write $q_i^{\max}(k_i)$. If the power allocated to the subband is greater than $q_{i,0}^{\text{thr}} = q_i^{\max}(0)$, improper signaling is optimal. □

According to Lemma 5.1, improper signaling may be beneficial on a subband depending on the channel coefficients. However, the power allocated to a subband plays an important role as well. Since the SU can allocate power to different subbands, proper transmissions may be the optimal solution even in subbands where improper signaling is potentially beneficial.

We propose an iterative algorithm to solve this problem. In general, if subband i is potentially beneficial for improper signaling, the rate of the SU in this subband can be written as [70]

$$R_{s,i} = \begin{cases} \log_2\left(1 + \frac{|f_i|^2 q_i}{\sigma^2 + |d_i|^2 p_{\text{PU},i}}\right) & \text{if} \quad 0 \leqslant q_i \leqslant q_{i,0}^{\text{thr}}, \\ \frac{1}{2}\log_2\left(C_i + D_i q_i\right) & \text{if} \quad q_{i,0}^{\text{thr}} \leqslant q_i \leqslant q_{i,1}^{\text{thr}}, \end{cases} \tag{5.12}$$

where C_i and D_i are constant coefficients, which can be obtained from [70]:

$$C_i = 1 + \frac{|f_i|^4}{|g_i|^4\left(p_{\text{PU},i}|d_i|^2 + \sigma^2\right)}\left(\frac{p_{\text{PU},i}^2|h_i|^4}{2^{2\overline{R}_i} - 1} - \sigma^4\right), \tag{5.13a}$$

$$D_i = \frac{2|f_i|^2}{p_{\text{PU},i}|d_i|^2 + \sigma^2} + \frac{2|f_i|^4}{|g_i|^2\left(p_{\text{PU},i}|d_i|^2 + \sigma^2\right)^2}\left(\frac{p_{\text{PU},i}|h_i|^2}{2^{2\overline{R}_i} - 1} - \sigma^2\right). \tag{5.13b}$$

Algorithm II Proposed solution for the rate constraint on each subband

Obtain C_i and D_i, for $i = 1, ..., N$, by (5.13),
For $i = 1, \ldots, N$
  If $D_i > 0$
    Improper is beneficial in this subband, and thus
    $R_{s,i} = \frac{1}{2}\log_2(C_i + D_i q_i)$,
    $q_i = q_{i,l}^{\text{thr}} = \frac{1}{|g_i|^2}\left(\frac{p_{\text{PU},i}|h_i|^2}{2^{\overline{R}_i}-1} - \sigma^2\right)$, and
    $q_{i,u}^{\text{thr}} = \frac{1}{2|g_i|^2}\left(\frac{p_{\text{PU},i}|h_i|^2}{2^{2\overline{R}_i - R_{p,i}^{\max}}-1} - \sigma^2\right)$
  Else
    Proper is beneficial in this subband, and thus
    $R_{s,i} = \log_2(1 + \frac{|f_i|^2}{\sigma^2+|d_i|^2 p_{\text{PU},i}} q_i)$, $q_i = q_{i,l}^{\text{thr}} = 0$, and
    $q_{i,u}^{\text{thr}} = \frac{1}{|g_i|^2}\left(\frac{p_{\text{PU},i}|h_i|^2}{2^{\overline{R}_i}-1} - \sigma^2\right)$
  End (If)
End (For)

While $q_i = q_{i,l}^{\text{thr}}$ for at least one improper subband **do**

$$q_i = \begin{cases} \left[\frac{1}{\mu} - \frac{C_i}{D_i}\right]_{q_{i,l}^{\text{thr}}}^{q_{i,u}^{\text{thr}}} & \text{if subband is improper} \\ \left[\frac{1}{\mu} - \frac{\sigma^2+|d_i|^2 p_{\text{PU},i}}{|f_i|^2}\right]_0^{q_{i,u}^{\text{thr}}} & \text{if subband is proper} \end{cases}$$

  for $i = 1, \ldots, N$, where μ is such that $\sum_{i=1}^{N} q_i = P_{\text{SU,max}}$
  For $i = 1, \ldots, N$
    If subband is improper and $q_i = q_{i,l}^{\text{thr}}$
      Make subband proper, and thus
      $R_{s,i} = \log_2(1 + \frac{|f_i|^2}{\sigma^2+|d_i|^2 p_{\text{PU},i}} q_i)$
      $q_{i,l}^{\text{thr}} = 0$, and $q_{i,u}^{\text{thr}} = \frac{1}{|g_i|^2}\left(\frac{p_{\text{PU},i}|h_i|^2}{2^{\overline{R}_i}-1} - \sigma^2\right)$
    End (If)
  End (For)
End (While)

Note that the first condition in Lemma 1 is equal to $D_i > 0$. Finally, the thresholds in (5.12) are

$$q_{i,0}^{\text{thr}} = \frac{1}{|g_i|^2}\left(\frac{p_{\text{PU},i}|h_i|^2}{2^{\overline{R}_i}-1} - \sigma^2\right), \tag{5.14a}$$

$$q_{i,1}^{\text{thr}} = \frac{1}{2|g_i|^2}\left(\frac{p_{\text{PU},i}|h_i|^2}{2^{2\overline{R}_i - R_{p,i}^{\max}}-1} - \sigma^2\right), \tag{5.14b}$$

where $R_{p,i}^{\max} = R_{p,i}(q_i = 0)$ refers to the maximum achievable rate of the PU on subband i. The thresholds in (5.14a) and (5.14b) are the maximum allowed power of the SU in proper, $k_i = 0$, and maximally improper, $k_i = 1$, cases, respectively.

In our proposed iterative algorithm, it is assumed in the first iteration that an improper signal is transmitted on a subband if an improper signal is potentially beneficial on that subband, i.e., the first condition in Lemma 5.1 is fulfilled. As a result, the allocated power is constrained to

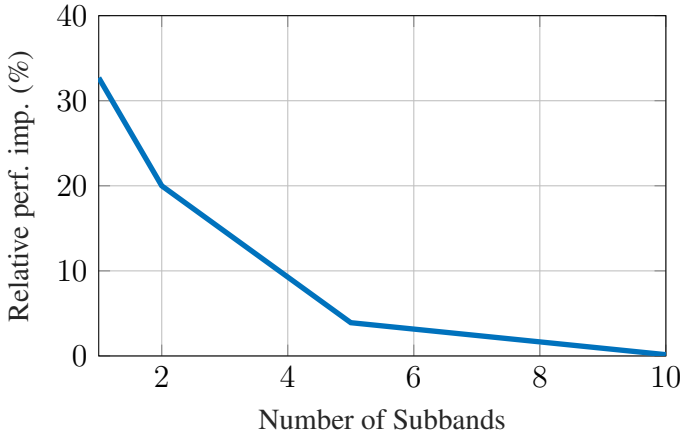

Figure 5.2: Improvement by employing improper signaling versus the number of subbands for $\alpha = 70\%$. The results are for the constraint on total rate.

be in the interval $[q_{i,0}^{\text{thr}}, q_{i,1}^{\text{thr}}]$. The rate of the SU is computed based on (5.12). The solution of this optimization problem is the well-known water-filling approach [24]. If, after solving the optimization in (5.3), the power allocated to an improper subband is equal to $q_{i,0}^{\text{thr}}$, proper signaling is the optimal solution for this subband. Thus, we update the set of proper and improper subbands and solve again the problem in (5.3). This procedure is iterated until all the powers allocated to all improper subbands are greater than $q_{i,0}^{\text{thr}}$. The proposed algorithm is summarized in Algorithm II. Note that $q_{i,l}^{\text{thr}}$ and $q_{i,u}^{\text{thr}}$ are lower and upper bounds of the power allocated to each subband in Algorithm II, respectively. Moreover, $[X]_a^b = \max\left(\min(X, b), a\right)$.

5.4 Numerical Results

In this section, we provide some numerical results. We consider Rayleigh fading channels, in which the real and imaginary parts of the channel coefficients are independent Gaussian random variables $\mathcal{N}(0, 1)$. For the sake of simplicity, it is assumed that the PU transmits with a fixed power P on each subband. The transmitted power of the PU on each subband, P, and variance of the additive Gaussian noise, σ^2 are equal to 1. The results are obtained by averaging over 100 independent channel realizations.

In Fig. 5.2, the improvement in rate obtained by employing improper signaling is shown for $\alpha = 70\%$, where $\alpha = \frac{\overline{R}}{R_p(\mathbf{q}=0)}$ is the loading factor. In order to consider the effect of identical parallel channels, we assumed that $P_{\text{SU,max}} = PN$. In other words, the power budget of the SU is increased at the same rate as the transmission power of the PU. The rate improvement by employing improper signaling decreases rapidly with increasing number of subbands, from 30% for $N = 1$ to less than 1% for $N = 10$. This is due to the fact that the SU can allocate power more flexibly when there are more subbands.

Let us now consider the problem where there is a rate constraint on each subband. Figure 5.3 shows the improvement obtained by employing improper signaling versus the number of subbands for $\alpha = 70\%$ and $P_{\text{SU,max}} = PN$. As before, the improvements rapidly decrease with an increasing number of subbands.

In Fig. 5.4, the improvements of improper signaling over proper signaling are shown as a function of α. The improvement is a decreasing function of α. When $N = 10$, which is a

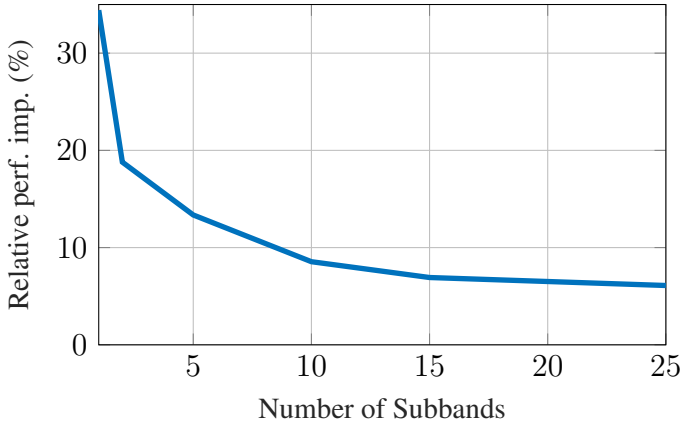

Figure 5.3: Improvement by employing improper signaling versus the number of subbands for $\alpha = 70\%$. The results are for the rate constraint on each subband.

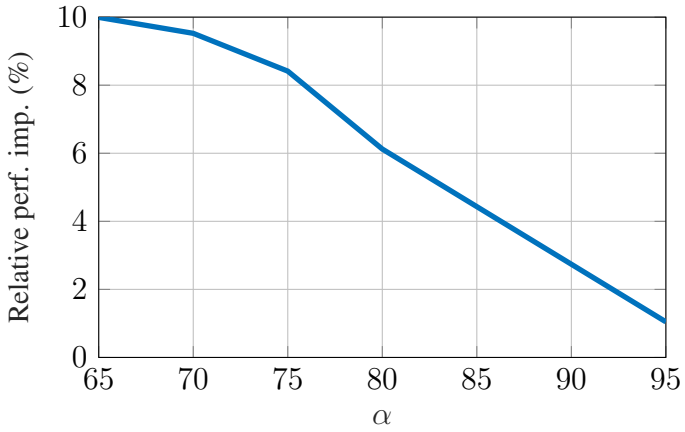

Figure 5.4: Improvement by employing improper signals versus α for $P_{\text{SU,max}} = 20$ and $N = 10$. The results are for the rate constraint on each subband.

relatively low number, the improvement is less than 10% for $\alpha > 65\%$. Moreover, as shown in Fig. 5.3, this gain decreases with increasing number of subbands.

We notice that improper signaling is more beneficial in the scenario where the rate threshold is on each subband. The reason is that, for example, when $\alpha = 80\%$ it is possible for the PU to neglect one subband out of five without violating the rate constraint. Thus, the SU can transmit proper signals with maximum power on that subband. As we observe in Fig. 5.3, even though improper signaling is more effective in the second scenario, the benefits also rapidly decrease with increasing number of subbands N.

5.5 Summary

Improper signaling has received quite a bit of attention lately as a means to improve achievable rates in interference channels. In this chapter, we investigated whether IGS is also beneficial in an OFDM UCR system. While there are indeed some benefits, these are minor and mainly apply to scenarios with small number of OFDM subbands. Such a rather negative result may be surprising, but it shows that improper signaling is not a magic tool that works in every case. Rather, its use needs to be justified on a case-by-case basis.

6 Achievable rate region of the K-user IC with asymmetric AHWD

In this chapter, we consider the achievable rate region of the K-user SISO IC with asymmetric AHWD. Since there are fewer optimization parameters in single antenna systems compared to multiple antenna systems, we are able to propose simpler and/or computationally less expensive algorithms for these systems. We first propose an iterative algorithm based on a sequential optimization method in which we solve a sequence of fractional optimization problems [6,108]. We derive the global optimal solution of each surrogate problem by fractional programming (FP) and the generalized Dinkelbach algorithm (GDA). In order to derive the achievable rate region, we rewrite the corresponding optimization problem as pseudo-signal-to-interference-plus-noise (PSINR) region, which is equivalent to the rate region problem. Our first proposed algorithm obtains a stationary point of the PSINR region. We then propose a simplified algorithm that is computationally less expensive than our proposed algorithm with FP. This simplified algorithm is based on a separate optimization of powers and complementary variances of users. We employ a bisection method to obtain the powers of the 2-user IC and derive a closed-form solution for powers in each iteration. Then, we employ difference of convex programming (DCP) to find the complementary variances. DCP falls into majorization minimization (MM) algorithms and can be applied to optimization problems in which either the objective and/or constraints are a difference of two concave/convex functions. Our results show that IGS enlarges the achievable rate of the two-user IC in the presence of asymmetric AHWD, and that there is a significant performance improvement by IGS for highly asymmetric HWD noise. Moreover, both of our proposed algorithms outperform existing PGS and other existing IGS algorithms. Results of this chapter have been published in [101].

6.1 Problem Statement

In this chapter, we aim at obtaining the boundary of the achievable rate region for the K-user SISO IC with asymmetric AHWD, which is described in Section 3.3.1. To this end, we employ the following definition of the Pareto boundary for the achievable rate region in Definition 4.1. As indicated in Section 4.3, the rate region is the union of all these achievable rate tuples, i.e.,

$$\mathcal{R} = \bigcup_{\{\mathbf{p},\mathbf{q}\}\in\Omega} (R_1, R_2, \cdots, R_K), \tag{6.1}$$

where Ω is the feasibility set of parameters, which is given by (3.38). Moreover, the boundary of the rate region can be derived by the rate profile technique as in the following optimization

problem [129]

$$\max_{R,\{\mathbf{p},\mathbf{q}\}\in\Omega} \quad R \qquad \text{s.t.} \qquad R_k \geq \lambda_k R, \qquad k = 1, 2, \cdots, K. \tag{6.2}$$

The paper in [64] proposed an algorithm based on DCP to maximize the achievable rate of a multihop relay system with asymmetric AHWD, in which all nodes transmit with maximum power, by optimizing over the complementary variances. Such algorithms cannot be applied for a joint optimization of powers and complementary variances since, in this case, the rates are not a difference of two jointly concave/convex functions in $\mathbf{p}$ and $\mathbf{q}$. Hence, we solve (6.2) by MM and FP. In MM, the objective function and constraints of an optimization problem are not required to follow a very specific structure such as being a difference of two convex/concave functions, which makes it more powerful than DCP.

To solve (6.2), we rewrite it such that it is more suitable to be solved with MM and FP. To this end, we employ the PSINR profile technique in [74, 92] to write an optimization problem that results in the solution of (6.2). We define the PSINR profile as

$$\max_{E,\{\mathbf{p},\mathbf{q}\}\in\Omega} \quad E \qquad \text{s.t.} \qquad E_k(\mathbf{p},\mathbf{q}) \geq 1 + \alpha_k E, \qquad k = 1, 2, \cdots, K, \tag{6.3}$$

where $\alpha_k \geq 0$ for all k are constants, $\sum_{k=1}^{K} \alpha_k = 1$, and

$$E_k(\mathbf{p},\mathbf{q}) \triangleq \frac{(\sigma^2 + \mathbf{a}_k^T\mathbf{p})^2 - |\mathbf{f}_k^H\mathbf{q} + \tilde{\mathbf{f}}_k^H\mathbf{p}|^2}{(\sigma^2 + \mathbf{b}_k^T\mathbf{p})^2 - |\mathbf{g}_k^H\mathbf{q} + \tilde{\mathbf{f}}_k^H\mathbf{p}|^2} = \frac{u_k(\mathbf{p},\mathbf{q})}{v_k(\mathbf{p},\mathbf{q})}. \tag{6.4}$$

We can derive the boundary of the PSINR region by varying α_ks. Note that $E_k(\mathbf{p},\mathbf{q}) \geq 1$ for all k since the rates are non-negative. Moreover, the numerator and denominator of $E_k(\mathbf{p},\mathbf{q})$ are strictly positive because the rates are bounded and non-negative. In the following lemma, we show that this technique results in the boundary of the rate region in (6.2).

Lemma 6.1 ([74, 92]) *Every point in the boundary of the rate region corresponds to a point in the boundary of the PSINR region, and vice versa.*

Proof. Assume there exists a vector $(R_1, R_2, \cdots, R_K)$ on the boundary of the achievable rate region that is not on the boundary of the PSINR region. In other words, the vector $(E_1 = 2^{R_1}, E_2 = 2^{R_2}, \cdots, E_K = 2^{R_K})$, which is a feasible PSINR pair, is not on the boundary of the PSINR region, and hence there exist $(E_1', E_2', \cdots, E_K') \neq (E_1, E_2, \cdots, E_K)$ such that the vector $(E_1', E_2', \cdots, E_K') \geq (E_1, E_2, \cdots, E_K)$ is feasible. Since the logarithm functions are monotonically increasing, the rate vector

$$(0.5\log_2(E_1'), 0.5\log_2(E_2'), \cdots, 0.5\log_2(E_K')) \geq (R_1, R_2, \cdots, R_K)$$

and $(0.5\log_2(E_1'), 0.5\log_2(E_2'), \cdots, 0.5\log_2(E_K')) \neq (R_1, R_2, \cdots, R_K)$ is achievable, which implies that $(R_1, R_2, \cdots, R_K)$ is not on the boundary of the rate region. Similarly, it can be shown that every point in the boundary of the PSINR region associates with a point in the boundary of the rate region. The inequalities $\geq$ are taken element-wise. □

Note that we can rewrite (6.3) as the following maximin optimization problem by removing

the variable E

$$\max_{\{\mathbf{p},\mathbf{q}\}\in\Omega} \quad \min_{k} \left\{ \frac{E_k(\mathbf{p},\mathbf{q})-1}{\alpha_k} \right\}. \tag{6.5}$$

6.2 Boundary of the rate region by Fractional Programming

In this section, we solve the PSINR profile problem in (6.3) by MM, which results in solving a sequence of fractional optimization problems. We solve each fractional optimization problem by FP and the generalized Dinkelbach algorithm [30, 98, 126]. Our proposed algorithm converges to a stationary point of (6.3). We can apply the generalized Dinkelbach algorithm to derive the boundary of the PSINR region since the optimization problem can be written as a maximin weighted problem as indicated in (6.5). However, since $u_k(\mathbf{p},\mathbf{q})$ and $v_k(\mathbf{p},\mathbf{q})$ are not, respectively, concave and convex in optimization variables, the corresponding optimization problem in each iteration of the generalized Dinkelbach algorithm is not convex. Indeed, $u_k(\mathbf{p},\mathbf{q})$ and $v_k(\mathbf{p},\mathbf{q})$ are a difference of two convex/concave functions:

$$u_k(\mathbf{p},\mathbf{q}) = \underbrace{-|\mathbf{f}_k^H\mathbf{q}+\tilde{\mathbf{f}}_k^H\mathbf{p}|^2}_{\text{concave part}} + \underbrace{(\sigma^2+\mathbf{a}_k^T\mathbf{p})^2}_{\text{convex part}}, \tag{6.6}$$

$$v_k(\mathbf{p},\mathbf{q}) = \underbrace{-|\mathbf{g}_k^H\mathbf{q}+\tilde{\mathbf{f}}_k^H\mathbf{p}|^2}_{\text{concave part}} + \underbrace{(\sigma^2+\mathbf{b}_k^T\mathbf{p})^2}_{\text{convex part}}. \tag{6.7}$$

Hence, to solve (6.5), we employ a sequential optimization approach by approximating $E_k(\mathbf{p},\mathbf{q})$ with a lower bound $\tilde{E}_k(\mathbf{p},\mathbf{q},\mu)$ in each iteration [6, 108]. Then, we obtain the global optimal solution of each surrogate optimization problem by the generalized Dinkelbach algorithm. To this end, in each iteration, we first approximate $u_k(\mathbf{p},\mathbf{q})$ by a lower bound concave function $\tilde{u}_k(\mathbf{p},\mathbf{q})$ and $v_k(\mathbf{p},\mathbf{q})$ by an upper bound convex function $\tilde{v}_k(\mathbf{p},\mathbf{q})$ as in the following lemma.

Lemma 6.2 *A concave lower bound for $u_k(\mathbf{p},\mathbf{q})$ in the mth iteration is*

$$\tilde{u}_k^{(m)}(\mathbf{p},\mathbf{q}) = -|\mathbf{f}_k^H\mathbf{q}+\tilde{\mathbf{f}}_k^H\mathbf{p}|^2 + (\sigma^2+\mathbf{a}_k^T\mathbf{p}^{(m)})^2 + 2(\sigma^2+\mathbf{a}_k^T\mathbf{p}^{(m)})\mathbf{a}_k^T(\mathbf{p}-\mathbf{p}^{(m)}), \tag{6.8}$$

Moreover, a convex upper bound for $v_k(\mathbf{p},\mathbf{q})$ in the mth iteration is

$$\begin{aligned}\tilde{v}_k^{(m)}(\mathbf{p},\mathbf{q}) =& (\sigma^2+\mathbf{b}_k^T\mathbf{p})^2 - |\mathbf{g}_k^H\mathbf{q}^{(m)}+\tilde{\mathbf{f}}_k^H\mathbf{p}^{(m)}|^2 - 2\Re\left[\tilde{\mathbf{f}}_k^H(\mathbf{g}_k^H\mathbf{q}^{(m)}+\tilde{\mathbf{f}}_k^H\mathbf{p}^{(m)})^*\right](\mathbf{p}-\mathbf{p}^{(m)}) \\ & - 2\Re\left[(\mathbf{g}_k^H\mathbf{q}^{(m)}+\tilde{\mathbf{f}}_k^H\mathbf{p}^{(m)})^*\mathbf{g}_k^H(\mathbf{q}-\mathbf{q}^{(m)})\right],\end{aligned} \tag{6.9}$$

where $\mathbf{p}^{(m)}$ and $\mathbf{q}^{(m)}$ are the power and complementary variances at the mth iteration, which are the solution of the previous iteration. Furthermore, $\Re[x]$ takes the real part of x.

Proof. Please refer to Section 6.6. □

Now, we are able to write the surrogate optimization problem in mth iteration as

$$\max_{E',\{\mathbf{p},\mathbf{q}\}\in\Omega} \quad E \qquad \text{s.t.} \qquad \tilde{E}_k^{(m)}(\mathbf{p},\mathbf{q}) \geq 1+\alpha_k E', \qquad k=1,2,\cdots,K, \tag{6.10}$$

Algorithm I Proposed sequential optimization algorithm.

Initialization

Set ε, M, $\mathbf{p}^{(0)} = \mathbf{0}$, $\mathbf{q}^{(0)} = \mathbf{0}$, $m = 1$, convergence=0

While convergence=0 and $m \leq M$ **do**

Construct $\tilde{E}_k^{(m)}(\mathbf{p}, \mathbf{q}) = \tilde{u}_k^{(m)}(\mathbf{p}, \mathbf{q})/\tilde{v}_k^{(m)}(\mathbf{p}, \mathbf{q})$ for $k = 1, 2, \cdots, K$, using Lemma 6.2

Obtain $\mathbf{p}^{(m+1)}$ and $\mathbf{q}^{(m+1)}$ by solving (6.10), i.e., run algorithm II

If $\|\mathbf{p}^{(m)} - \mathbf{p}^{(m+1)}\|/\|\mathbf{p}^{(m)}\| < \varepsilon$

and $\|\mathbf{q}^{(m)} - \mathbf{q}^{(m+1)}\|/\|\mathbf{q}^{(m)}\| < \varepsilon$

convergence=1

$\mathbf{p}^{(\star)} = \mathbf{p}^{(m+1)}$ and $\mathbf{q}^{(\star)} = \mathbf{q}^{(m+1)}$

End (If)

$m = m + 1$

End (While)

Return $\mathbf{p}^{(\star)}$ and $\mathbf{q}^{(\star)}$.

where $\tilde{E}_k^{(m)}(\mathbf{p}, \mathbf{q}) = \frac{\tilde{u}_k^{(m)}(\mathbf{p},\mathbf{q})}{\tilde{v}_k^{(m)}(\mathbf{p},\mathbf{q})}$ and $E_k(\mathbf{p}, \mathbf{q})$ fulfill the following conditions:

1. $\tilde{E}_k^{(m)}(\mathbf{p}, \mathbf{q}) \leq E_k(\mathbf{p}, \mathbf{q})$ for all feasible $\mathbf{p}, \mathbf{q}$ and $k = 1, 2, \cdots, K$.
2. $\tilde{E}_k^{(m)}(\mathbf{p}^{(m)}, \mathbf{q}^{(m)}) = E_k(\mathbf{p}^{(m)}, \mathbf{q}^{(m)})$ for $k = 1, 2, \cdots, K$.
3. $\frac{\partial \tilde{E}_k^{(m)}(\mathbf{p}^{(m)},\mathbf{q}^{(m)})}{\partial \mathbf{p}} = \frac{\partial E_k(\mathbf{p}^{(m)},\mathbf{q}^{(m)})}{\partial \mathbf{p}}$ and $\frac{\partial \tilde{E}_k^{(m)}(\mathbf{p}^{(m)},\mathbf{q}^{(m)})}{\partial \mathbf{q}} = \frac{\partial E_k(\mathbf{p}^{(m)},\mathbf{q}^{(m)})}{\partial \mathbf{q}}$ for $k = 1, 2, \cdots, K$.

These properties guarantee that the algorithm converges to a stationary point of (6.3) [6, Section II.B]. To solve (6.10) and obtain $\mathbf{p}^{(m+1)}$ and $\mathbf{q}^{(m+1)}$, we employ the GDA, which gives the global optimal solution of (6.10), as in the following. We summarize this procedure in Algorithm I.

Now we solve (6.10) and obtain its global optimal solution by FP, which is also an iterative algorithm as explained in Section 4.1.4. To this end, we introduce the following functions, which are the corresponding surrogate functions of $\frac{\tilde{E}_k^{(m)} - 1}{\alpha_k}$ for $k = 1, 2 \cdots, K$:

$$\hat{E}_k(\mathbf{p}, \mathbf{q}, \mu^{(l)}) \triangleq u_k^{(m)}(\mathbf{p}, \mathbf{q}) - (\mu^{(l)}\alpha_k + 1)v_k^{(m)}(\mathbf{p}, \mathbf{q}), \tag{6.11}$$

where $\mu^{(l)} \in \mathbb{R}$ is fixed and given by

$$\mu^{(l)} = \min_k \left(\frac{\tilde{E}_k(\mathbf{p}^{(l-1)}, \mathbf{q}^{(l-1)}) - 1}{\alpha_k} \right). \tag{6.12}$$

It is worth mentioning that the GDA requires an initial point $\mu^{(0)}$, which can be obtained by substituting $\mathbf{p}^{(m)}$ and $\mathbf{q}^{(m)}$ in (6.12). By substituting (6.11) in (6.10), the optimization problem at each iteration of the GDA is

$$\max_{E', \{\mathbf{p},\mathbf{q}\} \in \Omega} \quad E' \qquad \text{s.t.} \qquad \hat{E}_k(\mathbf{p}, \mathbf{q}, \mu^{(l)}) \geq E', \qquad k = 1, 2, \cdots, K. \tag{6.13}$$

We solve (6.13) for the given $\mu^{(l)}$, which results in $\mathbf{p}^{(l)}$ and $\mathbf{q}^{(l)}$. Then, we update $\mu^{(l)}$ by (6.12) and repeat the procedure until a convergence metric is met. As indicated in Section 4.1.4, the

Algorithm II Generalized Dinkelbach algorithm.

Initialization

Set ε, L, $l = 0$, $\mu^{(l)} = \min_{\forall k} \left(\frac{\tilde{E}_k(\mathbf{p}^{(m)}, \mathbf{q}^{(m)}) - 1}{\alpha_k} \right)$

Compute $\hat{E}_k(\mathbf{p}, \mathbf{q}, \mu^{(l)})$ for all k by (6.11)

While $\min_{\forall k} \{\hat{E}_k(\mathbf{p}, \mathbf{q}, \mu^{(l)})\} \geq \varepsilon$ and $l \leq L$ **do**

$l = l + 1$

Obtain $\mathbf{p}^{(l)}$ and $\mathbf{q}^{(l)}$ by solving (6.13)

If $\min_{\forall k} \{\tilde{E}_k(\mathbf{p}, \mathbf{q}, \mu^{(l)})\} < \varepsilon$

$\mathbf{p}^{(\star)} = \mathbf{p}^{(l)}$ and $\mathbf{q}^{(\star)} = \mathbf{q}^{(l)}$

Else

Update $\mu^{(l)}$ by (6.12)

End (If)

End (While)

Return $\mathbf{p}^{(\star)}$ and $\mathbf{q}^{(\star)}$.

convergence rate of the GDA is linear. The optimization problem (6.13) is convex, and its global optimal solution can be efficiently obtained [13]. We summarize this procedure in Algorithm II.

To sum up, the proposed algorithm works as follows. We solve the PSINR profile in (6.3) by solving a sequence of fractional optimization problems. Indeed, we employ a sequential optimization approach and approximate the PSINR term of each user by a lower bound. In order to derive the global optimal solution of each fractional optimization problem, we perform another iterative algorithm, i.e., the GDA. It is worth mentioning that this algorithm does not converge to the Pareto-optimal solution; however, it obtains a stationary point of (6.3).

6.3 Simplified algorithm

In this section, we propose a simplified version of the algorithm from Section 6.2, which exhibits a lower computational complexity. In the simplified algorithm, we first optimize the transmission power $\mathbf{p}$ for PGS, i.e., for $\mathbf{q} = \mathbf{0}$. This problem is addressed in Section 6.3.1. Then, in Section 6.3.2, we optimize the complementary variances for the resulting transmit power $\mathbf{p}$ such that the rates of all users are simultaneously increased.

6.3.1 Power optimization

In this subsection, we optimize the transmission power vector $\mathbf{p}$ for PGS, i.e., when $\mathbf{q} = \mathbf{0}$. In this case, deriving the boundary of the PSINR region can be cast as the optimization problem

$$\max_{E, \mathbf{p}} \; E \tag{6.14a}$$

$$\text{s.t.} \quad \frac{(\sigma^2 + \mathbf{a}_i^T \mathbf{p})^2 - |\tilde{\mathbf{f}}_i^H \mathbf{p}|^2}{(\sigma^2 + \mathbf{b}_i^T \mathbf{p})^2 - |\tilde{\mathbf{f}}_i^H \mathbf{p}|^2} \geq 1 + \alpha_k E, \qquad k = 1, 2, \cdots, K, \tag{6.14b}$$

$$0 \leq p_k \leq P_k, \qquad k = 1, 2, \cdots, K, \tag{6.14c}$$

for $\alpha_k \geq 0$ and $\sum_k \alpha_k = 1$. Unfortunately, the optimization problem in (6.14) is not convex due to (6.14b). In the following lemma, we derive a lower bound for (6.14b), which allows us to simplify (6.14) and derive a low-complexity algorithm.

Lemma 6.3 *A lower bound for the left-hand side of* (6.14b) *is*

$$\frac{(\sigma^2 + \mathbf{a}_i^T\mathbf{p})^2 - |\tilde{\mathbf{f}}_i^H\mathbf{p}|^2}{(\sigma^2 + \mathbf{b}_i^T\mathbf{p})^2 - |\tilde{\mathbf{f}}_i^H\mathbf{p}|^2} \geq \frac{(\sigma^2 + \mathbf{a}_i^T\mathbf{p})^2}{(\sigma^2 + \mathbf{b}_i^T\mathbf{p})^2}, \tag{6.15}$$

where the equality in (6.15) *holds if and only if the AHWD noise is proper, i.e.,* $\tilde{\mathbf{f}}_i = \mathbf{0}$.

Proof. It is easy to verify that $0 \leq |\tilde{\mathbf{f}}_i^H\mathbf{p}|^2 < (\sigma^2 + \mathbf{b}_i^T\mathbf{p})^2 < (\sigma^2 + \mathbf{a}_i^T\mathbf{p})^2$. Let us define

$$f(t) = \frac{\beta_1 - t}{\beta_2 - t}, \tag{6.16}$$

where $0 \leq t < \beta_2 < \beta_1$. The lower bound in (6.15) is then satisfied if $f(t)$ is increasing in t. This function is strictly increasing in $t \in [0, \beta_2)$ since

$$\frac{\partial f(t)}{\partial t} = \frac{\beta_1 - \beta_2}{(\beta_2 - t)^2} > 0, \tag{6.17}$$

Thus, we have

$$\frac{\beta_1 - t}{\beta_2 - t} \geq \frac{\beta_1}{\beta_2}, \tag{6.18}$$

with equality if and only if $t = 0$. □

For each point characterized by $\{\alpha_k\}_{k=1}^K$, we solve (6.14) for the lower bound in (6.15) as the optimization problem

$$\max_{E,\mathbf{p}} \quad E \tag{6.19a}$$

$$\text{s.t.} \quad \frac{\sigma^2 + \mathbf{a}_k^T\mathbf{p}}{\sigma^2 + \mathbf{b}_k^T\mathbf{p}} \geq \sqrt{1 + \alpha_k E}, \qquad k = 1, 2, \cdots, K, \tag{6.19b}$$

$$0 \leq p_k \leq P_k, \qquad k = 1, 2, \cdots, K. \tag{6.19c}$$

It is worth mentioning that the lower bound in Lemma 6.3 is employed to simplify (6.14) and obtain the powers, and the actual rates are derived by substituting the obtained powers in (3.47). Note that the region achieved by solving (6.14) includes the region achieved by solving (6.19). If the AHWD noise is proper, (6.19) is equivalent to (6.14)[1]. The global optimum solution of (6.19) can be derived by employing a bisection method and solving a sequence of feasibility problems [6]. That is, we fix E as E' and consider the feasibility problem

$$\text{find} \quad \mathbf{p} \in \mathbb{R}^2, \tag{6.20a}$$

$$\text{s.t.} \quad (\mathbf{a}_k^T - \sqrt{1 + \alpha_k E'}\mathbf{b}_k^T)\mathbf{p} \geq (\sqrt{1 + \alpha_k E'} - 1)\sigma^2, \qquad k = 1, 2, \cdots, K, \tag{6.20b}$$

$$0 \leq p_k \leq P_k, \qquad k = 1, 2, \cdots, K. \tag{6.20c}$$

[1]This is in line with [51], where it was shown that proper Gaussian noise is the worst case in a K-user MIMO IC with ideal devices.

If (6.20) is feasible for a given E', the optimal solution of (6.19) is greater than or equal to E', i.e., $E^{(\star)} \geq E'$. Otherwise, $E^{(\star)} < E'$. In order to find $E^{(\star)}$, we employ the well-known bisection method over E' solving (6.20) at each iteration, which yields, upon convergence, the global optimal solution of (6.19) [13]. Constraints (6.20b) and (6.20c) are linear in $\mathbf{p}$, which permits deriving a closed-form expression for a feasible point in the 2-user IC, as presented in the following theorem. It should be noted that this algorithm does not attain the global optimal solution of (6.14). There might be optimization approaches to obtain its global optimal solution such as the monotonic optimization framework [77, 90, 125], although the computational complexity of these approaches is high.

Theorem 6.1 *The optimization problem in* (6.20) *is feasible for a given E' in the 2-user IC if and only if $0 \leq p'_k \leq P_k$, for $k = 1, 2$, where*

$$\begin{bmatrix} p'_1 \\ p'_2 \end{bmatrix} = \mathbf{A}^{-1} \begin{bmatrix} (\sqrt{1+\alpha_1 E'} - 1)\sigma^2 \\ (\sqrt{1+\alpha_2 E'} - 1)\sigma^2 \end{bmatrix}. \tag{6.33}$$

$$\begin{aligned} \mathbf{A} &= \begin{bmatrix} \mathbf{a}_1^T - \sqrt{1+\alpha_1 E'}\mathbf{b}_1^T \\ \mathbf{a}_2^T - \sqrt{1+\alpha_2 E'}\mathbf{b}_2^T \end{bmatrix} \\ &= \begin{bmatrix} |h_{11}|^2 \left(1 - \sigma^2_{\eta_{11}}(\sqrt{1+\alpha_1 E'} - 1)\right) & -|h_{21}|^2(1+\sigma^2_{\eta_{21}})(\sqrt{1+\alpha_1 E'} - 1) \\ -|h_{12}|^2(1+\sigma^2_{\eta_{12}})(\sqrt{1+\alpha_2 E'} - 1) & |h_{22}|^2 \left(1 - \sigma^2_{\eta_{22}}(\sqrt{1+\alpha_2 E'} - 1)\right) \end{bmatrix}. \end{aligned} \tag{6.34}$$

Proof. Please refer to Section 6.7. □

We note that this algorithm leads to the optimal PGS only when AHWD noise is proper. Note that PGS is suboptimal, in *point-to-point* communications, in the presence of asymmetric AHWD [60, 61]. Thus, the users may improve the performance by employing IGS in asymmetric AHWD. It is worth noting that, in this paper, we aim at proposing PGS and IGS schemes for the two-user IC with asymmetric AHWD, but we do not derive sufficient and necessary conditions for the optimality of IGS or PGS in the two-user IC with asymmetric AHWD, which remains an open problem.

6.3.2 Complementary variance design

In this subsection, we optimize the complementary variances $\mathbf{q}$ for a given $\mathbf{p}^{(\star)}$, which has been obtained by solving (6.19). We obtain $\mathbf{q}$ such that the rates of both users exceed the rates achieved by PGS, which are the rates achievable with $\mathbf{q} = \mathbf{0}$ and the power vector $\mathbf{p}^{(\star)}$ obtained by solving (6.19). In other words, we want to solve the optimization problem

$$\max_{t,\mathbf{q}} \quad t \tag{6.35a}$$

$$\text{s.t.} \quad \frac{(\sigma^2 + \mathbf{a}_k^T\mathbf{p}^{(\star)})^2 - |\mathbf{f}_k^H\mathbf{q} + \tilde{\mathbf{f}}_k^H\mathbf{p}^{(\star)}|^2}{(\sigma^2 + \mathbf{b}_k^T\mathbf{p}^{(\star)})^2 - |\mathbf{g}_k^H\mathbf{q} + \tilde{\mathbf{f}}_k^H\mathbf{p}^{(\star)}|^2} \geq E_{p,k} + \alpha_k t, \quad k = 1, 2, \cdots, K, \tag{6.35b}$$

$$|q_k| \leq p_k^{(\star)}, \qquad k = 1, 2, \cdots, K. \tag{6.35c}$$

where $p_k^{(\star)}$ is the kth element of $\mathbf{p}^{(\star)}$. Moreover, $E_{p,k}$ is fixed and given by

$$E_{p,k} = \frac{(\sigma^2 + \mathbf{a}_k^T \mathbf{p}^{(\star)})^2 - |\tilde{\mathbf{f}}_k^H \mathbf{p}^{(\star)}|^2}{(\sigma^2 + \mathbf{b}_k^T \mathbf{p}^{(\star)})^2 - |\tilde{\mathbf{f}}_k^H \mathbf{p}^{(\star)}|^2}. \tag{6.36}$$

Unfortunately, (6.35) is not convex due to (6.35b). Hence, in order to efficiently solve (6.35), we first rewrite (6.35b) as

$$\frac{(\sigma^2 + \mathbf{a}_k^T \mathbf{p}^{(\star)})^2 - |\mathbf{f}_k^H \mathbf{q} + \tilde{\mathbf{f}}_k^H \mathbf{p}^{(\star)}|^2 - \alpha_k t_k}{(\sigma^2 + \mathbf{b}_k^T \mathbf{p}^{(\star)})^2 - |\mathbf{g}_k^H \mathbf{q} + \tilde{\mathbf{f}}_k^H \mathbf{p}^{(\star)}|^2} \geq E_{p,k}, \tag{6.37}$$

where $t_k = t\left[(\sigma^2 + \mathbf{b}_k^T \mathbf{p}^{(\star)})^2 - |\mathbf{g}_k^H \mathbf{q} + \tilde{\mathbf{f}}_k^H \mathbf{p}^{(\star)}|^2\right]$. We then relax the relation between $\{t_k\}_{k=1}^K$ and $\mathbf{q}$ and treat $\{t_k\}_{k=1}^K$ as new optimization variables. In other words, we approximate (6.35) as

$$\max_{\{t_k\}_{k=1}^K, \mathbf{q}} \quad \min_k \{t_k\} \tag{6.38a}$$

$$\text{s.t.} \quad \frac{(\sigma^2 + \mathbf{a}_k^T \mathbf{p}^{(\star)})^2 - |\mathbf{f}_k^H \mathbf{q} + \tilde{\mathbf{f}}_k^H \mathbf{p}^{(\star)}|^2 - \alpha_k t_k}{(\sigma^2 + \mathbf{b}_k^T \mathbf{p}^{(\star)})^2 - |\mathbf{g}_k^H \mathbf{q} + \tilde{\mathbf{f}}_k^H \mathbf{p}^{(\star)}|^2} \geq E_{p,k}, \quad k = 1, 2, \cdots, K, \tag{6.38b}$$

$$|q_k| \leq p_k^{(\star)}, \qquad k = 1, 2, \cdots, K. \tag{6.38c}$$

If $\min_k\{t_k\} > 0$, the rates of both users are simultaneously increased by employing IGS. Otherwise, we set $\mathbf{q} = \mathbf{0}$ and employ PGS. Note that the constraint (6.38b) can be rewritten as

$$E_{p,k}|\mathbf{g}_k^H \mathbf{q} + \tilde{\mathbf{f}}_k^H \mathbf{p}^{(\star)}|^2 - |\mathbf{f}_k^H \mathbf{q} + \tilde{\mathbf{f}}_k^H \mathbf{p}^{(\star)}|^2 + (\sigma^2 + \mathbf{a}_k^T \mathbf{p}^{(\star)})^2 - E_{p,k}(\sigma^2 + \mathbf{b}_k^T \mathbf{p}^{(\star)})^2 \geq \alpha_k t_k, \tag{6.39}$$

which is a difference of two convex functions. Thus, (6.38) is not a convex optimization problem, but it can be efficiently solved by difference of convex programming and a convex-concave procedure similar to (6.13) [31,75,76,108,124]. Hence, we employ DCP and solve (6.38) iteratively. At each iteration, we approximate the left-hand side of (6.39) by a concave function. To this end, we employ the first-order Taylor expansion and approximate the convex part of (6.39) around the point $\mathbf{q}^{(l)}$ by an affine function as

$$|\mathbf{g}_k^H \mathbf{q} + \tilde{\mathbf{f}}_k^H \mathbf{p}^{(\star)}|^2 \simeq |\mathbf{g}_k^H \mathbf{q}^{(l)} + \tilde{\mathbf{f}}_k^H \mathbf{p}^{(\star)}|^2 + 2\Re\left((\mathbf{g}_k^H \mathbf{q}^{(l)} + \tilde{\mathbf{f}}_k^H \mathbf{p}^{(\star)})^* \mathbf{g}_k^H (\mathbf{q} - \mathbf{q}^{(l)})\right), \tag{6.40}$$

where $\mathbf{q}^{(l)}$ contains the complementary variances of the users in the lth iteration. It is worth mentioning that $|\mathbf{g}_i^H \mathbf{q} + \tilde{\mathbf{f}}_i^H \mathbf{p}^{(\star)}|^2$ is always greater than or equal to the right-hand side of (6.40), and consequently, no trust region is required in DCP [31, 76, 124]. Finally, in the lth each iteration, (6.39) can be approximated by

$$\begin{aligned} -|\mathbf{f}_k^H \mathbf{q} + \tilde{\mathbf{f}}_k^H \mathbf{p}^{(\star)}|^2 + E_{p,k}|\mathbf{g}_k^H \mathbf{q}^{(l)} + \tilde{\mathbf{f}}_k^H \mathbf{p}^{(\star)}|^2 + 2E_{p,k}\Re\left((\mathbf{g}_k^H \mathbf{q}^{(l)} + \tilde{\mathbf{f}}_k^H \mathbf{p}^{(\star)})^H \mathbf{g}_k^H (\mathbf{q} - \mathbf{q}^{(l)})\right) \\ + (\sigma^2 + \mathbf{a}_k^T \mathbf{p}^{(\star)})^2 - E_{p,k}(\sigma^2 + \mathbf{b}_k^T \mathbf{p}^{(\star)})^2 \geq \alpha_k t_k. \end{aligned} \tag{6.41}$$

Finally, the convex optimization problem in the lth iteration is

$$\max_{\{t_k\}_{k=1}^K, \mathbf{q}} \quad \min_k \{t_k\} \qquad \text{s.t.} \qquad (6.41), (6.38c). \tag{6.42}$$

This problem can be easily solved by standard numerical tools [13]. Moreover, the proposed DCP algorithm converges to a stationary point of (6.38) [31, 75, 76, 108, 124]. It is worth mentioning that a stationary point of (6.38) is not necessarily a stationary point of (6.35).

The proposed simplified algorithm can be summarized as follows. The joint optimization problem for $\mathbf{p}$ and $\mathbf{q}$ is decoupled into two separate optimization problems. We derive the transmission powers by employing the well-known bisection method, which results, in each iteration, in a feasibility problem that has a closed-form solution. Then, we employ the DCP algorithm to derive the complementary variances for the given transmission powers.

6.4 Numerical Results

In this section, we present some numerical results to illustrate our findings. In the numerical results, we consider only the 2-user IC. For all examples, we set $\sigma^2 = 1$, $P_1 = P_2 = P$, $\varepsilon = 10^{-4}$, and $L = M = 20$, where ε, L, and M are, respectively, the threshold for convergence, and the maximum number of iterations for Algorithms I and II. Moreover, the maximum number of iterations for the algorithm in Section 6.3.2 is 40. We also define the signal-to-noise ratio (SNR) as the ratio of the power budget to σ^2, i.e., SNR$= \frac{P}{\sigma^2}$. We compare our proposed algorithms with PGS and the joint variance and complementary variance optimization algorithm in [129] for IGS, which is designed for ideal devices. To the best of our knowledge, there exists no PGS algorithm for asymmetric AHWD in the literature. Because of that, we optimize the PGS scheme by using the first step of our simplified algorithm (see Section 6.3.1). In the figures, we use the following labels:

- **S-IGS**: our proposed simplified design in Section 6.3,
- **FP-IGS**: our proposed design with FP in Section 6.2,
- **PGS**: the proposed PGS design in Section 6.3.1,
- **I-IGS**: the joint variance and complementary variance IGS design in [129] for ideal devices,
- **S-TS**: our proposed design in Section 6.3 with time sharing,
- **F-TS**: our proposed design in Section 6.2 with time sharing,
- **P-TS**: the proposed PGS design in Section 6.3.1 with time sharing.

Note that when time sharing (TS) is employed, it is allowed to average data rates and transmission powers over several transmission strategies [47]. Due to practical restrictions, it is not always possible to average power over different time slots, and the total power consumption is mostly restricted in each time slot. When power constraint is considered for each operational point, TS results in the convex hull operation. Throughout this dissertation, we derive the achievable rate region with TS by taking the convex hull operation over the corresponding

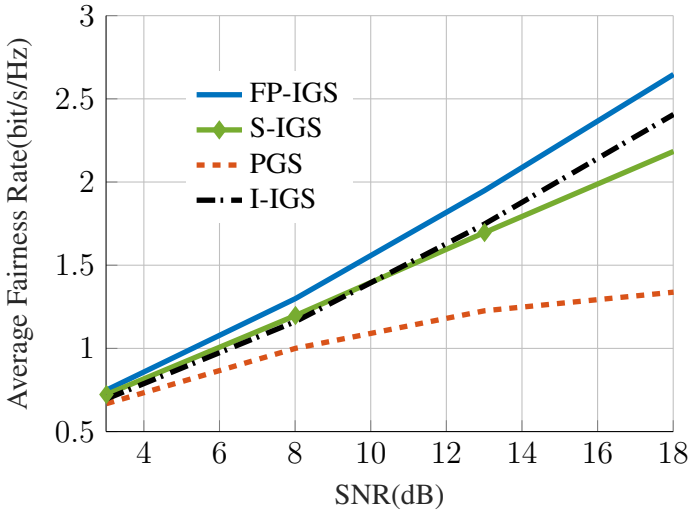

Figure 6.1: Average fairness rate for ideal devices versus the SNR.

achievable rate regions [129]. The achievable rate region with TS might be enlarged if an average power constraint over different operational point is considered [52]. However, this analysis is outside of the scope of this work.

6.4.1 Ideal devices

In this subsection, we compare the performance of our proposed algorithms with the joint variance and covariance IGS algorithm in [129] when there is no hardware distortion. In Fig. 6.1, we show the average fairness rate, i.e., the minimum rate allocated to the users, which is the fairness point of the rate region boundary and obtained by $\alpha_1 = \alpha_2 = 0.5$. We average the results over 100 channel realizations, where each channel realization is taken from a complex proper Gaussian distribution with variance 1, i.e., $\mathcal{CN}(0, 1, 0)$. As can be observed, our proposed algorithm based on FP outperforms the proposed algorithm in [129], especially at high SNR. Our simplified algorithm performs similarly to the proposed algorithm in [129] for low SNR. However, the algorithm in [129] performs better than the simplified algorithm in the moderate SNR regime. The reason is that the benefit of employing IGS increases with SNR. Thus, the performance differences of the IGS algorithms are clearer at higher SNR.

In Fig. 6.2, we also provide rate region examples for ideal devices and the channel realization

$$\mathbf{H}_1 = \begin{bmatrix} 1.4070e^{i0.2721} & 0.9288e^{i1.8320} \\ 0.9288e^{i1.8320} & 1.7367e^{i1.1136} \end{bmatrix}, \tag{6.43}$$

where $[\mathbf{H}_1]_{ij} = h_{ij}$ for $i, j \in \{1, 2\}$. As indicated before, the rate region figures highly depend on the channel realization. The advantage of these figures is that they provide a big picture of the system performance for different parameters. Although there are differences in the system performance for each channel realization, the main trends in the system operation remain unchanged. To cope with the changes for each channel realization, we also provide Monte Carlo-based simulations in which we have to consider a specific point of the rate region. In channel realization in (6.43), the direct links are stronger than the interference links. We can expect more benefits for IGS schemes when the interference links are stronger than the direct

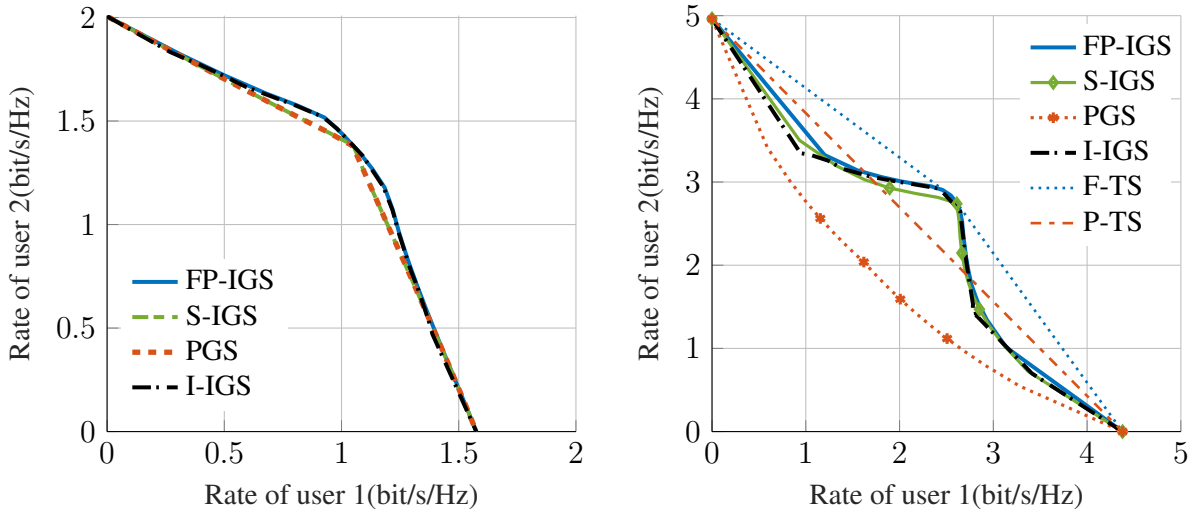

(a) $P = 1$ (SNR$=0$ dB) **(b)** $P = 10$ (SNR$=10$ dB)

Figure 6.2: Achievable rate region for ideal devices and channel realization $\mathbf{H}_1$ in (6.43).

links. As can be observed through Fig. 6.2, IGS can enlarge the achievable rate region for this channel realization and $P = 10$. Since the benefits of IGS are minor for low SNR, IGS does not provide any gain for $P = 1$. This is also in line with the averaged results in Fig. 6.1, where IGS has minor benefits at low SNR, while it improves the performance of the system significantly at moderate SNR. For this channel realization, our proposed algorithms and the algorithm in [129] perform very closely to each other. In Fig. 6.2b, we also consider the effect of TS on the achievable rate region. As can be observed, IGS with TS outperforms PGS with TS for this example. Since the IGS designs perform similarly, for this example, we provide only the TS for our proposed IGS design in Section 6.2.

The joint variance and covariance IGS algorithm in [129] is an iterative algorithm, based on a bisection method over the minimum weighted rates of users, and is proposed for *ideal devices*. The algorithm employs semidefinite relaxation (SDR) programming in order to solve the corresponding feasibility problem at each iteration of the bisection method. Since the solution of the SDR in [129] is not ensured to be rank-one, it does not necessarily obtain a valid solution, and a Gaussian randomization procedure is employed to obtain a rank-one solution. The solution obtained by the randomization procedure is not ensured to fulfill any optimality condition, which is in contrast with our proposed algorithm, which converges to a stationary point of (6.3). That may be the reason why our algorithm provides a better average fairness rate than SDR for high SNR in this scenario. It is also worth mentioning that our proposed algorithms are more general since they consider asymmetric AHWD, while the algorithm in [129] can only be applied for ideal devices.

6.4.2 Non-ideal devices

In this subsection, we consider the effect of AHWD on the performance of the two-user IC. Throughout this subsection, we consider the same statistics for AHWD in all devices. In Fig.

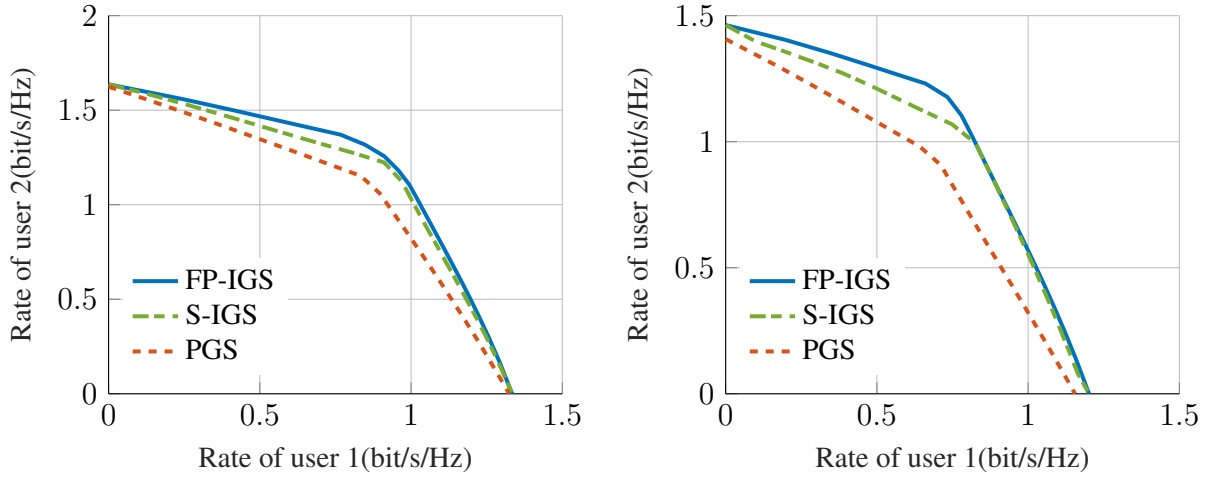

(a) $\sigma_\eta^2 = 0.2$ **(b)** $\sigma_\eta^2 = 0.5$

Figure 6.3: Achievable rate region for $|\tilde{\sigma}_\eta^2| = \sigma_\eta^2$, $P = 1$, and channel realization $\mathbf{H}_1$ in (6.43).

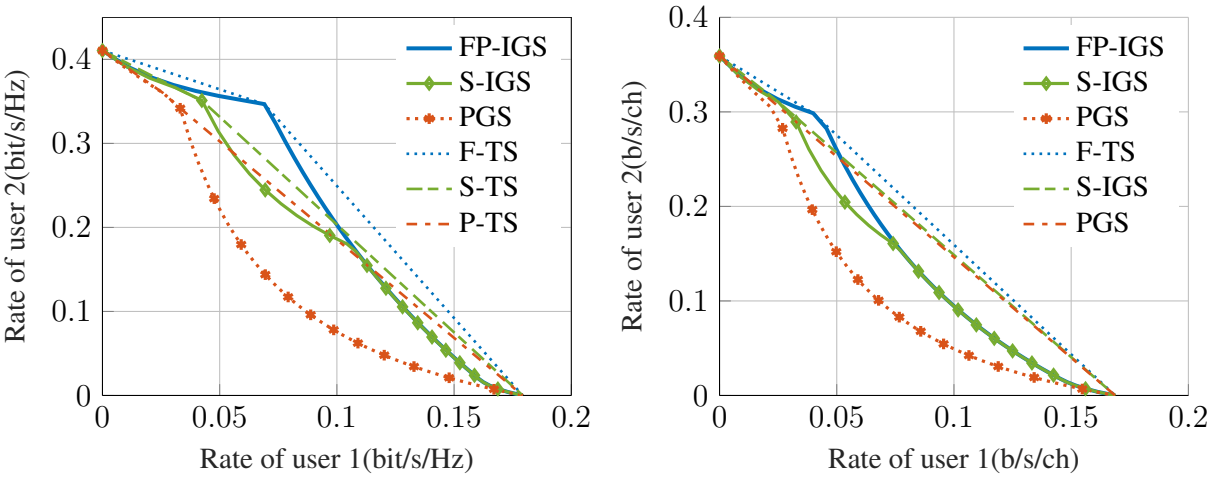

(a) $\sigma_\eta^2 = 0.5$ **(b)** $\sigma_\eta^2 = 1$

Figure 6.4: Achievable rate region for $\tilde{\sigma}_\eta^2 = 0$, $P = 1$, and channel realization $\mathbf{H}_2$ in (6.44).

6.3, we show the rate region for $\mathbf{H}_1$ and $P = 1$ under maximally improper AHWD[2] noise. As shown in Fig. 6.2a, IGS brings negligible gains when the transceivers are ideal, but, as observed in Fig. 6.3, IGS can significantly enlarge the rate region if there is asymmetric AHWD. Note that even in point-to-point communications, PGS is in general suboptimal for asymmetric AHWD, as it is shown in Fig. 6.3 for either $R_1 = 0$ or $R_2 = 0$.

In Fig. 6.4, we show the achievable rate region for $\tilde{\sigma}_\eta^2 = 0$, $P = 1$ (SNR$= 0$ dB), and channel realization

$$\mathbf{H}_2 = \begin{bmatrix} 0.3764e^{i1.4381} & 0.4029e^{i0.9486} \\ 1.8542e^{i2.8153} & 0.6277e^{i2.3697} \end{bmatrix}. \tag{6.44}$$

We take $\tilde{\sigma}_\eta^2 = 0$, i.e., symmetric (proper) AHWD. We can observe that IGS enlarges the rate

[2]Maximally improper AHWD happens when the in-phase and quadrature-phase noises are completely correlated [64].

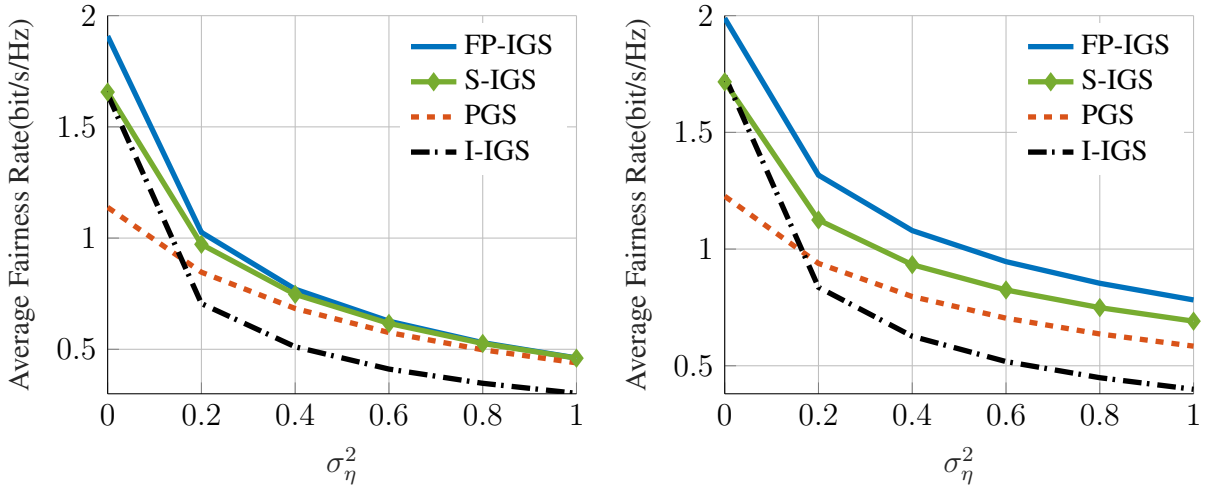

(a) $\tilde{\sigma}_\eta^2 = 0$ **(b)** $\tilde{\sigma}_\eta^2 = \sigma_\eta^2$.

Figure 6.5: Average fairness rate versus the variance of the AHWD noise for $P = 20$.

region even for proper AHWD with high noise variance, i.e., $\sigma_\eta^2 = 0.5$ and $\sigma_\eta^2 = 1$. Note that the PGS design is Pareto-optimal in the presence of symmetric AHWD. As can be observed, our IGS design in Section 6.2 with TS outperforms the Pareto-optimal PGS with TS for these examples.

In the following, we provide some averaged results for different parameters to illustrate different aspects of employing IGS. Similar to Fig. 6.1, we average the results over 100 channel realizations, where each channel realization is taken from a complex proper Gaussian distribution with variance 1, i.e., $\mathcal{CN}(0, 1, 0)$.

In Fig. 6.5, we consider the effect of the variance of the AHWD noise on the average fairness rate of users ($\alpha_1 = \alpha_2 = 0.5$) for $P = 20$. In this figure, we consider proper ($\tilde{\sigma}_\eta^2 = 0$) and maximally improper ($\tilde{\sigma}_\eta^2 = \sigma_\eta^2$) AHWD noise. We observe that our proposed algorithm with FP outperforms the other algorithms for maximally improper AHWD noise. Moreover, in Fig. 6.5a, our proposed IGS algorithms perform better than PGS for proper AHWD noise with different variances, which is Pareto-optimal PGS in this case. Furthermore, our simplified algorithm outperforms the IGS algorithm in [129] in the presence of AHWD. However, the performance improvement by our algorithms is minor for proper AHWD with high noise variance, where our algorithms only provide 5% improvement over PGS when $\sigma_\eta^2 = 1$ for this example.

Figure 6.6 shows the effect of the circularity coefficient of the AHWD noise on the fairness rate for $P = 20$. As can be observed, the benefits of employing IGS increase with the circularity coefficient of the AHWD noise, and there is a considerable performance improvement by IGS in maximally improper AHWD noise. We emphasize that PGS is suboptimal, even in interference-free communications, under asymmetric AHWD. Our proposed IGS design with FP outperforms the other algorithms, especially in highly asymmetric AHWD noise. When the variance of the AHWD noise is small, the gain of employing IGS is larger. The other interesting result in this figure is that our simplified algorithm performs very similarly to our proposed algorithm based on FP for proper AHWD. Since the simplified algorithm has less computational cost, it can be employed for proper AHWD noise when the variance of the AHWD noise is high, i.e., $\sigma_\eta^2 \geq 0.5$. However, our proposed algorithm based on FP outperforms the other algorithm in low-power AHWD noise and/or highly asymmetric AHWD noise. Note that, since the

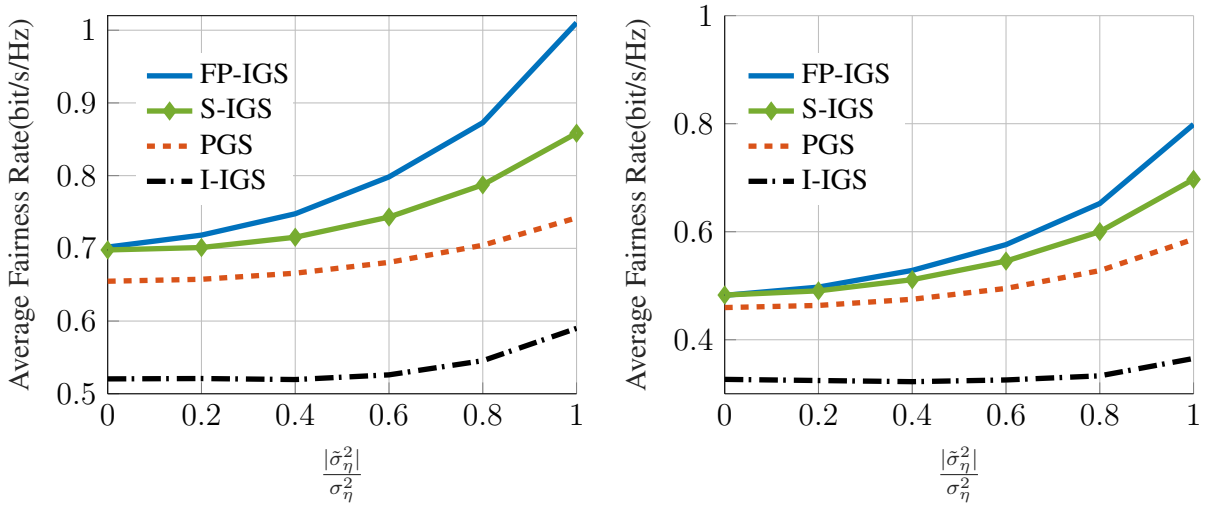

(a) $\sigma_\eta^2 = 0.5$ **(b)** $\sigma_\eta^2 = 1$

Figure 6.6: Average fairness rates versus the circularity coefficient of AHWD noise for $P = 20$.

IGS algorithm in [129] is proposed for ideal devices and does not consider AHWD, it performs worse than the proposed PGS, which considers symmetric AHWD, from the average fairness rate point of view, even when the AHWD noise is maximally improper.

In Fig. 6.7, we consider the effect of the power budget on the fairness rate of users. There is an almost constant performance gap between our proposed algorithms and the other algorithms. Similar to the other figures, our proposed IGS with FP outperforms our simplified algorithm.

6.5 Summary

In this chapter, we considered a K-user SISO IC with asymmetric AHWD at the transceivers based on the model in Section 3.3.1. Treating interference as noise, we addressed the problem of obtaining the achievable rate region for IGS and proposed two suboptimal algorithms. The first algorithm, which is based on MM and the GDA, obtains a stationary point of the PSINR region. In this algorithm, we jointly optimize the powers and complementary variances. We also proposed a simplified algorithm that has lower computational complexity. This simplified algorithm is based on the separate optimization of the powers and complementary variances. Through numerical examples, we showed that the proposed approaches enlarge the achievable rate region and outperform PGS and existing IGS algorithms, especially as the AHWD becomes more asymmetric.

6.6 Proof of Lemma 6.2

In order to approximate $u_k(\mathbf{p}, \mathbf{q})$ and $v_k(\mathbf{p}, \mathbf{q})$, we employ convex-concave (or concave-convex) procedure (CCP), in which the convex (concave) part is approximated as an affine function by the first-order approximation of the Taylor expansion. Note that we take the first-order term and employ an affine approximation since an affine function is the nearest concave approximation to a convex function. The first-order approximation of a real function $u(\mathbf{x})$ around the point $\mathbf{x}_0$

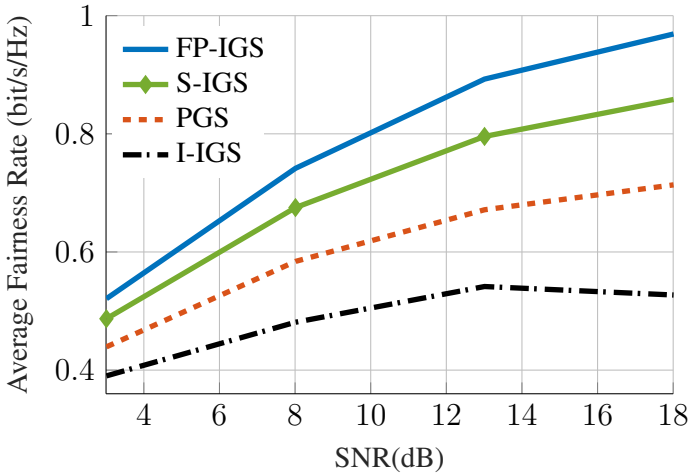

(a) $\sigma_\eta^2 = 0.5$

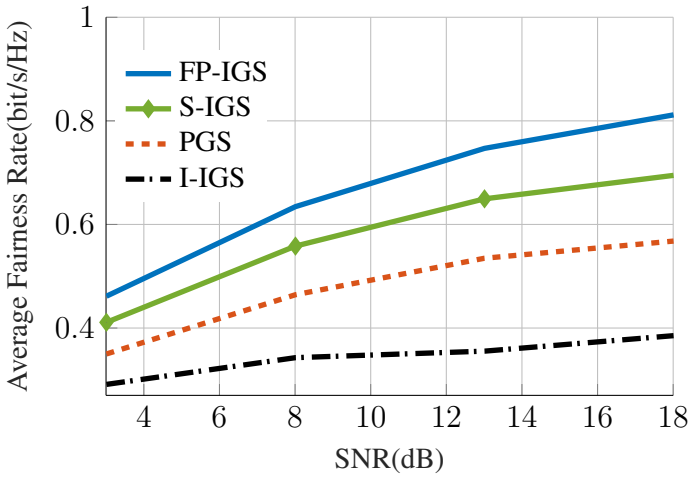

(b) $\sigma_\eta^2 = 1$

Figure 6.7: Average fairness rate versus SNR for $\tilde{\sigma}_\eta^2 = 0.9\sigma_\eta^2$.

is obtained through its Taylor expansion as [14, 94]

$$\Gamma(\mathbf{x}) \approx \Gamma(\mathbf{x}_0) + 2\Re\left[\left(\frac{\partial \Gamma(\mathbf{x})}{\partial \mathbf{x}}\Big|_{\mathbf{x}=\mathbf{x}_0}\right)^T(\mathbf{x}-\mathbf{x}_0)\right], \tag{6.45}$$

where $\mathbf{x}$ is a complex vector. In order to apply the CCP to $u_k(\mathbf{p},\mathbf{q})$, we have to differentiate the convex part in (6.6) with respect to $\mathbf{p}$, which is straightforward since it is a real function on a real domain and consequently, analytic in $\mathbf{p}$. The derivative of $(\sigma^2+\mathbf{a}_k^T\mathbf{p})^2$ with respect to $\mathbf{p}$ is

$$\frac{\partial(\sigma^2+\mathbf{a}_k^T\mathbf{p})^2}{\partial \mathbf{p}} = 2\mathbf{a}_k(\sigma^2+\mathbf{a}_k^T\mathbf{p}), \tag{6.46}$$

and the resulting first-order approximation around the power vector in the mth iteration, $\mathbf{p}^{(m)}$, is given by

$$(\sigma^2+\mathbf{a}_k^T\mathbf{p})^2 \simeq (\sigma^2+\mathbf{a}_k^T\mathbf{p}^{(m)})^2 + 2(\sigma^2+\mathbf{a}_k^T\mathbf{p}^{(m)})\mathbf{a}_k^T(\mathbf{p}-\mathbf{p}^{(m)}). \tag{6.47}$$

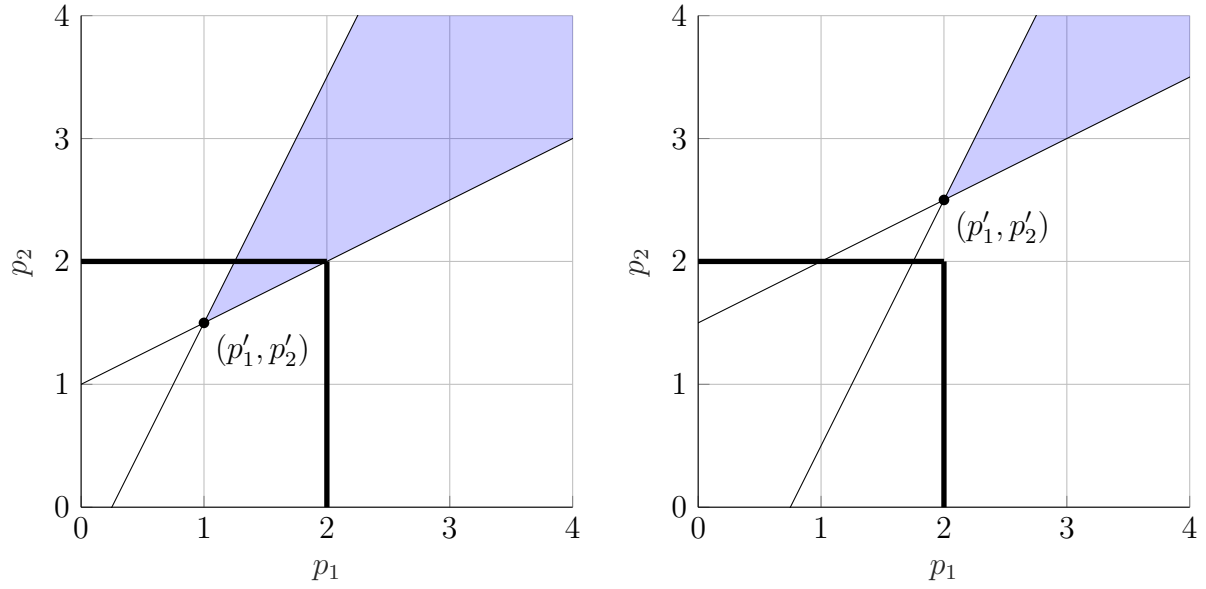

(a) Feasible E' **(b)** Infeasible E'

Figure 6.8: The constraints of (6.20) in the power plane.

In order to convexify $v_k(\mathbf{p}, \mathbf{q})$, we have to differentiate the concave part in (6.7) with respect to $\mathbf{p}$ and $\mathbf{q}$. The derivative of $|\mathbf{g}_k^H \mathbf{q} + \tilde{\mathbf{f}}_k^H \mathbf{p}|^2$ with respect to $\mathbf{p}$ is also straightforward since it is analytic in $\mathbf{p}$:

$$\frac{\partial |\mathbf{g}_k^H \mathbf{q} + \tilde{\mathbf{f}}_k^H \mathbf{p}|^2}{\partial \mathbf{p}} = 2\Re\left[\tilde{\mathbf{f}}_k (\mathbf{g}_k^H \mathbf{q} + \tilde{\mathbf{f}}_k^H \mathbf{p})\right]. \tag{6.48}$$

The term $|\mathbf{g}_k^H \mathbf{q} + \tilde{\mathbf{f}}_k^H \mathbf{p}|^2$, on the other hand, is not analytic in $\mathbf{q}$ since it is a real-valued function while $\mathbf{q}$ is a complex vector [14, 94]. Thus, we have to employ Wirtinger calculus to obtain the derivative of $|\mathbf{g}_k^H \mathbf{q} + \tilde{\mathbf{f}}_k^H \mathbf{p}|^2$ with respect to $\mathbf{q}$. By Wirtinger calculus, we treat $\mathbf{q}$ and $\mathbf{q}^*$ as two independent complex variables [14, 94]. Please refer to Section 2.4 for more details about Wirtinger calculus and complex analytic functions. Thus, we take the derivative of $|\mathbf{g}_k^H \mathbf{q} + \tilde{\mathbf{f}}_k^H \mathbf{p}|^2$ with respect to $\mathbf{q}$ while treating $\mathbf{q}^*$ as a constant, which results in

$$\frac{\partial |\mathbf{g}_k^H \mathbf{q} + \tilde{\mathbf{f}}_k^H \mathbf{p}|^2}{\partial \mathbf{q}} = \mathbf{g}_k^* (\mathbf{g}_k^H \mathbf{q} + \tilde{\mathbf{f}}_k^H \mathbf{p})^*. \tag{6.49}$$

Now by (6.45), we can approximate $|\mathbf{g}_k^H \mathbf{q} + \tilde{\mathbf{f}}_k^H \mathbf{p}|^2$ as an affine function as

$$\begin{aligned} |\mathbf{g}_k^H \mathbf{q} + \tilde{\mathbf{f}}_k^H \mathbf{p}|^2 \simeq |\mathbf{g}_k^H \mathbf{q}^{(m)} + \tilde{\mathbf{f}}_k^H \mathbf{p}^{(m)}|^2 + 2\Re\left(\tilde{\mathbf{f}}_k^H (\mathbf{g}_k^H \mathbf{q}^{(m)} + \tilde{\mathbf{f}}_k^H \mathbf{p}^{(m)})^*\right)(\mathbf{p} - \mathbf{p}^{(m)}) \\ + 2\Re\left((\mathbf{g}_k^H \mathbf{q}^{(m)} + \tilde{\mathbf{f}}_k^H \mathbf{p}^{(m)})^* \mathbf{g}_k^H (\mathbf{q} - \mathbf{q}^{(m)})\right). \end{aligned} \tag{6.50}$$

By substituting (6.50) in (6.7), we can obtain $\tilde{v}_k(\mathbf{p}, \mathbf{q})$.

6.7 Proof of Theorem 6.1

A given E' is feasible if and only if there exists at least a pair (p_1, p_2) that satisfies all the constraints in (6.20). Let us first consider the two linear constraints in (6.20b), which can be written as

$$|h_{11}|^2\Big(1-\sigma^2_{\eta_{11}}(\sqrt{1+\alpha_1 E'}-1)\Big)p_1-|h_{21}|^2(1+\sigma^2_{\eta_{21}})(\sqrt{1+\alpha_1 E'}-1)p_2\geq(\sqrt{1+\alpha_1 E'}-1)\sigma^2, \tag{6.51}$$

$$-|h_{12}|^2(1+\sigma^2_{\eta_{12}})(\sqrt{1+\alpha_2 E'}-1)p_1+|h_{22}|^2\Big(1-\sigma^2_{\eta_{22}}(\sqrt{1+\alpha_2 E'}-1)\Big)p_2\geq(\sqrt{1+\alpha_2 E'}-1)\sigma^2. \tag{6.52}$$

We can construct $\mathbf{A}$ in (6.34) by the coefficients of p_1 and p_2 in (6.51) and (6.52). It is worth mentioning that the non-diagonal elements of $\mathbf{A}$ in (6.34) are non-positive since $\sqrt{1+\alpha_1 E'} \geq 1$ and $\sqrt{1+\alpha_2 E'} \geq 1$. Thus, if the diagonal elements of $\mathbf{A}$ are not positive, there is no positive power pair that satisfies (6.51) and (6.52) simultaneously. Hence, in the following, we assume without loss of generality that $\mathbf{A}$ has strictly positive diagonal elements and strictly negative non-diagonal elements.

We can rewrite (6.51) and (6.52) as

$$[\mathbf{A}]_{11}p_1 \geq -[\mathbf{A}]_{12}p_2 + y_1, \tag{6.53}$$

$$[\mathbf{A}]_{22}p_2 \geq -[\mathbf{A}]_{21}p_1 + y_2, \tag{6.54}$$

where $\mathbf{y} = \begin{bmatrix} (\sqrt{1+\alpha_1 E'}-1)\sigma^2 & (\sqrt{1+\alpha_2 E'}-1)\sigma^2 \end{bmatrix}^T$. Moreover, $[\mathbf{A}]_{ij}$, and y_i for $i, j \in \{1, 2\}$ are the ijth element of $\mathbf{A}$, and the ith element of $\mathbf{y}$, respectively. If we decouple the inequalities, we end up with

$$\det(\mathbf{A})p_1 \geq [\mathbf{A}]_{22}y_1 - [\mathbf{A}]_{12}y_2, \tag{6.55}$$

$$\det(\mathbf{A})p_2 \geq -[\mathbf{A}]_{21}y_1 + [\mathbf{A}]_{11}y_2. \tag{6.56}$$

The right-hand sides (RHS) in (6.55) and (6.56) are positive for a feasible E' as mentioned before. Note that if $\det(\mathbf{A}) < 0$, there are no positive power pairs that satisfy (6.55) and (6.56) for the given structure of $\mathbf{A}$ in (6.34). Thus, we consider $\det(\mathbf{A}) > 0$, which yields

$$p_1 \geq p_1' = \frac{[\mathbf{A}]_{22}y_1 - [\mathbf{A}]_{12}y_2}{\det(\mathbf{A})}, \tag{6.57}$$

$$p_2 \geq p_2' = \frac{-[\mathbf{A}]_{21}y_1 + [\mathbf{A}]_{11}y_2}{\det(\mathbf{A})}, \tag{6.58}$$

or equivalently $\mathbf{p} = \begin{bmatrix} p_1 & p_2 \end{bmatrix}^T \geq \mathbf{A}^{-1}\mathbf{y}$, where p_1' and p_2' are the intersecting point given in (6.33). Hence, the intersecting point provides the minimum positive power pairs that satisfy (6.51) and (6.52). If p_1' and p_2' satisfy the power constraint, E' is feasible (Fig. 6.8.a). Otherwise, E' is infeasible (Fig. 6.8.b).

7 Energy-efficient IGS schemes for SISO systems

In this chapter, we consider the optimization of EE of IGS schemes in the K-user SISO IC and SISO UCR and study the potential benefits of IGS from this point of view. As indicated before, there are fewer optimization parameters in single-antenna systems compared to multiple antenna systems, which may allow us to propose computationally less expensive algorithms for single-antenna systems. We first consider the EE region of the K-user SISO IC and propose a suboptimal numerical solution for the corresponding optimization problem. We then consider EE maximization for the secondary user (SU) in an UCR system. To this end, we optimize the power and complementary variance of the SU to maximize its EE while a quality-of-service constraint for the primary user has to be met. In this case, the EE optimization problem is simplified with respect to the K-user SISO IC, which enables us to derive the necessary and sufficient conditions for the optimality of IGS from EE perspective. Our results show that IGS can improve the EE of the K-user SISO IC and SISO UCR systems. The work, presented in this chapter, has been published in [100] and [104].

7.1 K-user SISO interference channels

In this section, we propose a suboptimal IGS algorithm for obtaining the EE region of the K-user IC by employing a sequential optimization method, in which we first optimize the powers considering PGS, i.e., when the complementary variances are zero. We then optimize the complementary variances for the given powers. This suboptimal approach guarantees that the proposed IGS scheme is not worse than the PGS scheme. Our results show that IGS can substantially enlarge the EE region of the K-user IC.

7.1.1 Problem statement

We aim at deriving the EE region of the K-user IC, which can be cast as maximizing the weighted minimum EE (WMEE) as [126]

$$\max_{\{\mathbf{p},\mathbf{q}\}\in\Omega} \min_{k} \left\{ \frac{U_k}{\alpha_k} = \frac{R_k(\mathbf{p},\mathbf{q})}{\alpha_k \left(\zeta p_k + P_c\right)} \right\}, \tag{7.1}$$

where $(\alpha_k)^{-1}$ is the corresponding weight for user k, and $\sum_{k=1}^{K} \alpha_k = 1$. Moreover, Ω is the feasibility set of parameters, which is given by (3.38). Solving (7.1) is not straightforward since it is not a convex optimization problem. In order to solve (7.1), we employ a sequential optimization approach, in which we first obtain the powers that maximize the WMEE problem for $\mathbf{q} = \mathbf{0}$. To this end, we employ the PGS scheme in [126]. Then, we derive the complementary variances by optimizing (7.1) for the given power vector.

7.1.2 Optimization of the transmit powers

In this subsection, we obtain the powers, $\mathbf{p}$, that maximize the WMEE cost function when users employ PGS, i.e., $\mathbf{q} = \mathbf{0}$. In this case, (7.1) can be simplified to

$$\max_{\mathbf{p}} \min_{k} \left\{ \frac{U_k^p(\mathbf{p})}{\alpha_k} = \frac{R_k^p(\mathbf{p})}{\alpha_k \left(\zeta p_k + P_c\right)} \right\}, \quad \text{s.t.} \quad 0 \leq p_k \leq P_k, \quad k = 1, 2, \cdots, K, \tag{7.2}$$

where $U_k^p(\mathbf{p})$ and $R_k^p(\mathbf{p}) = \log_2(1 + \gamma_k(\mathbf{p}))$ are, respectively, the EE and rate of user k when all users employ PGS. Moreover, $\gamma_k(\mathbf{p})$ is the received signal-to-interference-plus-noise ratio (SINR) at the receiver of user k, which is given by

$$\gamma_k(\mathbf{p}) = \frac{p_k |h_{kk}|^2}{\sigma^2 + \sum\limits_{j \neq k} |h_{kj}|^2 p_j}. \tag{7.3}$$

The optimization problem (7.2) is not convex, but a suboptimal solution was proposed in [126], which is based on MM and GDA and obtains a stationary point of (7.2). For the sake of completeness, we describe the solution in the following.

To obtain a stationary point of (7.2), we first approximate the rates by a lower bound as [126]

$$R_k^p(\mathbf{p}) = \log_2(1 + \gamma_k(\mathbf{p})) \geq \tilde{R}_k^{(l)}(\mathbf{p}) = a^{(l)} \log_2(\gamma_k(\mathbf{p})) + b^{(l)}, \tag{7.4}$$

where

$$a^{(l)} = \frac{\gamma_k(\mathbf{p}^{(l-1)})}{1 + \gamma_k(\mathbf{p}^{(l-1)})}, \tag{7.5a}$$

$$b^{(l)} = \log_2\left(1 + \gamma_k(\mathbf{p}^{(l-1)})\right) - \frac{\gamma_k(\mathbf{p}^{(l-1)}) \log_2\left(\gamma_k(\mathbf{p}^{(l-1)})\right)}{1 + \gamma_k(\mathbf{p}^{(l-1)})}. \tag{7.5b}$$

Note that (7.4) holds with equality at $\gamma_k(\mathbf{p}) = \gamma_k(\mathbf{p}^{(l-1)})$. Moreover, the derivatives of the left-hand side and right-hand side of (7.4) are equal at $\gamma_k(\mathbf{p}^{(l-1)})$. Hence, we can derive a stationary point of (7.2) by solving the following optimization problem iteratively

$$\max_{\mathbf{p}} \min_{k} \left\{ \frac{\tilde{U}_k^{(l)}(\mathbf{p})}{\alpha_k} = \frac{a^{(l)} \log_2(\gamma_k(\mathbf{p})) + b^{(l)}}{\alpha_k \left(\zeta p_k + P_c\right)} \right\}, \quad \text{s.t.} \quad 0 \leq p_k \leq P_k, \quad k = 1, 2, \cdots, K. \tag{7.6}$$

The optimization problem (7.6) is not convex; however, we can derive its global optimal solution by the GDA, which is described in Section 4.1.4, Lemma 4.6. Applying the GDA to (7.6) results in the following optimization problem at the mth iteration of the GDA

$$\max_{\mathbf{p}} \min_{k} \; a^{(l)} \log_2(\gamma_k(\mathbf{p})) + b^{(l)} - \mu^{(l)} \alpha_k \left(\zeta p_k + P_c\right) \tag{7.7a}$$

$$\text{s.t.} \; 0 \leq p_k \leq P_k \qquad k = 1, 2, \cdots, K, \tag{7.7b}$$

where $\mu^{(m)} = \tilde{U}_k^{(l)}(\mathbf{p}^{(m-1)})$ is fixed at each iteration, and $\mathbf{p}^{(m-1)}$ is the solution of the $(m-1)$th

iteration. The optimization problem (7.7) can be rewritten as

$$\max_{\mathbf{p},e} \; e \tag{7.8a}$$

$$\text{s.t. } a_k^{(l)} \log_2(p_k|h_{kk}|^2) - a_k^{(l)} \log_2\left(\sigma^2 + \sum_{j\neq k}|h_{kj}|^2 p_j\right) + b_k^{(l)} - \mu^{(l)}\alpha_k\left(\zeta p_k + P_c\right) \geq e, \quad \forall k, \tag{7.8b}$$

$$0 \leq p_k \leq P_k, \qquad \forall k. \tag{7.8c}$$

Now we substitute p_k by $t_k = \log_2(p_k)$ and rewrite (7.8) as [126]

$$\max_{\mathbf{t},e} \; e \tag{7.9a}$$

$$\text{s.t. } a_k^{(l)} t_k + \log_2(|h_{kk}|^2) - a_k^{(l)} \log_2\left(\sigma^2 + \sum_{j\neq k}|h_{kj}|^2 2^{t_j}\right) + b_k^{(l)} - \mu^{(l)}\alpha_k\left(\zeta 2^{t_k} + P_c\right) \geq e, \quad \forall k, \tag{7.9b}$$

$$0 \leq t_k \leq \log_2(P_k), \qquad \forall k, \tag{7.9c}$$

where $\mathbf{t} = [t_1, t_2, ..., t_k]$. The problem (7.9) is convex in $\{t_k\}_{k=1}^K$ and can be solved efficiently.

7.1.3 Optimizing complementary variances

In this subsection, we maximize the WMEE function over $\mathbf{q}$ for the given $\mathbf{p}^{(\star)}$ obtained in Section 7.1.2. The corresponding optimization problem is again nonconvex and difficult to solve. Thus, we employ an iterative algorithm to find a suboptimal solution. This is accomplished by approximating the original optimization problem and solving each approximated problem by a sequence of convex feasibility problems.

For a given power vector $\mathbf{p}^{(\star)}$, (7.1) is equivalent to

$$\max_{\mathbf{q},e} \; e \tag{7.10a}$$

$$\text{s.t. } R_k(\mathbf{p}^{(\star)}, \mathbf{q}) \geq \alpha_k\left(\zeta p_k^{(\star)} + P_c\right) e, \quad \forall k, \tag{7.10b}$$

$$|q_k| \leq p_k^{(\star)}, \qquad \forall k. \tag{7.10c}$$

We can rewrite (7.10) as

$$\max_{\mathbf{q},e} \; e \tag{7.11a}$$

$$\text{s.t. } -\left((\sigma^2 + \mathbf{b}_k^T\mathbf{p}^{(\star)})^2 - |\mathbf{g}_k^H\mathbf{q}|^2\right) 2^{2\alpha_k\left(\zeta p_k^{(\star)} + P_c\right)e} + (\sigma^2 + \mathbf{a}_k^T\mathbf{p}^{(\star)})^2 - |\mathbf{f}_k^H\mathbf{q}|^2 \geq 0, \quad \forall k, \tag{7.11b}$$

$$|q_k| \leq p_k^{(\star)}, \qquad \forall k. \tag{7.11c}$$

The optimization problem in (7.11) is not convex since (7.11b) is not a concave function in $\mathbf{q}$ and e. Similar to the previous section, we first find a lower bound for (7.11b), such that it is a concave function in $\mathbf{q}$ for a fixed e. That is, we approximate the nonconvex part of (7.11b) by

an affine function of $\mathbf{q}$, using the first-order Taylor expansion at $\mathbf{q}^{(m)}$, i.e., [94]

$$|\mathbf{g}_k^H\mathbf{q}|^2 \geq |\mathbf{g}_k^H\mathbf{q}^{(m)}|^2 + 2\Re\left((\mathbf{g}_k^H\mathbf{q}^{(m)})^H\mathbf{g}_k^H(\mathbf{q}-\mathbf{q}^{(m)})\right), \tag{7.12}$$

where $\mathbf{q}^{(m)}$ is the solution obtained at the previous iteration, and $\Re(x)$ takes the real part of x. Note that the equality holds only at $\mathbf{q} = \mathbf{q}^{(m)}$. Furthermore, the derivatives of the left-hand side and right-hand side of (7.12) are equal at $\mathbf{q}^{(m)}$. Under these conditions, the approximated problem converges to a point satisfying the KKT conditions of (7.11) [6]. By plugging (7.12) into (7.11), the approximated optimization problem at the mth iteration becomes

$$\max_{\mathbf{q},e} \quad e \tag{7.13a}$$
$$\text{s.t.} \quad \tilde{E}^{(m)}(\mathbf{q},e) > 0, \qquad \forall k, \tag{7.13b}$$
$$|q_k| \leq p_k^{(\star)}, \qquad \forall k, \tag{7.13c}$$

where

$$\tilde{E}^{(m)}(\mathbf{q},e) = 2^{1+2\alpha_k\left(\zeta p_k^{(\star)}+P_c\right)e}\Re\left((\mathbf{g}_k^H\mathbf{q}^{(m)})^H\mathbf{g}_k^H(\mathbf{q}-\mathbf{q}^{(m)})\right) + 2^{2\alpha_k\left(\zeta p_k^{(\star)}+P_c\right)e}|\mathbf{g}_k^H\mathbf{q}^{(m)}|^2$$
$$+ (\sigma^2 + \mathbf{a}_k^T\mathbf{p}^{(\star)})^2 - |\mathbf{f}_k^H\mathbf{q}|^2 - 2^{2\alpha_k\left(\zeta p_k^{(\star)}+P_c\right)e}(\sigma^2 + \mathbf{b}_k^T\mathbf{p}^{(\star)})^2. \tag{7.14}$$

The optimization problem (7.13) is not convex, but we can obtain its optimal solution, $e^{(m)}$, by a bisection method, which results in a sequence of feasibility problems [13]. That is, we fix $e = e_0$ and solve

$$\text{find} \quad \mathbf{q} \tag{7.15a}$$
$$\text{s.t.} \quad \tilde{E}^{(m)}(\mathbf{q},e_0) > 0, \qquad \forall k, \tag{7.15b}$$
$$|q_k| \leq p_k^{(\star)}, \qquad \forall k. \tag{7.15c}$$

If (7.15) is feasible, $e^{(m)} > e_0$. Otherwise, $e^{(m)} < e_0$. As indicated formerly, the complete algorithm converges to a point satisfying the KKT conditions of (7.11).

7.1.4 Numerical results

In this subsection, we provide some numerical examples to illustrate the EE improvement achieved by IGS for the K-user SISO IC. We set $\sigma^2 = 10^{-4}$ W, $\zeta = 3$, and $P_k = 5$ mW for $k = 1, ..., K$ [80]. We average the results over 100 channel realizations. Every channel realization is drawn from a proper complex Gaussian distribution with zero mean and unit variance, i.e., $\mathcal{CN}(0,1,0)$.

In Figs. 7.1 and 7.2, we show the fairness point of the EE region boundary, which is given by $\alpha_k = 1/K$, versus P_c for the 2-user and 3-user IC, respectively. Notice that at this point the users achieve the same EE, and therefore it is typically denoted as symmetric EE. These figures show that IGS provides higher average symmetric EE than PGS. As expected, the EE decreases with P_c. In these figures, we also compare our proposed IGS scheme with an IGS scheme based on exhaustive search with 5×10^5 and 10^7 randomizations (labeled by IGS-E) for the 2-user and

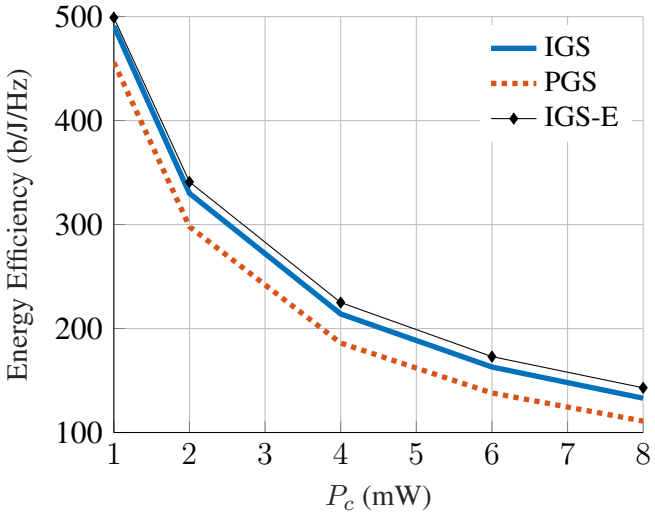

Figure 7.1: Fairness EE of the 2-user IC versus P_c.

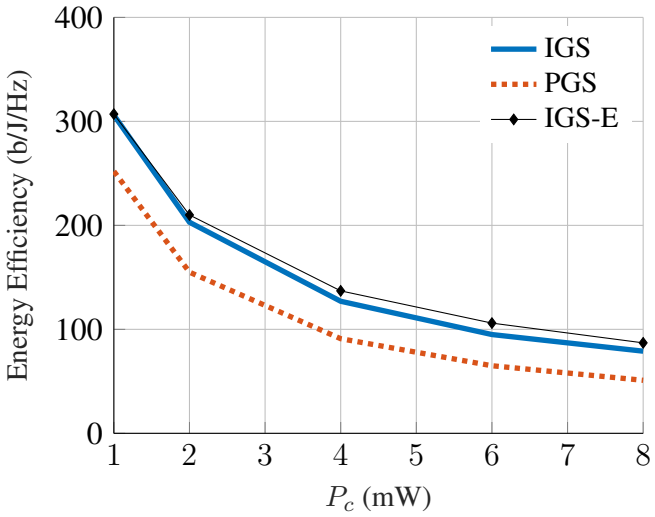

Figure 7.2: Fairness EE of the 3-user IC versus P_c.

3-user IC, respectively. This provides a hint on how close the proposed IGS suboptimal design is to the optimal solution. As can be observed, the proposed IGS scheme performs very close to IGS-E in this scenario. In particular, for the example in Fig. 7.1, our IGS scheme performs only 1.5% and 7.5% worse than the IGS-E at $P_c = 1$ mW and $P_c = 8$ mW, respectively. Similarly, for the example in Fig. 7.2, the IGS-E is 0.3% and 11.2% better than our scheme when $P_c = 1$ mW and $P_c = 8$ mW, respectively. Note that the IGS-E can be considered a lower bound for the optimal IGS solution.

In Fig. 7.3, we show the improvement in the average fairness EE by IGS versus P_c for the 2-user and 3-user ICs. As can be observed, the improvement by IGS increases with P_c. The reason is that the optimal powers for PGS increase with P_c, and the EE maximization is simplified to rate maximization when P_c is very high [15]. Since higher powers result in more improvement by optimizing over complementary variances [129], the improvement is also increasing with P_c. We can also observe in Fig. 7.3 that the improvement by IGS is more significant for the

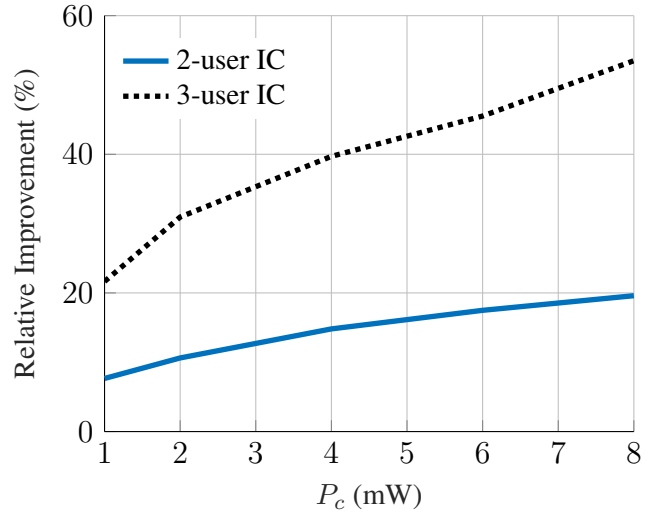

Figure 7.3: Relative improvement by employing IGS for the fairness EE versus P_c.

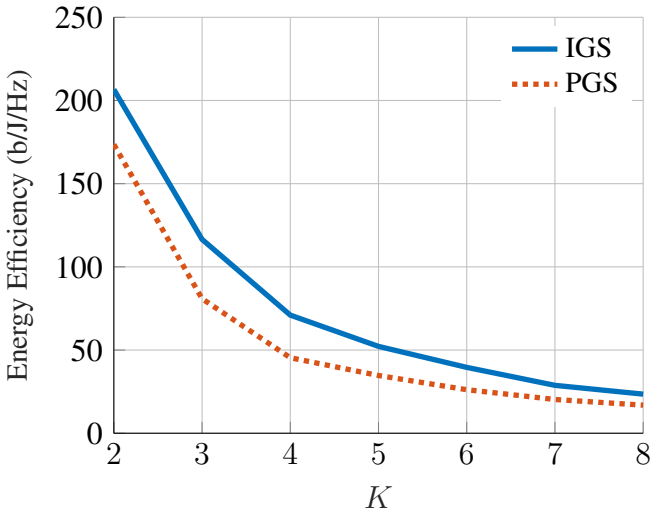

Figure 7.4: Fairness EE of the K-user IC versus K.

3-user IC. This is due to the fact that the higher the number of users is, the more interference they cause. As a result, the benefits of IGS are potentially higher in the 3-user IC.

In Fig. 7.4, we show the fairness EE versus the number of users, K, for $P_c = 4$ mW. As can be seen, the fairness EE decreases with K. In Fig. 7.5, we show the sum of the fariness EE versus the number of users, K, for $P_c = 4$ mW. As expected, the sum of the fairness EE decreases with K, which implies that the overall EE decreases when more users employ the same amount of resources. In these figures, we can observe that IGS significantly outperforms PGS for every K, where there is 19% and 56% improvement for $K = 2$ and $K = 4$, respectively.

Figure 7.6 shows the EE region of the 2-user IC for $P_c = 5$ mW and channel realization

$$\mathbf{H} = \begin{bmatrix} 1.3997e^{-i0.3803} & 1.5401e^{i1.0127} \\ 1.2250e^{i2.4311} & 0.9361e^{i0.8844} \end{bmatrix}. \tag{7.16}$$

For this channel realization, the interference link of each receiver is stronger than its corre-

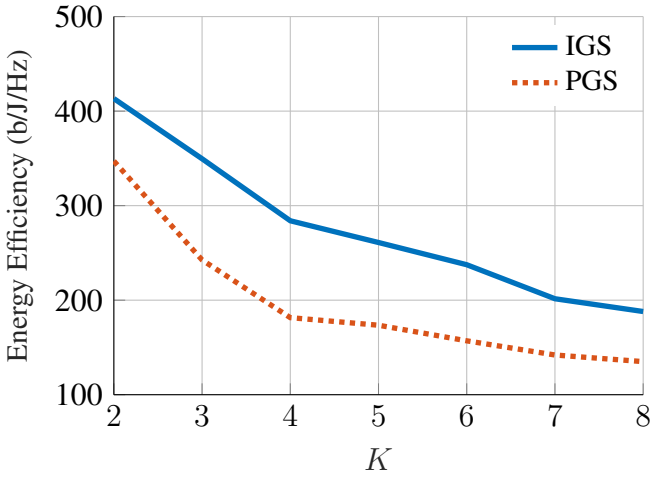

Figure 7.5: Sum of fairness EE of the K-user IC versus K.

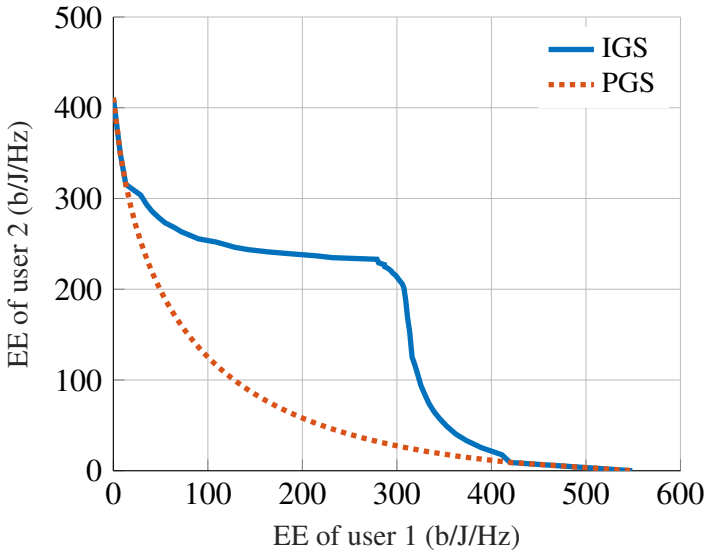

Figure 7.6: Energy efficiency region of of the 2-user IC for channel realization $\mathbf{H}$ in (7.16).

sponding direct link, which yields a strong interference regime. As can be observed, IGS can significantly enlarge the EE region for this example. It is worth mentioning that IGS does not provide any gain in noise-limited regimes, for which the interference is negligible. In other words, not surprisingly the benefits of IGS increase with the interference level.

7.2 Underlay Cognitive Radio

In this section, we consider the EE of IGS in single antenna UCR with ideal devices and perfect CSI. For this system, we derive a necessary and sufficient condition in closed form for IGS to be more energy efficient than PGS. We leverage this result to numerically obtain the optimal transmission parameters by the well-known bisection method. Our results show that IGS can improve the EE of the SU in UCR when interference is treated as noise.

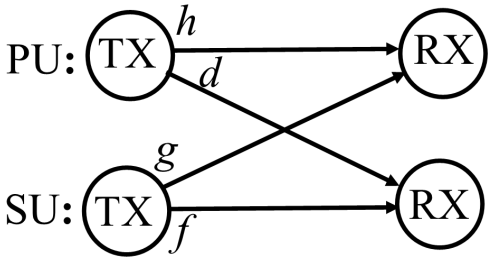

Figure 7.7: UCR channel model as a SISO two-user IC.

7.2.1 System model

We consider UCR system as depicted in Fig. 7.7, in which the PU, unaware of the SU, employs PGS with fixed transmit power P, while the SU can employ IGS. In particular we assume that the SU transmits a zero-mean complex Gaussian random variable with variance $q = \mathbb{E}\{|x|^2\}$, and circularity coefficient $\kappa = \frac{|\mathbb{E}\{x^2\}|}{\mathbb{E}\{|x|^2\}}$, where $\kappa \in [0, 1]$ [2, 94]. Thus, the rates of the PU and SU are, respectively, [71, 129]

$$R_p = \frac{1}{2}\log_2\left(\frac{(P|h|^2 + \sigma^2 + q|g|^2)^2 - (q\kappa|g|^2)^2}{(\sigma^2 + q|g|^2)^2 - (q\kappa|g|^2)^2}\right), \tag{7.17}$$

$$R_s = \frac{1}{2}\log_2\left(\frac{(\sigma^2 + q|f|^2 + P|d|^2)^2 - (q\kappa|f|^2)^2}{(\sigma^2 + P|d|^2)^2}\right), \tag{7.18}$$

where h, d, g, f, and σ^2 are the PU-PU, PU-SU, SU-PU, SU-SU channel coefficients, and noise variance, respectively.

7.2.2 Energy-Efficient IGS Design

We aim at maximizing the EE of the SU under the constraint that the rate of the PU is above a threshold. That is [80]

$$\max_{0\le q\le Q, 0\le\kappa\le 1} \quad U_s = \frac{R_s}{\zeta q + q_c} \tag{7.19a}$$

$$\text{s.t.} \quad R_p \ge \overline{R} = \alpha R_p^{\max}, \tag{7.19b}$$

where $R_p^{\max} = \log_2(1 + \frac{P|h|^2}{\sigma^2})$, $\overline{R}$, and Q are the maximum rate of the PU, the rate constraint for the PU and the power budget of the SU, respectively, and $\alpha \in [0, 1]$ is the loading factor.

To solve (7.19), we employ the analytical results in [70], which provide the conditions for the optimality of IGS in terms of achievable rate. It is evident that IGS may improve the EE of the SU only if IGS is able to increase the rate of the SU. For convenience, we restate these conditions in the following lemma.

Lemma 7.1 *IGS improves the rate of the SU if and only if:*

1. $\eta = \frac{|g|^2(\sigma^2+P|d|^2)}{|f|^2\sigma^2} + \frac{P|h|^2}{\sigma^2(2^{2\overline{R}}-1)} > 1$, *and*

2. $Q > q_0 = \frac{1}{|g|^2}\left(\frac{P|h|^2}{2^{\overline{R}}-1} - \sigma^2\right)$.

Proof. Refer to [70, Theorem 1] or [103, Lemma 1]. □

As mentioned before, the conditions in Lemma 1 are necessary, but not sufficient, for the optimality of IGS in the terms of EE. Thus, in the following we assume that these conditions are satisfied when we derive the additional conditions that are required for IGS to be also optimal in terms of EE. We also relax the power constraint when we study the behavior of the EE function of the SU. However, we finally consider all conditions for deriving the optimal parameters.

In order to simplify (7.19), we can rewrite (7.19b) in a more convenient way, i.e., by writing κ as a function of q, as [70]

$$\kappa^2(q) = \begin{cases} 0 & \text{if} \quad q < q_0 \\ \frac{2^{2\overline{R}}(q|g|^2+\sigma^2)^2-(q|g|^2+P|h|^2+\sigma^2)^2}{(1-2^{2\overline{R}})q^2|g|^4} & \text{if} \quad q_0 \leq q \leq q_1, \end{cases} \tag{7.20}$$

where

$$q_1 = \frac{1}{2|g|^2}\left(\frac{P|h|^2}{2^{2\overline{R}-R_p^{\max}}-1} - \sigma^2\right), \tag{7.21}$$

where $R_p^{\max}$ is defined as in (7.19). Note that the constraint (7.19b) is active only if $q_0 \leq q \leq q_1$. If $q < q_0$, (7.19b) is not active and the optimal circularity coefficient is $\kappa^* = 0$. Plugging (7.20) into (7.18), the SU rate as a function of the transmit power is [70, 103]

$$R_s(q) = \begin{cases} \log_2\left(1+\frac{|f|^2 q}{\sigma^2+|d|^2P}\right) & \text{if} \quad 0 \leqslant q \leqslant q_0, \\ \frac{1}{2}\log_2\left(a+bq\right) & \text{if} \quad q_0 \leqslant q \leqslant q_1, \end{cases} \tag{7.22}$$

where

$$a = 1 + \frac{|f|^4}{|g|^4\left(P|d|^2+\sigma^2\right)^2}\left(\frac{P^2|h|^4}{2^{2\overline{R}}-1} - \sigma^4\right), \tag{7.23a}$$

$$b = \frac{2|f|^2}{P|d|^2+\sigma^2} + \frac{2|f|^4}{|g|^2\left(P|d|^2+\sigma^2\right)^2}\left(\frac{P|h|^2}{2^{2\overline{R}}-1} - \sigma^2\right). \tag{7.23b}$$

Note that $\eta > 1$ is equivalent to $b > 0$, which implies that $R_s(q)$ is increasing in q when IGS is data-rate optimal. The following lemmas characterize the SU EE function.

Lemma 7.2 *The EE function of the SU is differentiable in $[0, q_1]$ except at q_0, where we have $\lim_{q\to q_0^-}\frac{\partial U(q)}{\partial q} > \lim_{q\to q_0^+}\frac{\partial U(q)}{\partial q}$. Moreover, the derivative of $U(q)$ with respect to q at $q \neq q_0$ is*

$$\frac{\partial U(q)}{\partial q} = \begin{cases} \frac{\frac{b'}{1+b'q}(q+q_c')-\ln(1+b'q)}{(\zeta\ln 2)(q+q_c')^2} & \textit{if} \quad 0 \leqslant q < q_0, \\ \frac{\frac{b}{a+bq}(q+q_c')-\ln(a+bq)}{(\zeta 2\ln 2)(q+q_c')^2} & \textit{if} \quad q_0 < q \leqslant q_1, \end{cases} \tag{7.24}$$

where $b' = \frac{|f|^2}{\sigma^2+|d|^2P}$ and $q_c' = q_c/\zeta$.

Proof. Please refer to Section 7.4. □

Lemma 7.3 *The EE function of the SU is maximized at a unique power q^*, where we have $U(q) < U(q^*)$ for $q \neq q^*$.*

Proof. Please refer to Section 7.5. □

The following theorem presents the optimality conditions of IGS.

Theorem 7.1 *IGS improves the EE of the SU if and only if* $\eta > 1$, $Q > q_0$ *and*

$$b(q_0 + q_c') > (2\ln 2)R_s(q_0)(2^{2R_s(q_0)}). \tag{7.25}$$

Proof. Since $U(q)$ is strictly increasing before the optimal point and strictly decreasing after the optimal point according to Lemma 3, it is sufficient to consider the behavior of $U(q)$ as $q \to q_0^+$ to verify optimality of IGS. $U(q)$ is strictly increasing as $q \to q_0^+$ if and only if (7.25) holds. Moreover, the power budget has to be sufficiently large, i.e., $Q > q_0$. □

Note that if $b < 0$, which is equivalent to $\eta < 1$, (7.25) does not hold. Thus, as indicated before, the optimality conditions for EE are stricter than those for data rate in Lemma 1.

We now obtain the optimal transmission parameters of the SU, which are the solution of (7.19). According to Theorem 1, IGS is optimal if and only if $Q > q_0$, and (7.25) holds. In this case, the optimal solution is $q^* = \min(Q, q', q_1)$, where q' is the solution of $\frac{\partial U(q)}{\partial q} = 0$ for $q > q_0$, or equivalently

$$\delta(q) = b(q + q_c') - (a + bq)\ln(a + bq) = 0. \tag{7.26}$$

Since there is no closed form solution for (7.26), we solve it numerically. As shown in the proof of Lemma 3, $\delta(q)$ is decreasing and crosses zero at only one point. As a result, if $\delta(q_1) \geq 0$, the optimal power is $q^* = \min(Q, q_1)$. Otherwise, the optimal power can be found using bisection in the interval $[q_0, q_1]$. Finally, the optimal circularity coefficient is obtained by (7.20) as $\kappa^* = \kappa(q^*)$.

If the conditions in Theorem 1 are not satisfied, PGS is optimal. In this case, the optimal solution is $\kappa^* = 0$ and $q^* = \min(Q, q'', q_0)$, where q'' is the solution of $\frac{\partial U(q)}{\partial q} = 0$ for $q < q_0$, or equivalently

$$\tilde{\delta}(q) = b'(q + q_c') - (1 + b'q)\ln(1 + b'q) = 0. \tag{7.27}$$

Since $\tilde{\delta}(q)$ exhibits the same properties as $\delta(q)$, we can again make use of a bisection method to find q''.

7.2.3 Numerical results

In this subsection we provide some numerical examples to illustrate our findings in the SISO UCR systems. We consider $\sigma^2 = 1$, $P = 20$, $Q = 10$, and the power efficiency $\zeta = 2.86$ as in [21, 56]. In order to illustrate the impact of the interference, we fix $|h|^2 = |d|^2 = |f|^2 = 1$ and vary $|g|^2$.

In Fig. 7.8, we show the EE of the SU for $q_c = 20$, and two values of α, namely, $\alpha = 0.5$ and $\alpha = 0.7$. As can be observed, IGS (indicated as "I" in the legend) can significantly improve the EE of the SU when the gain of the cross link exceeds a certain value. Interestingly, the EE is almost flat for IGS and $\alpha = 0.5$, showing a large improvement over PGS. This is due to the fact that, for $\alpha \leq 0.5$, the SU can transmit a maximally improper signal with an arbitrary large transmit power, hence this scenario is no longer being interference-limited.

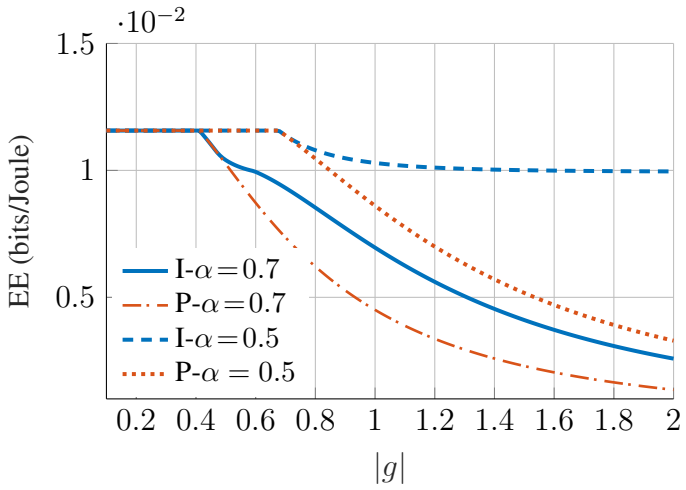

Figure 7.8: EE function for different values of α.

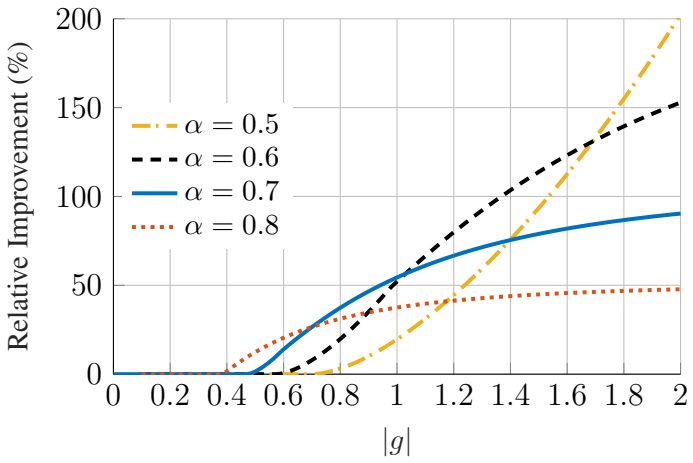

Figure 7.9: Percentage of improvement of EE by employing IGS as a function of $|g|$.

In Fig. 7.9, we show the relative improvement of EE function by employing IGS for different α. As can be observed, the improvement is more substantial for lower values of α. However, IGS is beneficial at a lower interference level when the loading factor, α, increases.

In Fig. 7.10, we consider the effect of constant power consumption for $\alpha = 0.7$. As can be observed, higher constant power results in a larger improvement by employing IGS. Indeed, as q_c grows, the EE function becomes dominated by the achievable rate. Since the optimality conditions for the achievable rate are less stringent than those for EE, the behavior observed in Fig. 7.10 follows.

Finally, Fig. 7.11 shows the relative improvement of EE function by employing IGS as a function of α for $Q = 20$, $q_c = 20$, and different $|g|$. As can be observed, there is a more substantial improvement at higher $|g|$ for every value of α. Moreover, the improvement is maximized at a fixed value α, which decreases with $|g|$.

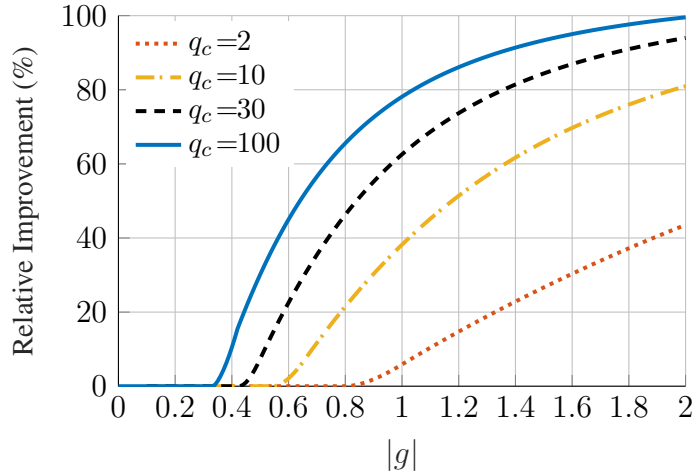

Figure 7.10: Percentage of improvement of EE by employing IGS as a function of $|g|$.

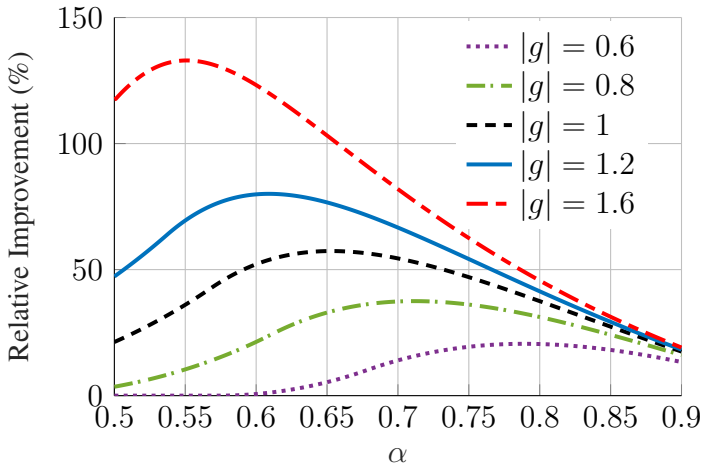

Figure 7.11: Percentage of improvement of EE by employing IGS as a function of α.

7.3 Summary

In this chapter, we proposed energy-efficient IGS schemes for the SISO K-user IC and SISO UCR. We first considered the SISO K-user IC. By maximizing the WMEE, we proposed an IGS design to operate at different points of the EE region. In order to find a suboptimal solution to the WMEE problem, we performed a separate optimization of the powers and complementary variances. For the former, we considered proper signaling and resorted to GDA and SCP to find a solution to the original non-convex problem satisfying the KKT conditions. The resulting solution was then improved by optimizing over the complementary variances. Again, this resulted in a non-convex problem, and a suboptimal solution was found by using bisection and SCP. Our numerical results showed that IGS is more energy efficient than its proper counterpart.

We also addressed the optimization of the EE function of the SU in UCR networks. We derived necessary and sufficient optimality conditions for IGS in closed form, and proposed a bisection method to find the optimal transmission parameters of PGS and IGS. Our results showed that IGS also pays off in terms of EE, although stricter conditions than those for rate optimization have to be fulfilled.

7.4 Proof of Lemma 9.2

$U(q)$ is continuous in q since $R_s(q)$ is continuous in q [70, 103]. It is also evident that $U(q)$ is differentiable for $q \neq q_0$, and its derivative is (7.24). In order to prove the lemma, we have to show that

$$\frac{\frac{b'}{1+b'q_0}(q_0+q_c') - \ln(1+b'q_0)}{(\ln 2)(q_0+q_c')^2} > \frac{\frac{b}{a+bq_0}(q_0+q_c') - \ln(a+bq_0)}{(2\ln 2)(q_0+q_c')^2}. \tag{7.28}$$

We know that $\log_2(a+bq_0) = 2\log_2(1+b'q_0)$, or equivalently $a+bq_0 = (1+b'q_0)^2$, since $R_s(q)$ is continuous. Taking this into account, we can simplify (7.28) as

$$2b'(1+b'q_0) > b, \tag{7.29}$$

where $b' = \frac{|f|^2}{\sigma^2+|d|^2P}$, and b is defined in (7.23). It is easy to verify that (7.29) holds by replacing the corresponding parameters into it, which concludes the proof.

7.5 Proof of Lemma 9.3

In order to prove the lemma, it is sufficient to show that the EE function of the SU is strictly increasing before the optimal point and strictly decreasing after the optimal point. Let us first consider the case $q_0 < q \leq q_1$. In this case, $U(q)$ is strictly increasing if and only if its derivative is non-negative, which yields

$$\delta(q) = b(q+q_c') - (a+bq)\ln(a+bq) > 0. \tag{7.30}$$

The function $\delta(q)$ decreases with q if and only if

$$b < b\ln(a+bq) + b, \tag{7.31}$$

which always holds since $a+bq > 1$. Therefore, if $\lim_{q\to q_0^+} \frac{\partial U(q)}{\partial q} < 0$, $U(q)$ is always decreasing in $q_0 < q \leq q_1$. Otherwise, there is a unique q' such that $U(q)$ is increasing in $q_0 < q \leq q'$ and decreasing in $q > q'$. However, it might happen that $q' > q_1$, in which case $U(q)$ is strictly increasing in $q_0 < q \leq q_1$.

Let us now consider the case $q < q_0$. $U(q)$ is increasing if and only if

$$\tilde{\delta}(q) = b'(q+q_c') - (1+b'q)\ln(1+b'q) > 0. \tag{7.32}$$

First, it is easy to verify that the above condition holds for $q = 0$. In order to find out how $\tilde{\delta}(q)$ behaves as q increases, we analyze its derivative with respect to q. Thus, we obtain that $\tilde{\delta}(q)$ is decreasing in q if and only if

$$b' < b'\ln(1+b'q) + b', \tag{7.33}$$

which is always true since $1+b'q > 1$. This means that there exists q'' such that $U(q)$ is increasing in $q < q''$ and decreasing in $q > q''$. Again, it might happen that $q'' > q_0$, in which case $U(q)$ is strictly increasing in the interval $0 \leq q < q_0$.

Since by Lemma 2, $\lim_{q\to q_0^-} \frac{\partial U(q)}{\partial q} > \lim_{q\to q_0^+} \frac{\partial U(q)}{\partial q}$, this behavior is maintained when regarding the whole interval $0 \leq q \leq q_1$, which concludes the proof.

8 New IGS schemes for the 2-user SISO Interference Channels

In previous chapters, we assume that transmitters have access to perfect and global instantaneous channel state information at the transmitter side (CSIT). In this chapter, we study the performance of IGS in the 2-user SISO IC and the Z-IC with realistic assumptions regarding CSIT. In Section 8.1, we assume that transmitters have access to imperfect instantaneous CSIT and derive the achievable worst-case rate region of the 2-user IC and the Z-IC. In the 2-user SISO IC and Z-IC, we are able to simplify the optimization problems and derive suboptimal closed-form solutions for the rate region as will be shown in this chapter. Moreover, in Section 8.2, we study the achievable ergodic rates of IGS schemes over the 2-user fading IC with TIN. We derive closed-form expressions for the ergodic rates for both users for the case where at most one user employs IGS (denoted as PGS/IGS scheme). In this chapter, we show that IGS can be also beneficial with realistic assumptions regarding CSIT. The results of this chapter have been presented in [102, 105].

8.1 Robust IGS with imperfect CSIT

In this section, we propose robust IGS designs for the 2-user IC and Z-IC. Assuming imperfect CSIT, we tackle the worst-case rate region problem and derive closed-form suboptimal solutions to operate at different points of the rate region. We derive sufficient conditions for the optimality of IGS. Our numerical results show that IGS can enlarge the worst-case achievable rate region of the 2-user and Z-IC with imperfect CSIT.

8.1.1 Channel uncertainty model

Throughout this section, we assume perfect channel state information (CSI) at the receivers but imperfect CSI at the transmitters. It is reasonable to assume that a receiver knows the CSI perfectly since acquiring CSI at the receiver side is relatively easy with training sequences or applying blind/semi-blind estimation methods [89, 97, 115]. On the other hand, the channel information is typically quantized and then sent to the transmitters through a noisy feedback link. Therefore we have imperfect CSIT [89, 95, 97, 115, 118]. In this chapter, we assume that the true channel, h_{ij} for $i, j \in \{1, 2\}$, lies in a vicinity of the channel estimate at the transmitter side, $\hat{h}_{ij}$, i.e., $\hat{h}_{ij} = h_{ij} + e_{ij}$, where e_{ij} accounts for all sources of error between the estimate and the true channel. We assume that the true channel h_{ij} belongs to an uncertainty set $\mathcal{E}_{ij}$, which includes $\hat{h}_{ij}$. We do not restrict our model to any specific error source and consider an arbitrary model for the uncertainty set, as illustrated in Fig. 8.1.

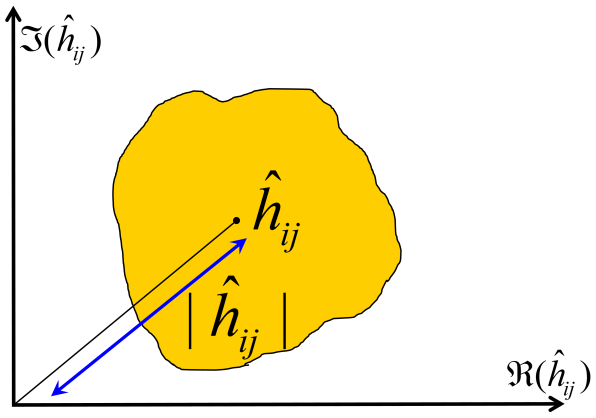

Figure 8.1: Arbitrary channel uncertainty region.

8.1.2 Problem statement

In this chapter, we aim at deriving the boundary of the robust rate region for a given channel uncertainty set. In the 2-user SISO IC with TIN and IGS, the achievable rate of user $i \in \{1,2\}$ is [71, 129]

$$R_i = \frac{1}{2}\log_2\left(\frac{\left(\sigma^2+\sum_{j=1}^{2} p_j|h_{ij}|^2\right)^2 - \left|\sum_{j=1}^{2} p_j\kappa_j|h_{ij}|^2 e^{j(2\measuredangle h_{ij}+\phi_j)}\right|^2}{(p_{\bar{i}}|h_{i\bar{i}}|^2+\sigma^2)^2-(p_{\bar{i}}\kappa_{\bar{i}}|h_{i\bar{i}}|^2)^2}\right), \tag{8.1}$$

where p_j, κ_j, and ϕ_j for $j=1,2$, are, respectively, the transmission power, circularity coefficient and phase of the complementary covariance of the signal transmitted by user j. Moreover, $|h_{ji}|$ and $\measuredangle h_{ji}$ for $i,j \in \{1,2\}$ are the magnitude and phase of the channel from the ith transmitter to the jth receiver, respectively. Note that the rate expressions in (8.1) are the maximum rates that can be supported by the channels.

In order to derive the robust rate region, we employ the definition of the Pareto boundary for the rate region, which is defined in Section 4.3 and Definition 4.1. Employing the concept of *worst-case robustness* [35, 88, 114], we define the boundary of the robust rate region as the Pareto-optimal points that are achievable for all possible channels inside the uncertainty region [82]. Therefore, the robust rate region is the union of all these achievable rate tuples, i.e.,

$$\mathcal{R} = \bigcup_{\varrho\in\Omega}\left(\min_{h_{ij}\in\mathcal{E}_{ij}} R_1, \min_{h_{ij}\in\mathcal{E}_{ij}} R_2\right), \tag{8.2}$$

where $\varrho = \{p_i,\kappa_i,\phi_i, i=1,2\}$, and $\Omega = \{p_i,\kappa_i,\phi_i : 0\le p_i\le P_i, 0\le\kappa_i\le 1, 0\le\phi_i\le 2\pi,\ i=1,2\}$ are the design parameters, and the feasible set of the design parameters, respectively, with P_i being the power budget of user i. Hereafter, we represent the worst-case rate of user i by $R_i^w \triangleq \min\limits_{h_{ij}\in\mathcal{E}_{ij}} R_i$ for $i\in\{1,2\}$.

In order to derive the boundary of the robust rate region, we do not need to optimize over all the six design variables, i.e., the powers, circularity coefficients, and the phases of the complementary variances. According to (8.1), the achievable rates are functions of the phase difference between the phases of the complementary variances, i.e., $\Delta_\phi = \phi_1 - \phi_2$. The reason is that, as

can be observed through (8.1), R_i depends on the phase parameters only through the term

$$\begin{aligned} t &\triangleq \left| p_i\kappa_i|h_{ii}|^2 e^{j(2\angle h_{ii}+\phi_i)} + p_{\bar{\imath}}\kappa_{\bar{\imath}}|h_{i\bar{\imath}}|^2 e^{j(2\angle h_{i\bar{\imath}}+\phi_{\bar{\imath}})}\right|^2, \\ &= \left| p_i\kappa_i|h_{ii}|^2 + p_{\bar{\imath}}\kappa_{\bar{\imath}}|h_{i\bar{\imath}}|^2 e^{j(2(\angle h_{i\bar{\imath}}-\angle h_{ii})+\phi_{\bar{\imath}}-\phi_i)}\right|^2 \end{aligned} \tag{8.4}$$

where $i, \bar{\imath} \in \{1, 2\}$ and $\bar{\imath} \neq i$. Furthermore, it is shown in [87, Theorem 2] that, in every point on the Pareto-optimal boundary of the rate region for this problem, at least one user transmits with maximum power. As a result, we can further simplify the problem by taking the power of one user equal to its maximum power, and solve two optimization problems with only *four* optimization parameters, namely the two circularity coefficients, Δ_ϕ, and the power of one of the users.

Let us denote the user that transmits with maximum power by i. The boundary of the robust rate region, when user i transmits with maximum power, can be derived by solving

$$\max_{\Delta_\phi,\, 0\leq p_{\bar{\imath}}\leq P_{\bar{\imath}},\, 0\leq\kappa_1,\kappa_2\leq 1} \quad R_{\bar{\imath}}^w \qquad \text{s.t.} \quad R_i^w \geq \alpha R_{i,\max}^w, \tag{8.5}$$

for $i, \bar{\imath} \in \{1, 2\}$ and $i \neq \bar{\imath}$, and a fixed $\alpha \in [0, 1]$, where $R_{i,\max}^w$ is the maximum worst-case rate of user i, which is obtained with $p_{\bar{\imath}} = 0$ and PGS [24]. That is, we maximize the worst-case rate of user $\bar{\imath}$ for every feasible worst-case rate of user i. It is worth mentioning that deriving the optimal solution of (8.5) in polynomial time is not possible in general since (8.5) is not convex and has an infinite number of non-convex constraints. These infinite number of constraints could be reduced to a single one if an expression for the worst-case channels within the uncertainty sets were identified. However, this is also not possible for arbitrary uncertainty regions. To the best of our knowledge, even with perfect CSIT, there are only numerical approaches that provide a suboptimal solution, e.g., [129], for the rate region of the 2-user IC.

8.1.3 Robust design for the 2-user IC

In this section, we propose a robust design for the 2-user IC by simplifying the original problem (8.5). In particular, by allowing only one user to employ IGS, i.e., by setting either κ_1 or κ_2 to zero, we can easily find the worst-case channels for arbitrary uncertainty sets. In turn, an optimization problem that approximates (8.5) is obtained, which, although still non-convex, its global optimal solution admits a closed form.

If at most one of the users employs IGS, the achievable rates are independent of the phases of the channel coefficients since R_i depends on the phase parameters only through the term t in (8.4). Thus, if $\kappa_i = 0$ or $\kappa_{\bar{\imath}} = 0$, t is independent of the phases of the channel coefficients and as a result, these phases are not required at the transmitter side in order to optimize the rate. Since our proposed robust algorithm is independent of the phases of the channels, it requires only the worst-case channel gains and consequently can be applied to any uncertainty model. In the following, we first derive the worst-case channel gains and then derive the optimal parameters in closed-form.

It is easy to see that the rate of each user is a strictly increasing function of the gain of the corresponding direct link, i.e., $\frac{\partial R_1}{\partial |h_{11}|^2} > 0$ and $\frac{\partial R_2}{\partial |h_{22}|^2} > 0$. Moreover, the rates of users are decreasing functions of the interference channel gain, i.e., $\frac{\partial R_1}{\partial |h_{12}|^2} \leq 0$ and $\frac{\partial R_2}{\partial |h_{21}|^2} \leq 0$. Thus, the worst-case channel gains are $|\tilde{h}_{11}|^2 = \min\limits_{x\in\mathcal{E}_{11}} |x|^2$, $|\tilde{h}_{22}|^2 = \min\limits_{x\in\mathcal{E}_{22}} |x|^2$, $|\tilde{h}_{21}|^2 = \max\limits_{x\in\mathcal{E}_{21}} |x|^2$, and

$|\tilde{h}_{12}|^2 = \max_{x \in \mathcal{E}_{12}} |x|^2$.

To derive the boundary of the robust rate region, we have to optimize only two parameters, i.e., the power of the user that may not transmit with maximum power, and the circularity coefficient of the user that may employ IGS. Thus, every point of the robust rate region that is achievable by this scheme can be derived by one of the following strategies:

1. Strategy 1: The PGS user transmits with maximum power,
2. Strategy 2: The IGS user transmits with maximum power.

Let us denote the rate region achieved by the kth strategy as $\mathcal{R}_k$. The robust rate region achieved by the proposed scheme is the union of the achievable rate regions of the above strategies, i.e., $\mathcal{R} = \bigcup_{k=1}^{2} \mathcal{R}_k$. It is worth mentioning that $\mathcal{R}_k$ is also a union of two different strategies since there is no difference between users and either of them can be the IGS user. In the following subsections, we derive the Pareto-optimal achievable rate region of each strategy.

Achievable rate region for strategy 1

In strategy 1 the PGS user transmits with maximum power. Without loss of generality, let us assume that the IGS user is user $\bar{\imath}$. Then, the optimization problem is

$$\max_{0 \le p_{\bar{\imath}} \le P_{\bar{\imath}},\ 0 \le \kappa_{\bar{\imath}} \le 1} \quad R_{\bar{\imath}}^w(p_{\bar{\imath}}, \kappa_{\bar{\imath}}) \tag{8.6a}$$

$$\text{s.t.} \quad R_i^w(p_{\bar{\imath}}, \kappa_{\bar{\imath}}) \ge \alpha R_{i,\max}^w, \tag{8.6b}$$

for $i, \bar{\imath} \in \{1, 2\}$ and $i \neq \bar{\imath}$, and a fixed $\alpha \in [0, 1]$, where $R_{i,\max}^w = \log_2(1 + \frac{P_i |\tilde{h}_{ii}|^2}{\sigma^2})$. Note that the worst-case rates are derived by replacing the worst-case channel gains in (8.1). The achievable robust rate region can be derived by varying $\alpha \in [0, 1]$. In [70], a similar scenario in the context of cognitive radio was studied, and (8.6) was solved. Thus, we can apply the results in [70] to obtain the Pareto-optimal parameters for strategy 1 as presented in the following theorem.

Theorem 8.1 *Let us define* $\gamma_i(\alpha) = 2^{\alpha R_{i,\max}^w - 1}$. *The Pareto-optimal parameters for transmission strategy 1 are given by*

$$\kappa_{\bar{\imath}} = \begin{cases} 0 & \text{if} \quad \frac{|\tilde{h}_{i\bar{\imath}}|^2(\sigma^2 + P_i|\tilde{h}_{\bar{\imath}i}|^2)}{|\tilde{h}_{\bar{\imath}\bar{\imath}}|^2\sigma^2} \le 1 - \frac{\gamma_i(1)}{\gamma_i(2\alpha)}, \\ \kappa^{(\star)} & \text{if} \quad \frac{|\tilde{h}_{i\bar{\imath}}|^2(\sigma^2 + P_i|\tilde{h}_{\bar{\imath}i}|^2)}{|\tilde{h}_{\bar{\imath}\bar{\imath}}|^2\sigma^2} > 1 - \frac{\gamma_i(1)}{\gamma_i(2\alpha)} \quad \text{and} \quad \mathcal{P}_{\bar{\imath}}(1) \le P_{\bar{\imath}}, \\ 1 & \text{otherwise}, \end{cases} \tag{8.7}$$

$$p_{\bar{\imath}} = \mathcal{P}_{\bar{\imath}}(\kappa_{\bar{\imath}}), \tag{8.8}$$

where

$$\kappa^{(\star)} = \sqrt{1 - \frac{\sigma^2}{p_{\bar{\imath}}|\tilde{h}_{i\bar{\imath}}|^2}\left[\left(\frac{\gamma_i(2)}{\gamma_i(2\alpha)} - 1\right)\frac{\sigma^2}{p_{\bar{\imath}}|\tilde{h}_{i\bar{\imath}}|^2} - 2(1 - \frac{\gamma_i(1)}{\gamma_i(2\alpha)})\right]}, \tag{8.9}$$

$$\mathcal{P}_{\bar{\imath}}(\kappa) = \left[\sqrt{(1 - \frac{\gamma_i(1)}{\gamma_i(2\alpha)})^2 + (1 - \kappa^2)\left(\frac{\gamma_i(2)}{\gamma_i(2\alpha)} - 1\right)} - (1 - \frac{\gamma_i(1)}{\gamma_i(2\alpha)})\right] \frac{\sigma^2}{|\tilde{h}_{i\bar{\imath}}|^2(1 - \kappa^2)}, \tag{8.10}$$

Proof. Please refer to Eq. (11) and Theorem 1 in [70] for more details. □

Achievable rate region for strategy 2

In strategy 2 the IGS user transmits with maximum power. Without loss of generality, let us assume that the IGS user is user $\bar{\imath}$. Then, the optimization problem is

$$\max_{0\leq p_i\leq P_i,\ 0\leq\kappa_{\bar{\imath}}\leq 1} \quad R_i^w(p_i,\kappa_{\bar{\imath}}) \tag{8.11a}$$

$$\text{s.t.} \quad R_{\bar{\imath}}^w(p_i,\kappa_{\bar{\imath}}) \geq \alpha R_{\bar{\imath},\max}^w, \tag{8.11b}$$

for $i,\bar{\imath}\in\{1,2\}$ and $i\neq\bar{\imath}$, and a fixed $\alpha\in[0,1]$, where $R_{\bar{\imath},\max}^w=\log_2(1+\frac{P_{\bar{\imath}}|\tilde{h}_{\bar{\imath}\bar{\imath}}|^2}{\sigma^2})$. Similar to (8.6), the robust achievable rate region can be derived by varying $\alpha\in[0,1]$. The optimization problem (8.11) resulting from strategy 2 has not been considered before in the literature. We present the Pareto-optimal parameters for this strategy in the subsequent theorem.

Theorem 8.2 *The Pareto-optimal signaling scheme for strategy 2 is IGS if and only if one of the following conditions is met. Additionally, the Pareto-optimal parameters for each condition are provided.*

1. $P_i\leq\mathcal{P}_i(1)$, $\Rightarrow p_i=P_i$ *and* $\kappa_{\bar{\imath}}=1$,

2. $P_i>\mathcal{P}_i(1)$, $(\zeta_1\beta_2-\zeta_2\beta_1)<0$ *and* $\tau<0$, $\Rightarrow p_i=\mathcal{P}_i(1)$ *and* $\kappa_{\bar{\imath}}=1$,

3. $P_i>\mathcal{P}_i(1)$, $(\zeta_1\beta_2-\zeta_2\beta_1)<0$, $\tau>0$, *and* $\mathcal{P}(0)>x_1^{(\star)}$, $\Rightarrow p_i=\max(x_1^{(\star)},\mathcal{P}_i(1))$ *and* $\kappa_{\bar{\imath}}=\mathcal{K}(p_i)$,

4. $P_i>\mathcal{P}_i(1)$, $(\zeta_1\beta_2-\zeta_2\beta_1)>0$, $\tau<0$, $\mathcal{P}_i(1)<x_2^{(\star)}$, *and* $R_i^w(\mathcal{P}(1))>R_i^w(\mathcal{P}(0))$, $\Rightarrow p_i=\mathcal{P}_i(1)$ *and* $\kappa_{\bar{\imath}}=1$,

where i and $\bar{\imath}$ are the users that employ PGS and IGS in the transmission strategy 2, respectively, $\gamma_{\bar{\imath}}(\cdot)$ is defined as in Theorem 8.1*, and*

$$x_1^{(\star)}=\frac{-\zeta_1\tau-\sqrt{(\zeta_1\tau)^2-\beta_1\tau(\zeta_1\beta_2-\zeta_2\beta_1)}}{\zeta_1\beta_2-\zeta_2\beta_1}, \tag{8.12}$$

$$x_2^{(\star)}=\frac{-\zeta_1\tau+\sqrt{(\zeta_1\tau)^2-\beta_1\tau(\zeta_1\beta_2-\zeta_2\beta_1)}}{\zeta_1\beta_2-\zeta_2\beta_1}, \tag{8.13}$$

$$\mathcal{P}_i(\kappa)=\frac{1}{|\tilde{h}_{\bar{\imath}i}|^2}\left[\left(\frac{1+\sqrt{1+\gamma_{\bar{\imath}}(2\alpha)(1-\kappa^2)}}{\gamma_{\bar{\imath}}(2\alpha)}\right)P_{\bar{\imath}}|\tilde{h}_{\bar{\imath}\bar{\imath}}|^2-\sigma^2\right], \tag{8.14}$$

$$\mathcal{K}(p_i)=\sqrt{1-\frac{(\sigma^2+p_i|\tilde{h}_{\bar{\imath}i}|^2)^2}{P_{\bar{\imath}}^2|\tilde{h}_{\bar{\imath}\bar{\imath}}|^4}\gamma_{\bar{\imath}}(2\alpha)+2\frac{\sigma^2+p_i|\tilde{h}_{\bar{\imath}i}|^2}{P_{\bar{\imath}}|\tilde{h}_{\bar{\imath}\bar{\imath}}|^2}}, \tag{8.15}$$

$$R_i^w(p_i)=\frac{1}{2}\log_2\left(1+\frac{\zeta_1p_i^2+\beta_1p_i}{\zeta_2p_i^2+\beta_2p_i+\tau}\right). \tag{8.16}$$

Moreover, β_1, ζ_1, β_2, ζ_2 *and* τ *are*

$$\begin{aligned}
\beta_1 &= 2|\tilde{h}_{ii}|^2(\sigma^2 + P_{\bar{i}}|\tilde{h}_{i\bar{i}}|^2), & \zeta_1 &= |\tilde{h}_{ii}|^4, \\
\beta_2 &= 2(\sigma^2\gamma_{\bar{i}}(2\alpha) - P_{\bar{i}}|\tilde{h}_{\bar{i}\bar{i}}|^2)\frac{|\tilde{h}_{i\bar{i}}|^4|\tilde{h}_{\bar{i}}i|^2}{|\tilde{h}_{\bar{i}\bar{i}}|^4}, & \zeta_2 &= \frac{|\tilde{h}_{i\bar{i}}|^4|\tilde{h}_{\bar{i}i}|^4}{|\tilde{h}_{\bar{i}\bar{i}}|^4}\gamma_{\bar{i}}(2\alpha), \\
\tau &= \sigma^4 + 2\sigma^2 P_{\bar{i}}|\tilde{h}_{i\bar{i}}|^2 - 2\sigma^2 P_{\bar{i}}\frac{|\tilde{h}_{\bar{i}i}|^2}{|\tilde{h}_{\bar{i}\bar{i}}|^2} + \sigma^4\gamma_{\bar{i}}(2\alpha)\frac{|\tilde{h}_{i\bar{i}}|^4}{|\tilde{h}_{\bar{i}\bar{i}}|^4}. & & \qquad (8.17)
\end{aligned}$$

Proof. Please refer to Section 8.4. □

Note that if none of the conditions in Theorem 8.2 is fulfilled, PGS is Pareto-optimal for both users in strategy 2. Moreover, the parameters of the users can be easily derived through (8.6) by taking $\kappa_{\bar{i}} = 0$.

The implication of Theorem 8.2 can be understood with the following example. If, e.g., user 2 employs IGS, it causes less interference to user 1. Thus, user 1 can decrease its transmission power in order to meet the rate constraint of user 2 in (8.11b). According to Theorem 8.2, this power reduction of user 1, alongside with employing IGS by user 2, may even result in a rate increase for user 1. In other words, IGS allows the users to decrease the transmission power and simultaneously increase the achievable rate, hence, improving as well the power efficiency. This is due to the fact that IGS can mitigate the negative effect of the interference, which may lead to an overall improvement of the system performance.

8.1.4 Robust design for the Z-IC

In this section, we consider the Z-IC and derive a closed-form robust design. The results in Section 8.1.3 can be applied to the Z-IC by taking $h_{21} = 0$. However, for this simplified scenario it is possible to obtain a better closed-form robust design for the Z-IC if we allow both users to employ IGS. When both users employ IGS, the phases of the channels are relevant for the optimal strategy. Thus, even though problem (8.5) is simpler for the Z-IC, it is still in general difficult to obtain the worst-case channels when both magnitude and phase are considered. Therefore, the constraint set of problem (8.5) cannot be reduced to a finite number of constraints and hence it is still difficult to solve in its current form. To overcome this, we approximate the original problem by considering a surrogate uncertainty region in which magnitude and phase are decoupled, so that their worst realizations can easily be found. It is also worth mentioning that this approach gives us a lower bound for the worst-case rates of problem (8.5). Note that the surrogate uncertainty region must contain the original region as illustrated in Fig. 8.2 in order for the constraints of (8.5) to be fulfilled after solving the approximated problem. Thus, we consider the enlarged uncertainty region $\tilde{\mathcal{E}}_{ij} = \{x \in \mathbb{C} \colon |x| = |\hat{h}_{ij}| + e_{|h_{ij}|}, \measuredangle x = \measuredangle\hat{h}_{ij} + e_{\measuredangle h_{ij}}, |e_{|h_{ij}|}| \leq \delta_{ij}, |e_{\measuredangle h_{ij}}| \leq \theta_{ij}\}$, where δ_{ij} and θ_{ij} are the largest uncertainties in magnitude and phase, respectively.

The enlarged uncertainty region permits decoupling the errors in phase and magnitude and hence allows us to find the worst-case phases and the worst-case channel gains independently. It is worth mentioning that, since the errors in phase and magnitude are not necessarily independent, a channel realization with both the worst-case channel phase and worst-case channel gains might not be in the original set. Hence, this approach provides a lower bound for the worst-case rates of (8.5). Note that the enlarged uncertainty region includes the original region as a subset,

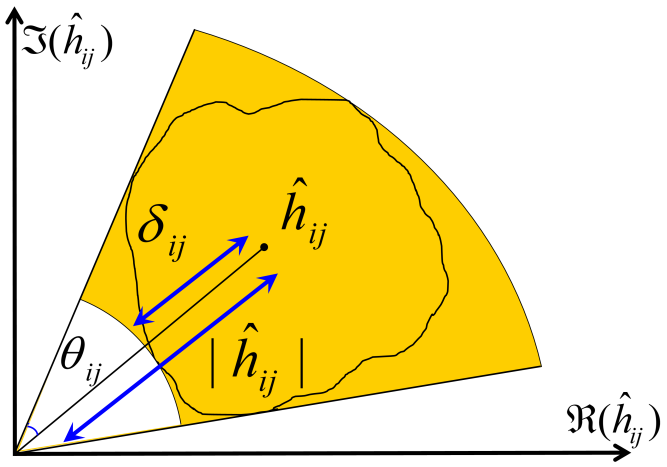

Figure 8.2: Enlarged channel uncertainty region for the uncertainty region in Fig 8.1.

and the bounds of the errors in phase and magnitude are the same for both uncertainty regions. Thus, this approach can be applied to any arbitrary uncertainty model.

In the Z-IC, since user 1 does not interfere with user 2, the optimal design parameters for user 1 are those maximizing its rate. Thus, every point in the Pareto boundary of the robust rate region can be achieved when user 1 transmits with maximum power, i.e., $p_1 = P_1$. Hence, in the rest of this section, we consider $p_1 = P_1$. The rate of user 2 in the Z-IC can be derived by taking $h_{21} = 0$ in (8.1) as

$$R_2 = \frac{1}{2}\log_2\left(\frac{(p_2|h_{22}|^2+\sigma^2)^2-(\kappa_2 p_2|h_{22}|^2)^2}{\sigma^4}\right). \tag{8.18}$$

Moreover, the robust rate region of the Z-IC for the enlarged uncertainty region can be derived by replacing $\mathcal{E}_{ij}$ with $\tilde{\mathcal{E}}_{ij}$ in (8.2) as

$$\tilde{\mathcal{R}} = \bigcup_{\varrho\in\Omega}\left(\min_{h_{ij}\in\tilde{\mathcal{E}}_{ij}} R_1, \min_{h_{ij}\in\tilde{\mathcal{E}}_{ij}} R_2\right), \tag{8.19}$$

where $\tilde{\mathcal{R}} \subset \mathcal{R}$. In the following, we first derive the worst-case channel coefficients in the enlarged uncertainty region, which are the solution of the minimization part in (8.19). Then, we will derive the transmission parameters that attain the boundary of the robust rate region for the enlarged uncertainty region, which is the solution of the optimization problem

$$\max_{\Delta_\phi, 0\le p_2\le P_2, 0\le\kappa_1,\kappa_2\le 1} \quad R_2^w, \qquad \text{s.t.} \quad R_1^w \ge \alpha R_{1,\max}^w, \tag{8.20}$$

for a fixed $\alpha \in [0,1]$. The robust rate region can be derived by varying $\alpha \in [0,1]$.

The worst-case gains are the same as those derived in Section 8.1.3, i.e., the minimum channel gain in the uncertainty region $\tilde{\mathcal{E}}_{ij}$ for the direct links, and the maximum channel gain in $\tilde{\mathcal{E}}_{ij}$ for the interference links. We rewrite them here as $|\tilde{h}_{11}|^2 = \min\limits_{x\in\mathcal{E}_{11}} |x|^2$, $|\tilde{h}_{22}|^2 = \min\limits_{x\in\mathcal{E}_{22}} |x|^2$, and $|\tilde{h}_{12}|^2 = \max\limits_{x\in\mathcal{E}_{12}} |x|^2$.

In the following, we derive the worst-case phase error along with the Pareto-optimal phases

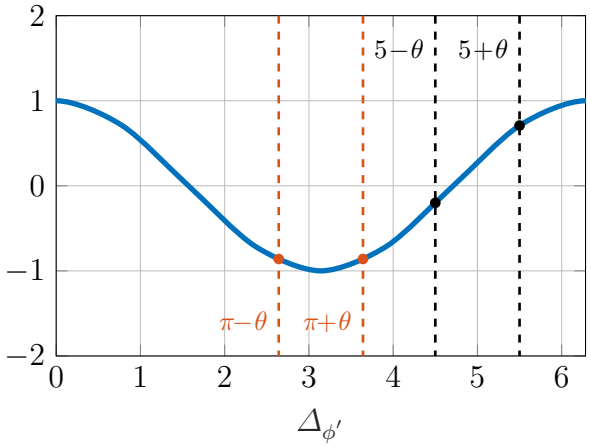

Figure 8.3: Function $\cos(\Delta_{\phi'} + \Delta_{ch})$ for two examples with $\theta = 0.5$, $\Delta_{\phi'} = \pi$ (red) and $\Delta_{\phi'} = 5$ (black).

ϕ_1 and ϕ_2 for the given worst-case channel gains. Through (8.1), it can be observed that R_1 depends on these quantities only through the term

$$A \triangleq \left| p_1 \kappa_1 |\tilde{h}_{11}|^2 e^{j(2\angle h_{11} - 2\angle h_{12} + \phi_1 - \phi_2)} + p_2 \kappa_2 |\tilde{h}_{12}|^2 \right|^2, \tag{8.21}$$

while the rate of user 2 is independent of them (see (8.18)). Replacing the true values by the estimated values, we have $2\angle h_{11} - 2\angle h_{12} = 2\angle \hat{h}_{11} - 2\angle \hat{h}_{12} \pm 2e_{\angle h_{11}} \pm 2e_{\angle h_{12}}$. Let us define $\Delta_{ch} \triangleq 2e_{\angle h_{11}} + 2e_{\angle h_{12}} \in [-\theta, \theta]$ as the aggregate uncertainty in phase, where $\theta = 2\theta_{11} + 2\theta_{12}$ is the magnitude of the maximum aggregate phase error. Note that $\theta = \pi$ means that there is no reliable information about the phase of the channels. Finally, the term A can be written as

$$A = p_2^2 \kappa_2^2 |\tilde{h}_{12}|^4 + 2p_1 \kappa_1 p_2 \kappa_2 |\tilde{h}_{12}|^2 |\tilde{h}_{11}|^2 \cos(\Delta_{ch} + \Delta_{\phi'}) + p_1^2 \kappa_1^2 |\tilde{h}_{11}|^4, \tag{8.22}$$

where $\Delta_{\phi'} = (\phi_1 + 2\angle \hat{h}_{11}) - (\phi_2 + 2\angle \hat{h}_{12})$. In the following lemma, we state the Pareto-optimal phase parameters.

Lemma 8.1 *In the Z-IC, each point of the boundary of the rate region defined in* (8.19) *can be achieved by* $\phi_1 = 0$ *and* $\phi_2 = 2\angle \hat{h}_{11} - 2\angle \hat{h}_{12} + \pi$. *Furthermore, the corresponding worst-case channel phases yield* $\Delta_{ch}^{(\star)} = \theta$.

Proof. Since Δ_{ch} and $\Delta_{\phi'}$ only affect R_1, their values describing the boundary of the rate region defined in (8.19) can be obtained as the solution of the maximin problem

$$(\Delta_{\phi'}^{(\star)}, \Delta_{ch}^{(\star)}) = \arg \max_{\Delta_{\phi'}} \min_{\Delta_{ch}} (R_1) \overset{(*)}{=} \arg \min_{\Delta_{\phi'}} \max_{\Delta_{ch}} (A) = \arg \min_{\Delta_{\phi'}} \max_{\Delta_{ch}} (\cos(\Delta_{\phi'} + \Delta_{ch})). \tag{8.23}$$

The equality $(*)$ in (8.23) holds since R_1 is a function of the phases only through A. Moreover, R_1 decreases with A. In order to solve this problem, we consider $\Delta_{\phi'}$ in a period, i.e., $0 \leq$

$\Delta_{\phi'} < 2\pi$, as depicted in Fig 8.3. Thus, the solution of the maximization problem in (8.23) is

$$\Delta_{ch}^{(\star)} = \begin{cases} \max(-\Delta_{\phi'}, -\theta) & \text{for} \quad 0 \leq \Delta_{\phi'} < \pi, \\ \min(2\pi - \Delta_{\phi'}, \theta) & \text{for} \quad \pi \leq \Delta_{\phi'} < 2\pi. \end{cases} \tag{8.24}$$

This is because $\cos(\phi)$ is decreasing in the interval $[0, \pi]$, increasing in the interval $[\pi, 2\pi]$ and maximized at $\phi = 0$, or $\phi = 2\pi$. Moreover, since $\cos(\phi)$ is decreasing (increasing) in the interval $[0, \pi]$ ($[\pi, 2\pi]$), it can be easily seen through Fig. 8.3 that $\Delta_{\phi'}^{(\star)}$ should be such that $\Delta_{\phi'} + \Delta_{ch}$ is as close as possible to π, which results in $\Delta_{\phi'} = \pi$. In other words, the solution of the minimax problem is $\Delta_{\phi'}^{(\star)} = \pi$ and $\Delta_{ch}^{(\star)} = \theta$. Through (8.18) and (8.1), we can see that the rate of user 2 is independent of the phase parameters, and the rate of user 1 is only a function of the phase difference. Thus, we can, without loss of generality, choose $\phi_1 = 0$ and $\phi_2 = 2\measuredangle \hat{h}_{11} - 2\measuredangle \hat{h}_{12} + \pi$. □

We now derive the optimal transmit powers and circularity coefficients for the worst-case channels, so that the boundary of the rate region (8.19) is attained. Since user 1 does not interfere with user 2, the optimal design parameters for user 1 maximize its rate. Thus, its circularity coefficient can be obtained as

$$\kappa_1^{(\star)} = \arg \max_{\kappa_1} \left(R_1^w\right) = \arg \min_{\kappa_1} \left(A^{(\star)}\right), \tag{8.25}$$

where $A^{(\star)}$ is obtained by taking the worst-case channels in (8.22). Since A^* is convex in κ_1, the solution of (8.25) can be derived as

$$\frac{\partial A^{(\star)}}{\partial \kappa_1} = -2P_1 p_2 \kappa_2 |\tilde{h}_{12}|^2 |\tilde{h}_{11}|^2 \cos\theta + 2P_1^2 \kappa_1 |\tilde{h}_{11}|^4 = 0. \tag{8.26}$$

Taking the feasible set of κ_1 into account, we obtain

$$\kappa_1^{(\star)} = \min\left(1, \left[\frac{p_2|\tilde{h}_{12}|^2}{P_1|\tilde{h}_{11}|^2}\kappa_2 \cos\theta\right]^+\right). \tag{8.27}$$

From this equation we can readily observe that, if the total uncertainty in phase is equal to or greater than $\frac{\pi}{2}$ (i.e., $\theta \geq \frac{\pi}{2}$), user 1 should transmit proper Gaussian signals. In such a case, the resulting problem becomes equivalent to the proposed robust algorithm for strategy 1 in Section 8.1.3, in which only one of the users employs IGS. Thus, in the following, we assume that $\theta < \pi/2$ and derive a condition for the optimality of IGS for user 2 in terms of θ, as well as its transmission parameters.

Plugging into (8.1) the optimal transmission parameters of user 1 yields the worst-case rates

$$R_1^w(p_2, \kappa_2) = \begin{cases} \frac{1}{2}\log_2\left(1 + \frac{2P_1|\tilde{h}_{11}|^2\left(\sigma^2 + p_2|\tilde{h}_{12}|^2(1+\kappa_2\cos\theta)\right)}{p_2^2|\tilde{h}_{12}|^4(1-\kappa_2^2) + 2\sigma^2 p_2|\tilde{h}_{12}|^2 + \sigma^4}\right) & \text{if} \quad \kappa_1^{(\star)} = 1, \\ \frac{1}{2}\log_2\left(\frac{\left(P_1|\tilde{h}_{11}|^2 + p_2|\tilde{h}_{12}|^2 + \sigma^2\right)^2 - p_2^2|\tilde{h}_{12}|^4\kappa_2^2\sin^2\theta}{p_2^2|\tilde{h}_{12}|^4(1-\kappa_2^2) + 2\sigma^2 p_2|\tilde{h}_{12}|^2 + \sigma^4}\right) & \text{if} \quad \kappa_1^{(\star)} < 1, \end{cases} \tag{8.28a}$$

$$R_2^w(p_2, \kappa_2) = \frac{1}{2}\log_2\left(p_2^2|\tilde{h}_{22}|^4\sigma^{-4}(1-\kappa_2^2) + 2p_2|\tilde{h}_{22}|^2\sigma^{-2} + 1\right). \tag{8.28b}$$

The Pareto-optimal boundary for the enlarged uncertainty region can then be obtained by rewriting (8.20) as

$$\underset{0\le p_2\le P_2, 0\le\kappa_2\le 1}{\text{maximize}} \quad R_2^w(p_2,\kappa_2), \tag{8.28a}$$

$$\text{s.t.} \quad R_1^w(p_2,\kappa_2)\ge \alpha R_{1,\max}^w, \tag{8.28b}$$

where $\alpha\in[0,1]$ is fixed and $R_{1,\max}^w$ is the maximum worst-case achievable rate for user 1, which is obtained with $p_2=0$ and PGS [24]. By varying α between 0 and 1, the solution of (8.28) provides every point of the robust rate region boundary in (8.19) [71]. Unfortunately, the optimization problem (8.28) is not convex due to constraint (8.28b). Furthermore, the results in [71] for perfect CSIT cannot be applied due to the phase error θ. In the following lemma, we rewrite constraint (8.28b) in a more convenient form to simplify the optimization problem.

Lemma 8.2 *The constraint* (8.28b) *is simplified to* $p_2\le q(\kappa_2,\theta)$*, where* $q(\kappa_2,\theta)$ *is*

$$q(\kappa_2,\theta)=\begin{cases}\dfrac{P_1|\tilde{h}_{11}|^2-\sigma^2(\gamma_1(2\alpha)+1)+\sqrt{(P_1|\tilde{h}_{11}|^2-\sigma^2\gamma_1(2\alpha))^2-\eta\left(\sigma^4(\gamma_1(2\alpha)+1)-2P_1|\tilde{h}_{11}|^2\sigma^2-P_1^2|\tilde{h}_{11}|^4\right)}}{|\tilde{h}_{12}|^2\eta} \\ \qquad \textit{if} \qquad \kappa_1<1, \\ \dfrac{P_1|\tilde{h}_{11}|^2(1+\kappa_2\cos\theta)-\sigma^2\gamma_1(2\alpha)+\sqrt{P_1^2|\tilde{h}_{11}|^4(1+\kappa_2\cos\theta)^2-2P_1|\tilde{h}_{11}|^2\gamma_1(2\alpha)\sigma^2\kappa_2(\cos\theta+\kappa_2)+\gamma_1^2(2\alpha)\kappa_2^2\sigma^4}}{|\tilde{h}_{12}|^2\gamma(2\alpha)(1-\kappa_2^2)} \\ \qquad \textit{if} \qquad \kappa_1=1,\end{cases} \tag{8.29}$$

where $\eta=((\gamma(2\alpha)+1)(1-\kappa_2^2)-1+\kappa_2^2\sin^2\theta)$ *and* $\gamma_1(x)\triangleq 2^{xR_{1,\max}^w}-1$.

Proof. Constraint (8.28b) can be simplified to a quadratic function of p_2 by plugging (8.28b) into (8.28b) as

$$\begin{gathered}p_2^2|\tilde{h}_{12}|^4\eta-2P_1|\tilde{h}_{11}|^2\sigma^2-P_1^2|\tilde{h}_{11}|^4+\sigma^4(\gamma_1(2\alpha)+1) \\ -2p_2|\tilde{h}_{12}|^2\left[P_1|\tilde{h}_{11}|^2-\sigma^2\gamma_1(2\alpha)\right]\le 0 \quad \text{if} \quad \kappa_1<1, \\ p_2^2|\tilde{h}_{12}|^4(1-\kappa_2^2)\gamma_1(2\alpha)+\gamma_1(2\alpha)\sigma^4-2P_1\sigma^2|\tilde{h}_{11}|^2 \\ +2p_2|\tilde{h}_{12}|^2\left[\sigma^2\gamma_1(2\alpha)-P_1|\tilde{h}_{11}|^2(1+\kappa_2\cos\theta)\right]\le 0 \qquad \text{if} \qquad \kappa_1=1.\end{gathered} \tag{8.30}$$

We consider (8.30) as two quadratic polynomials in p_2 and take the positive root in (8.30), which results in (8.29). □

According to Lemma 8.2, we can combine the power constraint and (8.28b) into $0\le p_2(\theta)\le \min\{P_2,q(\kappa_2,\theta)\}$. Similar to [71], we must set $p_2(\theta)=\min\{P_2,q(\kappa_2,\theta)\}$ in order to achieve the global optimum of (8.28). As a result, the rate of user 2 is only a function of κ_2 as

$$R_2^w(\kappa_2,\theta)=\frac{1}{2}\log_2\left(\frac{p_2^2(\kappa_2,\theta)|\tilde{h}_{22}|^4(1-\kappa_2^2)}{\sigma^4}+\frac{2p_2(\kappa_2,\theta)|\tilde{h}_{22}|^2}{\sigma^2}+1\right). \tag{8.31}$$

Finally, the optimization problem in (8.28) is simplified to

$$\underset{0\le\kappa_2\le 1}{\text{maximize}} \quad R_2^w(\kappa_2,\theta). \tag{8.32}$$

Notice that the difference between this problem and the one solved in [71] is in the error term θ, which makes its solution not straightforward as the results in [71] are not applicable. Taking

$\theta = 0$ makes (8.32) equivalent to the problem considered in [71].

Theorem 8.3 *The optimal transmission strategy for user 2 is IGS if* $P_2 > q(0, \theta)$ *and*

$$\frac{|\tilde{h}_{12}|^2}{|\tilde{h}_{22}|^2} > \frac{\sigma^2\gamma_1(2\alpha) - P_1|\tilde{h}_{11}|^2 - (\frac{P_1|\tilde{h}_{11}|^2}{\gamma_1(\alpha)} - \sigma^2)\cos^2\theta}{\sigma^2\left(\gamma_1(2\alpha) + \cos^2\theta\right)}. \tag{8.33}$$

In this case, the optimal circularity coefficient of user 2 is

$$\kappa = \begin{cases} 1 & \text{if } q(1,\theta) \leq P_2, \\ \kappa_{\max} & \text{otherwise}, \end{cases} \tag{8.34}$$

where $\kappa_{\max}$ *is the minimum value of* κ_2 *that results in* $P_2 \leq q(\kappa_{\max}, \theta)$ *and* $\gamma_1(x) \triangleq 2^{xR^w_{1,\max}} - 1$.

Proof. Please refer to Section 8.5. □

Remark 8.1 *According to Theorem* 8.3*, even if there is no reliable phase information, i.e., when* θ *is large, the optimal transmission strategy for user 2 may be IGS if the interference level is sufficiently high, i.e., if* (8.33) *holds.*

Notice that the condition presented in Theorem 8.3 is sufficient, but may not be necessary. As shown in Section 8.5, condition (8.33) is obtained by showing that $R_2^w(\kappa_2, \theta)$ is increasing at $\kappa_2 = 0$ if and only if this condition holds. However, IGS might provide a minor gain when (8.33) does not hold. As shown in [71], there is only a small performance advantage of IGS in perfect CSI when $R_2^w(\kappa_2, \theta)$ is not increasing around zero, which vanishes as κ_1 approaches 0. Therefore, the solution presented in Theorem 8.3 provides an almost-optimal characterization of the Pareto boundary for the enlarged uncertainty region.

8.1.5 Numerical Results

In this subsection we illustrate our findings with some numerical examples. Throughout this section, for the sake of illustration, we consider a proper complex Gaussian distribution for the aggregate CSI error similar to the models in [19, 88, 118]. Nevertheless, our proposed design can be applied to any uncertainty set, as mentioned before. We consider the uncertainty region as the region where the true channel lies with probability ψ. Thus, the uncertainty region for the SISO channel is a circle centered at $\hat{h}_{ij}$, as illustrated in Fig. 8.4. The radius of this circle is

$$\delta_{ij} = \sqrt{-\sigma_{ij}^2 \ln(1-\psi)}, \tag{8.35}$$

where σ_{ij}^2 is the variance of the channel estimation error. Hence, the uncertainty set for channel h_{ij} is $\mathcal{E}_{ij} = \{x \in \mathbb{C} : x = \hat{h}_{ij} + e_{ij}, |e_{ij}|^2 \leq \delta_{ij}^2\}$. Moreover, the enlarged uncertainty region is $\tilde{\mathcal{E}}_{ij} = \{x \in \mathbb{C} : |x| = |\hat{h}_{ij}| + e_{|h_{ij}|}, \measuredangle x = \measuredangle\hat{h}_{ij} + e_{\measuredangle h_{ij}}, |e_{|h_{ij}|}| \leq \delta_{ij}, |e_{\measuredangle h_{ij}}| \leq \theta_{ij}\}$, where $\theta_{ij} = \arcsin\frac{\delta_{ij}}{|\hat{h}_{ij}|}$ as depicted in Fig. 8.4.

In this section, we consider $\sigma^2 = 1$ and $P = P_1 = P_2$, unless it is explicitly mentioned. We also assume the same variance of the estimation error for all links, i.e., $\sigma_{e_{ij}}^2 = \sigma_e^2$ for $i, j \in \{1, 2\}$ unless it is explicitly mentioned. That yields the same size of the uncertainty region for all channels, i.e., $\delta_{ij} = \delta$ for $i, j \in \{1, 2\}$, where δ is given by (8.35). Furthermore, we compare our proposed robust designs with the existing non-robust designs [71] and [129]

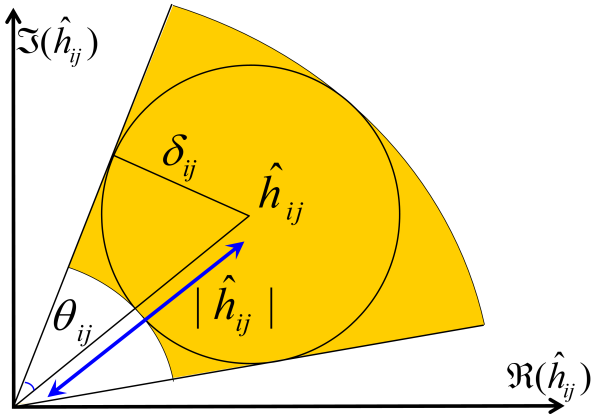

Figure 8.4: Channel uncertainty and enlarged channel uncertainty regions when the CSI errors are modeled as proper Gaussian.

for the Z-IC and 2-user IC, respectively. We choose the joint covariance and complementary covariance algorithm in [129] as a non-robust design for 2-user IC. Moreover, the robust PGS is the PGS design for the worst-case channels gains.

In the following subsections we provide two different types of numerical examples. In the first type, we provide results averaged over a large number of channel realizations for a specific point of the rate region. For example, we derive the average sum-rate for a specific point of the rate region averaged over 200 channel realizations in Figs. 8.5, 8.8 and 8.9. For this type of numerical examples, we employ the Monte Carlo method and generate the channels randomly. In each channel realization, each channel estimate is drawn from a proper complex Gaussian distribution with zero mean and unit variance. In the second type, we derive the whole rate region for a specific channel realization. It is worth mentioning that both types of numerical examples are common for rate region analysis (please refer to [69, 71, 129]).

Numerical results for the 2-user IC

In this subsection, we present the results for the 2-user IC. The proposed and existing techniques are denoted as follows.

- **R-IGS**: Our proposed robust IGS in Section 8.1.3.
- **R-PGS**: Robust PGS.
- **N-IGS**: Non-robust IGS, which is derived by our proposed scheme for the 2-user IC without considering errors in CSI.
- **2-IGS**: The joint variance and covariance IGS algorithm in [129].
- **TS-I**: Robust IGS with time sharing.
- **TS-P**: Robust PGS with time sharing.

In order to evaluate the effect of phase error on the transmitter side, we assume perfect CSI for the channel gains in Fig. 8.5. This figure shows the average sum-rate for signal-to-noise-ratio (SNR), i.e., $\frac{P}{\sigma^2}$, equal to 10 dB versus the accuracy of the phase information. We consider

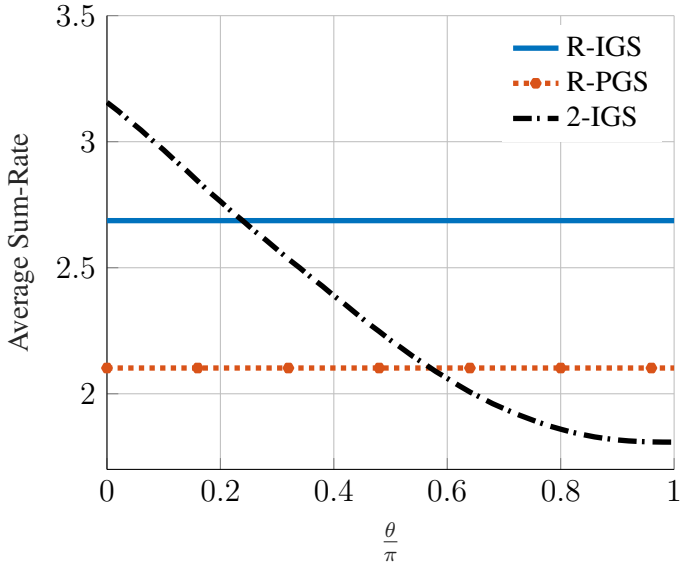

Figure 8.5: Average sum-rate of the 2-user IC for SNR= 10dB versus the phase error.

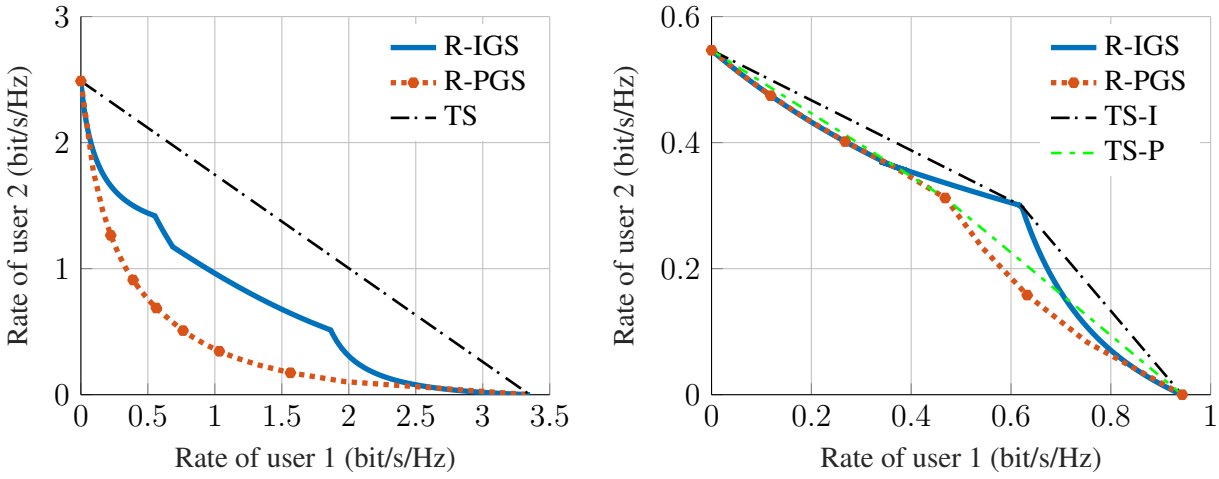

(a) SNR= 10 dB. **(b)** SNR= 0 dB.

Figure 8.6: Robust rate region of the 2-user IC for $\delta_{ij} = 0.5$ for $i, j \in \{1, 2\}$ and $i \neq j$.

a specific point in the rate region, which is given by the fairness point in the algorithm in [129]. In order to provide a fair comparison, we first derive the rates by the algorithm in [129] and then fix the rate of user 1 in our design to the worst-case rate of user 1 achieved by the algorithm in [129]. We average the results over 200 channel realizations, and consider the worst-case performance of the average sum-rate for a bounded error in the available phase information. The considered error is the aggregated error in phase information for both interference and direct links, i.e., $\theta_i = \theta_{ii} + \theta_{ji}$ for $i, j \in \{1, 2\}$, where $\theta_1 = \theta_2 = \theta$ is the horizontal axis of Fig. 8.5. The worst-case phase is the phase that minimizes the achievable rate of users. As can be observed, our proposed algorithm is suboptimal when perfect CSI is available, compared to the non-robust algorithm proposed in [129]. However, it outperforms this algorithm when the aggregated phase error increases. For this example, our robust algorithm performs better than the algorithm in [129] when $\theta \geq 42°$. Our robust proposed algorithm for the 2-user IC and

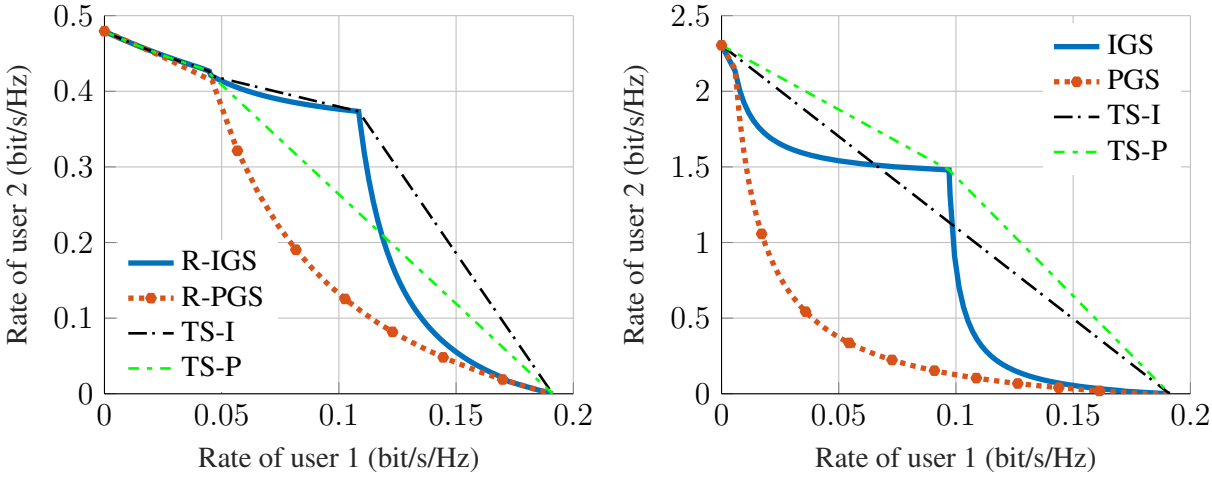

(a) SNR= 10 dB. **(b)** $\text{SNR}_1 = 0$ dB, $\text{SNR}_2 = 10$ dB.

Figure 8.7: Robust rate region for the 2-user IC and channel realization $\hat{\mathbf{H}}_2$.

robust PGS are both independent of phase information, hence their performance is independent of phase information. However, the performance of the non-robust algorithm highly depends on the accuracy of the phase information. Thus, our proposed algorithm outperforms existing methods when the error in the phase of the channels is high.

In Fig. 8.6, we show the achievable robust rate region of the 2-user IC for SNRs of 10 dB and 0 dB, and estimated channel

$$\hat{\mathbf{H}}_1 = \begin{bmatrix} 1.4833e^{-i2.5864} & 0.9367e^{-i3.0001} \\ 0.6375e^{-i1.3064} & 0.4118e^{i2.1234} \end{bmatrix}, \tag{8.36}$$

where $[\hat{\mathbf{H}}]_{ij} = \hat{h}_{ij}$. In this figure, we consider a scenario with perfect CSI for the direct links but imperfect CSI for the interference links. This may represent a scenario where less resources are devoted to acquiring the CSI of the interfering links, which is relevant because interfering signals are treated as noise at the receivers. In this figure, it can be observed that IGS can enlarge the robust rate region in both high and low SNR regimes. Moreover, the performance improvement of IGS in the high SNR regime is higher than in the low SNR regime for the same channels. For this channel realization, IGS with TS[1] performs the same as PGS with TS at 10 dB SNR, indicated by TS in Fig. 8.6a. However, at 0 dB SNR, IGS with TS outperforms PGS with TS in Fig. 8.6b.

In Fig. 8.7, we show the achievable rate region of the 2-user IC for perfect CSI, and channel

$$\hat{\mathbf{H}}_2 = \begin{bmatrix} 0.3764e^{i1.4381} & 1.8542e^{i2.8153} \\ 0.4029e^{i0.9486} & 0.6277e^{i2.3697} \end{bmatrix}. \tag{8.37}$$

[1] As indicated in Section 7.2.3, the achievable rate region with TS is derived by taking the convex-hull operation over the corresponding achievable rate region of each design [71, 129]. Note that TS yields the convex hull when the power constraint is satisfied in each operating point. The rate region may be enlarged by constraining the average transmit power over the different operation points instead. It is shown in [50, 52] for *perfect CSI* that IGS with TS does not provide any gain over PGS with TS in the Z-IC and 2-user IC. Repeating this analysis for the imperfect CSI case is by no means straightforward and falls outside the scope of this work.

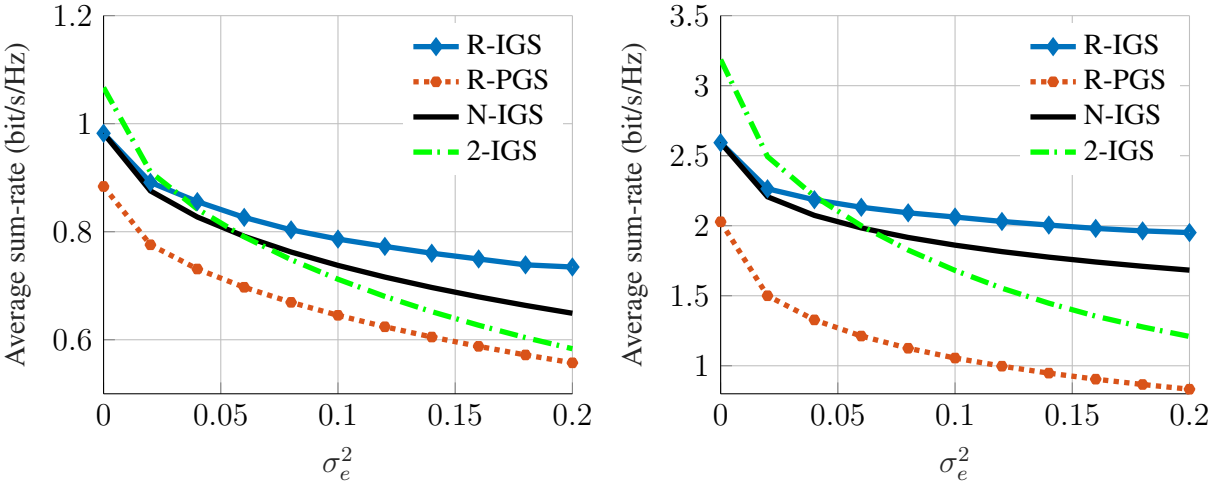

(a) SNR$=0$ dB. **(b)** SNR$=10$ dB.

Figure 8.8: Average sum-rate of the 2-user IC when only the CSI of the interference links is imperfect.

We consider SNR of 10 dB for Fig. 8.7a, and $\text{SNR}_1 = 0\,\text{dB}$, $\text{SNR}_2 = 10\,\text{dB}$ for Fig. 8.7b, where $\text{SNR}_i = \frac{P_i}{\sigma^2}$. As can be observed, IGS significantly enlarges the achievable rate region for $\hat{\mathbf{H}}_2$.

In Figs. 8.8 and 8.9, we consider the average sum-rate of the 2-user IC for SNRs of $0\,\text{dB}$ and $10\,\text{dB}$. In these figures, we consider the same point of the rate region described in Fig. 8.5 and average the results over 200 channel realizations. We set $\Pr = 95\%$ (which implies a maximum outage probability of 5%) and vary the variance of the estimation error, σ_e^2. Moreover, the radius of the uncertainty region is then obtained as (8.35).

In Fig. 8.8, we consider imperfect CSI only for the interference links, where $\delta_{11} = \delta_{22} = 0$ and $\delta_{21} = \delta_{12}$. As can be observed in Fig. 8.8, the IGS algorithms are always better than PGS. Since our proposed algorithm for the 2-user IC is suboptimal for perfect CSI, the non-robust algorithm in [129] performs better than our robust design. Specifically, it achieves 18% higher sum-rate for SNR$=10\,\text{dB}$ and 8% for SNR$=0\,\text{dB}$. However, as the error in the interference link increases, our proposed algorithm performs better than the non-robust algorithm, where there is a 61% and 25% improvement in achievable sum-rate for $\sigma_e^2 = 0.2$ when SNR$=10\,\text{dB}$ and SNR$=0\,\text{dB}$, respectively.

In Fig. 8.9, we consider errors in all links with the same size of the uncertainty region, i.e., $\delta_{ij} = \delta$ for $i, j \in \{1, 2\}$. We observe that the IGS algorithms always perform better than PGS. As also observed in Fig. 8.8, our algorithm performs better than the non-robust algorithm as the error in all links increases. For this example, there is a 200% and 137% improvement in average sum-rate when $\sigma_e^2 = 0.2$ for SNR$=10\,\text{dB}$ and SNR$=0\,\text{dB}$, respectively.

These figures show that our proposed algorithm is robust against imperfect CSI and provides a considerable gain in sum-rate compared to a non-robust approach in high estimation errors. This is a rather surprising result, which means that IGS is even more robust to imperfect CSI than its proper counterpart when the transmission parameters are optimized in a robust way.

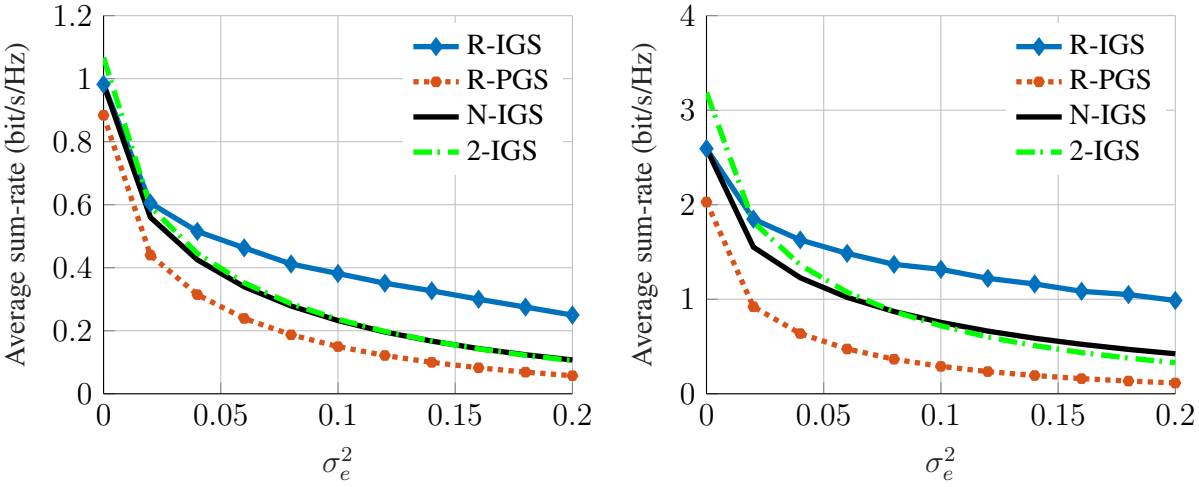

(a) SNR= 0 dB. **(b)** SNR= 10 dB.

Figure 8.9: Average sum-rate of the 2-user IC when the CSI of the direct and interference link is imperfect.

Numerical results for the Z-IC

In this subsection, we evaluate the robust design for the Z-IC. In the figures of this subsection, we use the following acronyms:

- **R-IGS**: Our proposed robust IGS in Section 8.1.4.
- **R-PGS**: Robust PGS.
- **N-IGS**: The non-robust IGS optimal solution in [71].
- **R-IGS-2IC**: Our proposed robust IGS in Section 8.1.3.

We first consider the enlarged uncertainty region to illustrate the effect of the aggregated phase uncertainty θ in the achievable worst-case rate region. Figure 8.10 shows the impact of the aggregated phase uncertainty on the rate region of the Z-IC. In this figure, the channel gains are equal to 1 for all links. In order to consider the effect of the phase uncertainty, we ignore at this point the estimation error in the channel gains. In other words, the channel gains are perfectly known in this example. There is a significant improvement over PGS when only user 2 employs IGS (which corresponds to the case $\theta \geq \pi/2$), whereas the performance gain slightly increases when user 1 also employs IGS (which corresponds to the case $\theta < \pi/2$). Notice that the proposed strategy for $\theta \geq \pi/2$ is the same as the one derived for the 2-user IC, where only one user employs IGS. This result corroborates again that allowing only one user to use IGS is an effective way of improving the performance with imperfect CSI.

In Figs. 8.11 and 8.12, we average the results over 10^3 channel realizations. In order to provide a fair comparison, we depict the rate of user 2 for a fixed rate of user 1. In other words, we reduce the power of user 2 in the non-robust PGS and IGS approaches to achieve the same worst-case rate for user 1 as with the robust schemes. The rate of user 1 is fixed to $\alpha\%$ of its maximum worst-case achievable rate for each channel realization.

In Fig. 8.11, we show the rate of user 2 versus the variance of the estimation error for SNR=10dB, $\alpha = 40\%$ and $\alpha = 60\%$. Figure 8.11 shows a gap between PGS and IGS as the

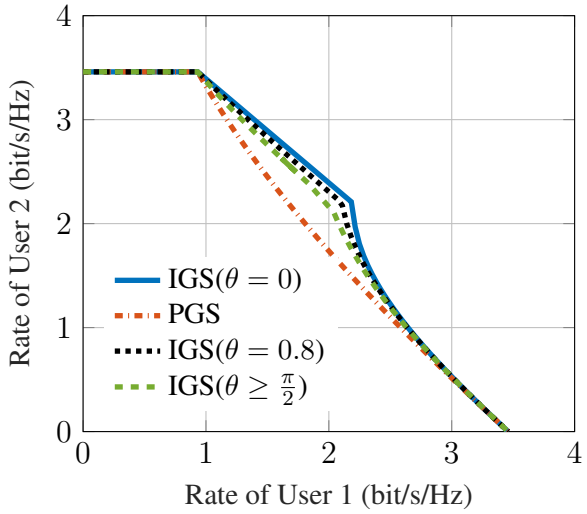

Figure 8.10: Achievable rate region boundaries of the Z-IC for different phase uncertainties and SNR=10dB.

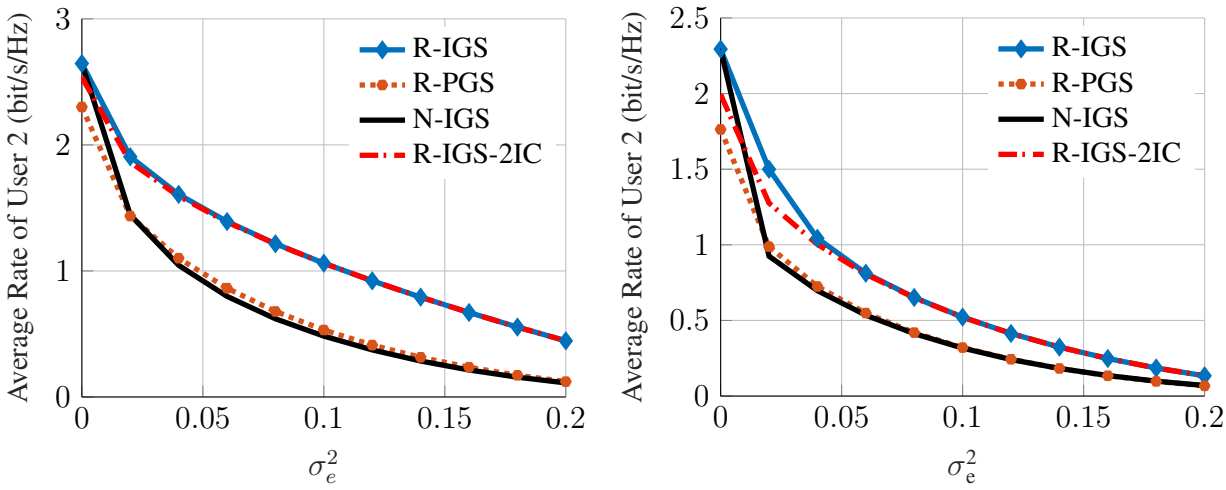

(a) $\alpha = 40\%$. **(b)** $\alpha = 60\%$.

Figure 8.11: Average rate of user 2 versus the variance of channel estimation error for SNR=10dB in the Z-IC.

channel estimation error increases. In Fig. 8.12, we represent the rate of user 2 versus SNR for $\alpha = 60\%$, $\sigma_e^2 = 0.01$, and $\sigma_e^2 = 0.03$. As can be observed, the robust IGS significantly outperforms the non-robust IGS as well as robust PGS. These figures show that the non-robust IGS does not provide any gain compared to the robust PGS in the Z-IC and may even perform worse than the robust PGS when the CSI is not accurate. However, if we design the parameters in a robust way, we can achieve a considerable gain even in presence of highly noisy CSI.

In these figures, we also compare our robust Z-IC design with our robust design for the 2-user IC, in which only one user (user 2) employs IGS. As can be observed, our robust Z-IC design performs better than our robust 2-user IC design for low channel estimation error; on the other hand, these algorithms perform similarly when the channel estimation error is high. This suggests that high-quality CSI permits both users to employ IGS in order to make the signal and

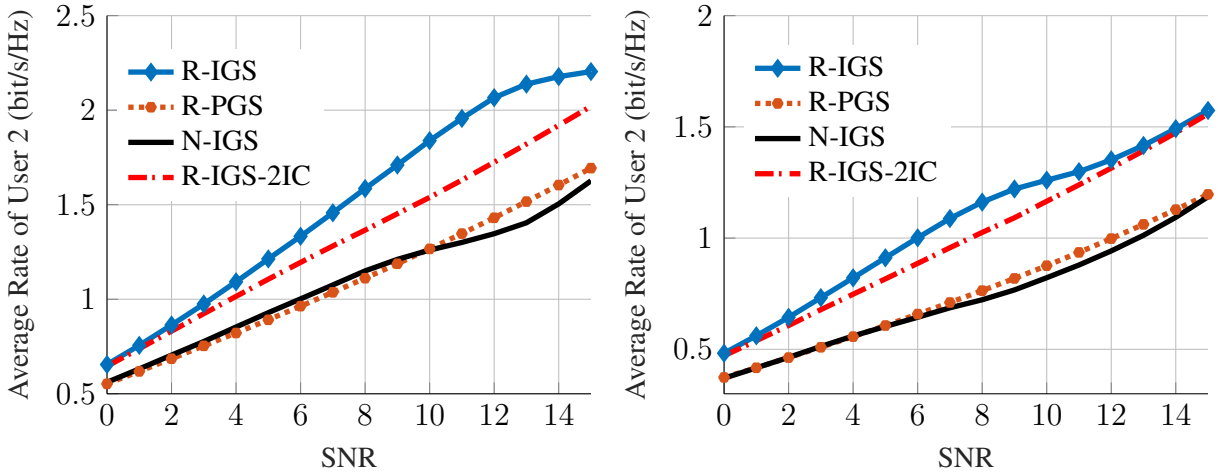

(a) $\sigma_e^2 = 0.01$.

(b) $\sigma_e^2 = 0.03$.

Figure 8.12: Average rate of user 2 versus SNR for $\alpha = 60\%$ in the Z-IC.

interference as close to orthogonal as possible. If the channel phase is not reliable ($\theta \geq \pi/2$), the robust design employs $\kappa_1 = 0$, which corresponds to the same robust design as for the 2-user IC. In this case, IGS still provides a significant performance increase (see Fig. 8.10), while keeping a CSI requirement similar to that of PGS.

8.2 IGS with Statistical CSIT: Ergodic rate analysis

In this section, we study the achievable ergodic rates of IGS schemes over the 2-user fading IC with TIN. We assume that the users have perfect and instantaneous CSI at the receiver side (CSIR) but they only have access to statistical CSIT. In other words, the transmitters know the parameters defining the Rayleigh fading distributions of the direct and interfering links. Note that the perfect instantaneous CSIR can be achieved using, for example, training sequences [97, 102] as indicated in Section 8.1. Under these assumptions, we derive closed-form expressions for the ergodic rates for both users for the case where at most one user employs IGS (denoted as PGS/IGS scheme). These rates can be attained using fixed-rate codebooks and no optimization is involved. The results of this section have been presented in [105].

8.2.1 System model

We consider a 2-user SISO IC, in which the users may employ IGS as described in Section 3.3.1 and Chapter 8. We assume that the users have access to only statistical CSIT and consider Rayleigh fading channels modeled as

$$h_{ii} \sim \mathcal{CN}(0, \sqrt{\text{snr}_i}, 0), \tag{8.38}$$

$$h_{\bar{i}i} \sim \mathcal{CN}(0, \sqrt{\text{inr}_i}, 0), \tag{8.39}$$

where snr_i and inr_i for $i, \bar{\imath} \in \{1, 2\}$ and $i \neq \bar{\imath}$ are, respectively, the average gain of the direct and interference links of receiver i. Additionally, the channel gains are Gamma distributed, that is,

$$|h_{ii}|^2 \sim \Gamma(1, 1/\text{snr}_i), \tag{8.40}$$
$$|h_{\bar{\imath}i}|^2 \sim \Gamma(1, 1/\text{inr}_i). \tag{8.41}$$

We assume that the transmitters know neither the fading states on which they transmit, nor the fading states of the interfering signal. On the other hand, we assume that the receivers have perfect knowledge of the channels. As indicated in Chapter 8, the instantaneous rate of user i in the 2-user IC is [102]

$$R_i = \frac{1}{2}\log_2\left(\frac{\left(\sigma^2 + \sum_{j=1}^{2} p_j|h_{ij}|^2\right)^2 - \left|\sum_{j=1}^{2} p_j\kappa_j|h_{ij}|^2 e^{j(2\measuredangle h_{ij}+\phi_j)}\right|^2}{(p_{\bar{\imath}}|h_{\bar{\imath}i}|^2 + \sigma^2)^2 - \left(p_{\bar{\imath}}\kappa_{\bar{\imath}}|h_{\bar{\imath}i}|^2\right)^2}\right), \tag{8.42}$$

where p_j, κ_j, and ϕ_j for $j = 1, 2$, are, respectively, the transmission power, circularity coefficient and phase of the complementary covariance of the signal transmitted by user j. Moreover, $\measuredangle h_{ji}$ for $i, j \in \{1, 2\}$ is the phase of the channel from the ith transmitter to the jth receiver. Hereafter, in this chapter, we consider $\sigma^2 = 1$ without loss of generality.

In this chapter, we consider the scenario, where at most one user may employ IGS. As indicated in Chapter 8, the instantaneous rates of users are independent of channels phases when at most one user may employ IGS. For notational simplicity in this section, we consider user 1 as the PGS user without loss of generality. Obviously, there is no difference between the users and either user can be the PGS user. The instantaneous rate of the PGS user is

$$R_1^{\text{PGS}} = \frac{1}{2}\log_2\left(1 + \frac{X_1}{1 + (1+\kappa)Y_1}\right) + \frac{1}{2}\log_2\left(1 + \frac{X_1}{1 + (1-\kappa)Y_1}\right), \tag{8.43}$$

where $X_i = p_i|h_{ii}|^2 \sim \Gamma(1, 1/(p_i\text{snr}_i))$ and $Y_i = p_{\bar{\imath}}|h_{\bar{\imath}i}|^2 \sim \Gamma(1, 1/(p_{\bar{\imath}}\text{inr}_i))$ are independent Gamma distributed random variables and κ is the circularity coefficient of the IGS user. The instantaneous rate of the IGS user is

$$R_2^{\text{IGS}} = \frac{1}{2}\log_2\left(1 + \frac{(1+\kappa)X_2}{1 + Y_2}\right) + \frac{1}{2}\log_2\left(1 + \frac{(1-\kappa)X_2}{1 + Y_2}\right). \tag{8.44}$$

A special case of this scheme is MIGS, that is, $\kappa = 1$. In this case, the rate of the PGS user simplifies to

$$R_1^{\text{PGS}} = \underbrace{\frac{1}{2}\log_2\left(1 + X_1\right)}_{\text{interference free}} + \underbrace{\frac{1}{2}\log_2\left(1 + \frac{X_1}{1 + 2Y_1}\right)}_{\text{with interference}}. \tag{8.45}$$

Since the MIGS user transmits only on one dimension, there is an interference-free dimension for the PGS user. We can exploit this interference-free dimension even without CSIT due to the fact that the receivers know the channels perfectly. Additionally, the rate of the MIGS user is

$$R_2^{\text{MIGS}} = \frac{1}{2}\log_2\left(1 + \frac{2X_2}{1 + Y_2}\right). \tag{8.46}$$

As we observe in (8.46), the PGS user causes less interference to the MIGS user because both

the PGS user and the noise divide their power between the two dimensions. The downside is that the MIGS user loses some rate because only one signal dimension is exploited for transmission. However, the MIGS user can compensate for this rate loss by increasing its transmission power if the power budget has not been fully used and the overall effect can be beneficial in terms of sum-rate. As indicated, the PGS user has an interference-free dimension, which ensures a minimum instantaneous achievable rate of

$$R_1^{\text{PGS}} > \frac{1}{2}\log_2\left(1+X_1\right). \tag{8.47}$$

8.2.2 Problem Statement

In this paper, we derive the achievable ergodic rates for the PGS/IGS scheme under fast fading channels (i.e., when the codewords span a large number of fading states). The achievable ergodic rate is defined as the expected achievable rate $\overline{R} = \mathbb{E}\{R\}$. In order to derive the achievable ergodic rate region, we employ the Pareto boundary, which is defined in Definition 4.1.

The whole achievable ergodic rate region can be obtained by varying the powers and complementary variances of the transmit symbols. In [20, 87] it is proven that the Pareto-optimal rates for the 2-user IC when interference is treated as noise are obtained when at least one user transmits at maximum power. This result, which was originally proved for the case where the transmitters have perfect CSIT, is also valid for our ergodic fast fading channel model.

8.2.3 PGS/IGS Scheme

In this section, our goal is to derive the achievable pair of ergodic rates $\left(\overline{R}_1^{\text{PGS}}, \overline{R}_2^{\text{IGS}}\right)$ obtained by taking the mathematical expectation of R_1^{PGS} in (8.43) and R_2^{IGS} in (8.44). We first present Lemma 8.3 in order to derive the ergodic rate of the users. Then we present the achievable ergodic rates in Theorem 8.4.

Lemma 8.3 *Let us define the random variable $Z = \frac{\beta X}{1+\alpha Y}$, where $\alpha \geq 0$ and $\beta \geq 0$ are given constants and $X \sim \Gamma(1, \frac{1}{snr})$ and $Y \sim \Gamma(1, \frac{1}{inr})$ are independent Gamma distributed random variables. The cumulative density function (CDF) of Z is*

$$F_Z(z) = 1 - \frac{e^{-\frac{z}{\beta snr}}}{1+\frac{\alpha inr}{\beta snr}z}. \tag{8.48}$$

The expectation of Z is

$$\mathbb{E}\{Z\} = \begin{cases} \beta snr & \text{if} \quad \alpha = 0, \\ \left(\frac{\beta snr}{\alpha inr}\right) e^{\frac{1}{\beta snr}} E_1\left(\frac{1}{\beta snr}\right) & \text{if} \quad \alpha > 0. \end{cases} \tag{8.49}$$

Additionally, the expectation of $R = \log(1+Z)$ *is*

$$f(\beta snr, \alpha inr) \triangleq \overline{R} = \begin{cases} e^{\frac{1}{\beta snr}} E_1\left(\frac{1}{\beta snr}\right) & \text{if} \quad \alpha = 0, \\ \frac{\beta snr\left(e^{\frac{1}{\beta snr}} E_1\left(\frac{1}{\beta snr}\right) - e^{\frac{1}{\alpha inr}} E_1\left(\frac{1}{\alpha inr}\right)\right)}{\beta snr - \alpha inr}, & \text{if} \quad \beta snr \neq \alpha inr > 0 \\ e^{\frac{1}{\beta snr}} E_2\left(\frac{1}{\beta snr}\right), & \text{if} \quad \beta snr = \alpha inr > 0 \end{cases} \tag{8.50}$$

where the $E_n(x)$ *function is defined by the integral (for* $n \geq 1$ *and* $x > 0$*)*

$$E_n(x) = \int_1^\infty \frac{e^{-xt}}{t^n} dt. \tag{8.51}$$

Proof of Lemma 8.3. Please refer to Section 8.6. □

Note that when $\beta = 0$, the variable Z defined in Lemma 8.3 is $Z = 0$. To include this case, we define $f(0, \alpha \text{inr}) \triangleq 0$. Moreover, notice that $E_n(x)$ can be written in terms of the upper incomplete gamma function as $E_n(x) = x^{n-1}\Gamma(1-n, x)$, where

$$\Gamma(s, x) = \int_x^\infty t^{s-1} e^{-t}. \tag{8.52}$$

It is worth mentioning that $E_1(x) = \Gamma(0, x)$ is the exponential integral. These functions can be computed using standard software packages.

Theorem 8.4 *The ergodic rates of the PGS and the IGS users are, respectively,*

$$\bar{R}_1^{PGS} = f(p_1 snr_1, (1+\kappa) p_2 inr_1) + f(p_1 snr_1, (1-\kappa) p_2 inr_1), \tag{8.53}$$

$$\bar{R}_2^{IGS} = f((1+\kappa) p_2 snr_2, p_1 inr_2) + f((1-\kappa) p_2 snr_2, p_1 inr_2), \tag{8.54}$$

where $f(x, y)$ *is given by* (8.50)*.*

Proof of Theorem 8.4. The ergodic rate of users are given by taking expectations of (8.43) and (8.44). Hence, by applying the results of Lemma 8.3 and substituting the corresponding α and β, we can prove the theorem. □

Remark 8.2 *The ergodic rate of the PGS user is strictly increasing in* κ*, while the ergodic rate of the IGS user is strictly decreasing in* κ*. This is due to the fact that the instantaneous rate of the PGS (IGS) user is strictly increasing (decreasing) in* κ*.*

We can derive the achievable ergodic rate region by varying the transmission power of the two users. As indicated in Section 8.2.2, every point on the boundary of the achievable ergodic rate region is obtained when at least one user transmits with maximum power [20, 87]. Thus, the whole Pareto optimal region for the PGS/IGS scheme can be derived as

$$\begin{aligned} \mathcal{S}^{IGS} = & \bigcup_{\substack{0 \leq \kappa_2 \leq 1 \\ 0 \leq p_2 \leq P_2}} \left(\overline{R}_1^{\text{PGS}}(P_1, p_2, \kappa_2), \overline{R}_2^{\text{IGS}}(P_1, p_2, \kappa_2)\right) \bigcup_{\substack{0 \leq \kappa_2 \leq 1 \\ 0 \leq p_1 \leq P_1}} \left(\overline{R}_1^{\text{PGS}}(p_1, P_2, \kappa_2), \overline{R}_2^{\text{IGS}}(p_1, P_2, \kappa_2)\right) \\ & \bigcup_{\substack{0 \leq \kappa_1 \leq 1 \\ 0 \leq p_2 \leq P_2}} \left(\overline{R}_1^{\text{IGS}}(P_1, p_2, \kappa_1), \overline{R}_2^{\text{PGS}}(P_1, p_2, \kappa_1)\right) \bigcup_{\substack{0 \leq \kappa_1 \leq 1 \\ 0 \leq p_1 \leq P_1}} \left(\overline{R}_1^{\text{IGS}}(p_1, P_2, \kappa_1), \overline{R}_2^{\text{PGS}}(p_1, P_2, \kappa_1)\right). \end{aligned} \tag{8.55}$$

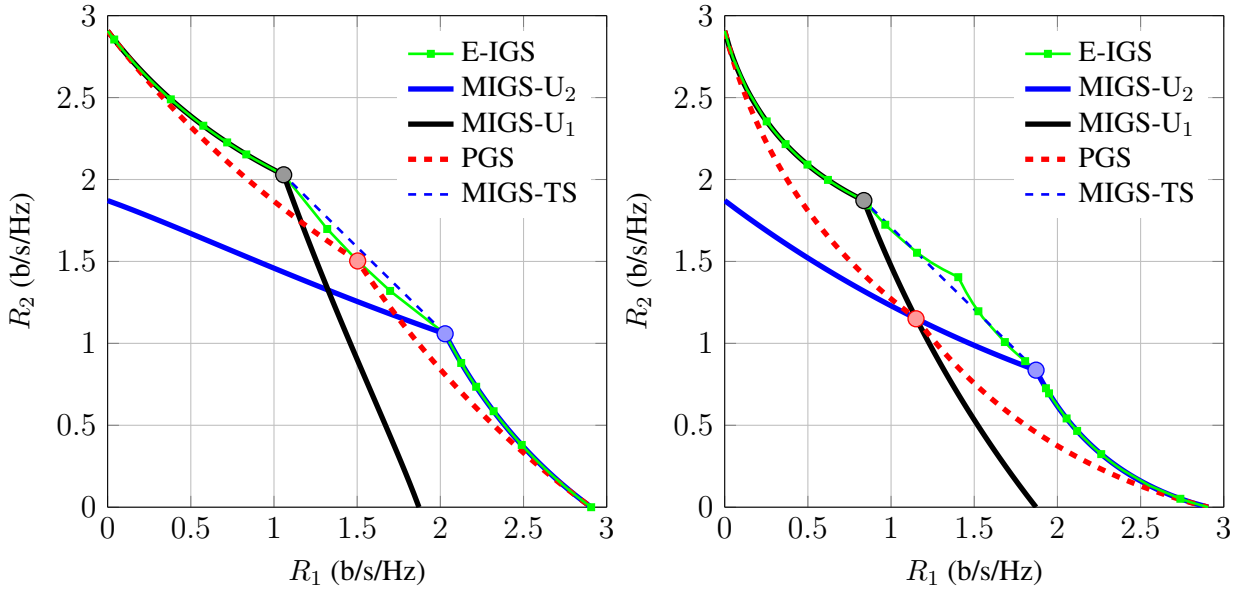

(a) inr= 7 dB. **(b)** inr= 10 dB.

Figure 8.13: PGS and IGS rate regions for a symmetric 2-user IC with snr= 10 dB.

Note that the achievable ergodic rate region in (8.55) is the union of the achievable ergodic rate region of two transmission strategies:

1. User 1 employs PGS, while user 2 may employ IGS,
2. User 2 employs PGS, while user 1 may employ IGS.

8.2.4 Numerical Examples

We consider a 2-user fading IC where the channel coefficients of the direct links are drawn from $h_{ii} \sim \mathcal{CN}(0, \sqrt{\text{snr}}, 0)$ and the channel coefficients of the interfering links are drawn from $h_{i\bar{i}} \sim \mathcal{CN}(0, \sqrt{\text{inr}}, 0)$. The four channel coefficients are independent random variables. In this way, the performance of the proposed schemes can be analyzed in terms of the average snr and inr, which are the same at both receivers. Moreover, we assume $P_1 = P_2 = 1$ and $\sigma^2 = 1$. Indeed, we reflect the effect of the transmission power as well as the noise power by the gain of the direct and interference links, that is, snr and inr. Since the fading direct and interference channels are symmetric, the two users send information at the same rate.

When at most one user employs IGS, the instantaneous rates are independent of the phases of the channels. Additionally, it allows us to find closed-form expressions of the ergodic rates. However, the question remains: *How far is the PGS/IGS scheme from the Pareto-optimal design of a scheme that would allow both users to use IGS on the 2-user IC?*

To answer the question, we compare the performance of our scheme with an exhaustive search over all design parameters $(\kappa_1, \kappa_2, p_1, p_2)$ when both users may employ IGS. Unfortunately, to the best of our knowledge, there is no closed-form solution for the ergodic rates when both users employ IGS. Thus, we estimate the ergodic rate of the 2-user IC when both users employ IGS by Monte Carlo simulations. That is, we generate a large number (10^5) of channels and compute the instantaneous rate achieved by the transmission parameters for each channel

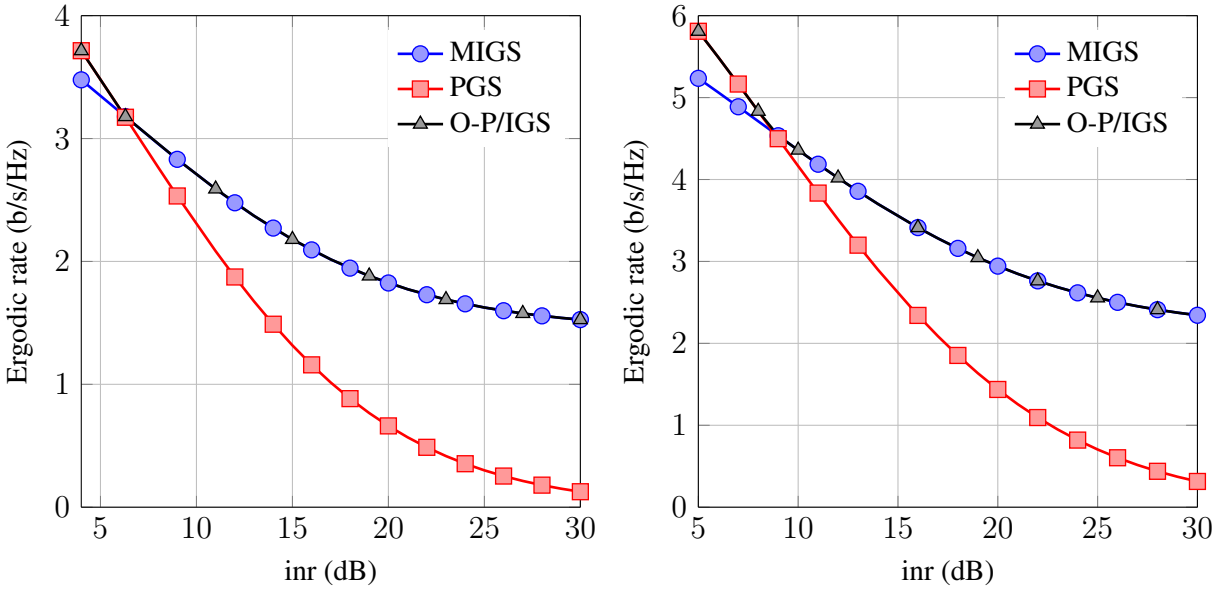

(a) snr= 10 dB. **(b)** snr= 15 dB.

Figure 8.14: Sum ergodic rate of the schemes as a function of inr.

realization. Finally, we estimate the ergodic rate by averaging the instantaneous rates. Once the ergodic rate pairs have been estimated for many different transmission parameters, the Pareto boundary for the IGS/IGS scheme can readily be estimated.

The considered schemes are denoted as follows.

- **PGS**: The PGS scheme with $\kappa_1 = \kappa_2 = 0$.
- **MIGS**: The PGS/MIGS scheme with $\kappa = 1$.
- **E-IGS**: The exhaustive search for IGS when both users may employ IGS.
- **O-P/IGS**: The PGS/IGS scheme with the optimal κ.
- **MIGS-U**$_i$: The PGS/MIGS scheme when the MIGS user is user i.
- **MIGS-TS**: The PGS/MIGS scheme with time sharing over the points with maximum power for both users.

In Figure 8.13, we depict the achievable ergodic rate region of our proposed schemes for snr $= 10$ dB. As can be observed, the union of the ergodic rate regions achievable by the PGS and MIGS schemes is very close to the optimal achievable ergodic rate region. If we employ time sharing over the points with maximum power for both users in the union of the PGS and PGS/MIGS schemes (indicated by circles in Figure 8.13), we attain almost the entire Pareto-optimal region of the 2-user IC when both users are allowed to employ IGS.

In Figure 8.14, we show the sum-ergodic rate as a function of the inrwhen both users transmit at maximum power. Note that, in this case, the sum-ergodic rate can be achieved by red points for the PGS scheme and by either black or blue points for the PGS/MIGS scheme in Figure 8.13. As can be observed in Figure 8.14, the PGS/MIGS scheme significantly outperforms the PGS scheme when the interference level is high. Interestingly, the sum-rate can be achieved by

either $\kappa = 0$ or $\kappa = 1$ and no optimization over κ is required for maximizing the sum-rate. Note that, for symmetric channels, both users can achieve the same ergodic rate in the PGS/MIGS scheme by letting each user be the MIGS user 50% of the time. Hence, the MIGS scheme with switching between proper and maximally improper users can substantially improve the performance of the 2-user IC. This scheme requires as little cooperation as possible between users and further it requires no optimization or power control at the transmitter side.

8.3 Summary

In this chapter, we investigated the performance of IGS in the 2-user SISO IC and Z-IC with realistic assumptions regarding CSIT. To this end, we first studied the robustness of IGS against imperfect CSIT in the single-antenna 2-user IC and Z-IC. We proposed robust designs for the 2-user IC and Z-IC, which have closed-form solutions for the transmission parameters. We derived closed-form conditions when IGS outperforms PGS for the 2-user IC and Z-IC in the presence of imperfect CSI. We showed through analytical studies that even if there is no reliable phase information, a robust IGS design can outperform a robust PGS design. In this case, one user may employ IGS, while the other employs PGS. We evaluated our analytical studies by simulations and showed that IGS permits a significant performance increase for the 2-user IC and Z-IC. Our numerical results showed that IGS is even more robust to imperfect CSI than PGS provided that the transmission parameters are properly designed, and thus IGS still pays off in the context of imperfect CSI.

In this chapter, we, furthermore, studied the ergodic rate of a PGS/IGS scheme in a 2-user Rayleigh IC treating interference as noise. Under the assumption that the users have perfect CSIR but they have access only to statistical CSIT, we derived closed-form expressions for the ergodic rates and characterized the boundary of the achievable ergodic rate region. We also proposed a practical IGS scheme which does not require any optimization and power control at the transmitter side. In this scheme, both users transmit with maximum power. One user employs MIGS while the other user employs PGS. By numerical examples, we showed that IGS can substantially increase the sum-rate and enlarge the ergodic rate region of the 2-user Rayleigh SISO-IC under strong interference.

8.4 Proof of Theorem 8.2

Here, we assume that user 2 employs IGS and transmits with maximum power without loss of generality. In this strategy, the worst-case rates of users are given by

$$R_1^w(p_1,\kappa_2) = \frac{1}{2}\log_2\left(1+\frac{p_1^2|\tilde{h}_{11}|^4+2p_1|\tilde{h}_{11}|^2(P_2|\tilde{h}_{12}|^2+\sigma^2)}{\sigma^4+2\sigma^2P_2|\tilde{h}_{12}|^2+(1-\kappa_2^2)P_2^2|\tilde{h}_{12}|^4}\right), \tag{8.56a}$$

$$R_2^w(p_1,\kappa_2) = \frac{1}{2}\log_2\left(\frac{P_2^2|\tilde{h}_{22}|^4(1-\kappa_2^2)}{(\sigma^2+p_1|\tilde{h}_{21}|^2)^2}+\frac{2P_2|\tilde{h}_{22}|^2}{\sigma^2+p_1|\tilde{h}_{21}|^2}+1\right). \tag{8.56b}$$

If $R_2^w(P_1,1) > \alpha R_{2,\max}^w$, maximally improper for user 2 and maximum power transmission for user 1, i.e., $p_1 = P_1$ and $\kappa_2 = 1$, is the solution of (8.6) since it maximizes the rate of user 1. Thus, in the following, we consider the case $R_2^w(P_1,1) < \alpha R_{2,\max}^w$. The constraint

$R_2^w(p_1, \kappa_2) = \alpha R_{2,\max}^w$ is equivalent to

$$1-\kappa_2^2 = \frac{(\sigma^2 + p_1|\tilde{h}_{12}|^2)^2}{P_2^2|\tilde{h}_{22}|^4}\gamma_2(2\alpha) - 2\frac{\sigma^2+p_1|\tilde{h}_{12}|^2}{P_2|\tilde{h}_{22}|^2}. \tag{8.57}$$

It can be easily verified that (8.57) results in (8.15). Moreover, if we consider (8.57) as a quadratic function in p_1 and take its positive root, we obtain (8.14). Additionally, plugging (8.57) into (8.56a) yields (8.16). Through (8.14), it is clear that p_1 is decreasing in κ_2. Thus, IGS can improve the performance of the system if and only if (8.16) is decreasing in p_1. This means that the argument of the logarithm function in (8.16) must be decreasing in p_1. Note that (8.16) holds if and only if $R_2^w(p_1, \kappa_2) = \alpha R_{2,\max}^w$, which results in $p_1 \in [\mathcal{P}(1), \mathcal{P}(0)]$. As a result, if $P_1 < \mathcal{P}(1)$, (8.16) does not hold, and maximally IGS is optimal for user 2 as indicated before. This case is mentioned as condition 1 of Theorem 8.2.

In the following, we derive the other conditions. Let us define $\bar{R}_1(p_1)$ as

$$\bar{R}_1(p_1) \triangleq \frac{\zeta_1 p_1^2 + \beta_1 p_1}{\zeta_2 p_1^2 + \beta_2 p_1 + \tau}, \tag{8.58}$$

where ζ_1, β_1, ζ_2, β_2, and τ are defined as in Theorem 1. The derivative of $\bar{R}_1(p_1)$ with respect to p_1 is

$$\frac{\partial \bar{R}_1(p_1)}{\partial p_1} = \frac{(2\zeta_1 p_1 + \beta_1)(\zeta_2 p_1^2 + \beta_2 p_1 + \tau) - (\zeta_1 p_1^2 + \beta_1 p_1)(2\zeta_2 p_1 + \beta_2)}{(\zeta_2 p_1^2 + \beta_2 p_1 + \tau)^2}, \tag{8.59a}$$

$$= \frac{(\zeta_1\beta_2 - \zeta_2\beta_1)p_1^2 + 2\zeta_1\tau p_1 + \beta_1\tau}{(\zeta_2 p_1^2 + \beta_2 p_1 + \tau)^2}. \tag{8.59b}$$

Note that ζ_1, ζ_2 and β_1 are always positive. Additionally, the denominator of $\frac{\partial \bar{R}_1(p_1)}{\partial p_1}$ is positive. Thus, the behavior of $\bar{R}_1(p_1)$ with respect to p_1 depends only on the sign of the numerator of $\frac{\partial \bar{R}_1(p_1)}{\partial p_1}$, which we denote as $\bar{r}_1(p_1)$. The sign of $\bar{r}_1(p_1)$ is related to $\zeta_1\beta_2 - \zeta_2\beta_1$ and τ as these terms can be either positive or negative. If $\zeta_1\beta_2 - \zeta_2\beta_1$ and τ have the same sign, $\bar{R}_1(p_1)$ is monotone in p_1. Otherwise, there is a positive extreme point, which is equal to the positive root of $\bar{r}_1(p_1)$ and given by $x_1^{(\star)}$ in (8.12) if $(\zeta_1\beta_2 - \zeta_2\beta_1) < 0$, and $x_2^{(\star)}$ in (8.13) otherwise. Thus, $\bar{R}_1(p_1)$ is strictly decreasing in p_1 if $\zeta_1\beta_2 - \zeta_2\beta_1 < 0$ and $\tau < 0$. Hence, the rate of user 1 is maximized if user 1 transmits with $p_1 = \mathcal{P}(1)$, and user 2 employs maximally IGS, which results in condition 2 of Theorem 8.2. If $\zeta_1\beta_2 - \zeta_2\beta_1 > 0$ and $\tau > 0$, $\bar{R}_1(p_1)$ is strictly increasing in p_1, and PGS is the optimal solution for both users.

Now we consider the case that $\bar{R}_1(p_1)$ is not necessarily monotone in $p_1 \in [\mathcal{P}(1), \mathcal{P}(0)]$, i.e., when $(\zeta_1\beta_2 - \zeta_2\beta_1)\tau < 0$. Figure 8.15 shows the behavior of $\bar{r}_1(p_1)$ when $(\zeta_1\beta_2 - \zeta_2\beta_1)\tau < 0$. Note that the extreme point can be outside of $[\mathcal{P}(1), \mathcal{P}(0)]$. In other words, there is at most one extreme point in $p_1 \in [\mathcal{P}(1), \mathcal{P}(0)]$. Since $\bar{r}_1(p_1)$ is a quadratic function of p_1, $\bar{r}_1(p_1)$ is either convex or concave. Let us first consider the concave case, i.e., $\zeta_1\beta_2 - \zeta_2\beta_1 < 0$ and $\tau > 0$. In this case, if $\mathcal{P}(0) < x_1^{(\star)}$, $\bar{R}_1(p_1)$ is strictly increasing in $p_1 \in [\mathcal{P}(1), \mathcal{P}(0)]$, and thus, $p_1 = \mathcal{P}(0)$ and PGS is optimal for both users. Therefore, we consider $\mathcal{P}(0) > x_1^{(\star)}$, which implies $\frac{\partial R_1^w(p_1)}{\partial p_1}|_{p_1=\mathcal{P}(0)} < 0$. In this case, $\bar{R}_1(p_1)$ is maximized at $p_1 = x_1^{(\star)}$ if $x_1^{(\star)} \in [\mathcal{P}(1), \mathcal{P}(0)]$, and at $p_1 = \mathcal{P}(1)$ otherwise, which results in condition 3 of Theorem 8.2.

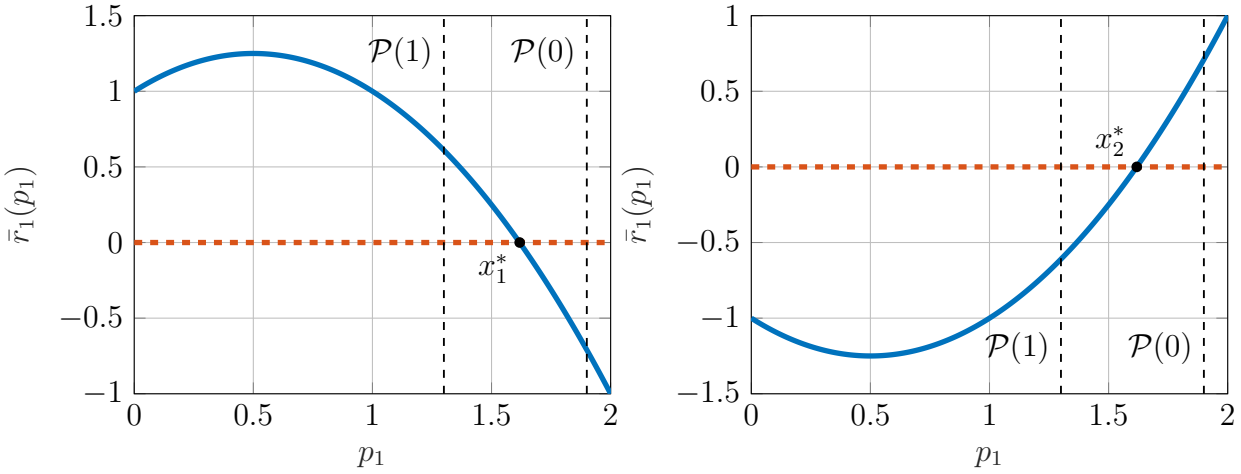

(a) $\zeta_1\beta_2 - \zeta_2\beta_1 = -\zeta_1\tau p_1 = -\beta_1\tau = -1$. **(b)** $\zeta_1\beta_2 - \zeta_2\beta_1 = -\zeta_1\tau p_1 = -\beta_1\tau = 1$.

Figure 8.15: Function $\bar{r}_1(p_1)$ versus p_1.

Now we consider the case that $\bar{r}_1(p_1)$ is convex, i.e., $\zeta_1\beta_2 - \zeta_2\beta_1 > 0$ and $\tau < 0$. In this case, $\bar{R}_1(p_1)$ is strictly increasing in $p_1 \in [\mathcal{P}(1), \mathcal{P}(0)]$ if $\mathcal{P}(1) > x_2^{(\star)}$, where $x_2^{(\star)}$ is given by (8.12), which results in PGS being optimal. Moreover, $\bar{R}_1(p_1)$ is strictly decreasing in $p_1 \in [\mathcal{P}(1), \mathcal{P}(0)]$ if $\mathcal{P}(0) < x_2^{(\star)}$, and thus, $p_1 = \mathcal{P}(1)$ and maximally IGS is optimal for user 2 in this case. If $x_2^{(\star)} \in [\mathcal{P}(1), \mathcal{P}(0)]$, $R_1(p_1)$ is strictly increasing in $p_1 \in [x_2^{(\star)}, \mathcal{P}(0)]$ and strictly decreasing in $p_1 \in [\mathcal{P}(1), x_2^{(\star)}]$, as illustrated in Fig. 8.15b. Thus, IGS is beneficial in this case only if $R_1^w(\mathcal{P}(1)) > R_1^w(\mathcal{P}(0))$, and maximally IGS is then the optimal strategy, which results in condition 4 of Theorem 8.2.

8.5 Proof of Theorem 8.3

We first derive the condition that results in $\frac{\partial R_2^w(\kappa_2,\theta)}{\partial \kappa_2^2}\Big|_{\kappa_2=0} > 0$. Then, we prove that if $\frac{\partial R_2^w(\kappa_2,\theta)}{\partial \kappa_2^2}\Big|_{\kappa_2=0} > 0$ holds, we have $\frac{\partial R_2^w(\kappa_2,\theta)}{\partial \kappa_2^2} > 0$ for $\kappa_2 > 0$. The term $\frac{\partial R_2^w(\kappa_2,\theta)}{\partial \kappa_2^2} > 0$ is equivalent to

$$2\frac{\partial q(\kappa_2,\theta)}{\partial \kappa_2^2}\left[|\tilde{h}_{22}|^2 q(\kappa_2,\theta)\sigma^{-2}(1-\kappa_2^2)+1\right] > q^2(\kappa_2,\theta)|\tilde{h}_{22}|^2\sigma^{-2}. \tag{8.60}$$

Now we first consider (8.30) for $\kappa_1 < 1$, and then prove that if $\frac{\partial R_2^w(\kappa_2,\theta)}{\partial \kappa_2^2}|_{\kappa_2=0} > 0$, the rate of user 2 remains strictly increasing in κ_2 when $q(\kappa_2,\theta)$ is derived based on the expression in (8.30) for $\kappa_1 = 1$. We can obtain $\frac{\partial q(\kappa_2,\theta)}{\partial \kappa_2^2}$ by taking the derivative of (8.30) with respect to κ_2^2 for $\kappa_1 < 1$. That is

$$2\frac{\partial q(\kappa_2,\theta)}{\partial \kappa_2^2} = \frac{q^2(\kappa_2,\theta)|\tilde{h}_{12}|^2(\gamma_1(2\alpha)+\cos^2\theta)}{q(\kappa_2,\theta)|\tilde{h}_{12}|^2\left[(\gamma_1(2\alpha)+1)(1-\kappa_2^2)-1+\kappa_2^2\sin^2\theta\right]+\sigma^2\gamma_1(2\alpha)-P_1|\tilde{h}_{11}|^2}. \tag{8.61}$$

By replacing (8.61) in (8.60), we have

$$\frac{|\tilde{h}_{12}|^2(\gamma_1(2\alpha)+\cos^2\theta)\left[|\tilde{h}_{22}|^2 q(\kappa_2,\theta)\sigma^{-2}(1-\kappa_2^2)+1\right]}{q(\kappa_2,\theta)|\tilde{h}_{12}|^2\left[(\gamma_1(2\alpha)+1)(1-\kappa_2^2)-1+\kappa_2^2\sin^2\theta\right]+\sigma^2\gamma_1(2\alpha)-P_1|\tilde{h}_{11}|^2} > |\tilde{h}_{22}|^2\sigma^{-2}. \tag{8.62}$$

Equation (8.62) is simplified to

$$\frac{|\tilde{h}_{21}|^2}{|\tilde{h}_{22}|^2} > \frac{\sigma^2\gamma_1(2\alpha)-P_1|\tilde{h}_{11}|^2-q(\kappa_2,\theta)|\tilde{h}_{21}|^2\cos^2\theta}{\sigma^2(\gamma(2\alpha)+\cos^2\theta)}. \tag{8.63}$$

From (8.29), it can be seen that $q(\kappa_2,\theta)|\tilde{h}_{21}|^2$ is independent of $\frac{|\tilde{h}_{21}|^2}{|\tilde{h}_{22}|^2}$, and $q_2(\kappa_2=0,\theta)|\tilde{h}_{21}|^2 = \frac{P_1}{\gamma_1(\alpha)}-\sigma^2$ which results in (8.33). Moreover, $q(\kappa_2,\theta)$ is a strictly increasing function of κ_2, which implies that the inequality holds when $\kappa_2 > 0$. Now we prove that if (8.63) holds, $\frac{\partial R_2^w(\kappa_2,\theta)}{\partial\kappa_2^2} > 0$ for the case $\kappa_1 = 1$. In this case, we have

$$2\frac{\partial q(\kappa_2,\theta)}{\partial\kappa_2^2} = \frac{q(\kappa_2,\theta)|\tilde{h}_{21}|^2\gamma_1(2\alpha)-\frac{q(\kappa_2,\theta)P_1|\tilde{h}_{11}|^2\cos\theta}{\kappa_2}}{q(\kappa_2,\theta)|\tilde{h}_{21}|^2\gamma_1(2\alpha)(1-\kappa_2^2)+\sigma^2\gamma_1(2\alpha)-P_1|\tilde{h}_{11}|^2(1+\kappa_2\cos\theta)}. \tag{8.64}$$

Thus, $\frac{\partial R_2^w(\kappa_2,\theta)}{\partial\kappa_2^2}\Big|_{\kappa_2=0} > 0$ is equivalent to

$$\frac{[q(\kappa_2,\theta)|\tilde{h}_{21}|^2\gamma_1(2\alpha)-\frac{P_1|\tilde{h}_{11}|^2\cos\theta}{\kappa_2}]\left[|\tilde{h}_{22}|^2 q(\kappa_2,\theta)(1-\kappa_2^2)+\sigma^2\right]}{q(\kappa_2,\theta)|\tilde{h}_{21}|^2\gamma_1(2\alpha)(1-\kappa_2^2)+\sigma^2\gamma_1(2\alpha)-P_1|\tilde{h}_{11}|^2(1+\kappa_2\cos\theta)} > q(\kappa_2,\theta)|\tilde{h}_{22}|^2. \tag{8.65}$$

The expression in (8.65) is simplified to

$$q(\kappa_2,\theta)\left[(|\tilde{h}_{21}|^2-|\tilde{h}_{22}|^2)\gamma_1(2\alpha)\sigma^2+P_1|\tilde{h}_{11}|^2|\tilde{h}_{22}|^2\left(1+2\kappa_2\cos\theta-\frac{\cos\theta}{\kappa_2}\right)\right]-\sigma^2P_1|\tilde{h}_{11}|^2\frac{\cos\theta}{\kappa_2} > 0. \tag{8.66}$$

It is easy to see that the left-hand side of (8.66) is strictly increasing in κ_2 as we are considering $0 \le \theta \le \frac{\pi}{2}$. Therefore, if (8.66) holds for $\kappa_2 = \overline{\kappa}$, it will hold as well for $\kappa_2 > \overline{\kappa}$. We now show that such a $\overline{\kappa}$ exists. We have proved that, if (8.63) holds, we have $\frac{\partial R_2^w(\kappa_2,\theta)}{\partial\kappa_2^2} > 0$ as long as $q(\kappa_2,\theta)$ is derived from the first equation in (8.30). This implies that $\frac{\partial R_2^w(\kappa_2,\theta)}{\partial\kappa_2^2} > 0$ for $\kappa_2 = \overline{\kappa} = \frac{P_1|\tilde{h}_{11}|^2}{q(\kappa_2,\theta)|\tilde{h}_{21}|^2\cos\theta}$, where $\overline{\kappa}$ is the smallest value of κ_2 such that $\kappa_1 = 1$ (see (8.27)). Hence, (8.62) and (8.63) are equivalent for $\kappa_2 = \overline{\kappa}$, which results in (8.66) holding as well for $\kappa_2 = \overline{\kappa}$. As a result, the rate of user 2 is strictly increasing in κ_2 if $\frac{\partial R_2^w(\kappa_2,\theta)}{\partial\kappa_2^2} > 0$ holds for $\kappa_2 = 0$. Thus, we choose the maximum possible κ_2 when improper signaling is optimal, which results in (8.34).

8.6 Proof of Lemma 8.3

By definition, the CDF of Z is

$$\begin{aligned} F_Z(z) &= Pr(Z \leq z) = 1 - Pr(\beta X \geq z(1+\alpha Y)) \\ &= \int_0^\infty \frac{e^{-y/\text{inr}}}{\text{inr}} \int_{\frac{z(1+\alpha y)}{\beta}}^\infty \frac{e^{-x/\text{snr}}}{\text{snr}} dxdy = 1 - \frac{e^{-\frac{z}{\beta\text{snr}}}}{1+\frac{\alpha\text{inr}}{\beta\text{snr}}z}. \end{aligned} \tag{8.67}$$

Furthermore, since Z is a positive random variable, its expectation can be obtained as

$$\mathbb{E}\{Z\} = \int_0^\infty (1 - F_Z(z))\, dz = \begin{cases} \beta\text{snr} & \text{if} \quad \alpha = 0, \\ \left(\frac{\beta\text{snr}}{\alpha\text{inr}}\right) e^{\frac{1}{\beta\text{snr}}} E_1\left(\frac{1}{\beta\text{snr}}\right) & \text{if} \quad \alpha > 0. \end{cases} \tag{8.68}$$

It can be easily verified that $\bar{R} = e^{\frac{1}{\beta\text{snr}}} E_1\left(\frac{1}{\beta\text{snr}}\right)$ when $\alpha = 0$. Hence, in the following, we consider $\alpha > 0$. In this case, the CDF of $R = \log(1+Z)$ is

$$F_R(r) = 1 - e^{\frac{1}{\beta\text{snr}}} e^{-\frac{e^r}{\beta\text{snr}}} \left(\frac{1}{1 - \frac{\alpha\text{inr}}{\beta\text{snr}} + \frac{\alpha\text{inr}}{\beta\text{snr}} e^r}\right), \quad r \geq 0. \tag{8.69}$$

Since R is a positive random variable, its expectation may be found from its CDF as

$$\mathbb{E}\{R\} = \int_0^\infty (1 - F_R(r))\, dr. \tag{8.70}$$

Making the change of variables $e^r = 1 + z$ in (8.70), $\overline{R}$ is given by the integral

$$\mathbb{E}\{R\} = \int_0^\infty \frac{e^{-\frac{z}{\beta\text{snr}}}}{1 + \left(\frac{\alpha\text{inr}}{\beta\text{snr}} + 1\right) z + \left(\frac{\alpha\text{inr}}{\beta\text{snr}}\right) z^2} dz. \tag{8.71}$$

If $\beta\text{snr} \neq \alpha\text{inr}$, the integrand in (8.71) has two simple poles at $z = -1$ and $z = -\beta\text{snr}/\alpha\text{inr}$. Decomposing the integrand into simple fractions we arrive, after some change of variables, at

$$\overline{R} = \left(\frac{\beta\text{snr}}{\beta\text{snr} - \alpha\text{inr}}\right) \left[e^{\frac{1}{\beta\text{snr}}} E_1\left(\frac{1}{\beta\text{snr}}\right) - e^{\frac{1}{\alpha\text{inr}}} E_1\left(\frac{1}{\alpha\text{inr}}\right) \right]. \tag{8.72}$$

On the other hand, if $\beta\text{snr} = \alpha\text{inr}$, the integrand in (8.71) has a double pole at $z = -1$. Then, (8.71) becomes

$$\overline{R} = \int_0^\infty \frac{e^{-\frac{z}{\beta\text{snr}}}}{1+z^2} dz = e^{\frac{1}{\beta\text{snr}}} \int_{\frac{1}{\beta\text{snr}}}^\infty \frac{e^{-t}}{t^2} dt = e^{\frac{1}{\beta\text{snr}}} E_2\left(\frac{1}{\beta\text{snr}}\right), \tag{8.73}$$

thus proving Lemma 8.3.

9 Conclusion

9.1 Summary of contributions

In this dissertation, we proposed some IGS schemes for various interference-limited systems with practical assumptions regarding CSIT and hardware. We aimed at improving the spectral and energy efficiency of some interference-limited systems by improper signaling. We considered both single-antenna and multiple-antenna systems when interference is treated as noise. Our proposed schemes in multiple-antenna systems could be also applied to single-antenna systems. However, in single-antenna systems, we were able to propose computationally less expensive algorithms. In the following subsections, we summarize our contributions.

9.1.1 Multiple-antenna systems

We studied the performance of IGS in interference-limited multiple-antenna systems with imperfect hardware by considering two main performance metrics, i.e., achievable rate and EE. To this end, we considered achievable rate region, weighted-sum-rate maximization, energy-efficiency region and global energy-efficiency maximization problems as well as the rate maximization of the SU in a MIMO OFDM UCR. In order to solve these non-convex optimization problems, we employed a suboptimal optimization framework for interference-limited multiple-antenna systems, which was based on MM. This optimization framework obtains a stationary point of every optimization problem in which either the objective function and/or the constraints are linear functions of the achievable rates. Our numerical results showed that IGS can outperform PGS from both achievable rate and EE points of view.

Our contribution for the multiple-antenna systems can be summarized as follows:

- We observed that the benefits of IGS as an interference-management technique increase with the number of users. This is due to the fact that the interference level increases with the number of users, and the higher the interference level is, the more need for managing the interference, and consequently, the more improvements by IGS.

- We also observed that the benefits of employing IGS decrease with the number of antennas. The reason is that, interference can be managed easier when there are more resources. This is in line with the results in Chapter 5, in which it was shown that IGS cannot provide considerable benefits in OFDM UCR systems due to existence of parallel channels. Moreover, in [52], it was shown that the benefits of IGS disappear with time sharing when the average power consumption is constrained, instead of the *instantaneous power*, which allows a more flexible power allocation. To sum up, the benefits of IGS decrease or even vanish by increasing the number of resources either by increasing the number of antennas or number of time slots, by time sharing, and/or the number of parallel channels by OFDM.

- Our results showed that IGS can improve the performance of the MIMO K-user IC with HWI from both achievable rate and EE point of view. Moreover, we observed that IGS provides more benefits from achievable rate point of view than from EE perspective.
- In the presence of I/Q imbalance, we also observed that the benefit of employing IGS increases with the imbalance level for a fixed number of antennas. The reason is that, the more improper the noise is, the more benefits by IGS.

9.1.2 Single-antenna systems

In this work, we considered different SISO interference-limited systems such as K-user IC, 2-user IC, Z-IC and UCR. We made different practical assumptions regarding channels and hardware as summarized in the following parts.

IGS for SISO OFDM underlay-cognitive-radio systems

IGS has been shown to be successful to improve the performance of different interference-limited systems. Hence, it might appear that IGS is always able to outperform PGS; however, it is not necessarily the case in all scenarios as indicated before. In chapter 5, we investigated whether improper signaling is also beneficial in an UCR OFDM system. While there are indeed some benefits, these are minor and mainly apply to scenarios with small number of OFDM subbands. Such a rather negative result may be surprising, but it shows that improper signaling is not a magic tool that works in every case. Indeed, by increasing the number resources, interference can be managed easier by PGS, and the benefits of employing IGS decrease or even may vanish.

K-user SISO IC with asymmetric AHWD

We addressed the problem of obtaining the achievable rate region by IGS in the K-user SISO IC with asymmetric AHWD and proposed two suboptimal algorithms. To this end, we rewrote the corresponding optimization problem as the pseudo-signal-to-interference-plus-noise-rate (PSINR) region problem. We then tackled the corresponding optimization problem by MM. Our first algorithm, which was based on MM and the GDA, obtained a stationary point of the PSINR region. In this algorithm, we jointly optimized the powers and complementary variances. Furthermore, we proposed a simplified algorithm that has lower computational complexity. This simplified algorithm was based on the separate optimization of the powers and complementary variances. Through numerical examples, we showed that the proposed approaches enlarge the achievable rate region and outperform PGS and existing IGS algorithms, especially as the AHWD becomes more asymmetric.

Energy-efficient IGS for K-user IC

We also proposed energy-efficient IGS schemes for the K-user IC and UCR. We first aimed at enlarging the EE region of the K-user IC. By maximizing the weighted minimum energy efficiency (WMEE) of users, the proposed design permitted operating at different points of the EE region. In order to find a suboptimal solution to the WMEE maximization problem, we performed a separate optimization of the powers and complementary variances. For the former, we

considered PGS and resorted to MM and the GDA to find a solution to the original non-convex problem satisfying the KKT conditions. The resulting solution was then improved by optimizing over the complementary variances. Again, this has resulted in a non-convex problem, and a suboptimal solution was found by using bisection and MM. Our numerical results, presented in Section 7.1.4, show that IGS is more energy efficient than its proper counterpart.

We also considered the EE of IGS in UCR. We addressed the maximization of the EE function for the SU in UCR networks and derived necessary and sufficient optimality conditions for IGS in closed form. Additionally, we proposed a bisection method to find the optimal transmission parameters of PGS and IGS. Our results showed that IGS also pays off in terms of EE, although stricter conditions than those for rate optimization have to be fulfilled.

IGS with realistic CSIT assumptions

The aforementioned results were obtained assuming perfect, instantaneous and global channel state information (CSI) at transceivers. This assumption might not be realistic in every practical scenarios. In general, it is reasonable to assume that a receiver knows the CSI perfectly since acquiring CSI at the receiver side is relatively easy with training sequences or applying blind/semi-blind estimation methods [89, 97, 115]. However, the channel information is typically quantized and then sent to the transmitters through a noisy feedback link, which results in noisy CSI at transmitter side (CSIT). Therefore, we considered imperfect CSIT in Chapter 8 and investigated the robustness of IGS against imperfect CSIT in the single-antenna 2-user IC and Z-IC. We studied 2-user SISO IC and Z-IC since we were able to propose robust designs for IGS with closed-form solutions. We also derived closed-form conditions when IGS outperforms PGS for the 2-user IC and Z-IC in the presence of imperfect CSI. We showed through analytical studies that even if there is no reliable phase information, a robust IGS design can outperform a robust PGS design. In this case, one user may employ IGS, while the other employs PGS. We evaluated our analytical studies by simulations and showed that IGS permits a significant performance increase for the 2-user IC and Z-IC. Our numerical results show that IGS is even more robust to imperfect CSI than PGS provided that the transmission parameters are properly designed, and thus IGS still pays off in the context of imperfect CSI.

The instantaneous CSIT might not be always available. Hence, it is interesting to investigate the performance of IGS in fading channels, where the transmitters have access to only statistical CSIT. We addressed this problem in Section 8.2 and studied the ergodic rate of a PGS/IGS scheme in a 2-user Rayleigh IC with TIN. Under the assumption that the users have perfect CSIR but they have access only to statistical CSIT, we derived closed-form expressions for the ergodic rates and characterized the boundary of the achievable ergodic rate region. We also proposed a practical IGS scheme which does not require any optimization and power control at the transmitter side. In this scheme, both users transmit with maximum power. One user employs MIGS while the other user employs PGS. By numerical examples, we showed that IGS can substantially increase the sum-rate and enlarge the ergodic rate region of the 2-user Rayleigh SISO-IC under strong interference.

Summary of findings in SISO systems

To sum up, the results in the single antenna systems are generally in line with the results in the multiple antenna systems. We summarize our findings on IGS in single-antenna interference-limited systems as:

- The benefits of IGS increases with the number of users in the K-user SISO IC, similar to the K-user MIMO IC.

- IGS can improve the performance of single-antenna interference-limited systems from both achievable rate and EE point of view. However, we observed that IGS provides more benefits from achievable rate point of view than from EE perspective, similar to the MIMO systems.

- IGS my provide only minor improvements in OFDM UCR systems. The reason is that PGS can simpler manage interference when there are more resources, which is in line with the results in MIMO systems.

- IGS can outperform PGS in the 2-user SISO IC with imperfect CSIT if IGS is designed in a robust way.

- IGS can provide a better performance from the achievable ergodic rate point of view in the 2-user SISO IC with fading channels.

9.2 Future Studies

In this work, we considered various SISO and MIMO antenna systems with different realistic assumptions, which can open a path for further studies on improper signaling and interference-limited systems. In this section, we provide an insight for future works in the following subsections.

9.2.1 Statistical and/or imperfect CSIT

In this work, we considered realistic assumptions regarding CSIT in 2-user SISO IC. For instance, we considered the performance of IGS in the 2-user SISO IC without instantaneous CSIT. Additionally, we studied the performance of IGS in the 2-user IC and Z-IC with imperfect CSIT. In our IGS schemes for the 2-user IC with imperfect CSIT or perfect statistical CSIT, only one user may employ IGS, which allows us to find closed-form solutions for the design parameters. It has to be investigated whether these schemes can provide a considerable gain in a multiple-user and/or multiple-antenna system.

As indicated, PGS requires only channel gains to design parameters. However, IGS needs both channel gains and phases to optimize powers and complementary variances. Hence, it might be expected that the benefits of IGS vanish by imperfect CSIT or lack of instantaneous CSIT. It has been shown that IGS can improve the performance of multi-user (more than two users) and/or multiple-antenna systems in the presence of perfect instantaneous CSIT [17, 69, 100, 121]. However, perfect and instantaneous CSIT might not be available in practical scenarios. Thus, the following question arises, which has to be answered in future works. *Does IGS provide some gains, in multi-user (large scale scenarios) and/or multiple antenna systems when CSIT is noisy or instantaneous CSIT is not available?*

9.2.2 Global optimal

In this work, we mainly proposed suboptimal algorithms. Precisely, except the algorithm in Chapter 7.2, we obtained only suboptimal solutions for the optimization problems. For example, we presented a framework to obtain a stationary point of various optimization problems for the K-user MIMO IC with hardware imperfections. It is interesting to find out how close are theses solutions to the corresponding global optimal solutions. Moreover, in some scenarios, it is possible to derive necessary and sufficient conditions for the optimality of IGS. For example, these conditions are derived in Chapter 7.2 for the energy efficiency optimality of IGS in UCR. It is also interesting to obtain such conditions for the other considered problems. For example, it is known that IGS is optimal in the presence of improper noise in a point-to-point communication. It is reasonable to employ IGS in the K-user SISO IC with asymmetric AHWD, but it is not proved that IGS is optimal for this scenario. These problems can be addressed in future studies.

9.2.3 Distributed algorithms

All optimizations in this work are solved with centralized algorithms, which might not be applicable in some practical scenarios. By increasing the number of user, it might be very challenging to cooperate with all users. Hence, distributed algorithms can be studied in further studies. Additionally, acquiring global CSI is very complicated when the number of users grows. Thus, suboptimal algorithms, in which the users require only partial CSI, are also interesting and have to be addressed in further studies.

9.2.4 Discrete constellation

In this work, we considered only Gaussian signaling. Assuming Gaussian signaling simplifies the corresponding optimization problems and gives an insight on the system performance. In practice, discrete rather than Gaussian signaling is employed (see, e.g., [62, 86, 91]), which will lead to performance degradation with respect to IGS. The significance of studying improper Gaussian signals is that it shows us whether *improper* signaling may in principle achieve performance improvements over *proper* signaling. However, the following questions arise, which have to be addressed for implementation of improper signals: *What is the optimal discrete improper constellation? How is the performance of improper signaling with discrete constellation? Does discrete improper signal outperform its proper counterpart?*

List of Publications

The work presented in this thesis has been published in the following blind peer-reviewed journals and international conference proceedings:

Journal papers

1. **Mohammad Soleymani**, Christian Lameiro, Ignacio Santamaria, and Peter J Schreier, "Robust improper signaling for two-user SISO interference channels," *IEEE Trans. Commun.*, 67(7):4709–4723, July 2019.

2. **Mohammad Soleymani**, Christian Lameiro, Ignacio Santamaria, and Peter J Schreier, "Improper signaling for SISO two-user interference channels with additive asymmetric hardware distortion," *IEEE Trans. Commun.*, 67(12):8624–8638, Dec. 2019.

3. **Mohammad Soleymani**, Ignacio Santamaria, Christian Lameiro, and Peter J Schreier, "Ergodic rate for fading interference channels with proper and improper Gaussian signaling," *Entropy*, 21(10):922, 2019.

4. **Mohammad Soleymani**, Ignacio Santamaria, and Peter J Schreier, "Improper Gaussian signaling for the K-user MIMO interference channels with hardware impairments," *IEEE Trans. Veh. Technol.*, 69(10): 11632–11645, Oct. 2020.

Conference papers

1. **Mohammad Soleymani**, Christian Lameiro, Peter J Schreier, and Ignacio Santamaria, "Improper signaling for OFDM underlay cognitive radio systems," In *IEEE Statistical Signal Process. Workshop (SSP)*, pages 722–726. IEEE, 2018.

2. **Mohammad Soleymani**, Christian Lameiro, Peter J Schreier, and Ignacio Santamaria, "Energy-efficient design for underlay cognitive radio using improper signaling," In *Proc. IEEE Int. Conf. on Acoust., Speech and Signal Process. (ICASSP)*, pages 4769–4773, 2019.

3. **Mohammad Soleymani**, Christian Lameiro, Ignacio Santamaria, and Peter J. Schreier, "Energy-efficient improper signaling for K-User interference channels," In *Proc. IEEE European Signal Process. Conf. (EUSIPCO)*, pages 1–5, 2019.

4. **Mohammad Soleymani**, Ignacio Santamaria, Behrouz Maham, and Peter J Schreier, "Rate region of K-user MIMO interference channels with imperfect transmitters," In *Proc. IEEE European Signal Process. Conf. (EUSIPCO), accepted*, 2020.

Bibliography

[1] Tülay Adali and Peter J Schreier. Optimization and estimation of complex-valued signals: Theory and applications in filtering and blind source separation. *IEEE Signal Process. Mag.*, 31(5):112–128, 2014.

[2] Tülay Adali, Peter J Schreier, and Louis L Scharf. Complex-valued signal processing: The proper way to deal with impropriety. *IEEE Trans. Signal Process.*, 59(11):5101–5125, 2011.

[3] Osama Amin, Walid Abediseid, and Mohamed-Slim Alouini. Underlay cognitive radio systems with improper Gaussian signaling: Outage performance analysis. *IEEE Trans. Wireless Commun.*, 15(7):4875–4887, 2016.

[4] Osama Amin, Walid Abediseid, and Mohamed-Slim Alouini. Overlay spectrum sharing using improper Gaussian signaling. *IEEE J. Sel. Areas Commun.*, 35(1):50–62, 2017.

[5] Jeffrey G Andrews, Stefano Buzzi, Wan Choi, Stephen V Hanly, Angel Lozano, Anthony CK Soong, and Jianzhong Charlie Zhang. What will 5G be? *IEEE J. Sel. Areas Commun.*, 32(6):1065–1082, 2014.

[6] Augusto Aubry, Antonio De Maio, Alessio Zappone, Meisam Razaviyayn, and Zhi-Quan Luo. A new sequential optimization procedure and its applications to resource allocation for wireless systems. *IEEE Trans. Signal Process.*, 66(24):6518–6533, 2018.

[7] Aharon Ben-Tal, Laurent El Ghaoui, and Arkadi Nemirovski. *Robust Optimization*. Princeton University Press, 2009.

[8] Emil Björnson, Jakob Hoydis, Marios Kountouris, and Merouane Debbah. Massive MIMO systems with non-ideal hardware: Energy efficiency, estimation, and capacity limits. *IEEE Trans. Inf. Theory*, 60(11):7112–7139, 2014.

[9] Emil Björnson, Michail Matthaiou, and Merouane Debbah. A new look at dual-hop relaying: Performance limits with hardware impairments. *IEEE Trans. Commun.*, 61(11):4512–4525, 2013.

[10] Emil Björnson, Per Zetterberg, Mats Bengtsson, and Bjorn Ottersten. Capacity limits and multiplexing gains of MIMO channels with transceiver impairments. *IEEE Commun. Lett.*, 17(1):91–94, 2013.

[11] Elena Boshkovska, Derrick Wing Kwan Ng, Linglong Dai, and Robert Schober. Power-efficient and secure WPCNs with hardware impairments and non-linear EH circuit. *IEEE Trans. Commun.*, 66(6):2642–2657, 2018.

[12] Alexandros-Apostolos A Boulogeorgos, Nestor D Chatzidiamantis, and George K Karagiannidis. Energy detection spectrum sensing under RF imperfections. *IEEE Trans. Wireless Commun.*, 64(7):2754–2766, 2016.

[13] Stephen Boyd and Lieven Vandenberghe. *Convex Optimization*. Cambridge University Press, 2004.

[14] DH Brandwood. A complex gradient operator and its application in adaptive array theory. In *IEE Proc. F Commun., Radar Signal Process.*, volume 130, pages 11–16. IET, 1983.

[15] Stefano Buzzi, I Chih-Lin, Thierry E Klein, H Vincent Poor, Chenyang Yang, and Alessio Zappone. A survey of energy-efficient techniques for 5G networks and challenges ahead. *IEEE J. Sel. Areas Commun.*, 34(4):697–709, 2016.

[16] Viveck R Cadambe and Syed Ali Jafar. Interference alignment and degrees of freedom of the K-user interference channel. *IEEE Trans. Inf. Theory*, 54(8):3425, 2008.

[17] Viveck R Cadambe, Syed Ali Jafar, and Chenwei Wang. Interference alignment with asymmetric complex signaling–Settling the Høst-Madsen-Nosratinia conjecture. *IEEE Trans. Inf. Theory*, 56(9):4552–4565, 2010.

[18] Xun Cai, Yik-Chung Wu, Hai Lin, and Katsumi Yamashita. Estimation and compensation of CFO and I/Q imbalance in OFDM systems under timing ambiguity. *IEEE Trans. Veh. Technol.*, 60(3):1200–1205, 2011.

[19] Zheng Chang, Tapani Ristaniemi, and Zhisheng Niu. Radio resource allocation for collaborative OFDMA relay networks with imperfect channel state information. *IEEE Trans. Wireless Commun.*, 13(5):2824–2835, 2014.

[20] Mohamad Awad Charafeddine, Aydin Sezgin, Zhu Han, and Arogyaswami Paulraj. Achievable and crystallized rate regions of the interference channel with interference as noise. *IEEE Trans. Wireless Commun.*, 11(3):1100–1111, 2012.

[21] Yan Chen, Shunqing Zhang, and Shugong Xu. Impact of non-ideal efficiency on bits per Joule performance of base station transmissions. In *Proc. VTC - Spring*, pages 1–5. IEEE, 2011.

[22] Songlin Cheng, Rui Wang, Jun Wu, Wei Zhang, and Zhijun Fang. Performance analysis and beamforming designs of MIMO AF relaying with hardware impairments. *IEEE Trans. Veh. Technol.*, 67(7):6229–6243, 2018.

[23] Yuan-Hwui Chung and See-May Phoong. Joint estimation of I/Q imbalance, CFO and channel response for MIMO OFDM systems. *IEEE Trans. Commun.*, 58(5):1485–1492, 2010.

[24] Thomas M Cover and Joy A Thomas. *Elements of Information Theory*. John Wiley & Sons, 2012.

[25] Jean-Pierre Crouzeix and Jacques A Ferland. Algorithms for generalized fractional programming. *Math. Programm.*, 52(1-3):191–207, May 1991.

[26] Arash Gholami Davoodi and Syed Ali Jafar. Aligned image sets under channel uncertainty: Settling conjectures on the collapse of degrees of freedom under finite precision CSIT. *IEEE Trans. Inf. Theory*, 62(10):5603–5618, 2016.

[27] Arash Gholami Davoodi and Syed Ali Jafar. Transmitter cooperation under finite precision CSIT: A GDoF perspective. *IEEE Trans. Inf. Theory*, 63(9):6020–6030, 2017.

[28] Zhiguo Ding, Xianfu Lei, George K Karagiannidis, Robert Schober, Jinhong Yuan, and Vijay K Bhargava. A survey on non-orthogonal multiple access for 5G networks: Research challenges and future trends. *IEEE J. Sel. Areas Commun.*, 35(10):2181–2195, 2017.

[29] Zhiguo Ding, Yuanwei Liu, Jinho Choi, Qi Sun, Maged Elkashlan, I Chih-Lin, and H Vincent Poor. Application of non-orthogonal multiple access in LTE and 5G networks. *IEEE Commun. Mag.*, 55(2):185–191, 2017.

[30] Werner Dinkelbach. On nonlinear fractional programming. *Management Science*, 13(7):492–498, 1967.

[31] John Duchi. Sequential convex programming. *Lecture Notes, EE364b, Stanford University*, 2018.

[32] Alex Dytso, Daniela Tuninetti, and Natasha Devroye. Interference as noise: Friend or foe? *IEEE Trans. Inf. Theory*, 62(6):3561–3596, 2016.

[33] Albrecht Fehske, Gerhard Fettweis, Jens Malmodin, and Gergely Biczok. The global footprint of mobile communications: The ecological and economic perspective. *IEEE Commun. Mag.*, 49(8):55–62, 2011.

[34] Junjuan Feng, Shaodan Ma, Sonia Aïssa, and Minghua Xia. Two-way massive MIMO relaying systems with non-ideal transceivers: Joint power and hardware scaling. *IEEE Trans. Commun.*, 2019.

[35] Renhai Feng, Quanzhong Li, Qi Zhang, and Jiayin Qin. Robust secure transmission in MISO simultaneous wireless information and power transfer system. *IEEE Trans. Veh. Technol*, 64(1):400–405, 2015.

[36] Mohamed Gaafar, Osama Amin, Walid Abediseid, and Mohamed-Slim Alouini. Underlay spectrum sharing techniques with in-band full-duplex systems using improper Gaussian signaling. *IEEE Trans. Wireless Commun.*, 16(1):235–249, 2017.

[37] Mohamed Gaafar, Mohammad Galal Khafagy, Osama Amin, Rafael F Schaefer, and Mohamed-Slim Alouini. Full-duplex relaying with improper Gaussian signaling over Nakagami-m fading channels. *IEEE Trans. Commun.*, 66(1):64–78, 2018.

[38] Chunhua Geng, Navid Naderializadeh, Amir Salman Avestimehr, and Syed A Jafar. On the optimality of treating interference as noise. *IEEE Trans. Inf. Theory*, 61(4):1753–1767, 2015.

[39] Gye-Tae Gil, Il-Hyun Sohn, Jin-Kyu Park, and Yong Hoon Lee. Joint ML estimation of carrier frequency, channel, I/Q mismatch, and DC offset in communication receivers. *IEEE Trans. Veh. Technol.*, 54(1):338–349, 2005.

[40] Andrea Goldsmith, Syed Ali Jafar, Ivana Maric, and Sudhir Srinivasa. Breaking spectrum gridlock with cognitive radios: An information theoretic perspective. *proc. IEEE*, 97(5):894–914, 2009.

[41] Michael Grant, Stephen Boyd, and Yinyu Ye. CVX: MATLAB software for disciplined convex programming, 2008.

[42] Ali Haghi, Neda Mohammadizadeh, and Amir K Khandani. Delay in cooperative communications: Achieving higher multiplexing gain in Gaussian interference channels with full-duplex transmitters. *IEEE Trans. Inf. Theory*, 2019.

[43] Muhammad Fainan Hanif, Zhiguo Ding, Tharmalingam Ratnarajah, and George K Karagiannidis. A minorization-maximization method for optimizing sum rate in the downlink of non-orthogonal multiple access systems. *IEEE Trans. Signal Process.*, 64(1):76–88, 2015.

[44] Simon Haykin. Cognitive radio: brain-empowered wireless communications. *IEEE J. Sel. Areas Commun.*, 23(2):201–220, 2005.

[45] Robert W Heath, Nuria Gonzalez-Prelcic, Sundeep Rangan, Wonil Roh, and Akbar M Sayeed. An overview of signal processing techniques for millimeter wave MIMO systems. *IEEE J. Sel. Topics Signal Process.*, 10(3):436–453, 2016.

[46] Christoph Hellings, Michael Joham, and Wolfgang Utschick. QoS feasibility in MIMO broadcast channels with widely linear transceivers. *IEEE Signal Process. Lett.*, 20(11):1134–1137, 2013.

[47] Christoph Hellings, Bho Matthiesen, Eduard A Jorswieck, and Wolfgang Utschick. Globally optimal TIN strategies with time-sharing in the MISO interference channel. In *Proc. IEEE European Signal Process. Conf. (EUSIPCO)*, pages 1–5. IEEE, 2019.

[48] Christoph Hellings and Wolfgang Utschick. Performance gains due to improper signals in MIMO broadcast channels with widely linear transceivers. In *Proc. IEEE Int. Conf. on Acoust., Speech and Signal Process. (ICASSP)*, pages 4379–4383. IEEE, 2013.

[49] Christoph Hellings and Wolfgang Utschick. Block-skew-circulant matrices in complex-valued signal processing. *IEEE Trans. Signal Process.*, 63(8):2093–2107, 2015.

[50] Christoph Hellings and Wolfgang Utschick. Improper signaling versus time-sharing in the SISO Z-interference channel. *IEEE Commun. Lett.*, 21(11):2432–2435, 2017.

[51] Christoph Hellings and Wolfgang Utschick. On the worst-case noise in Gaussian MIMO systems with proper and with improper signaling. In *WSA 2017; 21th International ITG Workshop on Smart Antennas*, pages 1–7. VDE, 2017.

[52] Christoph Hellings and Wolfgang Utschick. Improper signaling versus time-sharing in the two-user Gaussian interference channel with TIN. *IEEE Trans. Inf. Theory*, 66(5):2988–2999, 2020.

[53] Zuleita Ho, Alessio Zappone, and Eduard Jorswieck. Optimal non-regenerative relay processing with improper signals. In *Proc. ISWCS*, pages 1–5. Ilmenau, Germany, Aug. 2013.

[54] Zuleita KM Ho and Eduard Jorswieck. Improper Gaussian signaling on the two-user SISO interference channel. *IEEE Trans. Wireless Commun.*, 11(9):3194–3203, 2012.

[55] Chiachi Huang, Viveck R Cadambe, and Syed Ali Jafar. Interference alignment and the generalized degrees of freedom of the X channel. *IEEE Trans. Inf. Theory*, 58(8):5130–5150, 2012.

[56] Christian Isheden, Zhijiat Chong, Eduard Jorswieck, and Gerhard Fettweis. Framework for link-level energy efficiency optimization with informed transmitter. *IEEE Trans. Wireless Commun.*, 11(8):2946–2957, 2012.

[57] Syed A Jafar. Interference alignment—a new look at signal dimensions in a communication network. *Found Trends® in Commun. Inf. Theory*, 7(1):1–134, 2011.

[58] R Jagannathan. On some properties of programming problems in parametric form pertaining to fractional programming. *Management Science*, 12(7):609–615, 1966.

[59] Sidrah Javed, Osama Amin, and Mohamed-Slim Alouini. Full-duplex relaying under I/Q imbalance using improper Gaussian signaling. In *Proc. IEEE Int. Conf. on Acoust., Speech and Signal Process. (ICASSP)*, pages 6538–6542, 2017.

[60] Sidrah Javed, Osama Amin, Salama S Ikki, and Mohamed-Slim Alouini. Asymmetric hardware distortions in receive diversity systems: Outage performance analysis. *IEEE Access*, 5:4492–4504, 2017.

[61] Sidrah Javed, Osama Amin, Salama S Ikki, and Mohamed-Slim Alouini. Impact of improper Gaussian signaling on hardware impaired systems. In *Proc. IEEE Int. Conf. Commun. (ICC)*, pages 1–6, 2017.

[62] Sidrah Javed, Osama Amin, Salama S Ikki, and Mohamed-Slim Alouini. Asymmetric modulation for hardware impaired systems-error probability analysis and receiver design. *IEEE Trans. Wireless Commun.*, 18(3):1723–1738, 2019.

[63] Sidrah Javed, Osama Amin, Salama S Ikki, and Mohamed-Slim Alouini. Multiple antenna systems with hardware impairments: New performance limits. *IEEE Trans. Veh. Technol.*, 68(2):1593–1606, 2019.

[64] Sidrah Javed, Osama Amin, Basem Shihada, and Mohamed-Slim Alouini. Improper Gaussian signaling for hardware impaired multihop full-duplex relaying systems. *IEEE Trans. Commun.*, 67(3):1858–1871, 2019.

[65] Sidrah Javed, Osama Amin, Basem Shihada, and Mohamed-Slim Alouini. A journey from improper Gaussian signaling to asymmetric signaling. *IEEE Commun. Surveys & Tutorials*, 2020.

[66] Eduard A Jorswieck, Erik G Larsson, and Danyo Danev. Complete characterization of the Pareto boundary for the MISO interference channel. *IEEE Trans. Signal Process.*, 56(10):5292–5296, 2008.

[67] Ernest Kurniawan and Sumei Sun. Improper Gaussian signaling scheme for the Z-interference channel. *IEEE Trans. Wireless Commun.*, 14(7):3912–3923, 2015.

[68] Sandra Lagen, Adrian Agustin, and Josep Vidal. Coexisting linear and widely linear transceivers in the MIMO interference channel. *IEEE Trans. Signal Process.*, 64(3):652–664, 2016.

[69] Sandra Lagen, Adrian Agustin, and Josep Vidal. On the superiority of improper Gaussian signaling in wireless interference MIMO scenarios. *IEEE Trans. Commun.*, 64(8):3350–3368, 2016.

[70] Christian Lameiro, Ignacio Santamaría, and Peter J Schreier. Benefits of improper signaling for underlay cognitive radio. *IEEE Wireless Commun. Lett.*, 4(1):22–25, 2015.

[71] Christian Lameiro, Ignacio Santamaría, and Peter J Schreier. Rate region boundary of the SISO Z-interference channel with improper signaling. *IEEE Trans. Commun.*, 65(3):1022–1034, 2017.

[72] Christian Lameiro, Wolfgang Utschick, and Ignacio Santamaría. Spatial interference shaping for underlay MIMO cognitive networks. *Signal Processing*, 134:174–184, 2017.

[73] Cristian Lameiro and Ignacio Santamaría. Degrees-of-freedom for the 4-user SISO interference channel with improper signaling. In *Proc. IEEE Int. Conf. Commun. (ICC)*, pages 3053–3057, 2013.

[74] Cristian Lameiro, Javier Vía, and Ignacio Santamaría. Amplify-and-forward strategies in the two-way relay channel with analog Tx-Rx beamforming. *IEEE Trans. Veh. Technol.*, 62(2):642–654, 2013.

[75] Gert R Lanckriet and Bharath K Sriperumbudur. On the convergence of the concave-convex procedure. In *Proc. Adv. Neural Inf. Process. Syst*, pages 1759–1767, 2009.

[76] Thomas Lipp and Stephen Boyd. Variations and extension of the convex–concave procedure. *Optim. Eng.*, 17(2):263–287, 2016.

[77] Liang Liu, Rui Zhang, and Kee-Chaing Chua. Achieving global optimality for weighted sum-rate maximization in the K-user Gaussian interference channel with multiple antennas. *IEEE Trans. Wireless Commun.*, 11(5):1933–1945, 2012.

[78] Zhi-Quan Luo, Wing-Kin Ma, Anthony Man-Cho So, Yinyu Ye, and Shuzhong Zhang. Semidefinite relaxation of quadratic optimization problems. *IEEE Signal Process. Mag.*, 27(3):20–34, 2010.

[79] Mohammad Ali Maddah-Ali, Abolfazl Seyed Motahari, and Amir Keyvan Khandani. Communication over MIMO X channels: Interference alignment, decomposition, and performance analysis. *IEEE Trans. Inf. Theory*, 54(8):3457–3470, 2008.

[80] Junling Mao, Gang Xie, Jinchun Gao, and Yuanan Liu. Energy efficiency optimization for OFDM-based cognitive radio systems: A water-filling factor aided search method. *IEEE Trans. Wireless Commun.*, 12(5):2366–2375, 2013.

[81] Barry R Marks and Gordon P Wright. A general inner approximation algorithm for nonconvex mathematical programs. *Operations Research*, 26(4):681–683, 1978.

[82] Rami Mochaourab and Eduard A Jorswieck. Robust beamforming in interference channels with imperfect transmitter channel information. *Signal Processing*, 92(10):2509–2518, 2012.

[83] G Mohamed. Massive relaying communication system under I/Q imbalance and hardware manufacturing problems. *IEEE Systems Journal*, 2019.

[84] Abolfazl Seyed Motahari and Amir Keyvan Khandani. Capacity bounds for the Gaussian interference channel. *IEEE Trans. Inf. Theory*, 55(2):620–643, 2009.

[85] Ali Arshad Nasir, Hoang Duong Tuan, Trung Q Duong, and H Vincent Poor. Improper Gaussian signaling for broadcast interference networks. *IEEE Signal Process. Lett.*, 26(6):808–812, 2019.

[86] Hieu Duy Nguyen, Rui Zhang, and Sumei Sun. Improper signaling for symbol error rate minimization in K-user interference channel. *IEEE Trans. Commun.*, 63(3):857–869, 2015.

[87] Haewook Park, Seok-Hwan Park, Jin-Sung Kim, and Inkyu Lee. SINR balancing techniques in coordinated multi-cell downlink systems. *IEEE Trans. Wireless Commun.*, 12(2):626–635, 2013.

[88] Antonio Pascual-Iserte, Daniel Pérez Palomar, Ana I Pérez-Neira, and Miguel Ángel Lagunas. A robust maximin approach for MIMO communications with imperfect channel state information based on convex optimization. *IEEE Trans. Signal Process.*, 54(1):346–360, 2006.

[89] Yiyang Pei, Ying-Chang Liang, Kah Chan Teh, and Kwok Hung Li. Secure communication in multiantenna cognitive radio networks with imperfect channel state information. *IEEE Trans. Signal Process.*, 59(4):1683–1693, 2011.

[90] Alexander Rubinov, Hoang Tuy, and Heather Mays. An alogrithm for monotonic global optimization problems. *Optimization*, 49(3):205–221, 2001.

[91] Ignacio Santamaria, Pedro Crespo, Christian Lameiro, and Peter Schreier. Information-theoretic analysis of a family of improper discrete constellations. *Entropy*, 20(1):45, 2018.

[92] Ignacio Santamaría, Javier Vía, Alfredo Nazábal, and Christian Lameiro. Capacity region of the multiantenna Gaussian broadcast channel with analog Tx-Rx beamforming. In *Proc. 5th Int. ICST CHINACOM*, pages 1–6, Aug. 2010.

[93] Tim Schenk. *RF imperfections in high-rate wireless systems: impact and digital compensation*. Springer Science & Business Media, 2008.

[94] Peter J Schreier and Louis L Scharf. *Statistical Signal Processing of Complex-Valued Data: the Theory of Improper and Noncircular Signals*. Cambridge University Press, 2010.

[95] Ararat Shaverdian and Mohammad Reza Nakhai. Robust distributed beamforming with interference coordination in downlink cellular networks. *IEEE Trans. Commun.*, 62(7):2411–2421, 2014.

[96] Changyang She, Chenyang Yang, and Lingjia Liu. Energy-efficient resource allocation for MIMO-OFDM systems serving random sources with statistical QoS requirement. *IEEE Trans. on Commun.*, 63(11):4125–4141, 2015.

[97] Hong Shen, Jiaheng Wang, Bernard C Levy, and Chunming Zhao. Robust optimization for amplify-and-forward MIMO relaying from a worst-case perspective. *IEEE Trans. Signal Process.*, 61(21):5458–5471, 2013.

[98] Kaiming Shen and Wei Yu. Fractional programming for communication systems–Part I: Power control and beamforming. *IEEE Trans. Signal Process.*, 66(10):2616–2630, 2018.

[99] Hun-Young Shin, Seok-Hwan Park, Haewook Park, and Inkyu Lee. A new approach of interference alignment through asymmetric complex signaling and multiuser diversity. *IEEE Trans. Wireless Commun.*, 11(3):880–884, 2012.

[100] Mohammad Soleymani, Christian Lameiro, Ignacio Santamaria, and Peter J. Schreier. Energy-efficient improper signaling for K-User interference channels. In *Proc. IEEE European Signal Process. Conf. (EUSIPCO)*, pages 1–5, 2019.

[101] Mohammad Soleymani, Christian Lameiro, Ignacio Santamaria, and Peter J Schreier. Improper signaling for SISO two-user interference channels with additive asymmetric hardware distortion. *IEEE Trans. Commun.*, 67(12):8624–8638, 2019.

[102] Mohammad Soleymani, Christian Lameiro, Ignacio Santamaria, and Peter J Schreier. Robust improper signaling for two-user SISO interference channels. *IEEE Trans. Commun.*, 67(7):4709–4723, 2019.

[103] Mohammad Soleymani, Christian Lameiro, Peter J Schreier, and Ignacio Santamaria. Improper signaling for OFDM underlay cognitive radio systems. In *IEEE Statistical Signal Process. Workshop (SSP)*, pages 722–726. IEEE, 2018.

[104] Mohammad Soleymani, Christian Lameiro, Peter J Schreier, and Ignacio Santamaria. Energy-efficient design for underlay cognitive radio using improper signaling. In *Proc. IEEE Int. Conf. on Acoust., Speech and Signal Process. (ICASSP)*, pages 4769–4773, 2019.

[105] Mohammad Soleymani, Ignacio Santamaria, Christian Lameiro, and Peter J Schreier. Ergodic rate for fading interference channels with proper and improper Gaussian signaling. *Entropy*, 21(10):922, 2019.

[106] Mohammad Soleymani, Ignacio Santamaria, Behrouz Maham, and Peter J Schreier. Rate region of K-user MIMO interference channels with imperfect transmitters. In *Proc. IEEE European Signal Process. Conf. (EUSIPCO), accepted*, 2020.

[107] Mohammad Soleymani, Ignacio Santamaria, and Peter J Schreier. Improper Gaussian signaling for the K-user MIMO interference channels with hardware impairments. *IEEE Trans. Veh. Technol., accepted*, 2020.

[108] Ying Sun, Prabhu Babu, and Daniel P Palomar. Majorization-minimization algorithms in signal processing, communications, and machine learning. *IEEE Trans. Signal Process.*, 65(3):794–816, 2017.

[109] Kuang-Yu Sung and Chi-chao Chao. Estimation and compensation of I/Q imbalance in OFDM direct-conversion receivers. *IEEE J. Sel. Topics Signal Process.*, 3(3):438–453, 2009.

[110] Ravi Tandon, Syed Ali Jafar, Shlomo Shamai, and H Vincent Poor. On the synergistic benefits of alternating CSIT for the MISO broadcast channel. *IEEE Trans. Inf. Theory*, 59(7):4106–4128, 2013.

[111] Leila Tlebaldiyeva, Behrouz Maham, and Theodoros A Tsiftsis. Device-to-device mmwave communication in the presence of interference and hardware distortion noises. *IEEE Commun. Lett.*, 2019.

[112] Leila Tlebaldiyeva, Theodoros A Tsiftsis, and Behrouz Maham. Performance analysis of improved energy detector with hardware impairments for accurate spectrum sensing. *IEEE Access*, 7:13927–13938, 2019.

[113] Hoang Duong Tuan, Ali Arshad Nasir, Ha H Nguyen, Trung Q Duong, and H Vincent Poor. Non-orthogonal multiple access with improper Gaussian signaling. *IEEE J. Sel. Topics Signal Process.*, 13(3):496–507, 2019.

[114] Jiaheng Wang, Mats Bengtsson, Björn Ottersten, and Daniel P Palomar. Robust MIMO precoding for several classes of channel uncertainty. *IEEE Trans. Signal Process.*, 61(12):3056–3070, 2013.

[115] Jiaheng Wang and Daniel P Palomar. Worst-case robust MIMO transmission with imperfect channel knowledge. *IEEE Trans. Signal Process.*, 57(8):3086–3100, 2009.

[116] Liang Wang, Min Sheng, Yan Zhang, Xijun Wang, and Chao Xu. Robust energy efficiency maximization in cognitive radio networks: The worst-case optimization approach. *IEEE Trans. Commun.*, 63(1):51–65, 2015.

[117] Yan Wang, Wenjun Xu, Kewen Yang, and Jiaru Lin. Optimal energy-efficient power allocation for OFDM-based cognitive radio networks. *IEEE Commun. Lett.*, 16(9):1420–1423, 2012.

[118] Zhiqiang Wei, Derrick Wing Kwan Ng, Jinhong Yuan, and Hui-Ming Wang. Optimal resource allocation for power-efficient MC-NOMA with imperfect channel state information. *IEEE Trans. Commun.*, 65(9):3944–3961, 2017.

[119] Wilhelm Wirtinger. Zur formalen Theorie der Funktionen von mehr komplexen Veränderlichen. *Math. Ann.*, 97(1):357–375, 1927.

[120] Xiaochen Xia, Dongmei Zhang, Kui Xu, Wenfeng Ma, and Youyun Xu. Hardware impairments aware transceiver for full-duplex massive MIMO relaying. *IEEE Trans. Signal Process.*, 63(24):6565–6580, 2015.

[121] Lu Yang and Wei Zhang. Interference alignment with asymmetric complex signaling on MIMO X channels. *IEEE Trans. Commun.*, 62(10):3560–3570, 2014.

[122] Yang Yang and Marius Pesavento. A unified successive pseudoconvex approximation framework. *IEEE Trans. Signal Process.*, 65(13):3313–3328, 2017.

[123] Talha Younas, Jiandong Li, and Jehangir Arshad. On bandwidth efficiency analysis for LS-MIMO with hardware impairments. *IEEE Access*, 5:5994–6001, 2017.

[124] Alan L Yuille and Anand Rangarajan. The concave-convex procedure. *Neural computation*, 15(4):915–936, 2003.

[125] Alessio Zappone, Emil Björnson, Luca Sanguinetti, and Eduard Jorswieck. Globally optimal energy-efficient power control and receiver design in wireless networks. *IEEE Trans. Signal Process.*, 65(11):2844–2859, 2017.

[126] Alessio Zappone and Eduard Jorswieck. Energy efficiency in wireless networks via fractional programming theory. *Found Trends® in Commun. Inf. Theory*, 11(3-4):185–396, 2015.

[127] Alessio Zappone, Pin-Hsun Lin, and Eduard A Jorswieck. Secrecy energy efficiency for MIMO single-and multi-cell downlink transmission with confidential messages. *IEEE Trans. Inf. Forensics Security*, 14(8):2059–2073, 2019.

[128] Alessio Zappone, Luca Sanguinetti, Giacomo Bacci, Eduard Jorswieck, and Merouane Debbah. Energy-efficient power control: A look at 5G wireless technologies. *IEEE Trans. Signal Process.*, 64(7):1668–1683, 2015.

[129] Yong Zeng, Cenk M Yetis, Erry Gunawan, Yong Liang Guan, and Rui Zhang. Transmit optimization with improper Gaussian signaling for interference channels. *IEEE Trans. Signal Process.*, 61(11):2899–2913, 2013.

[130] Yong Zeng, Rui Zhang, Erry Gunawan, and Yong Liang Guan. Optimized transmission with improper Gaussian signaling in the K-user MISO interference channel. *IEEE Trans. Wireless Commun.*, 12(12):6303–6313, 2013.

[131] Jiayi Zhang, Linglong Dai, Xinlin Zhang, Emil Björnson, and Zhaocheng Wang. Achievable rate of Rician large-scale MIMO channels with transceiver hardware impairments. *IEEE Trans. Veh. Technol*, 65(10):8800–8806, 2016.

[132] Jiayi Zhang, Yinghua Wei, Emil Björnson, Yu Han, and Shi Jin. Performance analysis and power control of cell-free massive MIMO systems with hardware impairments. *IEEE Access*, 6:55302–55314, 2018.

[133] Qi Zhang, Tony QS Quek, and Shi Jin. Scaling analysis for massive MIMO systems with hardware impairments in Rician fading. *IEEE Trans. Wireless Commun.*, 17(7):4536–4549, 2018.

[134] Xianyu Zhang, Daoxing Guo, Kang An, and Bangning Zhang. Secure communications over cell-free massive MIMO networks with hardware impairments. *IEEE Systems Journal*, 2019.

[135] Jun Zhu, Derrick Wing Kwan Ng, Ning Wang, Robert Schober, and Vijay K Bhargava. Analysis and design of secure massive MIMO systems in the presence of hardware impairments. *IEEE Trans. Wireless Commun.*, 16(3):2001–2016, 2017.